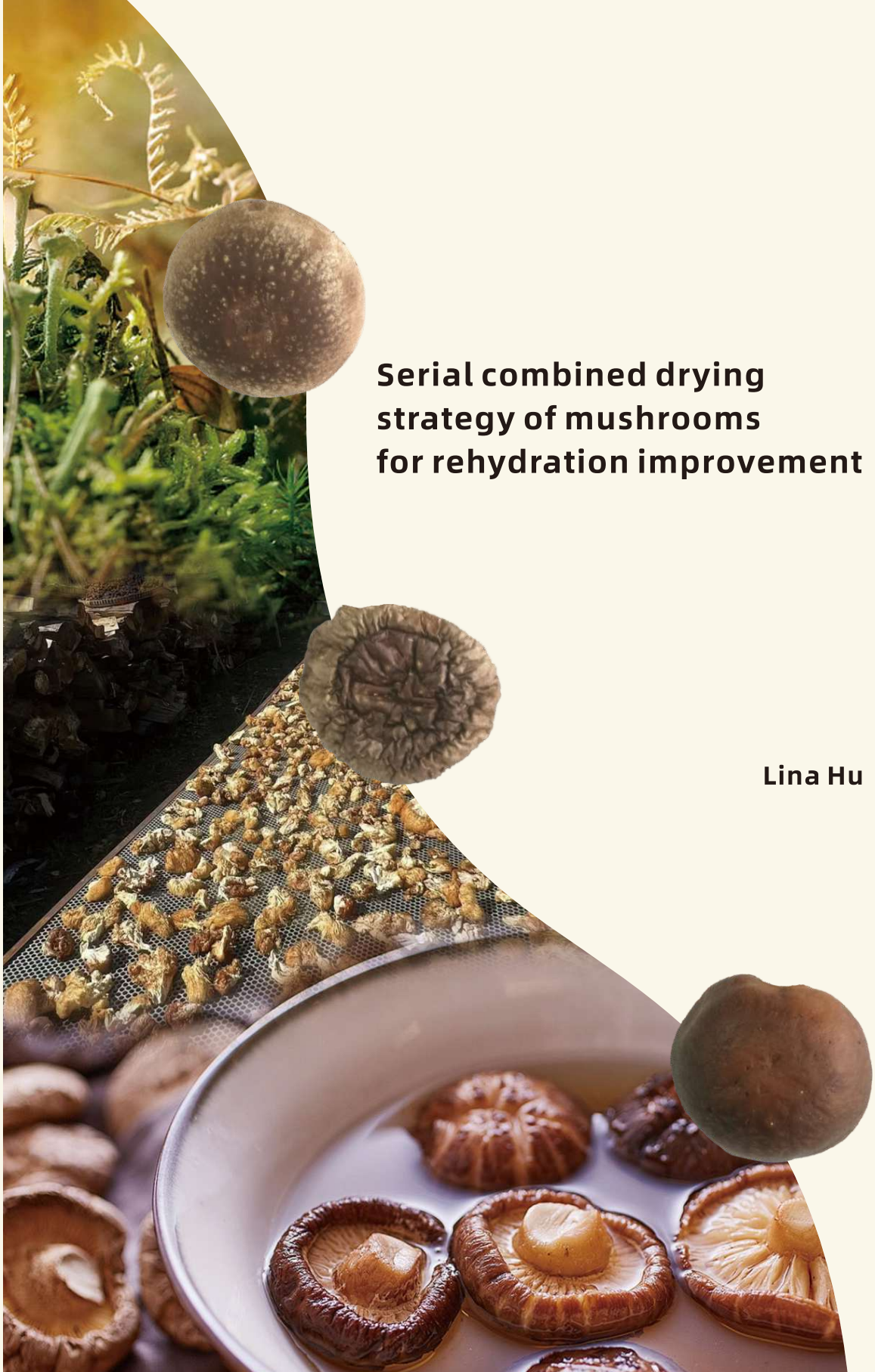


Serial combined drying strategy of mushrooms for rehydration improvement

Lina Hu

Propositions

1. Drying processes will never be optimized efficiently for rehydration as long as researchers ignore the microstructure.
   (this thesis)
2. The explanatory power of models outweighs their predictive accuracy.
   (this thesis)
3. On-site processing of perishable agricultural products adds values by reducing waste and freight cost, while enhancing product quality.
4. Pre-preparation is a fundamental driver of efficiency across diverse scientific disciplines.
5. Dedicated reflection time is an essential prerequisite for productivity.
6. Divergent values and aims within academic systems raise challenges for communication in international PhD programs.

Propositions belonging to the thesis, entitled
Serial Combined Drying Strategy of Mushrooms for Rehydration Improvement

Lina Hu
Wageningen, 6 May 2026

Serial combined drying strategy of mushrooms for rehydration improvement

Lina Hu

Thesis committee

Promotors

Prof. Dr Ruud G.M. van der Sman

Special professor in Food Process Engineering

Wageningen University & Research

Prof. Dr Jinfeng Bi

Professor, Institute of Food Science and Technology

Chinese Academy of Agricultural Sciences(CAAS), Beijing, China

Co-promotor

Dr Xin Jin, Institute of Food Science and Technology

Chinese Academy of Agricultural Sciences (CAAS) , Beijing, China

Other members

Prof. Xiao Dong Chen, Institute of Biopharmaceutical and Health Engineering-Tsinghua Shenzhen International Graduate School, Shenzhen, China

Prof. Thijs Defraeye, Wageningen University & Research

Dr. Camilla Terenzi, Wageningen University & Research

Dr. Joanna Siccama, Wageningen Food & Biobased Research- Wageningen University & Research

This research was conducted under the auspices of the Graduate School VLAG (Biobased, Biomolecular, Chemical, Food and Nutrition Sciences)

Serial combined drying strategy of mushrooms for rehydration improvement

Lina Hu

Thesis

submitted in fulfilment of the requirements for the degree of doctor
at Wageningen University
by the authority of the Rector Magnificus,
Prof. Dr C. Kroeze,
in the presence of the
Thesis Committee appointed by the Academic Board
to be defended in public
on Wednesday 6 May 2026
at 10:30 a.m. in the Omnia Auditorium.

Lina Hu

Serial combined drying strategy of mushrooms for rehydration improvement

196 pages

PhD thesis, Wageningen University, Wageningen, the Netherlands (2026)

With references, with summary in English

ISBN: 978-94-6534-342-6

DOI: https://doi.org/10.18174/680980

Contents

Chapter 1	Introduction	1
Chapter 2	Study on the rehydration quality improvement of *shiitake* mushroom by combined drying methods	13
Chapter 3	Microstructure evolution affecting the rehydration of dried mushrooms during instant controlled pressure drop combined hot air drying (DIC-HA)	45
Chapter 4	Impact of physical changes in mushroom on variation in moisture sorption	71
Chapter 5	A multiphase and multiscale mechanistic model for hot air drying of shiitake mushroom	97
Chapter 6	General discussion	141
References		151
Summary		185
Appendices		189

Chapter 1

Introduction

1.1. General introduction

Drying is a widely adopted method for preserving agricultural products, such as vegetables and fruits, effectively extending their shelf life and minimizing post-harvest loss (Ratti, 2001). It can offer a sustainable solution for long distance transport of agricultural products, if the energy input for drying does not outweigh the energy gained for transporting it in the dry state (instead of the fresh state)(Mujumdar, 2007). Before consumption the dried products typically require rehydration (Lewicki, 2006). Optimal rehydration performance in dried products is characterized by a rapid rehydration rate, minimal nutrient loss, and the restoration of satisfactory sensory and textural quality, such as good chewiness (Krokida and Philippopoulos, 2005). Ideally, the rehydrated product has similar texture to that of the fresh products (Aguilera, 2006).

However, the results of common drying methods are far from ideal. It is known that freeze-dried products exhibit fast rehydration rates due to their high porosity. However, the freezing step causes significant structural damage during the ice formation process, which leads to solutes loss and a too fragile texture of the dried products (Marques et al., 2009; Siebert et al., 2018; Vergeldt et al., 2014). In contrast, air-dried products exhibit slow rehydration rates and tough texture due to their compact structure (Krokida and Philippopoulos, 2005). Yet, after the (long) rehydration their texture is reasonable (Marabi et al., 2006). Currently, no single drying method delivers the "ideal" product with reasonable rehydration time, and a texture similar to that of fresh produce. To overcome the drawbacks of single drying methods, the combined drying techniques have been investigated in terms of their ability to enhance product quality (Siebert et al., 2018; Xu et al., 2006; Xu et al., 2005; Zhang et al., 2017).

There are two principal ways of combined drying: serial and parallel. Serial combined drying involves the sequential application of one drying method, followed by another. For example, Siebert et al. (2018) investigated all possible combinations of hot air drying (HAD), microwave vacuum drying (MVD), and freeze drying (FD). In contrast, parallel combinations involve the simultaneous implementation of two or more drying methods, for example microwave heating with vacuum drying (MWVD) or freeze drying (MWFD) (Jiang et al., 2010; Zhang et al., 2010; Zhang et al., 2006; Zielinska et al., 2017). Serial combined drying can easily be implemented with existing drying equipment, while parallel combined drying requires specialized equipment (Zhang et al., 2017), which hinders their adoption at industrial scale. Therefore, in this thesis we will focus on serial combined drying. As a case study, we selected *shiitake* mushrooms for their economic importance in China, and their

unique property of having an initial porous structure, which supports efficient water uptake. Moreover, the drying process can significantly enhance the levels of vitamin D_2 and umami compounds (Hiraide et al., 2004; Mattila et al., 2002; Rathore et al., 2017).

Designing and optimizing combined drying techniques require a thorough understanding of the microstructural changes induced by drying, and their subsequent impact on rehydration and texture (Aguilera, 2006; Rojas and Augusto, 2018; Zhao et al., 2019). Porosity is a well-known factor for the fast rehydration of dried products (Benseddik et al., 2019; Lopez-Quiroga et al., 2019; Marabi and Saguy, 2004; Witrowa-Rajchert and Lewicki, 2006). The role of cell membrane integrity in rehydration performance has received increasing attention in recent years (Qiu et al., 2021; Wang et al., 2024). Therefore, the identification and evolution of key microstructural properties affecting rehydration enhancement during drying of *shiitake* mushrooms is essential.

Due to the large complexity of the drying and rehydration problems, in relation to microstructure, we believe that good insight can only be obtained via physical modeling. The insight gained from coupling theoretical models with experiments allows for the iterative refinement of hypotheses, and targeted experimentation. Mathematical modeling of drying, grounded in the physical description of transport phenomena within the products, coupled with large deformation mechanics, provides a powerful tool for designing complicated (serial combined) drying process to obtain products with good rehydration and texture properties. By establishing a model that describes the physical state changes of products, including temperature, moisture content and microstructure, one can probe the optimal setting of the sequential steps of the drying conditions. Zhu et al.(2021) developed a convective drying model for *shiitake* mushrooms, incorporating thermo-hydro-mechanical coupling and considering the effect of shrinkage on heat and mass transfer. However, they have yet to account for the unique microscopic structure of mushrooms, such as the porous and connective hyphal network as well as the cell membrane that set them apart from homogeneous materials (Zecchi et al., 2011; Zhu et al., 2021). Therefore, the existing model for mushroom drying is still limited in offering a good understanding of the transport phenomena, and a fully mechanistic model development considering the microstructure properties is necessary.

The primary goal of this research was to investigate a novel drying strategy for mushrooms, with a specific focus on improving the rehydration performance of the final dried product. To achieve this, the study has several objectives: 1) To evaluate a number of serial combined drying methods to improve the microstructure of the products. 2) To characterize the

evolution of the microstructure during drying and identify the critical microstructural properties that most significantly impact rehydration. 3) To develop a theoretical mushroom drying model for better insights into the changes in the microstructure.

In the following sections, we describe the state of the art for our research problems, identify the knowledge gaps of optimal drying methods for rehydration, combined drying and microstructure, motivate our choices, and formulate the research questions to be investigated.

1.2 Rehydration, microstructure and combined drying technology

Rehydration is a process of water imbibition that consists of two steps: water enters the pores within the matrix via capillary suction, and is then absorbed by the matrix. The rehydration performance strongly depends on the microstructure properties that significantly vary with drying methods (Lewicki and Pawlak, 2003). Therefore, having a good knowledge of the impact of drying on microstructure properties is essential.

Conventional drying methods, such as air drying will cause 1) reduced porosity and a collapse (irreversible shrinkage) of cellular materials (Prothon et al., 2003);2) cell membrane disruption (Prothon et al., 2003; Wang et al., 2024), and 3) degradation of cell wall materials like pectin (via beta-elimination) if the drying temperature exceeds 80°C (van der Sman, 2020; Xin et al., 2015). During freeze drying, another drying method that is widely used in academia and the food industry, the intracellular ice crystals puncture the cell wall and cell membrane at the freezing step, resulting in: 1) loss of cell membrane integrity; and 2) the brittle cell wall with fractures and micro-cracks.

Upon rehydration, high permeability is essential for fast rehydration performance, which depends heavily on porosity according to the Carman-Kozeny equation (Dadmohammadi and Datta, 2020). Porosity comprises open pores (connected to the surface) and closed pores (isolated within the core), which do not contribute to the permeability (Marabi and Saguy, 2004; Sam Saguy et al., 2005). Besides, pore connectivity is also essential for optimal hydration, otherwise air bubbles remain trapped and poorly connected.

We propose that the good rehydration performance also hinges on the critical role of cell membrane integrity in restoring osmotic pressure and cellular turgor (Mari et al., 2024; Singh et al., 2014). Cell membrane is impermeable to solutes, but permeable to water. In mushrooms, cell membranes envelope the hyphae and the vacuole. The presence of solutes in the vacuole generates an osmotic pressure, which attracts water and thereby results in an increase of cell volume, leading to stretching of the cell wall, which generates an elastic stress,

i,e, turgor pressure. The swelling of the vacuole will continue until the elastic stress equals the osmotic pressure. Intact cell membranes allow dried vegetables to (partially) recover their turgid state upon rehydration (Wang et al., 2024), as shown in Fig.1.1a. If the cell membrane is disrupted (Fig. 1.1b), a significant solute leaching occurs. Upon turgor loss, water and dissolved solutes leave the vacuole. The water is then either absorbed by the cell wall or exists as capillary water within the extracellular pores (Paudel et al., 2016). If the cell wall is damaged by ice crystals during freezing drying (as shown by the microcracks Fig. 1.1c), the tissue will develop a fragile texture upon rehydration (Gruber et al., 2021).

Consequently, the desired microstructure properties for good rehydration performance should include high porosity, good connectivity as well as intact cell membranes.

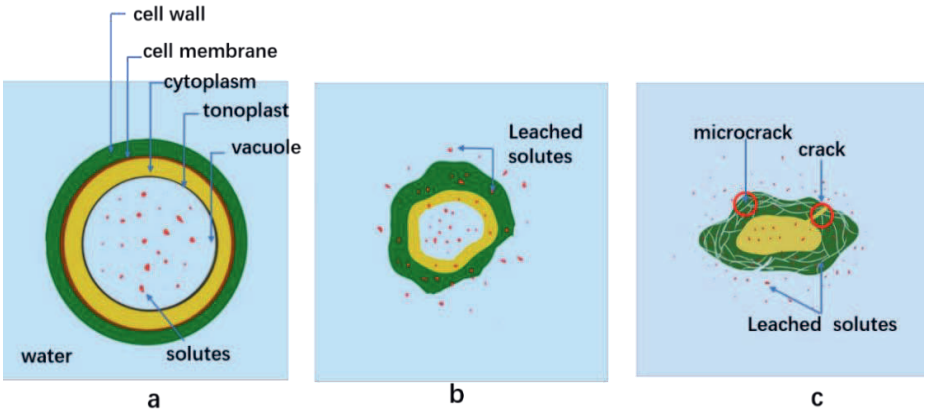


Fig.1.1. *Schematic diagram of cross section of rehydrated hypha (a: cell with intact cell membrane, b: cell with damaged cell membrane (air dried sample), c: cell with damaged cell wall and membrane (freezing dried sample)).*

The collapse of cellular tissue is a complex phenomenon that occurs during drying, and has significant effects on both texture properties and rehydration performance. As described by (Prothon et al., 2003), collapse occurs when a reduction in cell volume leads to the buckling of the cell wall. The underlying process can be explained as follows: during drying, moisture loss leads to the replacement of water with air, leaving cavities within the hyphae. The water/air interface gives rise to capillary pressure (Heila et al., 2008; Leibler and Sekimoto, 1993; Paudel et al., 2016). If the capillary pressure exceeds the critical elastic stress of the cell wall matrix, the wall becomes mechanically unstable and undergoes buckling. It is thought to be irreversible if the two opposing cell walls touch with each other, and form permanent bonds (Carvalho et al., 2025; Li et al., 2025). Hence, the cell volume and texture

cannot be recovered upon rehydration, even when cell membrane remains intact. Fig.1.2 shows the different states of the dried hypha after rehydration.

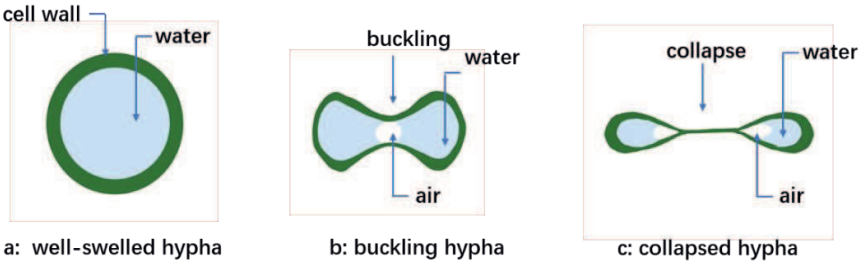


Fig.1.2. *Schematic diagram of cross section of hypha after rehydration (adapted from (Heila et al., 2008))*

One method to counter the collapse is to generate (gas) pressure differences between product and environment, which can be achieved via microwave heating or vacuum drying. Microwave heating is a volumetric heating method, with maximum temperature inside the food (Rakesh and Datta, 2011; Zhang et al., 2010). The local heating leads to the internal evaporation of moisture into extracellular pores, generating a pressure gradient between the inside and outside of the food, resulting in the convection transport of vapor (Jiang et al., 2017). The high pressure inside the material counteracts the elastic stress and capillary force that would otherwise lead to the collapse of the cellular structure. At sufficiently high gas pressure, the food material expands into a more open porous structure (Rakesh and Datta, 2011). In extreme cases, one can even obtain puffed structures with microwave-assisted drying, as in button mushrooms (Argyropoulos et al., 2011), mangoes (Pu and Sun, 2017), and cranberry fruits (Zielinska et al., 2017). Vacuum drying is a technique which allows moisture removal at low pressures. This reduction in ambient pressure lowers the boiling point of water (<100°C), hence, the water at the food surface exhibits strong evaporation (boiling) (Ajani et al., 2023; Ranjbaran and Datta, 2019). The temperature reaches the boiling point, corresponding to the ambient pressure (Erriguible et al., 2007). There is an ingress of the boiling front, leaving an interconnected, porous crust. These pathways allow for faster re-entry of water during rehydration, as compared to air-dried samples (Nadi and Tzempelikos, 2018).

Based on the knowledge of microstructure properties of dried and rehydrated cellular samples, we hypothesize that desired microstructure property, especially porosity can be obtained by serial combined drying strategy: the first drying step is used to porosity enhancement, when the risk of collapse is reduced, one can switch over to an efficient finish-drying step. Siebert

et al. (2018) applied freeze-drying as porosity enhancing pretreatment before hot air (HA) to increase product quality, such as volume retention, which could be attributed to the formation of a porous surface layer resulting from FD pretreatment. An extreme case of porosity enhancement is the instant controlled pressure drop (DIC) technology, where a preheated/pre-dried sample is subjected to a sudden decrease in environmental gas pressure, resulting in an expanded (puffed) structure. The final drying step is performed using vacuum drying. The typical application of DIC combined drying is the puffing of dried fruit/vegetable snacks (Lyu et al., 2015; Mounir et al., 2012; Peng et al., 2018). The common DIC drying method is quite disruptive to the microstructure of these pre-dried products, however, for puffed snack applications, this disruption is acceptable. Therefore, we assume that DIC might exert a mild pore-opening treatment if the products are fresh or sufficiently wet, as in their fresh state.

Consequently, we start our research with the question: which serial combined drying technique should be applied? Is it advantageous to have porosity-enhancement in the first step?

1.3 Microstructure measurement techniques

Nowadays, a suite of powerful experimental techniques enables the multi-scale characterization of the microstructure properties either visually or quantitatively, such as light microscope(Chen et al., 2021), scanning electron microscope (SEM)(Harnkarnsujarit et al., 2016), environmental scanning electron microscope (ESEM)(Metilli et al., 2020; Stokes, 2013), focused ion beam-scanning electron microscopy (FIB-SEM)(Pang and Xu, 2023), transmission electron microscopy (TEM)(Abdollah Hajalilou, 2019; Stadtländer, 2007; Yang et al., 2023), Raman microscopy (Jayan et al., 2025), confocal laser scanning microscopy (CSLM)(Onipe et al., 2020), X-ray micro-computed tomography (μCT)(Chanvrier et al., 2014; Demirkesen et al., 2014; Herremans et al., 2014; Schoeman et al., 2016), low-field nuclear magnetic resonance (NMR) and magnetic resonance imaging (MRI)(Chen et al., 2021). The applications of these techniques enable the quantification of microstructural metrics such as porosity, connectivity, pore size distribution, cell wall thickness, and cell membrane integrity(Deng et al., 2014; Harnkarnsujarit et al., 2016; Lewicki and Pawlak, 2003; Rojas and Augusto, 2018; Voda et al., 2012).

Among these characterization technologies, SEM is widely used to observe cell-scale changes in dried samples and quantify pore diameter and wall thickness using scale bars (Harnkarnsujarit et al., 2016). However, the SEM technique primarily images material surfaces(Inkson, 2016). Quantitative analysis of porosity and connectivity requires 3D

imaging. Transmission electron microscopy (TEM) examines internal structures at higher resolution, evaluates organelle/cell membrane integrity, and quantifies membrane pores (Inkson, 2016; Ogawa et al., 2001). It can complement SEM by examining thinly sliced sections of samples, allowing definitive cell membrane identification. However, its sampling via a microtome is complicated , more time-consuming and expensive than that for SEM. X-ray microtomography (X-ray mCT) can nondestructively image the 3D internal structures of foods at high resolution (Demirkesen et al., 2014; Naji-Tabasi and Mohebbi, 2015). After comprehensive data analysis, the porosity (both open and closed pores), pore connectivity and pore wall thickness can be quantified. Although the cost of X-ray microtomography is much higher than that of SEM and TEM, it generates a wealth of useful quantitative data. MRI could also be an instructive method to measure the microstructure evolution via the imaging the moisture change, and it can even be applied for in-line monitoring of drying (Borompichaichartkul et al., 2005; Foley et al., 2016; Hertig et al., 2021) . Its resolution is significantly lower than that of XRT, but it can be applied throughout the drying process, and can better image moisture gradients. Hence, XRT is usually applied to the fully-dried product. Conventionally, NMR quantifies the water distribution over different physical phases in food rather than providing spatial resolution. Crucially, this water distribution is a powerful indicator of cellular microstructure and integrity of the cells. Intact cell membranes compartmentalize water, resulting in specific NMR relaxation times. When membranes are damaged, water migrates, and its relaxation behavior changes characteristically. Thus, by tracking these changes, low-field NMR holds great potential for directly evaluating the integrity of cell membranes.

Although numerous studies have been conducted on the changes in microstructure parameters during drying via these characterization technologies (Chen et al., 2021; Huang et al., 2012; Rojas and Augusto, 2018; Wang et al., 2023; Zhang et al., 2018), few researchers have attempted to apply them to gain insight into the optimization of drying strategies aimed at improving rehydration and texture properties.

Hence, we pose the research questions: Can these technologies enhance our understanding of the role of microstructure changes during serial combined drying techniques?

1.4 Theoretical model for water activity

A pre-requisite for mechanistic drying model is a sound model for moisture sorption. Among food scientists, the GAB equation is the most commonly used, probably due to its high degrees of freedom (Wolf et al., 1985). However, it is doubtful if the GAB model holds for

foods, as it based on the BET model, which describes gas adsorption models on hard surfaces. Actually, mixtures of biopolymers, plasticizers and water should be regarded as a polymer solution, following the Flory-Huggins theory (Hancock and Zografi, 1993; Taylor et al., 1961; van der Sman and Meinders, 2011). When the food material is in glassy state, viscoelastic relaxation times are slow and stresses in the matrix can be locked in, for example during drying. Therefore, one needs to account for the contribution of this elastic stress to the chemical potential (the driving force for moisture transfer), cf. Flory-Rehner theory of swelling gels. Earlier, our research groups described it by the Free Volume theory (van der Sman et al., 2013; Vrentas and Vrentas, 1991), which has been applied to meat proteins, starch, maltodextrin (van der Sman, 2012; van der Sman and Meinders, 2011). However, the Flory-Huggins Free Volume theory (FHFV) is still phenomenological and does not directly account for the mechanical stress. It cannot explain the hysteresis phenomena widely observed during MSI measurement for many materials (Caurie, 2007; Hill et al., 2012; Leibler and Sekimotot, 1993; Patera et al., 2016; Salmén and Larsson, 2018; van der Sman, 2015). Recently, the theory has been updated via the inclusion of the true elastic stress, subject to viscoelastic relaxation, and has been applied to the dynamic vapor sorption (DVS) of maltodextrins (van der Sman, 2023). However, extensive characterization of rheology, such as physical elastic properties, is required. A less complex alternative is provided by (Leibler and Sekimoto, 1993), who includes a purely elastic stress only in the glassy state, and it was shown to be applicable to vegetable seed material (Veser et al., 2025). In this thesis, we will pursue the question that whether viscoelastic relaxation needs to be included in mushroom MSI models.

1.5 Mechanistic modeling for the drying process

Various mathematical models of drying processes have been developed (Aregawi et al., 2014; Castro et al., 2018; Demir et al., 2020; Hou et al., 2020; Zhu et al., 2021). In comparison to experimental methods that require extensive labor work, validated drying models provide a powerful tool for optimizing the drying process and designing dryers (Castro et al., 2018; Rahman et al., 2018). However, the development and validation of mechanistic drying models require substantial time investment. Nevertheless, the mechanistic drying model enables a deeper physical insight and understanding of the complex drying process, and consequently allows extrapolation for (Defraeye, 2014): 1) conditions outside the experimental domain, and 2) drying of other fruits or vegetables. With well-characterized material properties, this extrapolation can optimize the drying processes for a wider variety

of fruits and vegetables.

A key ingredient of mechanistic drying models is the coupling of large mechanical deformation to the heat and mass transport, which is still rarely done in food science, with exceptions by (Banaszak and Kowalski, 2002; Defraeye and Radu, 2018; Gulati and Datta, 2016; Rakesh and Datta, 2011). In particular, Datta's group follows the poro-mechanics approach, where liquid water is viewed as a separate phase (as capillary water), next to a non-hygroscopic solid phase. This is clearly not in agreement with the Flory-Huggins theory. Alternatively, in the work of Suo (Hong et al., 2009b), the Flory-Rehner theory was extended to inhomogeneous deformations, as occurred during food drying. This framework has been applied to broccoli drying (Jin and van der Sman, 2022), and pore formation in spherical viscoelastic foods (van der Sman et al., 2024). Large-deformations are coupled to moisture transfer, as the hydrostatic pressure appears in both the stress tensor, as well as the chemical potential of water (the driving force for moisture transport). In viscoelastic foods the stress can be dissipated via viscoelastic relaxation – as described by the seminal Maxwell model. We note that the classical Maxwell model assumes small strains, but it can be extended to large deformations (Gulati et al., 2016; Hong et al., 2009a; van der Sman, 2023).

In fact, modeling large deformation is mathematically much more complex than modeling small deformations, because the mesh of the materials used for the calculation deforms simultaneously, requiring intricate tensor calculations (Gulati and Datta, 2016). Mechanistic models involving large deformations of foods are still in their infancy, with the exception of the work of Datta as mentioned above. Within the framework of Suo, a model for food materials with closed pores has been developed (Hong et al., 2009b; van der Sman et al., 2024). Models for open pores, as in fresh mushrooms, still need further development. Furthermore, the multiscale characteristics of fruit and vegetables are hardly acknowledged in drying models, with the exception of (Welsh et al., 2026), who developed a multiscale downscaling model for apple drying that represents the most advanced approach toward a serially-coupled multiscale framework. Recognizing that a parallel-coupled multiscale model for drying has not yet been established, we take an initial step in this direction in our work by introducing a two-compartment cellular representation for the sorption isotherm, as described previously.

Hence, in this thesis, we investigate the extent to which mechanistic, multiscale drying model can be developed for mushroom drying, which is coupled to a realistic model of moisture sorption, accounting for viscoelastic relaxation.

1.6 Outline of the thesis

Our work is based on the hypothesis that combined drying techniques under optimal conditions can mitigate the limitations of individual drying methods. *Shiitake* mushrooms were chosen as the model food product for this study. The goal of this thesis is to develop a serial combined drying technology that enhances rehydration performance and to investigate the transport phenomena mechanisms during mushroom drying using a hot air drying model.

Initially, we explored various combinations of drying methodologies to produce dried mushrooms and evaluated their rehydration characteristics (Chapter 2). Subsequently, we identified the parameters that impact rehydration performance by investigating the microstructural evolution during the selected combined drying treatment (Chapter 3). Prior to modeling the drying process, we analyzed the impact of physical changes on moisture sorption in mushroom samples and suggested improvements to the theoretical model for predicting moisture sorption isotherms (Chapter 4), which were effectuated in Chapter 5, and integrated into a semi-mechanistic drying model that accounts for the multiphase and character of mushrooms. The validated drying model was subsequently used to analyze the conditions for loss of cell membrane integrity, as analyzed using T_2-NMR. Finally, we conclude with the reflections on the research performed in the complete thesis, and recommendations for future research (Chapter 6).

Chapter 2

Study on the rehydration quality improvement of *shiitake* mushroom by combined drying methods

This chapter has been published as Hu, L.; Bi, J.; Jin, X.; Qiu, Y.; van der Sman, R.G.M.. Study on the rehydration quality improvement of *shiitake* mushroom by combined drying methods. Foods, 2021, 10, 769.https://doi.org/10.3390/foods10040769

Abstract

The aim of study is to improve the rehydration quality of dried *shiitake* mushrooms for their promising requirement in instant food manufacturers and fast restaurants. Serial combined drying methods were investigated to achieve this objective: either instant controlled pressure drop drying (DIC) or freezing drying (FD) was used as the treatments for microstructure improvement, and they were applied either before or after an additional drying step at low (35 °C) or high (65 °C) temperatures. Dried mushrooms were assessed for quality indicators like relative volume, rehydration rate, dry matter loss and sensory scores. Microstructure properties were inferred to understand the physical mechanisms of quality changes. Principal component analysis (PCA) was used to cluster treatments, and to identify combinations of drying techniques rendering improved quality. Consequently, it was shown that DIC treatment before hot air drying at 35 °C was shown to be the most promising combined drying method to enhance the rehydration quality, leading to a high volume recovery ratio, low dry matter loss after rehydration, and high rehydration rates. The good performance could be explained by the retention of pore interconnectivity resulting from the slight expansion of porous structure during DIC and the retention of cell membrane integrity.

2.1 Introduction

Mushroom production has increased faster and accounted for over 70% of the world's production in China (FAO,2019). Among them, the *shiitake* mushroom is always the most commonly cultivated in China and is mainly processed by drying. Drying processes of *shiitake* mushrooms are widely investigated because drying not only prolongs their shelf life but also helps to generate their umami flavor (Tian, et al., 2016; Hiraide & Miyazaki & Shibata, 2004). In general, dried *shiitake* mushrooms are required to be rehydrated before being consumed. The ideal quality attributes of rehydrated products are expected to be high convenience (high rehydration rates) and similar appearance, texture and juiciness as fresh products. However, most studies have focused on the drying characteristics and quality attributes of dried products, while problems with rehydration properties have not been investigated thoroughly.

It is known that different drying methods and conditions can result in large quality differences of dried and rehydrated products (Seremet Ceclu et al., 2016; Zou et al., 2013; Voda et al., 2012; Doymaz et al., 2012; Contreras et al., 2012; Winiczenko et al., 2018a&b). As the major drying methods in industrial production, hot air drying (HA) and freeze drying (FD) have been investigated from both the academic and industrial points of view for many years. However, both methods still have problems in producing desired products with good rehydration quality. In particular, hot air drying (HA) always leads to slow rehydration and tough texture (Winiczenko et al., 2018a&b). While freeze-drying (FD) shows good rehydration and volume retention, texture is considered too fragile when eaten (Winiczenko et al., 2018a&b; Vergeldt et al., 2014; Ratti et al., 2001), which make freeze-dried products less attractive for consumers. The rehydration performance of a dried food product is largely determined by the changes in food structure resulting from microscale deformation during drying (Rahyan et al., 1971; Pedro et al., 2010; Lewicki& Pawlak, 2003). An interconnected, porous structure is critical for good rehydration, and this can be obtained by freezing drying (FD), microwave drying, frying, and instant controlled pressure drop (DIC) (Rahyan et al., 1971; Joardder et al., 2019; Joardder et al., 2018).

From previous studies, combined drying methods show advantages in improving drying times, the rehydration and sensorial qualities of vegetable products (Mounir et al., 2014; Malik et al., 2018; Pei et al., 2014; Wang et al., 2015; Zhang et al., 2017), which could be a promising way of obtaining "ideal" rehydrated mushrooms. Generally, there are two kinds of combined drying methods: serial and parallel drying. Serial combined drying involves the

use of one drying method followed by another. Parallel combined drying includes two or more drying methods implemented simultaneously. Notably, parallel combined drying requires specialized equipment, involving high investment and knowledge development for proper process design. Contrastingly, serial combined drying can easily be performed with existing drying equipment.

Several earlier studies have investigated the serial combined drying (Zhang et al., 2017; Siebert 2017&2019; Huang et al., 2012; Antal et al., 2014). Siebert et al. (2019) found that FD as pretreatment before hot air or microwave-vacuum drying creates a porous surface layer, which prevents case hardening, and retains volume similar to FD. Furthermore, FD pretreatment accelerates overall drying time. However, HA pre-drying before FD promoted tissue collapse, which could not be undone by FD, rendering poor rehydration and prolonged drying time. Besides, because the least efficient part of a conventional drying system (hot air or freeze drying) is near the end of the process (the falling rate period), when most of the time may be spent removing the small remaining portion of moisture content, an efficient drying method or treatment, such as infrared drying or instant controlled pressure drop (DIC), can be used at the second stage to reduce the drying time (Wang, et al., 2015, Yi et al., 2018). It can be concluded that the proper combination of drying methods needs to be designed carefully to improve both the quality and drying efficiency.

This study therefore set out to investigate the proper combination of drying methods to obtain products with the desired rehydration quality. Based on the earlier experience of (Siebert et al., 2018&2019) and (Zhang et al., 2017&2019), we have devised the following serial combined drying strategy: one drying method (DIC or FD) is used to enhance the porous structure, while another conventional drying method is used to remove the water efficiently. The latter methods are applied either before or after the DIC or FD treatments, and they are chosen on the basis of their reported good rehydration performance and drying efficiency. Accordingly, in this study, we investigated the most promising combination of drying techniques that overcomes the disadvantages of single drying methods like HA or FD. Quality indicators linked to rehydration properties and sensorial attributes of *shiitake* mushrooms were measured. PCA analysis was applied to the large data set to obtain the most discriminating quality traits amongst treatments, and to clustering them for more in-depth analysis with regard to microstructural changes due to drying. From the PCA results and our subsequent analysis the most promising combined drying method was selected.

2.2. Materials and Methods

2.2.1 Experimental design

Our experiments with serial combined drying are performed using either instant controlled pressure drop (DIC) or freeze-drying (FD) to enhance the porous structure. They are combined with the following conventional drying methods for moisture removal: 1) hot air drying (HA), 2) heat pump drying (HP), 3) vacuum drying (VD), and 4) infrared drying (IRD). These conventional drying methods were selected due to their practical or promising application in industry, where hot air drying methods are the most widely used for their low cost and ease of control; the heat pump and infrared drying methods have advantages in lower energy consumption or high drying efficiency, and they have been increasingly used as the technique for drying of agricultural products in recent years; vacuum drying is used when the product is heat-sensitive. These conventional drying methods were performed either before or after the DIC/FD treatments at two different temperatures: 35 °C and 65 °C. These conventional drying

methods were performed either before or after the DIC/FD treatments. Besides, the effect of the drying temperature of conventional drying techniques on the rehydration quality was assessed with two extreme temperatures, a higher temperature (65 °C) and a lower temperature (35 °C). The two temperatures were chosen based on the capacity of our equipment and assumed to give acceptable quality performance according to previous studies, whose drying temperature varies from 40 °C to 70 °C (Artnaseaw et al., 2010; Duangkhamchan, Wiset & Poomsa, 2013;Qi et al., 2014).This made a total of 32 different treatments, and for convenient discussion we abbreviated the treatments as either predrying35/65-DIC/FD, or DIC/FD-postdrying35/65, with pre-drying and post-drying indicating that the (conventional) drying method is applied before or after the DIC/FD treatment, respectively. The results of the serial combined drying methods were compared to single drying techniques, namely hot air drying at 35 °C and 65 °C (denoted as HA35 and HA65 respectively), and freeze-drying (FD), which all serve as reference drying methods.

An important design parameter for the combined drying methods was the switch-over condition: when the mushroom was transferred between drying methods. For the porosity enhancing methods, DIC and FD, we used fixed treatment times, which were shorter than for the reference single drying treatments, which were 44 h for HA35, 16 h for HA65, and 48 h for FD. The chosen treatment times for the porosity enhancing methods were chosen as 3 h for DIC, and 8 h for FD in case of the post-drying treatments. This resulted in 30% remaining

moisture content (wet basis) for the FD treatment, and 80% remaining moisture content for the DIC treatment. For the pre-drying treatments, we had determined that the switch-over was to happen at 30% moisture content (wet basis), as earlier preliminary studies had shown a remarkably decrease of the drying rate at this point. The corresponding switch-over time was determined via preliminary drying experiments, where mushrooms were weighed each hour using a digital balance (Sartorius BSA223S, Germany). For the post-drying we had determined their treatment times required to obtain a final moisture content of 13% (wet basis), which are also listed in Table 2.1.

Samples obtained from all drying treatments were evaluated for various quality traits after drying or after rehydration. The following quality indicators were measured: 1) the volume retention ratio after drying, 2) the volume recovery ratio after rehydration, 3) the rehydration rate, 4) the dry matter loss ratio during rehydration, 5) the water holding capacity (WHC), 6) the hardness and 7) the sensorial scores of cooked mushrooms. Other measurements targeted at changes in microstructure: 8) the porosity after drying, 9) the porosity after rehydration, and 10) the cell membrane integrity. Because of the large amount of data generated we used principal component analysis (PCA) to determine the principal quality traits distinguishing all treatments, and to guide us in the discussion of the large number of results.

Table. 2.1 *Overview of the combined drying methods with applied temperature and drying time.*

Combined methods / Group name /Temperature	DIC combined			FD combined	
	A	B		C	D
	35℃	65℃		35℃	65℃
DIC-postdrying	DIC-HA35 (33h)	DIC-HA65 (13h)	FD-postdrying	FD-HA35 (20h)	FD-HA65 (15h)
	DIC-HP35 (31h)	DIC-HP65 (13h)		FD-HP35 (18h)	FD-HP65 (14h)
	DIC-VD35 (43h)	DIC-VD65(27h)		FD-VD35 (26h)	FD-VD65 (18h)
	DIC-IRD35 (27h)	DIC-IRD65 (10h)		FD-IRD35 (17h)	FD-IRD65 (13h)
predrying-DIC	HA35-DIC (41h)	HA65-DIC (16h)	predrying-FD	HA35-FD (46h)	HA65-FD (21h)
	HP35-DIC (38h)	HP65-DIC (13h)		HP35-FD (43h)	HP65-FD (18h)
	VD35-DIC (49h)	VD65-DIC (25h)		VD35-FD (53h)	VD65-FD (30h)
	IRD35-DIC(33h)	IRD65-DIC (12h)		IRD35-FD (38h)	IRD65-FD (17h)

HA35,HP35,VD35,IRD35 means hot air drying, heat pump drying, vacuuming drying, infrared drying at 35°C, HA65,HP65,VD65,IRD65 means hot air drying, heat pump drying, vacuuming drying, infrared drying at 65°C.

2.2.2 Materials

Fresh cultivated *shiitake* mushrooms were purchased from a mushroom farm in Beijing (China), where they were graded to have a uniform maturity and size. All mushroom samples were transported to the laboratory and used for experiments within 48 h after harvest. Before experiments, they were put temporarily in a cold store at a temperature of 4 °C and 95% relative humidity. The average dimension of the mushroom cap was 60.2 ± 3.1 mm. The initial moisture content of the whole mushroom was 85.2 ± 1.7% (wet basis: w.b.), as measured by heating triplicate samples in a drying oven at 105°C for 24 h (AOAC. 1990).

2.2.3 Drying methods

The applied drying methods were performed as follows:

1. Freeze drying (FD): Fresh *shiitake* mushrooms were frozen in a refrigerator at -80 °C for

6 h, and then they were put in a lab-scale freeze dryer (Alpila-aplus 4Lplus, Christ Co. Ltd, Osterode am Harz, Germany). The corresponding drying stage of 24 h was performed at a chamber pressure of 37 Pa, a condenser temperature of -55 °C and a heating plate temperature of 20 °C. The drying time was 24 h for the FD reference, and 8 h in the serial combined treatments.

2. The DIC treatment was carried out by using a pilot-scale apparatus (QDPH1021, Tianjin Qin-de New Material Scientific Development Co. Ltd., Tianjin, China) according to previous studies (Yi et al., 2015; Gao et al., 2016; Peng et al., 2018; Li et al., 2019). The DIC treatment was conducted in two stages: in the first stage, the processing vessel was preheated via steel pipes, where steam was injected. Subsequently, the samples were put on wire mesh trays, which were placed on top of the steel pipes in the processing vessel. The samples were heated for 10 min with a processing vessel at 95 °C. In the second vacuum drying stage, the decompression valve was opened to a vacuum chamber to obtain an instant pressure drop ($t<0.2$ s) to vacuum (3-5 kPa, absolute pressure), at which the boiling temperature of water is about 24-32 °C. While maintaining this vacuum with a pump, the samples were dried with a processing vessel temperature of 50 °C for 2 h. The processing vessel temperature was maintained via proper steam injection into the steel pipes.

3. Hot air drying (HA): Samples were dried by a hot air drier (DHG-9123A, Shanghai Jinghong Experiment Facility Co., Ltd., Shanghai, China) at 35 °C and 65 °C at an air velocity of 1.2 m/s. The drying times for the single reference treatments were 44 and 16 h for HA35 and HA65, respectively, following the study (Zhao et al., 2019).

4. Heat pump drying (HP) was conducted with a heat pump drier (ZWH-KFY-BT4I/HG, ZhengXu New Energy Technology Co., Ltd, Dongguan, China. The airflow velocity was 2.4 m/s and the relative humidity was below 20% (Zhao et al., 2019).

5. Vacuum drying (VD) was conducted with a vacuum drier (VO200, Memmert, Germany) at 35 °C and 65 °C, respectively. The absolute pressure was 5 kPa for the drying process, which took about 20 min to reach. This pressure was selected so that the oven temperature was above the boiling point of water (Quintero et al., 2014).

6. Infrared radiation drying (IRD) experiments were conducted at 35 °C and 65 °C respectively by a laboratory-type short- and medium-wave infrared dryer (STC, Senttech Infrared Technology Co., Ltd, Taizhou, China) (Wang et al., 2015; Si et al., 2016).

2.2.4 Rehydration method

After drying, the mushrooms were immersed in distilled water at room temperature (25 ± 2°C) for either 15 min (to determine rehydration rate) or 24 h (to determine volume recovery and WHC). The ratio of the weight of dried mushrooms compared to water was 1:20 (w/w). At the end of rehydration, these samples were removed from the rehydration water. The excess water was drained off from the mushroom surface before measuring its weight and volume. The remaining rehydration water was analyzed for conductivity and dry matter content.

2.2.5 Quality indicators of mushroom

2.2.5.1 Volumetric changes of mushroom after drying and rehydration

The volume of fresh, dried, and rehydrated mushrooms was measured by a volume analyzer (VolScan Profiler300, Stable MicroSystem Co., England). The Volscan performed 3D imaging, and its software determined the mushroom volume. The volume change of dried and rehydrated mushrooms was expressed relative to the volume of the fresh mushroom. Thus, the volume ratios after drying and rehydration (νD and νR) were calculated via:

$$\nu_D = \frac{V_D}{V_0}; \nu_R = \frac{V_R}{V_0},$$

with V_0, V_D, and V_R (ml) were the scanned volumes of fresh, dried, and rehydrated mushrooms, respectively. Measurements were performed in quadruplicate. In the presentation of the results ν_D is denoted as the volume retention ratio, and ν_R is denoted as the volume recovery ratio.

2.2.5.2 Rehydration rate

The speed of rehydration is important for the convenience of the consumer. As a measure of the rehydration rate, we determined the change of the weight after 15 min of immersion in the rehydration liquid (tap water at room temperature). This short time was chosen in consideration of the practice of consumers preparing *shiitake* mushrooms and the sensitivity of the measurements. The rehydration rate of dried mushrooms was determined as follows:

$$R = \frac{M_1 - M_0}{M_0 \times 87\% * 15},$$

where M_0 and M_1 were sample weights at 0 min and 15 min. 87% was the average dry matter

content of dried mushrooms. 15 refers to the 15 min of immersion. The measurements were conducted in quadruplicate.

2.2.5.3 Dry matter loss ratio of rehydrated mushroom

We measured the dry matter loss during rehydration, via collecting the rehydration liquid after the 24 h of rehydration treatment. Both the rehydration liquid and the rehydrated mushrooms were dried in an oven at 105°C for 24 h (cf. AOAC. 1990) to determine their dry matter contents. The dry matter loss was expressed as the ratio of the weight of dry matter in rehydration liquid to the sum of dry matter in rehydration liquid and rehydrated mushroom.

2.2.5.4 Water holding capacity

Water holding capacity is regarded as a measure of the juiciness of mushrooms. In this experiment, we computed the WHC of rehydrated samples collected via the data from rehydration experiments. WHC was defined as:

$$WHC = \frac{W_r - W_d}{W_d},$$

where W_r was the weight of the rehydrated mushroom (after removal of surface water), and W_d was the dry matter weight of the same rehydrated mushroom without dry matter loss after being dried at 105 °C for 24 h.

2.2.5.5 Hardness

The hardness of the rehydrated mushrooms was measured by a texture analyzer (Stable Micro System Co., Ltd, Surrey, UK). A cylindrical probe (P/36) was used to compress cubical samples (measuring 0.5×0.5×0.5 cm^3). The compression distance on samples was fixed at 50% of their original height. The test speed was 1.5 mm/s. Measurements were performed with 10 repetitions for each sample.

2.2.5.6 Sensory evaluation

Sensory evaluation was conducted by a scaling method (Lawless and Heymann, 2010), where untrained panelists were asked to score the rehydrated samples regarding the intensity of taste and juiciness. We used a 7-point scale with the maximal score representing the highest juiciness or strongest taste. The taste of fresh mushroom was defined as scale 4 and its juiciness was defined as scale 7.

To simulate practical consumer use, dried mushrooms were rehydrated in boiling water for 5 min and provided to panelists after cooling to room temperature (25 °C). In the sensory tests, we used fresh mushrooms as a reference, which received the same boiling procedure as the

dried mushrooms. Because panelists were able to evaluate only a limited number of samples per session, the treated samples were divided into 4 groups (A-D), as shown in Table 2.1. In separate sessions, each group, together with the fresh, HA35 and FD references, were evaluated.

2.2.6 Microstructural properties

2.2.6.1 Porosity of mushrooms after drying

The porosity (i.e. the volume fraction of air) of the mushroom was calculated following a simple mass balance, as follows:

$$Porosity = \frac{V_a - V_{th}}{V_a} = 1 - \frac{\frac{M}{\rho_{th}}}{V_a}$$

in this equation V_a is the actual volume of mushroom determined by the Volscan, V_{th} is the theoretical volume and ρ_{th} is the theoretical density of the solid/liquid phase of mushroom, which is calculated from its composition estimated via averaging values from various literature sources, as indicated in Table 2.2. M is the mass of the sample. We assumed the following mass densities of the ingredient (van der Sman, 2008): water (ρw=1000 kg/L), carbohydrates (ρc=1550 kg/L), lipids (ρl =920 kg/L), proteins (ρp=1330 kg/L), and minerals (ρm=2440 kg/L). The theoretical density was then computed from the individual densities following the relation (van der Sman, 2008):

$$\frac{1}{\rho_{th}} = \sum_i \frac{y_i}{\rho_i},$$

where y_i is the mass fraction of component i.

Table. 2.2 *Fraction of ingredients in dry matter of shiitake mushrooms*

Number	Carbohydrates	Soluble carbohydrate (Mannitol+ Trehalose)	Insoluble carbohydrate (Fiber)	Protein *	Fat	Ash(K3PO4)	References
1	0.82	0.36	---	0.13	0.01	0.042	[Carneiro et.al,2013]
2	---	---	0.28	0.17	---	0.063	[Buwjoom et.al,2004]
3	0.71	---	0.46	0.14	0.031	0.072	[Julita,et al.2007]
4	0.87	0.13	---	0.044	0.017	0.067	[Reis et. al, 2012]
Average	0.72±0.14			0.17±0.11	0.024±0.007	0.067±0.007	

*In all these data sources protein content is determined with nitrogen-to-protein conversion factor of 4.38, which is required for correction of nitrogen-containing chitin.

2.2.6.2 Porosity after rehydration

After rehydration, some air can still remain trapped inside the pores. To quantify this we determined the porosity of rehydrated samples. The method for determining the porosity of rehydrated samples was the same as given in 2.6.1.1.

2.2.6.3 Cell integrity of rehydrated mushrooms

Cell membrane integrity was measured indirectly via measuring the electrical conductivity of rehydration liquid by electrolyte conductivity meter (DDS-307A, Leici New Energy Technology Co., Ltd, Shanghai, China). If the cell membrane loses its integrity, one can assume that the conductivity of rehydration liquid has changed significantly compared to tap water. We expressed the conductivity per gram dry matter relative to that of the fresh mushroom.

2.2.7 Statistical analysis

All the measurements were performed at least in triplicate (or more if stated otherwise), and the results were presented in the figures by their averaged values and error bars representing

standard errors (computed from standard deviations and 95% confidence intervals). Statistical analysis was carried using SPSS software (Version 18.0, Chicago, USA). Significant differences among product quality attributes were expressed with small letters a-t in the bar graphs showing the results. This was obtained by one-way analysis of variance (ANOVA) for significance at the $p < 0.05$ level and Duncan's test. Notably, due to the sensory evaluations conducted in 4 separated trials, ANOVA comparison of the common references from the 4 trials was conducted to assure no significant difference between them, and hence the sensory scores of the 4 trials can be compared together. Furthermore, principal component analysis (PCA) involving all indicators was carried out by employing SIMCA software (Version13.0, Umetrics, Sweden) to identify clustering within the different treatments, and possible correlations between quality parameters.

2.3. Results

2.3.1. Quality and microstructure performance of dried or rehydrated mushrooms with different combined drying methods

2.3.1.1. Volumetric changes comparison of mushrooms after drying

The volume retention ratios of mushrooms are shown in Fig.2.1. The FD and HA65 references show the highest and the lowest volume retention ratio, 0.75 and 0.27, respectively. Among the combined drying methods, DIC-postdrying65 show the lowest volume retention, while FD-postdrying35 and 65, show the highest volume retention, (0.60–0.69), excluding FD-VD35, but similar to the FD reference (0.75). It is also striking that all pre-drying treatments show poor volume retention. The DIC- postdrying35 shows overall similar volume retention (0.37-0.45) as the HA35 reference (0.41), except for the vacuum drying step: DIC-VD35.

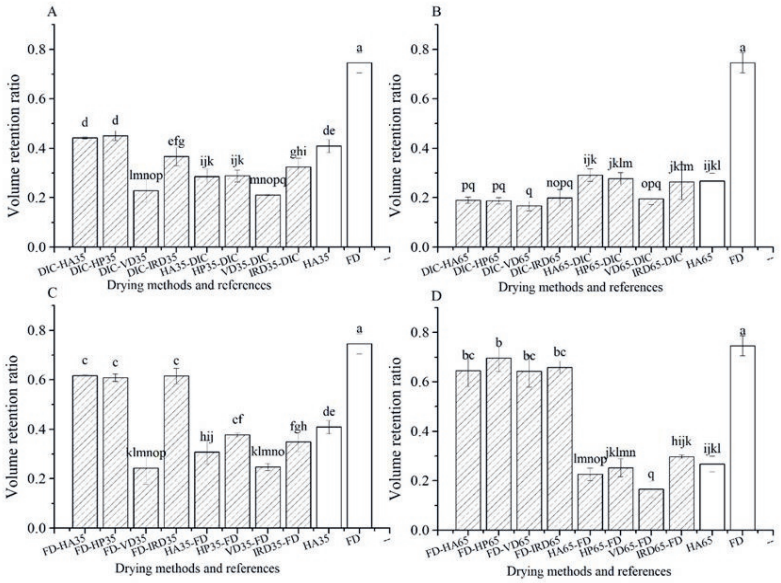


Fig. 2.1. *Volume retention ratio of mushrooms, directly after drying, for the different combined drying methods (☑) and reference methods (□). (A–D): group names as shown in Table 2.1.*

2.3.1.2. Volumetric changes comparison of mushrooms after rehydration

The relative volume recovery after rehydration of all samples is given in Fig.2.2. Of all dried samples, the highest volume recovery is shown by HA35 (0.95), for which we note that the samples are given 24h for rehydration. In comparison, the other references HA65 and FD show little volume recovery (0.37,0.52). The combined drying treatments involving FD show lower or similar volume recovery (0.29-0.51) to FD reference (0.52). Surprisingly, the volumes of the rehydrated FD and the FD-post-drying are smaller than shown in Fig.2.1: the samples have shrunk during rehydration. Amongst the combined dried samples, the best volume recovery is shown by DIC-postdrying35, especially, DIC-HA35 (0.74) and DIC-HP35 (0.64). Notice that the volume recovery ratio of the rehydrated fresh mushrooms (which we also treat as a reference) is larger than unity, namely 1.25, meaning that the fresh mushroom swells if immersed in pure water.

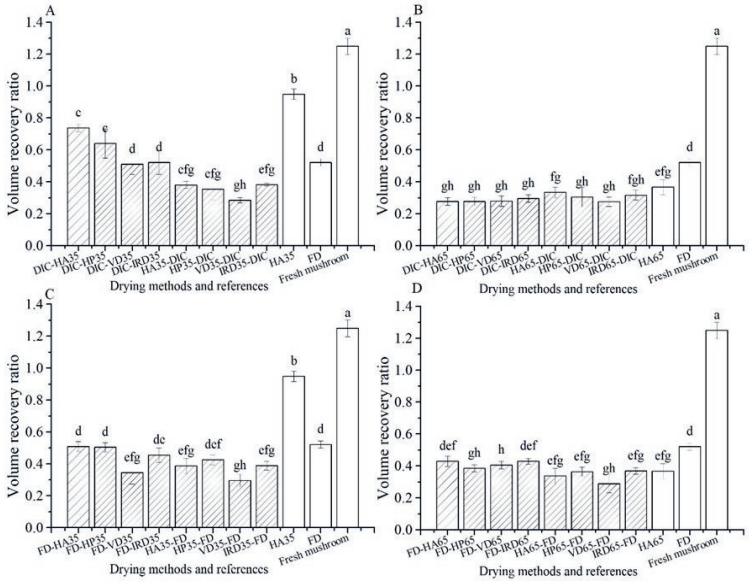


Fig. 2.2. *Volume recovery ratio of mushrooms after rehydration with different drying methods (▨) and references (□). (A–D): group names as shown in Table 2.1.*

2.3.1.3. Rehydration rate comparison of mushrooms

As shown in Fig.2.3. FD samples give the fastest rehydration rate (0.34 $g \cdot g^{-1} \cdot min^{-1}$) amongst all treatments, while HA35 and HA65 show a quite low rehydration rate (0.10,0.045 $g \cdot g^{-1} \cdot min^{-1}$). The result of HA35 is striking, because of its high volume retention after 24 h. However, note that the rehydration rate is based on the volume recovery after the initial 15 min of rehydration. The FD-postdrying35/65 treatments show high rehydration rates, comparable to the FD reference. Further, we note that the rehydration rates o f all pre-dried samples are low (0.032-0.11$g \cdot g^{-1} \cdot min^{-1}$), which complies with their low volume recovery, as shown in Fig.2.2. While DIC-postdrying65 is showing quite poor rehydration (0.020-0.028 $g \cdot g^{-1} \cdot min^{-1}$), DIC-postdrying35 shows good to moderate rehydration rates. Especially, DIC-HA35 stands out, having a comparable rehydration rate as the FD reference, which is also much higher than the HA35 reference.

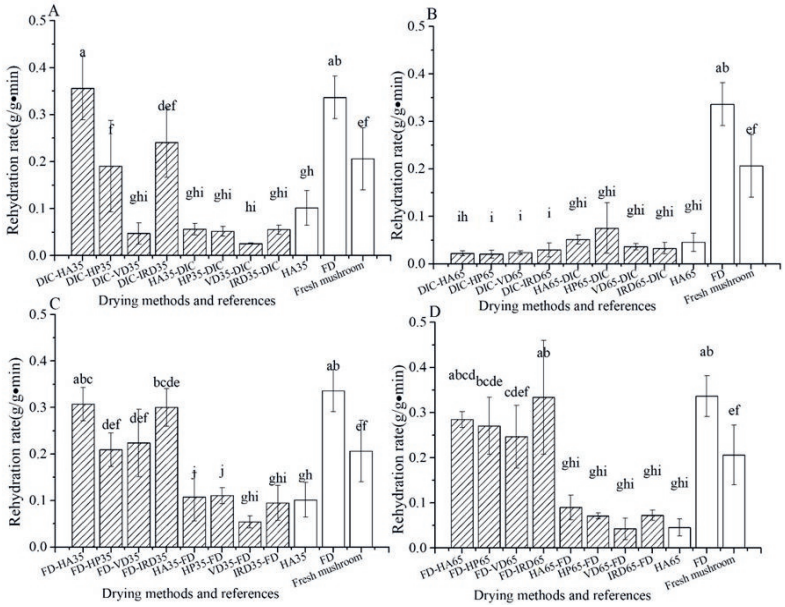


Fig. 2.3. *Rehydration rate of mushrooms with different drying methods (▨) and references (□). (A–D): group names as shown in Table 2.1.*

2.3.1.4. Dry matter loss ratio comparison of mushrooms

As shown in Fig.2.4, after rehydration, the dry matter loss of FD samples is the highest, as high as 50% of its total dry matter content. The dry matter loss of HA35 samples is lowest for all dried samples, accounting for 10% of its total dry matter content, while the dry matter loss is negligible for fresh mushrooms. Among combined drying treatments, DIC-postdrying35/65 shows the lowest dry matter loss, but it is comparable to HA65. For FD-post-drying treatments the dry matter loss is similar to FD reference, but it is slightly lower for pre-drying-FD.

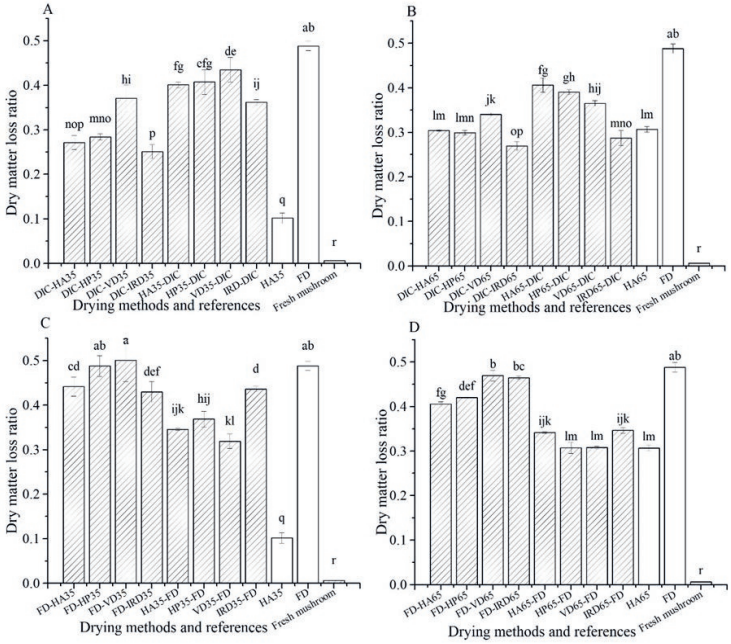


Fig. 2.4. *Dry matter loss ratio of rehydrated mushroom with different drying methods (▨) and references(□). (A–D): group names as shown in Table 2.1.*

2.3.1.5. Water holding capacity comparison of mushrooms after rehydration

As shown in Fig.2.5, HA35 and FD treatments have high WHC, similar to that of fresh mushrooms (0.95), but also comparable to several combined drying treatments, namely FD-post-drying and DIC-postdrying35. Poor WHC is shown by DIC-postdrying65 and predrying65-DIC treatments, varying from 0.70-0.79.

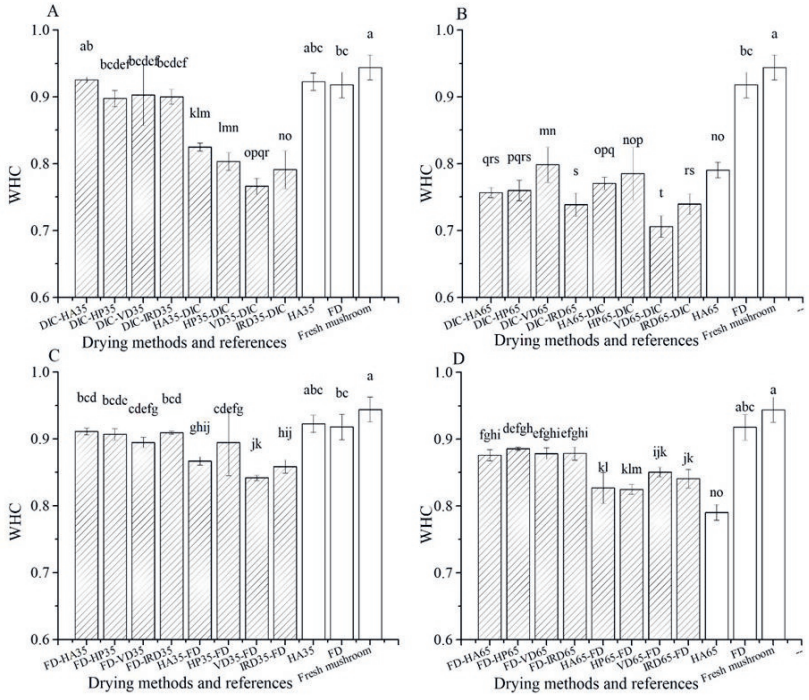


Fig. 2.5. *WHC of rehydrated mushrooms with different drying methods (▨) and references (□). (A–D): group names as shown in Table 2.1.*

2.3.1.6. Hardness comparison of fresh and rehydrated mushrooms

As shown in Fig.2.6 many of the treatments show similar hardness (after rehydration) as the fresh mushrooms (433 g), namely FD-post-drying, predrying35-FD and DIC-postdrying35 (except DIC-VD35). The highest values of hardness are shown by DIC-postdrying65, and several treatments within pre-drying-DIC, varying from 1295 g to 2018 g .

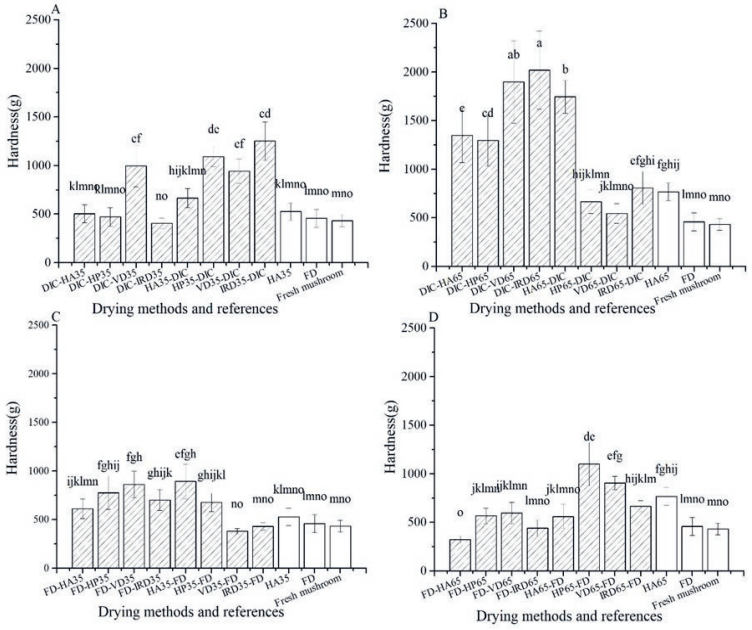


Fig.2.6. *Harness of rehydrated mushrooms with different drying methods (▨) and references(□). (A–D): group names as shown in Table 2.1.*

2.3.1.7. Sensory evaluation of mushrooms after rehydration

The sensory scores of the panelists are listed in **Appendix 2**. As illustrated above, the fresh mushroom was taken as the anchor for all the other evaluated samples. Among the shared references, HA35 shows similar taste as the fresh mushroom, but the FD samples show lower taste. HA35 and FD references show similar juiciness, which is lower than that of the fresh mushroom. Due to the large variations in the sensory scores amongst panelists, it is difficult to draw conclusions directly from the tables in the **Appendix 2**. We rely on the PCA analysis to obtain trends from the sensory evaluation.

2.3.1.8. Porosity after drying

As shown in Fig.2.7, the porosity of all dried samples increases when compared to that of fresh ones (0.61). FD gives the highest porosity (0.94), while HA65 gives the lowest one (0.76). For both DIC and FD treatments, it holds that combining with post-drying gives higher porosity than combining with pre-drying. We observe that, for DIC treatments, this porosity enhancement only remains when the post-drying temperature is lower (35 °C), the porosity of DIC-postdrying65 is the lowest amongst the combined drying treatments, and

similar to that of the fresh mushroom. FD-post-drying treatments show a porosity as high as the FD reference.

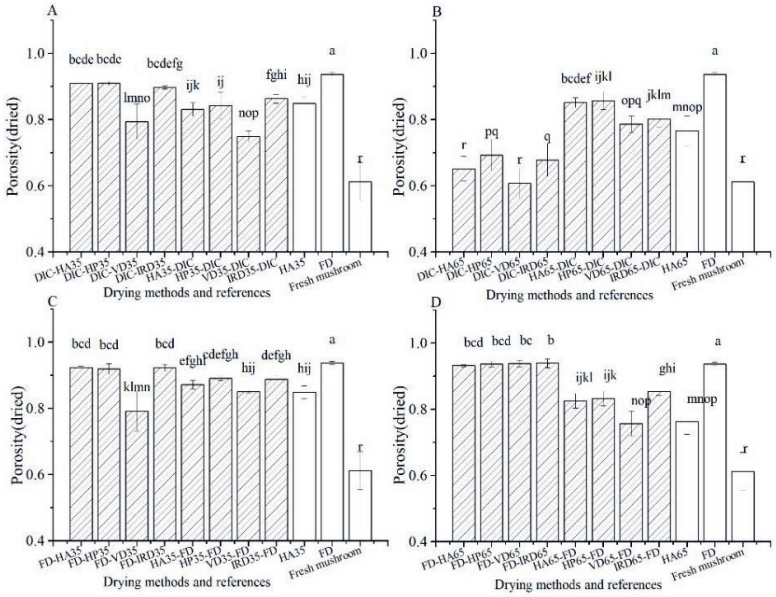


Fig. 2.7. *Porosity of dried mushrooms treated with different drying methods (▨) and references(□). (A–D): group names as shown in Table 2.1.*

2.3.1.9. Porosity after rehydration

The porosity after rehydration, entails pores where air is entrapped. As explained below, we will regard the porosity of rehydrated samples as a measure of the interconnectivity of the dried mushroom. For samples with high porosity, and thus much entrapped air, we assume a low interconnectivity. According to Fig.2.8, the porosity of rehydrated FD reference samples is the lowest (0.11), corresponding with the highest interconnectivity. Among the combined drying treatments, samples dried by FD-postdrying35/65 show the lowest values of porosity, but only slightly lower than DIC-postdrying35 (0.21-0.29). The porosity of pre-drying samples is overall higher than post-drying samples, with the worst performance by DIC-postdrying65 (0.32-0.37).

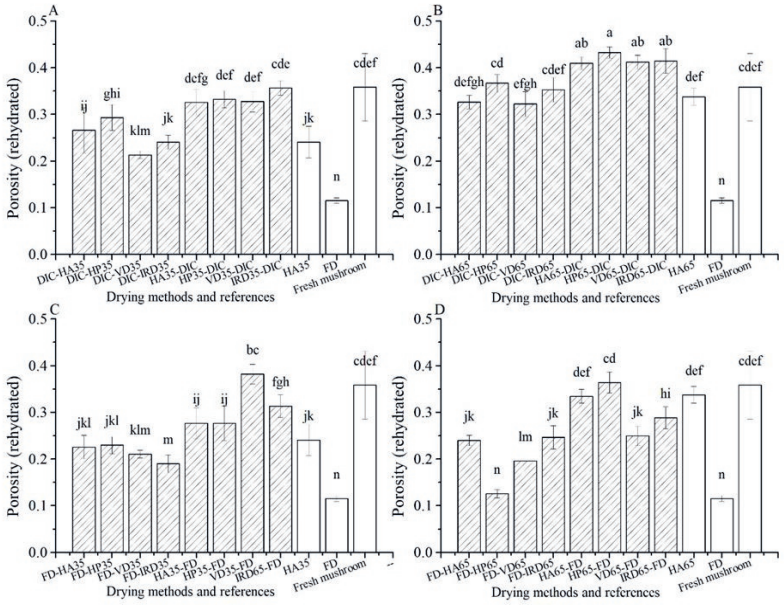


Fig. 2.8. *Porosity of rehydrated and fresh mushrooms treated with different drying methods (▨) and references(□). (A–D): group names as shown in Table 2.1.*

2.3.1.10. Cell membrane integrity

It is shown in Fig.2.9 that the relative conductivity of rehydration liquid of all dried samples is higher than 1, indicating that all drying methods cause the damage to the cell membrane. The lowest and highest relative conductivity ratios are shown by the HA35 and FD references, respectively. Among the combined drying methods, DIC-postdrying35 performs best with relative conductivity ratio only slightly higher than HA35. Most FD combined treatments perform better ratios than FD reference, excluding FD-postdrying65. The DIC-treatments, other than DIC-postdrying35, show similar behavior as these FD combined treatments.

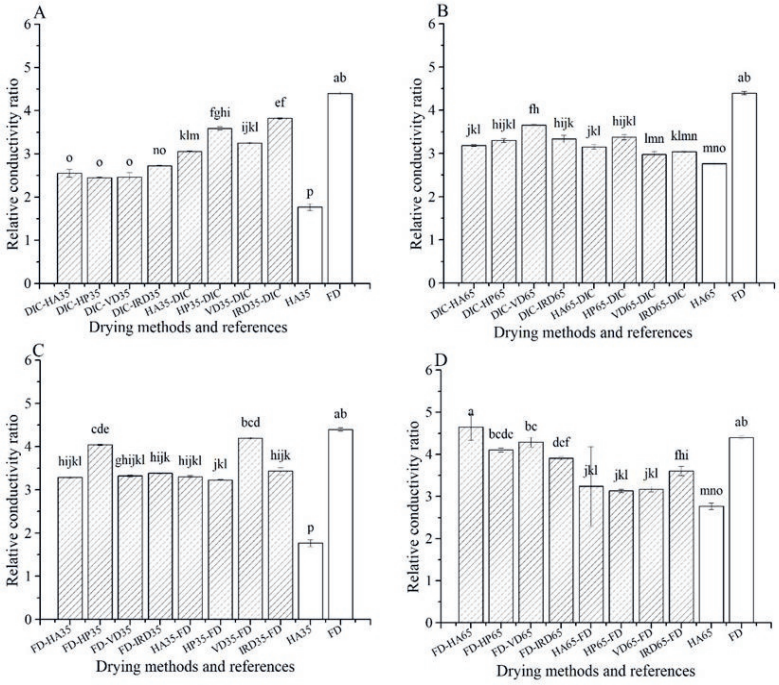


Fig. 2.9. *Relative conductivity ratio of rehydration liquid with different drying methods (▨) and references (□). (A–D): group names as shown in Table 2.1.*

2.3.2. PCA analysis

The loading plot and the score plot of the PCA analysis are shown in Fig. 2.10 and Fig. 2.11. PC1 and PC2 explain together 73% of the total variance. The loading plot has shown that many of the quality indicators have a high degree of correlation. PC1 is positively correlated with WHC, juiciness, rehydration rate, and volume recovery after rehydration, and is negatively correlated with hardness. These quality indicators are indeed related, namely to juiciness and texture. PC2 is positively correlated with dry matter loss, relative conductivity of the rehydration liquid, and slightly (negatively) correlated with taste. The porosity indicators depend on both PC1 and PC2.

As shown by the score plot in Fig.2.11, we observe a large difference between the single-drying methods, i.e. the references FD and HA35, which can be considered as two extremes in drying performance, as we have discussed in the introduction. Furthermore, we observe that there is a large degree of clustering amongst the combined drying methods. Thus, the clustering is probably due to the fact that the type of conventional drying method (HA, HP,

IR, VD) had limited impact on the quality indica-tors in general, except for the DIC-postdrying35 treatments.

In Fig.2.11 we have indicated the following clusters:

a) FD-postdrying35/65

b) predying35/65-DIC+predrying35/65-FD

c) DIC-postdrying65

d) DIC-postdrying35

From the results of clustering, it can be seen that cluster a) FD-postdrying35/65 is very close to the FD reference, giving a high volume retention after drying, a high rehydration rate, but accompanied by a high dry matter loss. Cluster b) is located to HA65, giving low quality performance such as a low volume retention after both drying and after rehydration, a quite low rehydration rate, but a moderate dry matter loss. The cluster c) DIC-postdrying65 also gives poor performance like cluster b), albeit with lower rehydration rate, and lower loss of dry matter. Compared with the other combined drying methods, the cluster d) DIC-postdrying35 shows improved quality, combining good volume recovery and a fast rehydration rate, but with a low dry matter loss. Its response is about midway references HA35 and FD, as has been our target for the combined drying method.

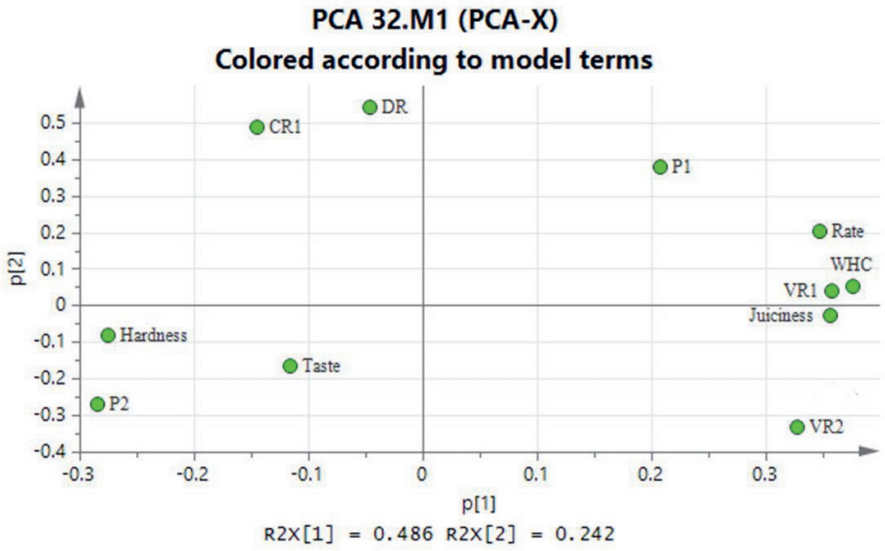


Fig.2.10. *Correlation loadings plot from PCA on mean-centered data. VR1: volume ratio of dried samples, VR2: volume ratio of rehydrated samples, P1: porosity of dried samples, P2: porosity of rehydrated samples, Rate: rehydrate rate; CR1: relative con-ductivity ratio DR: dry matter loss ratio.*

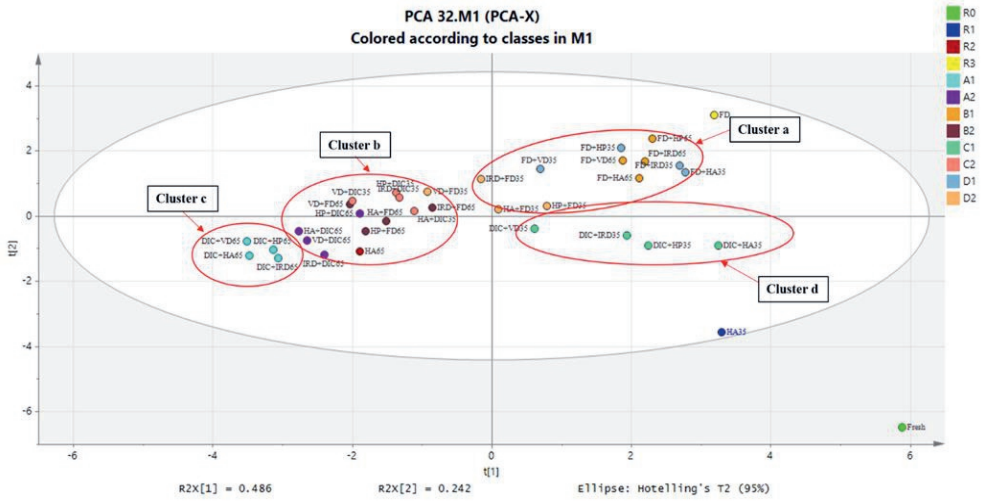


Fig.2.11. *Score plot of the products of treatments and references (listed in Table 1) showing clustering of the following treatments: cluster a, FD-postdrying35/65; cluster b, predying35/65-DIC+predrying35/65-FD; cluster c, DIC-postdrying65; cluster d, DIC-postdrying35.*

2.4. Discussion

Due to the large amount of generated data, we use the results of the PCA analysis to guide our discussion of the combined drying methods. The PCA analysis showed a strong clustering amongst the combined drying methods, and consequently we have performed our discussion mainly on the level of these clusters. For each cluster, we explained the observed differences in quality indicators in terms of microstructural changes. Before that, we list some generally accepted hypotheses relating quality to microstructure, which are used in the following discussion.

Among all drying methods, extreme differences were found in different indicators. HA35 gives the highest volume recovery ratio and the least dry matter loss. FD performs the largest volume retention ratio and rehydrates fastest, but it shows the most dry matter loss value. DIC-postdrying65 treatments leads to the least volume retention ratio, volume recovery ratio, rehydration rates and WHC value, but gives the highest hardness. The underlying mechanism for the difference can be explained by microstructure characteristics.

High rehydration rates are explained by high permeability, which is attributed to both a high porosity (after drying) as well as a high interconnectivity (Marabi et al., 2004). The porosity after rehydration can be viewed as a measure of this interconnectivity, air bubbles trapped during rehydration determines the (final) porosity of rehydrated samples. The trapped air bubbles have not escaped due to the poor interconnectivity (Vergeldt et al., 2014; Lewicki 1998, Prothon, Ahrne &Sjoholm, 2003). In our study, the high interconnectivity between pores in dried samples like FD combined treatments is corroborated by 1) the high rehydration rate, whose magnitudes are similar to those of the single FD treatment, and 2) the low porosity after rehydration.

Poor rehydration rates are generally attributed to (pore) collapse of tissue and subsequent case hardening (Lawless & Heymann, 2010). Recent literature on soft porous polymer gels (Kovalenko et al., 2016) relates the prevention of pore collapse during drying to interconnectivity between pores, which is shown earlier. The collapse of water-filled pore occurs only when they are not interconnected. Similarly, we assume water-filled cells in vegetables will collapse if a porous structure with sufficient interconnecting channels is present. The size of these channels defines the capillary pressure, and if the capillary pressure is smaller than the elastic modulus of the tissue, collapse does not occur (Kovalenko et al., 2016).

The loss of cell membrane integrity results in dry matter loss, i.e. the leaching of solutes from

the vacuole. During freeze-drying one can expect that all cell membrane integrity is lost due to ice crystals puncturing the cell membrane (Voda et al., 2012), or due to the high osmotic pressures – leading to osmotic lysis (Simonin, Beney & Gervais, 2007). This leads to high leaching of solutes into the rehydration water and high (relative) conductivity of the rehydration water. Besides, solute leaching is found to be independent of the microstructure (remaining after the loss of cell membrane integrity) of the dried vegetable (Vergeldt, et al 2014). In contrast, fresh mushrooms without cell damage give negligible dry matter loss and notably, grows 1.25 times larger in volume, meaning cell integrity is also critical for high volume recovery ratio (Lewicki & Pawlak, 2003).

For cluster a) FD-postdrying35/65, the FD treatment before post-drying can help to improve the volume retention after drying (except FD-VD35) and the rehydration rate when compared with HA35/65 dried samples. The results of improved volume retention and rehydration rate can be attributed to the higher porosity and interconnectivity created by the freeze-drying pretreatment (shown in Fig.2.7 and 2.9). The porosity values are similar to that of the single FD treatment. Notably, although the duration of the FD pretreatment (8 h) is shorter than the single FD drying (24 h), it is sufficient to create similar porosity. Apparently, ice sublimation finishes within the first 8 h of the (single) FD treatment. The porous structure is thus already created at the end of the ice sublimation; it enhances the mass transfer in the subsequent drying in the vacuum stage of FD. The created interconnected, porous tissue prevents the subsequent collapse of the structure during the post-drying, as commonly happens during hot air drying, like in the HA35 or HA65 reference treatments. Similar prevention of collapse by a freeze-drying pretreatment is also demonstrated for serial combined drying applied to mushrooms and carrots (Argyropoulos, Heindl &Müller, 2011; Siebert, et al., 2019).

Furthermore, we note that the dry matter leached during rehydration of FD treated samples (50% on dry weight basis) is larger than the amount of solutes from the vacuole (which is about 30% on dry weight basis, see Table 2.2). The loss of cell membrane integrity is thought to happen already in the freezing step, before the actual (freeze) drying via ice sublimation. Hence, one can indeed expect similar dry matter loss for FD-post-drying as for the single FD treatment. As illustrated above, we think that dry matter loss is also partly due to the damaged or fractured cell wall material. The extend of the damage to the cell wall material has probably led to the low hardness.

FD-postdrying35/65 gives a lower volume recovery than HA35, but similar to that of single FD treatments. If we compare the sample volume after drying with those after rehydration, we observe a decrease of volume due to rehydration similar to single FD treatments. This

reduction of volume during rehydration is hardly observed in literature and therefore, it is an important finding. This reduction of volume could be due to the mechanical stresses, frozen-in during freeze-drying, which are dissipated via re-laxation of the stretched cell wall material, leading to further shrinkage.

We attribute the high WHC and juiciness to the large amount of water contained in the pores after rehydration, which is pressed out easily during eating. The latter can be attributed to the high permeability of FD pretreated samples, which also facilitates the high rehydration rate.

For cluster b) predrying35/65-FD/DIC, poor product quality is observed, comparable to the HA65 reference. Similar as found by (Siebert et al., 2019), the microstructural damage imparted by pre-drying cannot be undone by pore-enhancing treatments, i.e., FD or DIC. The pre-drying samples showed low volume retention, and if compared to the volume after drying, one observes there is little water uptake by the pre-drying samples. This is also indicated by the low rehydration rate. Furthermore, there is little connectivity between pores as indicated by the high porosity after rehydration. As stated above, collapse happens if there is little interconnectivity between pores. In line with the poor rehydration, the pre-drying samples show low WHC, low juiciness, and high hardness. Unexpectedly, the pre-drying-DIC samples performed as bad as the pre-drying-FD samples. Commonly, pre-drying is a required pretreatment before puffing via the DIC treatment (Mounir et al., 2012). In our case, the volume expansion did not happen, probably due to the severity of case hardening caused by our pre-drying treatment. The compacted structure had probably a too high hardness, which could not be overcome by the pressure drop induced by DIC (Yi et al.,2016). For cluster c), the DIC-postdrying65 treatments show poor performance in hydration properties, such as low volume recovery, low rehydration rate, low WHC, and high hardness. Regarding th is, it scores even worse than the HA65 references. On the other hand, their dry matter loss is lower than the FD treatments, but comparable to HA65 and DIC-postdrying35. Remarkably, their volume retention after drying is the lowest of all treatments. Their poor performance is in stark contrast to DIC-postdrying35, which does show good hydration properties. Hence, the poor performance of DIC-postdrying65 must be sought in the combined effect of the high drying temperature and the long duration of the post-drying65 treatment. If we include the 2 h of the vacuum drying stage of the DIC treatment, the total drying time is similar or even longer than that of the HA65 reference. The severity of the postdrying65 treatment is indicated by the lowest volume retention, and lowest porosity after drying (Fig. 2.7). The high drying temperature leads to a higher loss of cell membrane integrity, as indicated by the higher relative conductivity ratio as compared to DIC-postdrying35. Besides, the

postdrying65 might lead to strong case hardening, resulting in very little and slow water uptake during rehydration. Any benefit of the DIC treatment, which is present as shown by the performance of DIC-postdrying35, has been eliminated by the severity of the postdrying65 treatment.

Unexpectedly, cluster d), the DIC-postdrying35 treatments show a good performance, namely a high volume recovery ratio and a high rehydration rate, but a low loss of dry matter and cell membrane integrity. The volume recovery is similar to the HA35 reference, but higher than the FD reference, while the rehydration rate is much higher than the HA35, and in the case of DIC-HA35 even higher than the FD reference. The dry matter loss is lower than FD, comparable to that of HA65, but lower than HA35. Within this cluster the DIC-HA35 has shown the best performance. The DIC-HA35 treatment combines the good traits of freeze-drying (FD) treatments with the good traits of mild hot air drying (HA35), which is indeed the objective of this study. Furthermore, as shown in Table 2.1, the total processing time of the serial combined drying of DIC-HA35 (3+33h) is significantly shorter than the HA35 reference (44 h). The stark difference in performance between DIC-postdrying35 and DIC-postdrying65 is likely due to the prevention of severe case hardening, i.e. collapse of the surface layer. This assumption is supported by the moderate volume shrinkage and high porosity after drying, the good volume recovery after rehydration (even better than FD), good rehydration rates (comparable to FD), and reasonably low porosity after rehydration for DIC-postdrying35. Earlier, we have explained the prevention of collapse in terms of good interconnectivity between pores. The high rehydration rate and low porosity after rehydration indicate that this indeed the case. This prevention of collapse is quite surprising, compared to the performance of HA35 and DIC-postdrying65. HA35 does have a good volume recovery, but its rehydration rate is quite poor, indicating a low permeability and interconnectivity. We think that low permeability and interconnectivity of HA35 especially holds in the surface layer, as the (average) volume shrinkage, the porosity after drying and after rehydration of HA35 is similar to DIC-HA35. The surface layer of DIC-HA35 has somehow retained the good permeability and interconnectivity, as one can find back in fresh mushrooms.

It is not likely that the DIC-pretreatment acts on the porosity of the mushroom. Our measurements have shown that the moisture content decreases only minutely from 82% to 80% during the DIC-pretreatment. For the creation of a high porosity the food material needs to be pre-dried, as shown by (Allaf et al.,2014). We think in our case the DIC-pretreatment acts at the level of the interconnectivity of pores. During the puffing stage of the DIC treatment, there is an instant drop in pressure of about 1 bar. The gas inside the mushroom

can probably not escape directly and it will expand due to the lower ambient pressure. Consequently, the gas expansion increases the volume of the mushroom and the size of interconnecting channels between pores. Subsequently, the (expanded) mushroom will be subjected to vacuum drying for 2 h. The mass transport during this vacuum drying is driven by pressure differences, similar to vacuum drying of wood (Chen, Z. et al. 2001). The pressure in the mushroom remains at the saturated vapor pressure at the governing product temperature (which is about 40 degrees due to evaporative cooling), thus retaining the pressure gradient for convective mass transport. Due to the high initial porosity of the fresh mushroom, the dehydration during the 2 h vacuum drying of DIC treatment happens throughout the whole tissue of the mushroom, in contrast to HA35 – where dehydration happens mainly at the surface layer in the first 2 h of drying. Besides, the increase in atmospheric pressure at the end of the DIC treatment is performed slowly such that the volume of the mushroom does not implode. Hence, the advantageous microstructural properties are retained throughout the DIC treatment. The same DIC treatment has been performed in both the DIC-postdrying35, as well as the DIC-postdrying65. While the post-drying at 65 °C destroys the advantageous microstructure, the post-drying at 35 °C can still retain it. Comparison of HA65 with HA35 indicates that drying at 65 °C is more severe leading to lower volume shrinkage, lower volume recovery, lower rehydration rates, lower porosity after drying, and a high porosity after rehydration (indicating the lower interconnectivity). Furthermore, the relative conductivity and dry matter loss in HA35 is much lower than HA65. Thus, the cell membrane integrity is better preserved during drying at 35 °C, which also happens during the DIC-post-drying as shown by the difference in relative conductivity between DIC-postdrying35 and DIC-postdrying65. If cell membrane integrity is (partially) retained, the turgor pressure is also (partially) retained. The turgor pressure makes that the effective elastic modulus is higher than that of the mushroom dried at 65 °C, where turgor pressure is lost. The higher elastic modulus retained by the low drying temperature combined with the better interconnectivity caused by the DIC treatment is the probable reason for the prevention of collapse during the post-drying at 35 °C, which does happen at the post-drying at 65 °C. Additionally, if the cell membrane loses integrity, intracellular water is pressed out to the extracellular space (pores and interconnecting channels) by the relaxing (previously stretched) cell walls. Due to capillarity effects, this water will predominantly be captured by the small interconnecting channels, rather than the large pores. Loss of membrane integrity will first happen at the surface layer in the DIC-HA65, thus closing the interconnection of (air-filled) pores with the environment. This loss of interconnectivity leads to the collapse of the surface layer. During DIC-HA35, loss of cell

membrane integrity happens much less, and probably at the late stage of the post-drying treatment. Hence, the collapse of the surface layer is probably prevented. Future research will have to substantiate our hypothesis.

2.5. Conclusions

The changes of quality and microstructure properties of mushrooms treated by serially combined drying with FD and DIC as pore-creation methods were analyzed. Among the serially combined drying treatments, there are only a few treatments which perform better than HA and FD references. The observed behavior of the different treatments has been explained in terms of changes of microstructure during drying and rehydration.

The best performance is shown by DIC-HA35 dried samples which show high volume recovery like that of HA35, but with a much shorter drying time; they can rehydrate as fast as the FD dried samples but with less dry matter loss. The unexpectedly good performance could be due to the retention of pore interconnectivity during the DIC-HA35 treatment, resulting from a) the slight expansion of structure during DIC, and b) the retention of cell membrane integrity, avoiding extracellular water filling the interconnecting channels between pores.

On the other hand, FD or DIC after drying cannot undo the damage imparted by pre-drying. No advantage is found of FD-post-drying over FD, which is probably due to the long duration of the freezing step. Quality might be improved via shorter freezing time. Nevertheless, we are inclined to select DIC-HA35 as the combined drying method in our further research, as it has been shown to improve the quality performance of rehydrated mushrooms when compared to single convective drying methods.

In future study, we think it is worthwhile investigating the DIC-HA35 serial combined drying method for a) the validation of our hypothesis, and b) the optimization of drying of mushrooms. Besides, whether the DIC-post-drying is beneficial to other vegetables or fruits remains to be seen.

Appendix 2

Table A2.1. *Sensory evaluation of DIC combined drying at 35℃*

	DIC-HA	**DIC-HP**	**DIC-VD**	**DIC-IRD**
Taste	4.3 ± 1.56^{ab}	3.5 ± 1.35^{bcd}	2.4 ± 1.42^{c}	5 ± 0.94^{a}
Juiciness	5.1 ± 0.99^{bc}	4.9 ± 0.73^{bc}	4.2 ± 0.91^{cd}	5.2 ± 1.03^{b}
	HA-DIC	**HP-DIC**	**VD-DIC**	**IRD-DIC**
Taste	3.6 ± 1.64^{bcd}	3 ± 0.94^{bcd}	2.6 ± 1.07^{cd}	3 ± 1.63^{bcd}
Juiciness	2.9 ± 0.73^{e}	3.8 ± 0.91^{d}	3.9 ± 1.66^{d}	4.4 ± 1.42^{bcd}
	HA35	**FD**	**Fresh sample**	
Taste	3.9 ± 1.59^{abc}	3.1 ± 0.87^{bcd}	4 ± 0^{ab}	
Juiciness	5.3 ± 0.94^{b}	6.4 ± 0.69^{a}	7 ± 0^{a}	

Values in the same indicator followed by different letters are significantly ($p < 0.05$) different

TableA2.2. *Sensory evaluation of DIC combined drying at 65℃*

	DIC-HA	**DIC-HP**	**DIC-VD**	**DIC-IRD**
Taste	5.2 ± 0.42^{abc}	4.4 ± 1.64^{bcde}	4.2 ± 1.47^{bcde}	3.8 ± 1.68^{de}
Juiciness	2.2 ± 0.63^{e}	2.9 ± 0.99^{cde}	2.4 ± 1.17^{de}	4.1 ± 1.44^{c}
	HA-DIC	**HP-DIC**	**VD-DIC**	**IRD-DIC**
Taste	5.8 ± 1.54^{a}	4.9 ± 0.73^{abcd}	5.4 ± 1.07^{ab}	5.2 ± 1.31^{abc}
Juiciness	3.4 ± 1.17^{cd}	3.8 ± 1.13^{c}	3.9 ± 1.44^{c}	3.6 ± 1.34^{c}
	HA35	**FD**	**Fresh sample**	
Taste	3.9 ± 1.59^{de}	3.2 ± 0.91^{e}	4 ± 0^{cde}	
Juiciness	5.7 ± 1.71^{b}	5.9 ± 1.45^{b}	7 ± 0^{a}	

Values in the same indicator followed by different letters are si=gnificantly ($p < 0.05$) different

TableA2.3. *Sensory evaluation of FD combined drying at 35℃*

	FD-HA	**FD-HP**	**FD-VD**	**FD-IRD**
Taste	3.6±1.57[a]	3±1.82[a]	3.7±1.88[a]	3.5±1.71[a]
Juiciness	5.5±1.95[b]	4.6±1.83[b]	5.5±2.06[b]	5.5±1.43[b]
	HA-FD	**HP-FD**	**VD-FD**	**IRD-FD**
Taste	4.3±1.56[a]	4.2±1.98[a]	3.6±1.42[a]	3±1.94[a]
Juiciness	4.7±0.67[b]	4.9±1.72[b]	4.9±1.28[b]	3.2±1.47[b]
	HA35	**FD**	**Fresh sample**	
Taste	4.4±1.72[a]	3.1±1.28[b]	4±0[a]	
Juiciness	5.7±0.82[b]	6.1±1.28[ab]	7±0[a]	

Values in the same indicator followed by different letters are significantly ($p < 0.05$) different

TableA2.4. *Sensory evaluation of FD combined drying at 65℃*

	FD-HA	**FD-HP**	**FD-VD**	**FD-IRD**
Taste	4.7±1.25[a]	4.1±0.99[ab]	4.3±1.15[a]	4.6±1.07[a]
Juiciness	5±0.81[b]	5±1.41[b]	4.6±1.42[b]	5.1±1.10[b]
	HA-FD	**HP-FD**	**VD-FD**	**IRD-FD**
Taste	5±1.33[a]	4.5±1.08[a]	4.9±1.1[a]	4.6±0.69[a]
Juiciness	2.6±0.96[c]	2.8±0.91[c]	2.3±0.67[c]	3.3±0.94[c]
	HA35	**FD**	**Fresh sample**	
Taste	4.4±1.72[a]	3.2±1.54[c]	4±0[ab]	
Juiciness	5.0±1.05[b]	5.3±1.63[b]	7±0[a]	

Values in the same indicator followed by different letters are significantly ($p < 0.05$) different.

Chapter 3

Microstructure evolution affecting the rehydration of dried mushrooms during instant controlled pressure drop combined hot air drying (DIC-HA)

This chapter has been published as Hu, L., Bi, J., Jin, X., & van der Sman, R. G. M. Microstructure evolution affecting the rehydration of dried mushrooms during instant controlled pressure drop combined hot air drying (DIC-HA). Innovative Food Science and Emerging Technologies,2022, 79,103056. https://doi.org/10.1016/j.ifset.2022.103056

Abstract

This paper presents a study on the microstructure evolution providing good rehydration performance of *shiitake* mushroom after instant controlled pressure drop combined with hot air drying (DIC-HA). The effect of variations of DIC process parameters on the cell membrane was studied via the electrical conductivity of rehydration liquid as well as transmission electron microscopy (TEM). Microstructural properties of dried products, including porosity and connectivity, were studied by scanning electron microscopy (SEM) and X-ray micro-computed tomography (μCT). The results confirm that DIC pretreatment can facilitate a higher porosity of mushroom tissue, thus preventing collapse during subsequent hot air drying – provided that the product temperature remains below a critical temperature for retaining the integrity of the cell membrane. A new insight into the role of instant controlled pressure drop is to improve the microstructure of the samples. The porous structure implies potential innovative applications in the production of dry foods distinguished by good rehydration behavior.

3.1 Introduction

There exist obvious drawbacks to the rehydration performance of dried food products obtained by conventional drying methods like freeze-drying (FD) and hot air drying (HA). After rehydration, the texture of FD dried samples was considered too fragile when eaten, giving a sudden release of moisture but low sustained juiciness, which is combined with a severe solute leaching, resulting in loss of nutritional value (Marabi, Dilak, Shah, & Saguy, 2004; Rahyan, Henning, & Westcott, 1971; Vergeldt, et al., 2014). On the other hand, HA dried samples show the irreversible collapse of a structure, a hard texture, and solids leaching after rehydration (Marabi, et al., 2004; Marabi, Thieme, Jacobson, & Saguy, 2006). The solutions to this poor performance of conventional dried products imply combining drying processes, which can take place in parallel or series. Similar to previous studies(Siebert, Becker, et al., 2020; Siebert, Gall, Karbstein, & Gaukel, 2018), we perceive a greater potential in serial combined drying, as operators can easily implement existing technologies.

In our previous work, we took *shiitake* mushrooms for the case study. Concerning a variety of serial combined drying methods of *shiitake* mushrooms, we selected the instant controlled pressure drop (DIC) pretreatment before hot air drying as a promising method for combined drying (Hu, Bi, Jin, Qiu, & van der Sman, 2021). The DIC combined with hot air drying at 35°C (DIC-HA35) dried samples showed a high volume recovery ratio after rehydration, a fast rehydration rate, as well as a decreased drying time and dry matter loss. The improved microstructure of the serially dried mushrooms is responsible for the difference in rehydration performance. The DIC treatment would mitigate the risk of case hardening and microstructure collapse during subsequent HA drying. This case hardening and collapse often happen during single drying methods using hot air drying. We hypothesize that the better the porosity and the higher connectivity, the better the rehydration performance of DIC-HA35 dried mushrooms. Pores provide the space for moisture transfer in the food matrix, while the connectivity, which is defined as the maximal number of particles that may be cut without separating the food structure (Pasquale M. Falcone, et al., 2006), reflects the profile of the pathway for the moisture transfer. They could together characterize the microstructure of final food products that is highly correlated to the physical and sensory properties. For mushrooms, the original connective hypha structure makes the mass transfer throughout the whole tissue. Hence, little connectivity between pores in dried mushrooms indicates the collapse of the structure and means poor rehydration (Hu, et al., 2021). Besides, we also assumed that this porosity or connectivity improvement could be retained in the final dried

products only when the temperature of subsequent post-drying is low (35°C), which might enable the retention of membrane integrity. Post-drying at temperatures above the critical temperature still leads to cell membrane damage and irreversible structure collapse.

To our knowledge, most applications involving DIC aimed at the texturing of pre-dried products by puffing, with pre-drying to a low moisture content of about 10%, and researchers mostly paid attention to the microstructure properties related to textures like hardness and crispy of final products (Allaf & Allaf, 2014; Fan, Wang, Zou, Wu, & Ying, 2018; Li, Bi, Chen, Jin, Wu, & Zhou, 2019; S. Mounir, Besombes, Al-Bitar, & Allaf, 2011). However, in our last study, we used the DIC to improve the microstructure of mushrooms for better rehydration performance. Therefore, we also require a fundamental understanding of the effect of DIC process parameters (such as temperature, moisture content) on the evolution of microstructure characteristics relevant to rehydration performance, like cell membrane integrity and porosity.

Therefore, the main objectives of this work were 1) first to make clear how the microstructural properties, such as membrane integrity and porosity of the porous structure, change with different DIC operating parameters. 2) based on the proper DIC operating parameters, to verify the hypothesis that DIC pretreatment before hot air drying at 35°C (HA35) facilitates a higher porosity and better connectivity of mushrooms. The microstructural changes were evaluated by electrical conductivity, transmission electron microscopy (TEM), scanning electron microscope (SEM), and X-ray micro-computed tomography (μCT) measurements. The obtained knowledge on microstructural development can be further used to optimize DIC combined drying of mushrooms in the future and be the reference for the rehydration improvement study of other dried food materials with porous structures.

3.2 Materials and methods

3.2.1 Materials

Fresh *shiitake* mushrooms were obtained from a local mushroom farm in Beijing (China). The mushroom stems were cut, leaving mushroom caps for experiments. The average moisture content of mushroom caps was 88.5 ± 2.0% (wet basis: w.b.), which was measured in a drying oven (DHG-9123A, Shanghai Jinghong Experiment Facility Co., Ltd., Shanghai, China) at 105°C for 24 h (AOAC. 1990).

3.2.2 Hot air drying/ DIC treatment/ DIC combined hot air drying

Hot air drying was conducted with a hot air drier (DHG-9123A, Shanghai Jinghong Experiment Facility Co., Ltd., Shanghai, China) with controlled temperatures (33,38,45, and 51 °C for only hot air dried samples) and air velocity of 1.2 m/s at the mushroom surface.

The DIC treatment was carried out by using a pilot-scale apparatus (QDPH1021, Tianjin Qinde New Material Scientific Development Co. Ltd., Tianjin, China) according to our previous study (Hu, et al., 2021). DIC treatment involves 4 main stages: 1) heating, 2) puffing, 3) vacuuming, and 4) cooling stages. During DIC-heating fresh mushrooms (300 g) were increased in temperature via heat conduction from hot pipes in the vessel. The pipes were heated by the steam (105-120°C) produced with a steamer. The duration of DIC-heating was determined by inserting a thermocouple in the center of the sample and measuring the time to reach the target temperature (around 45°C), which was about 10min. The DIC-puffing stage involves an abrupt pressure drop towards the vacuum by opening the decompression valve. The resulting gas pressure is about 3-5 kPa, which agrees with the saturated vapor pressure of water at 25-37°C. Subsequently, during the DIC-vacuuming, samples were maintained at the vacuum for several hours. According to preliminary trials, the DIC-vacuuming stage were the important step significantly affecting the moisture content after DIC treatment, and product temperature variation as well as the total drying time of DIC-HA. Besides, the mass transport during the DIC-vacuuming is also driven by pressure differences, which is different from DIC-heating and hot air drying (Hu, et al., 2021), and could lead to a different microstructure evolution compared to hot air drying. Hence, in this study, we vary the operation time and temperature during the DIC-vacuuming stage as listed in Table1. The DIC treatment was terminated with the DIC-cooling achieved by replacing the heating steam inside the pipes with cool tap water. We took the samples out of the vessel when the final center temperature of samples reached about 25°C and used them to investigate the microstructure change.

For DIC combined hot air drying, we first selected proper DIC treatment based on its effect on the microstructure of samples, and then, to combine it with hot air drying at 35°C and 65°C to produce dried mushrooms abbreviated as DIC-HA35, DIC-HA65, respectively.

Table3. 1 *The conditions of different DIC treatments of mushroom*

DIC treatment	DIC-vacuuming time (h)	DIC-vacuuming temperature (℃)
DIC1	1	75
DIC2	2	75
DIC3	3	75
DIC4	2	50
DIC5	2	100

During hot air drying and DIC treatment, the temperatures of the surface and center of mushrooms as well as the ambient temperature in the DIC treatment vessel were monitored by type-K thermocouples (TT-K-30, Omega Engineering Inc., Stamford, Connecticut, USA)) and recorded by a data recorder (PicoLogTC-08, Pico Technology, England). The center temperature was measured with the thermocouple inserted into the cap of the mushroom at a 10 mm depth, while the surface temperature was measured under the skin of the cap at a 0.2 mm depth.

3.2.3 Cell integrity measurement by electrical conductivity

As in our earlier work, we investigated the conductivity of rehydration liquid as the indicator of cell membrane integrity (Hu, et al., 2021). After rehydration, due to the disruption of cell membrane, the leaching of ions of the cytoplasm and vacuoles leads to enhanced conductivity of rehydration liquid (Lewicki & Pawlak, 2003). Hence, the lower conductivity, the better cell membrane integrity (Angersbach, Heinz, & Knorr, 1999). To establish critical conditions for the loss of cell membrane integrity, we specially prepared dried mushrooms with different moisture content via hot air drying performed at different temperatures i.e. 33,38,45, and 51 ℃. At one-hour intervals, we sampled the mushrooms to measure moisture content and obtain the drying curves. At the same time, we collected samples with the moisture content of 10%, 30%, 50%, 70% (wet basis, w.b.). The samples obtained from hot air drying and DIC treatments (in Table1) were rehydrated in distilled water at room temperature (25 ± 2℃) for 24 h. The electrical conductivity of the rehydration liquid of these samples was measured in triplicate using an electrolyte conductivity meter (DDS-307A, Leici New Energy Technology Co., Ltd., Shanghai, China).

3.2.4 Cell integrity measurement by transmission electron microscopy (TEM)

We observed the cellular structure of fresh and semi-dried samples according to the method of Hayat (2012) with some modifications: samples were first prefixed in 2.5% glutaraldehyde, then they were immersed in 1% osmium tetroxide and fixed for 2 h after washing with 0.2 M

phosphate buffer (pH 7.2) for three times. Then samples were dehydrated in an ethanol series (30%, 50%, 60%, 70%, 80%, 90%, and 100%) and then immersed in acetone solutions for 60 min to replace the ethanol. The samples were embedded in a mixture of Spurr's low viscosity resin and acetone solutions, followed by one week's polymerization process at 35 °C. In the end, TEM images of ultra-thin slices obtained with an ultramicrotome were recorded with a Hitachi H-7500 TEM (Hitachi, Tokyo, Japan). At least 6 images were collected for each sample.

3.2.5 Microstructural observation by scanning electron microscope (SEM)

We observed the different DIC samples (shown in Table1) using the scanning electron microscope to examine the porous characteristics change of samples, as compared to fresh mushrooms. Sliced samples about 2 mm thick were obtained from three parts of the mushroom cap: skin, lamella, and the fruit body. The samples used for SEM were prefixed and dehydrated with the same method as those for TEM measurement. Afterward, samples were dried by critical point drying using a LeicaCPD 030 CO2 (Leica, Germany). The dried samples were fixed on the scanning stub with the aid of adhesive tape, and the skin, fracture surface of the fruit part as well as the lamella of samples were placed upward. Subsequently, the samples were sputter-coated with gold through an ion sputtering apparatus (MCI000, Hitachi Co., Tokyo, Japan). The images of the sample microstructure were taken by using a scanning electron microscope (SU8010, Hitachi Co., Tokyo, Japan) which had an acceleration voltage of 10 kV. At least 6 images were collected for each sample.

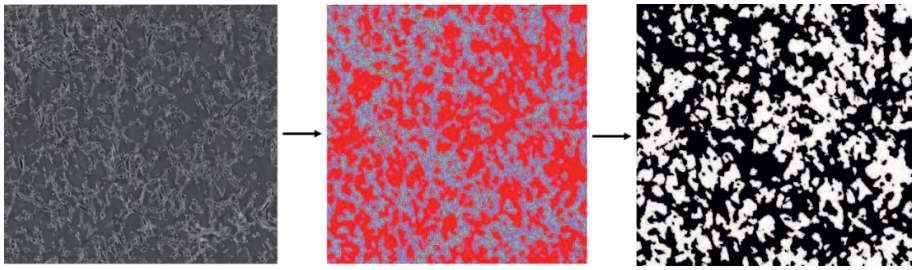
3.2.6 Porosity and connectivity measurement by X-ray micro-computed tomography (μCT)

To quantitatively capture the microstructural changes such as porosity and connectivity of DIC and DIC-HA mushroom samples, we performed X-ray micro-computed tomography (μCT) using Bruker Skyscan 1272 (Kontich, Belgium). Samples for μCT scanning were prepared from DIC-HA35 combined dried mushrooms (with MC about 10%, w.b.), DIC treated semi-dried mushrooms (with MC 79.03%, w.b.), and fresh ones. For semi-dried and fresh samples, due to the cell walls and water showing quite similar density, the internal structure of wet samples cannot be visualized with micro-CT except the air-filled pores (Siebert, Zuber, Engelhardt, Baumbach, Karbstein, & Gaukel, 2018). To identify the pores within the fresh or semi-dried *shiitake* mushroom, a high resolution for scanning is required, which was 0.8μm in this study. However, this will result in long measurement times up to

hours. Consequently, the undesired significant moisture loss and deformation will happen. Although a gas flow such as sublimated CO2 or liquid nitrogen can lower the temperature of the sample it is still impossible to keep the internal structure fixed within a few hours due to the high-moisture content and the use of high-resolution scanning (Siebert, Zuber, Hamann, Baumbach, Karbstein, & Gaukel, 2020). Therefore, to fixate the structure as much as possible, we treated and dried these cubes by critical point drying similar to the method applied for SEM measurement. These critically dried samples were used for µCT scanning.

The µCT scanning process was similar to (Peng, et al., 2018), with modifications conducted with a tungsten anode X-ray tube set to 50 kV and 90 µA. The sample was fixed on a specimen holder and rotated over 180 ∘ in angular steps of 0.15 ∘. The readout time for one sample was about 2.5 hours. The optical axis was 684 mm, and the center of the sample to source was 14.7 mm. After tomography reconstruction of projection images, we obtained a stack of about 1286 flat cross-sections. We used the reconstruction NRecon software (version 1.6.9.18, Bruker, Kontich, Belgium) to reconstruct the two-dimensional (2D) images and the software CTAn (version 1.16.4.1, Bruker) to analyze the three-dimensional images.

For dried samples, to distinguish the pores from the solid matrix, an interval threshold which was 106-107 was set. The space where the intensity was less than 106-107 were assumed pores. Equivalent diameters were defined as the diameter of the inscribed sphere in the pores of the sample. While for fresh and semi-dried samples, we have intracellular and extracellular pores, and the porosity of these samples referred to the volume ratio of extracellular pores compared to the whole sample. Therefore, the intracellular pores obtained by critical point drying were not our objective and hence excluded from the porosity estimation. The exclusion or image segmentation was achieved by the Trainable Weka Segmentation (TWS) plugin which uses machine learning algorithms to classify greyscale images into different classes (Arganda-Carreras, et al., 2017; Lormand, et al., 2018). As shown in Fig.3.1, the hypha, pores inside the hyphae, pores between hyphae were divided into three categories, which were manually marked respectively by drawing traces over a region of interest (ROI) for each category (this process is also called classifier training). Then TWS identified the pores according to the markers and segment the image. More details about the Weka segmentation process can be referred from(Arganda-Carreras, et al., 2017; Lormand, et al., 2018). After thresholding and removing noises processing, analysis of the images for porosity was conducted using CTAn..



(1) (2) (3)

Fig. 3.1. Automation protocol to derive porosity and connectivity using the Trainable Weka Segmentation (TWS) plugin of ImageJ. (1) CT images of the samples are obtained using a microCT (2) Result of the TWS using the input of sets of training pixels (STP's). Red, green, and purple are, respectively, pores between hyphae, inner pores in hyphae, and solid matrix of hyphae (3) Post segmentation image processing including thresholding, removing noises

The connectivity indicates the number of connected structures and is related to a topological number Eu known as Euler characteristic or Euler number (Gundersen, Boyce, Nyengaard, & Odgaard, 1993), which has been widely used for the microstructure analysis of cellular food matrices such as pear, mango, wheat, and bread (Cantre, Herremans, Verboven, Ampofo-Asiama, & Nicolaï, 2014; Lomolino, Morari, Dal Ferro, Vincenzi, & Pasini, 2017; Muziri, et al., 2016; Rzigue, et al., 2016). The Euler characteristic describes the structure of a topological space. It presents the degree to which parts of the object are multiply connected. The Euler number can be expressed as:

$$Eu = (separate\ parts - extra\ connections + enclosed\ cavities)$$

Hence, the more connections than separate parts and enclosed cavities, the higher connectivity the sample will be. While the pore network is well connected, Eu will be negative. More details about the Euler number and definitions of separate parts, extra connections, and enclosed cavities can be referred to (Gundersen, et al., 1993). The computation of the Euler number is performed using the post-processing software of the Skyscan micro-CT instrument (CTAn).

For the µCT analysis of fresh and DIC-treated mushrooms, we took cubic samples of size 0.8-1 mm, including the skin of the cap and lamella, respectively (shown in Fig.3.2a and Fig.3.2b). For convenience, these mushroom cubes including skin and lamella, respectively were named fresh-skin, fresh-lamella, DIC-skin, and DIC-lamella, respectively. The final dried samples used for the µCT analysis were cubic ones including the skin, shown as Fig.3.2c. They were named the same as the applied drying methods, which are referred to as

HA35, DIC-HA35, and DIC-HA65, respectively. Subsequently, we first investigated the porosity changes with the position for fresh-skin, fresh-lamella, DIC-skin, and DIC-lamella samples. For calculation convenience, these samples were divided into 10 layers, respectively. The porosity calculated from three cross-sections was used to indicate the porosity of the layer where they were. The locations of these images are shown by red lines on the cross-section of the cubic sample in Fig.3.2a and Fig.3.2b. For dried samples, HA35, DIC-HA35, DIC-HA65, the porosity, and connectivity change with depth were obtained from the top, middle, and bottom layers. The porosity and connectivity of each layer are the average values of 3 sub-cuboids in it, as shown in Fig.3.2c.

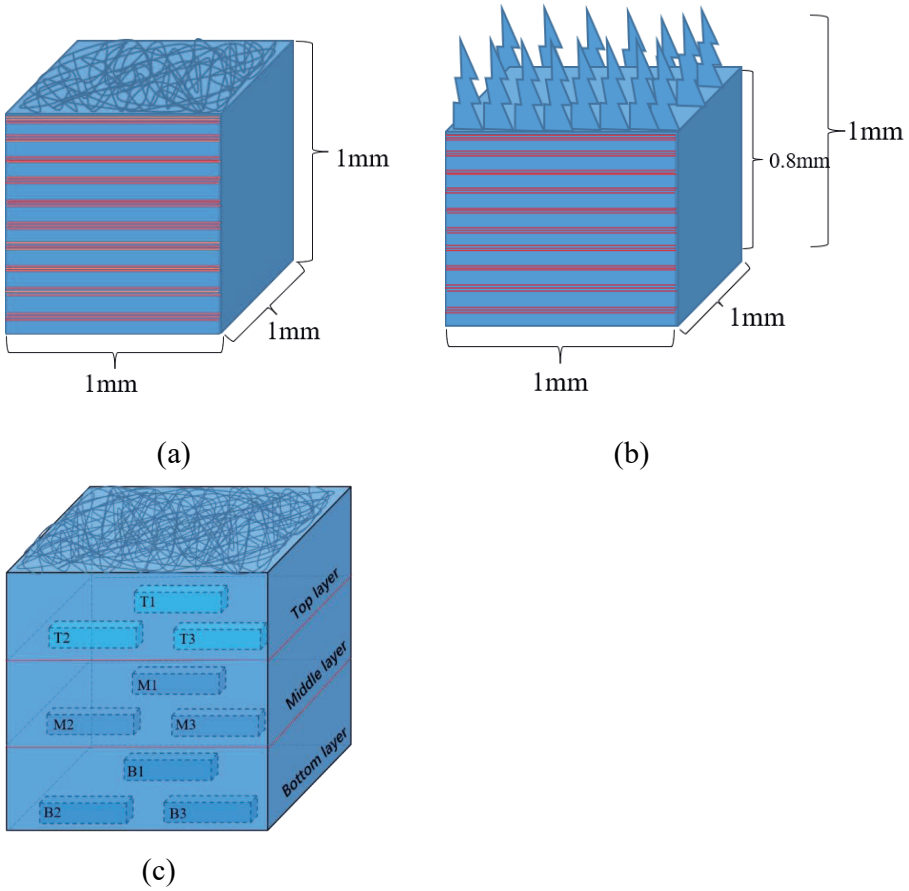


Fig. 3.2. *Mushroom cubes including skin and lamella parts (a,b: red lines indicate the location of images used for porosity calculation; c: T1-3, M1-3, B1-3 indicate the region of interest (ROI) for porosity and connectivity calculation in each layer)*

3.3. Results and discussion

3.3.1 Temperature and moisture dependency of cell membrane integrity

For the validation of our hypothesis, and also for the optimal process design of the serial combined drying process, it is required to know at which conditions the mushroom loses its cell membrane integrity. For yeast, it is known that cell membrane integrity is dependent on both temperature and moisture content (i.e. water potential) (Beney, de Maranon, Marechal, & Gervais, 2000). We, therefore, have subjected *shiitake* mushrooms to hot air drying at different temperatures first (33, 38, 45, 51 °C), as a means to vary both moisture content (MC) and product temperature (T_p), and monitored the changes of MC and T_p during the drying (see **Appendix** Fig.A1). For the relation between conductivity (i.e. cell membrane integrity), T_p, and MC we have used the average values of the surface and center temperatures for T_p. Fig. 3.3 shows the contour plot of conductivity as a function of T_p and MC. The color bar indicates the values of conductivity. We observe that conductivity is only a function of temperature when MC>40%. For MC < 40% the conductivity also shows a strong dependency with MC. Higher drying temperature results in higher conductivity, indicating increased cell membrane damage, as also found by (Lewicki, et al., 2005). At 51°C, we assume all membranes are fully destroyed and the conductivity is maximal. We propose as a critical condition regarding cell membrane integrity the contour line, with conductivity midway the minimal value of a fresh mushroom and the maximal value. We aim to confirm these critical conditions via TEM observations on DIC treated samples.

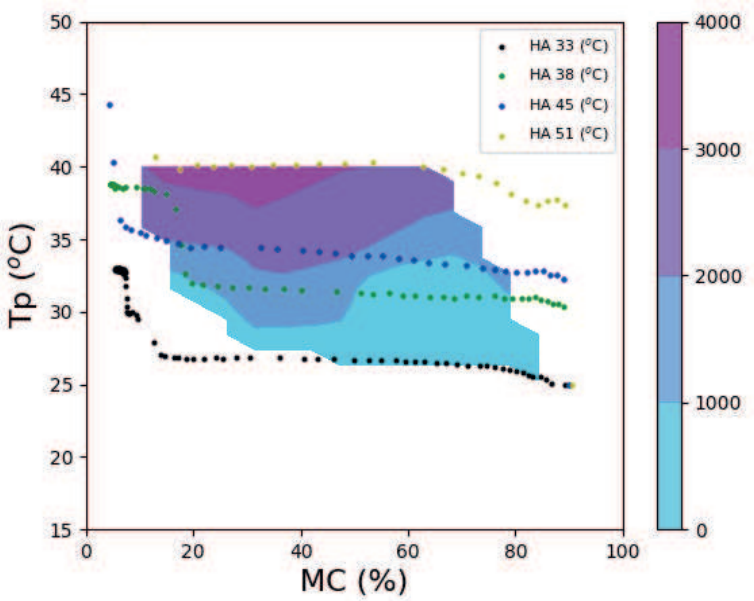


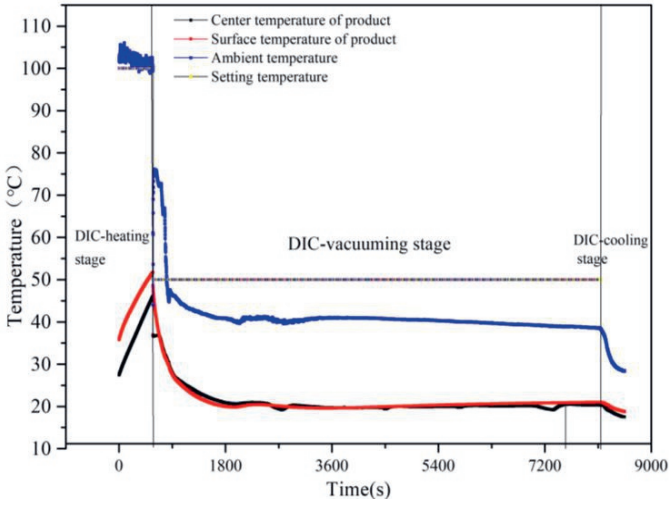
Fig 3.3. *Moisture–temperature state diagram of hot air treated mushrooms with contour lines for the electrical conductivity (μS/ cm) of their rehydration liquid*

3.3.2 Cell integrity after different DIC treatments

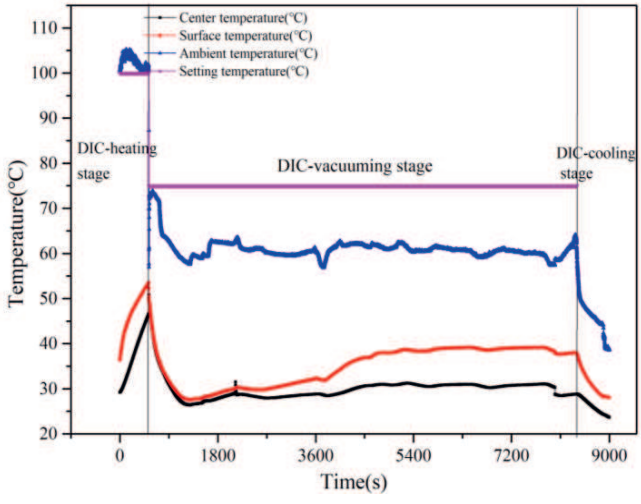
3.3.2.1 Temperature curves of DIC treatments

Mushrooms were subject to DIC treatments with different process parameters, as listed in Table 3.1. We recorded the product temperature throughout all the DIC treatments. The product temperature history of DIC treatments with different vacuuming temperatures (DIC2,4,5) is shown in Fig.3.4, and that for DIC1 and DIC3 showing different vacuuming times is given in **Appendix** Fig.A3.2(a) and Fig.SA.2(b). Note, the product temperature is much lower than the air temperature due to the evaporative cooling effect on the surface of mushrooms. During the heating stage, the center and the surface temperature have risen to 45°C and 50°C, respectively. After the abrupt evacuation, both of the temperatures decreased rapidly. A similar dramatic temperature change at the moment of evacuation was also observed by (Sabah Mounir, Allaf, Mujumdar, & Allaf, 2012) and (Louka & Allaf, 2004). The instant pressure drop could explain this, triggering the rapid liquid vaporization and causing drastic cooling. Furthermore, due to the porous structure of the mushroom, vaporization occurs through the whole sample, leading to the synchronous decrease of surface and center product temperatures. Via heat transfer from the ambient (with different ambient temperatures of 80, 60, and 40°C shown in Fig.3.4) the corresponding average

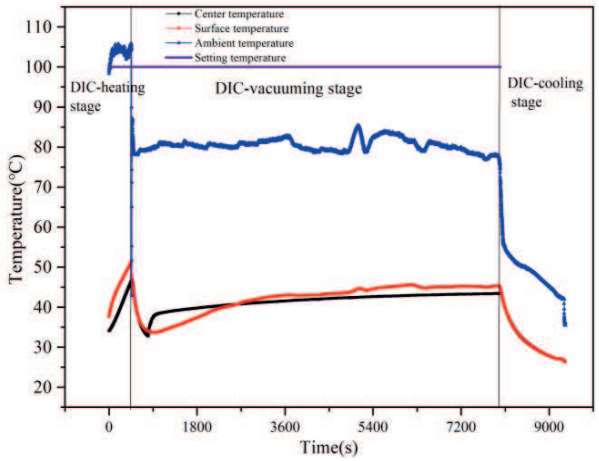
product temperature remains at 41.3, 29.9, and 21.0℃, respectively. In some cases, the surface temperature was not following the center temperature, which is probably due to the unstable pressure during the DIC-vacuuming stage or the poor contact between skin and thermocouple, mediated by the shrinkage of tissue. Overall, the variation of product temperature during different DIC treatments is in the range that can remain the cell membrane integrity, as will be discussed in the coming sections.



(a) DIC-vacuuming at 50℃



(b) DIC-vacuuming at 75℃



(c) DIC-vacuuming at 100°C

Fig. 3.4. *Product temperature changes of mushrooms during DIC-vacuuming stages at 50°C (a), 75°C(b), 100°C(c) for 2 hours*

3.3.2.2 Cell integrity indicated by transmission electron microscopy (TEM)

The integrity of the vacuole was taken as a direct indicator of overall cell membrane integrity, which has been observed via TEM images of the various DIC treated samples. We have taken samples from three regions: a) the cap's skin, b) the fruit body of the cap, and c) the lamella at the underside of the cap. The samples from the fresh mushroom serve as a reference with intact vacuole structures. Fig.3.5 shows the results, indicating that there were no intact vacuoles in the skin samples for all DIC treatments. We attributed it to the high surface temperature (up to 50 °C) during the DIC-heating stage. However, we observed that the vacuole was scarcely disintegrated for the fruit body and lamella samples. Apparently, during the subsequent DIC-vacuuming stage the critical conditions endured for a too short amount of time to inflict cell membrane damage (Fig.3.5a), or the subsurface product temperature remained low enough to preserve membrane integrity (Fig.3.5b). Only obvious tonoplast disintegration was detected in the fruit body samples at the vacuuming temperature of 100 °C (DIC5, where the average product temperature was above 40 °C). The effect of temperature on cell membrane integrity of fruit hyphae during DIC treatment is consistent with our previous observations (Qiu, Bi, Jin, Hu, Lyu, & Wu, 2021), in which the cell structure of dried samples obtained from hot air drying at different temperatures of 30 – 90 °C was studied via TEM. In that study, it was observed that vacuoles disappeared when the product temperature exceeded 40 °C. These results indicated that the critical condition for tonoplast and cell membrane rupture occurs somewhere in the interval at 30 °C < T_p < 40 °C.

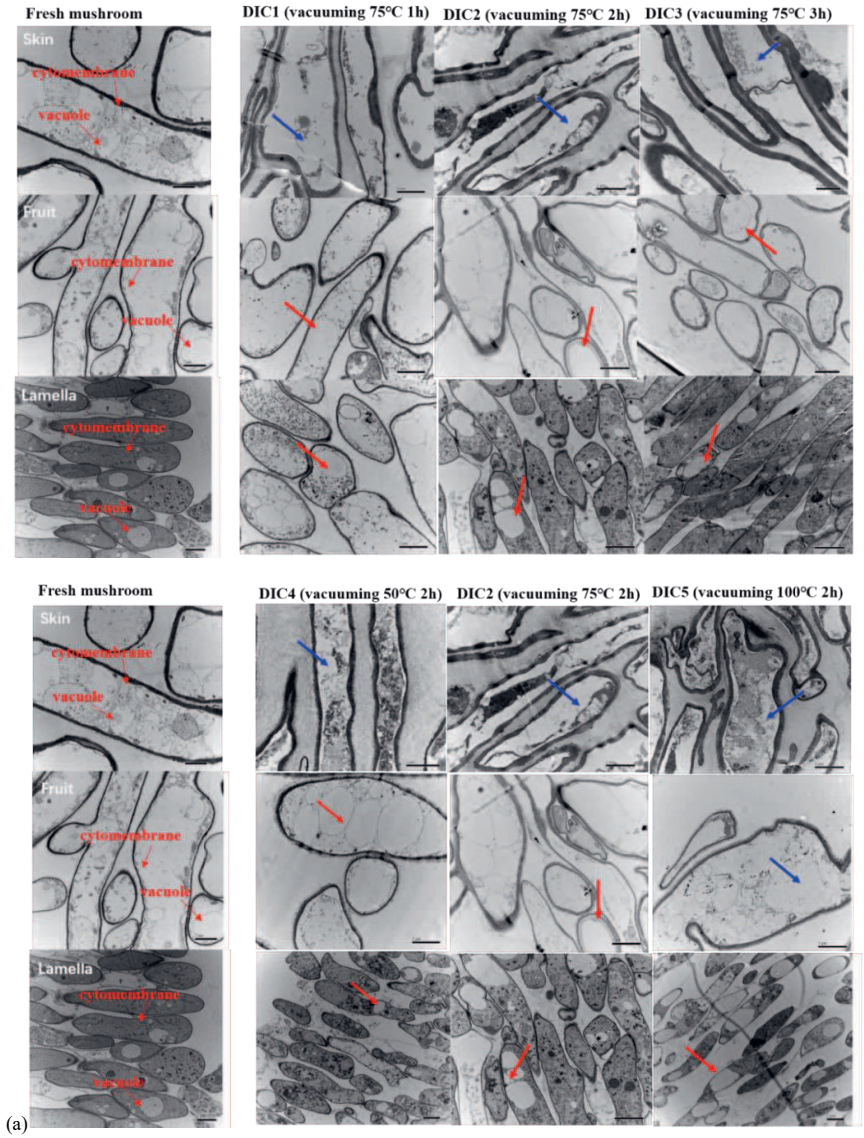


Fig. 3.5. *TEM images of mushrooms, (a): fresh and DIC treated mushrooms with different vacuuming time; (b): fresh and DIC treated mushrooms with different vacuuming temperatures (8000×for fresh mushroom,10000× for DIC treated samples, blue and red arrows indicate disrupted and intact vacuoles, respectively)*

3.3.2.3 Cell integrity indicated by conductivity

For samples taken at the end of the DIC-vacuuming stage, we have measured their moisture content and conductivity, with values shown in Table 3.2. Their values are consistent with those measured from hot air-dried samples, as shown in Fig.3.3. We have plotted the state of the sample (in terms of product temperature and moisture content) in the conductivity contour plot in Fig.3.6, with the red circle indicating an intact cell membrane, and the blue star indicating a ruptured cell membrane. We observe that DIC treated samples with product temperatures lower than 30°C have conductivity lower than the critical value. Hence, the conductivity and TEM measurements confirm that the critical temperature for cell membrane damage is indeed in the interval 30 < Tcr < 40°C, and likely Tcr = 35°C, as indicated by the contour plots of Fig.3.3 and Fig.3.6.

Table 3.2 *Cell membrane integrity changes with different DIC treatments*

DIC treatments	Average product temperature (°C)	Moisture content(%,w.b.)	Electrical conductivity (μS/cm)
Fresh		89.2±1.2[a]	149.80±0.6[e]
DIC1	29.9	84.98±1.0[b]	1185.83±9.63[c]
DIC2	29.9	77.69±0.4[c]	1262.04±7.93[b]
DIC3	29.9	76.12±2.1[c]	1275.74±7.6[b]
DIC4	21.0	79.03±4.0[c]	864.97±1.65[d]
DIC5	41.3	73.46±3.46[d]	2960.90±12.59[a]

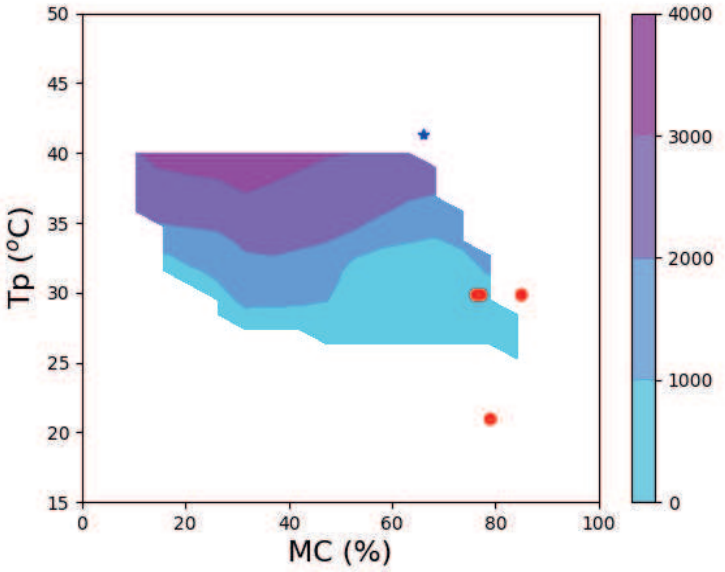


Fig. 3.6. *Moisture–temperature state diagram of hot air-dried mushrooms with contour lines for the electrical conductivity (μS/cm) of their rehydration liquid (red dots indicate the conductivity of DIC1-4 treated samples, whose vacuuming temperatures are 50 or 75°C and the blue star indicates that of the DIC5 treated one, whose vacuuming temperature is 100°C)*

3.3.3 Porosity and connectivity development during DIC combined drying

3.3.3.1 Scanning electron microscope (SEM) observation of mushrooms

To make clear how the microstructure of mushroom cap develops after DIC treatment and DIC combined drying, the scanning electron microscope (SEM) observation of mushrooms was first conducted. As retention of cell membrane integrity is a precondition for the enhancement/maintenance of porosity, we performed the analysis on the DIC4 pretreatment and its combination with hot air drying at either 35°C or 65°C. Thereafter, the DIC refers to the DIC4 with a vacuuming stage at 50°C for 2 h. The moisture contents of mushrooms after DIC treatment was 79.03% (w.b.), while was about 10% (w.b.) after DIC-HA35/65 combined drying and HA35 drying.

Similar to TEM investigation, samples from the skin, fruit body, and lamella parts of mushrooms were analyzed by SEM (Fig.3.7). The intercellular spaces between hyphae constitute the pore space, of which we analyze the porosity. From the SEM images, it is clear that the hyphae in the skin and fruit body have collapsed already after the DIC pretreatment, which is consistent with the observation by TEM, which shows that cell membrane integrity

is not retained in the skin region. After subsequent hot air drying at 35°C and 65°C, the skin samples of DIC-treated mushrooms are further compacted, and they eventually show a similar structure as the HA35 sample. For the fruit body part, DIC-HA35 performs similar shrinkage as HA35, but less cell collapses than DIC-HA65. All dried samples show a more open structure than the fresh and DIC-treated ones for the lamella part. Although the state of hypha and microstructure characteristics of the fracture surface of samples can be observed from SEM, it is not definite to compare the porosity and connectivity for these samples. Accurate quantitative analysis and comparison are still required, which is given in the following section by μCT.

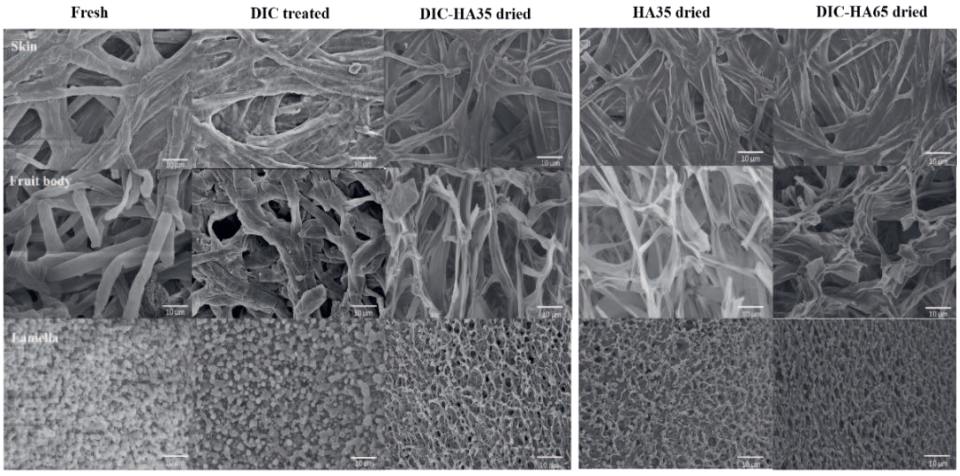


Fig. 3.7. *SEM images of fresh, DIC treated, DIC-HA35 dried, HA dried and DIC-HA65 dried mushrooms*

3.3.3.2 μCT images analysis of mushrooms

μCT analysis of fresh and DIC treated mushrooms

From the observation of TEM and SEM images, we found a significant difference in the microstructure development at the skin, fruit, and lamella parts of mushrooms during DIC treatment. Therefore, we first prepared such cubes from fresh mushrooms and DIC4 treated ones and examined cubical samples including the skin (fresh/DIC-skin) and lamella parts (fresh/DIC-lamella) with μCT respectively. Note, the porosity within the mushroom only refers to the intercellular space between hyphae.

According to the μCT images shown in Fig.3.8, the change of porosity of these cubes reveals the evolution process of the microstructure of mushrooms by DIC treatment. In Fig.3.8a and

Fig.3.8b, we observe that the closer to the skin, the lower porosity. For the fresh-skin sample, the porosity of the layer most close to the skin is 0.64%, while that for the layer most close to the fruit part is 45%. Compared to the fresh-skin sample, the porosity of most layers in the DIC-skin sample decreases significantly after DIC treatment, up to 30%, which could be attributed to the shrinkage and collapse caused by the moisture loss. On the other hand, Fig.3.8 also shows that the porosity of the layers below the lamella develops oppositely after DIC treatment. Namely, compared to the fresh-lamella sample whose porosity ranges from 18% to 25%, the DIC-lamella one gives a higher porosity (30%-35%), which is consistent with the looser structure shown by SEM images. The detailed microstructure of these samples can be visualized through μCT images shown in Fig.3.9 as well as the videos shown by (Hu, Bi, Jin, & van der Sman, 2022).

Thus, after DIC treatment, the porosity of the lamella region increases while that of the skin decreases. According to the previous study, the moisture loss of the lamella part of mushroom largely lags behind the skin region during drying (Cheng, Li, Yang, Wang, & Tan, 2020), hence we speculate that the moisture loss for the lamella part of the mushroom after such a short DIC-heating stage is negligible. Therefore, assuming the moisture content of the lamella part of DIC treated mushrooms is similar to that of fresh ones, it can be concluded that the DIC treatment induces the increased porosity of the lamella part. The results to some extent prove our assumption that DIC improves the porosity of mushrooms at the surface layer of samples.

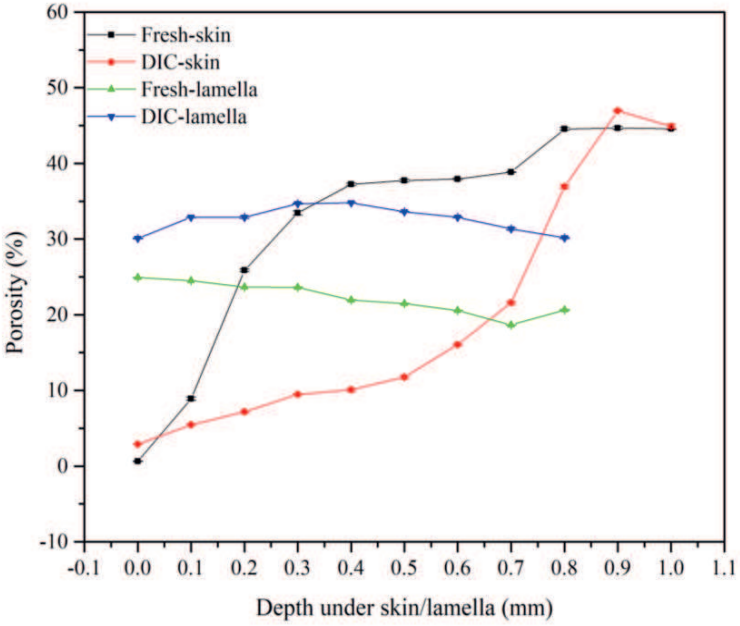


Fig. 3. 8. *Porosity changes of fresh and DIC treated (DIC4) mushrooms with the depth under skin/lamella*

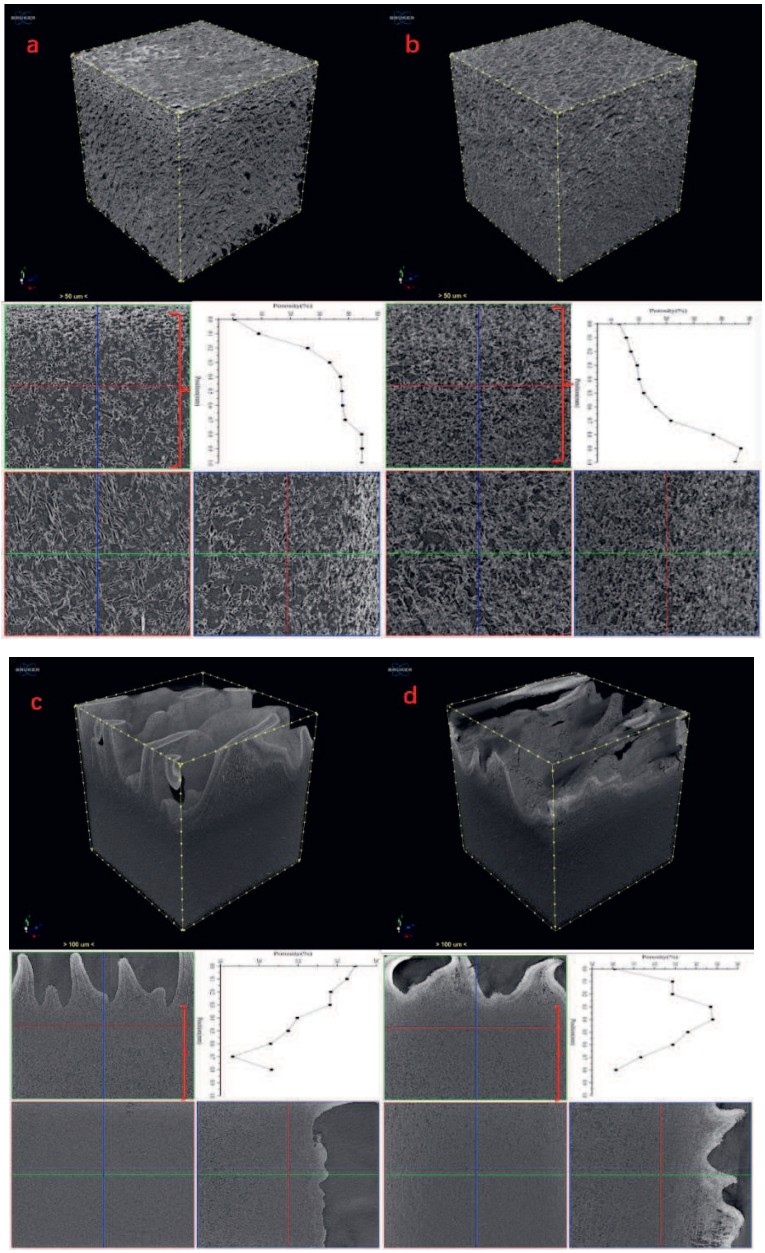


Fig. 3.9. *Microstructure (X-ray μCT images) and porosity (line figure) comparison of fresh and DIC4 treated mushrooms (a, b, c, and d represent X-ray μCT images for samples of fresh-skin, DIC-skin fresh-lamella, DIC-lamella respectively; the top parts of images a-d are the 3D structure of samples, the bottom parts are images from samples' frontal view, horizontal view, and sagittal view)*

μCT analysis of DIC-HA35/65 and HA35 dried mushrooms

To further prove our hypothesis regarding the microstructural changes of DIC-HA samples, we compared the porosity and connectivity of DIC-HA35, DIC-HA65, and HA35 dried mushrooms (with moisture content about 10%, w.b.). Only the mushroom cubes, including skin, were taken as objects. As shown in Fig.10 and Table 3.3, the DIC-HA35 dried sample presents higher porosity, but similar Eu numbers as the HA35 dried one at the top and middle parts, indicating the DIC treatment improves the porous structure, but has only a slight influence on connectivity. Compared to DIC-HA35 and HA35 samples, the DIC-HA65 sample gives the lowest Eu numbers at the top, middle, and bottom parts and presents the best connectivity. The fracturing of hyphae that we observed in the SEM images can explain this behavior revealing more connections among these disrupted hyphae and leading to improved connectivity. Hu, et al. (2022) visualized through a video and detailed the microstructure difference between dried samples.

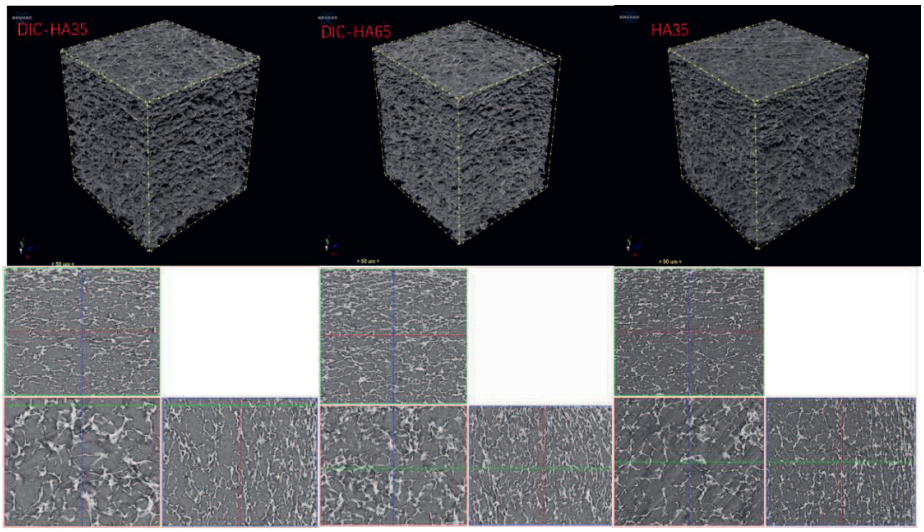


Fig.3.10. *Microstructure (X-ray μCT images) of DIC-HA35, DIC-HA65, HA35 dried mushrooms (The top parts represent the 3D structure of samples, and the bottom parts are the samples' frontal view, horizontal view, and sagittal view)*

Table 3.3 *Porosity and Eu numbers of DIC-HA35/65 and HA35 dried mushrooms*

Samples \ Position		Top	Middle	Bottom
DIC- HA35	Porosity	78.4±0.60^{D}	91.34±1.00^{A}	90.97±0.59^{A}
	Eu number	-6389.67±69.21^{cd}	-5116.33±419.40^{ef}	-4696.33±1045.09^{f}
DIC- HA65	Porosity	72.23±2.55^{F}	80.54±1.41^{D}	85.15±1.28^{C}
	Eu number	-8195±760.43^{b}	-8434.67±541.30^{b}	-11043±700.86^{a}
HA35	Porosity	75.34±1.53^{E}	87.88±0.55^{B}	90.70±0.26^{A}
	Eu number	-7181.33±686.76^{c}	-5388±130.33^{ef}	-7147±367.76^{c}

Notes: Values in the table are means ± standard deviation, and significant differences ($p<0.05$) among samples were expressed with capital letters A–F for porosity and with small letters a–f for Eu numbers.

3.3.4. General discussion

Due to this paper being a follow-up hypothesis verification work, a critical reflection based on our previous assumptions and practical experimental results will be given in this section. In our last paper, we mainly attributed the unexpected good rehydration performance of DIC-HA35 dried mushrooms to the retained connectivity, which is assumed to be the resultant of the slight expansion of structure during DIC and the retention of cell membrane integrity – preventing the collapse of the structure. However, the experimental results obtained from μCT scanning of mushrooms show that DIC (DIC4, with the 50°C of vacuuming temperature for 2 h) impacts the porosity of the surface layers rather than the connectivity. Even, slightly higher connectivity was obtained by DIC-HA65, due to the disruption of hyphae during the subsequent HA65. Our previous study showed that DIC-HA65 had a slower rehydration rate than DIC-HA35. Hence, we hold the reflection that the retention of connectivity to better rehydration is only valid when the porosity is increased or maintained.

In many previous studies, DIC was used as a process of texturing for pre-dried products at the middle or last stage of the combined drying (Louka, et al., 2004; Sabah Mounir, et al., 2012; Yi, Zhou, Bi, Wang, Liu, & Wu, 2016). But our studies also present the potential to act at the first step of combined drying by modifying the original microstructure of fresh samples. In addition to our research, S. Mounir, Amami, Allaf, Mujumdar, & Allaf (2020) used the DIC as the pretreatment before the intermittent microwave/airflow drying (DIC-IMAD), and obtained a significant expansion of shrimp snacks and hence an improved rehydration

performance. Interestingly, an increase in the drying rate was found in both cases of DIC-IMAD and DIC-HA35, and this could be explained by the structure expansion of original samples, which allows a higher internal moisture diffusion and a more effective final drying stage.

Compared to many other dried vegetables and fruits products as commonly treated with DIC, the *shiitake* mushroom structure is unique due to its high original porosity and connectivity in the fruit body, while having a compact skin structure. For products like carrot and apple, the task of the DIC treatment is to generate a porous (dried) structure (Li, et al., 2020; Peng, et al., 2018; Zhou, Wang, Bi, Liu, Yi, & Wu, 2018), while the task of DIC for *shiitake* mushroom is to *retain* its original porous structure. With the original porous structure of *shiitake* mushroom, one can also benefit from a reduction of drying time via the extension of the vacuum stage of DIC, where the mushroom experiences a significant internal vapor flow and the consequent evaporative cooling that keeps the product temperature below the critical point for the loss of cell membrane integrity. Furthermore, retention of cell membrane integrity prevents collapse of the surface layer, as observed for single dried HA35 and DIC-HA65 mushrooms, as indicated by the lower porosity at the top and middle position (Table.3.3).

3.4. Conclusion

In this work, we have obtained detailed knowledge about the development of the microstructure of fresh mushrooms after DIC treatment, which enabled us to verify the hypothesis of the beneficial effects of DIC-HA combined drying upon rehydration. It is proven that the DIC pretreatment produces a porous microstructure with a higher porosity on the sub-surface layer of mushroom (not including the skin), provided that the product temperature remains below the critical temperature of 35 °C causing membrane rupture. Otherwise, there is a collapse of the pore structure, inhibiting good rehydration. Evaporative cooling during the DIC-vacuuming stage of the DIC treatment and HA drying is an important factor in keeping the product temperature below the critical temperature. We view there is ample opportunity for further optimization of the combined DIC-HA treatments, which can profit from the development of a numerical model of the physics during the DIC-HA drying, which will be the subject of our future research.

Appendix 3

Supplementary data

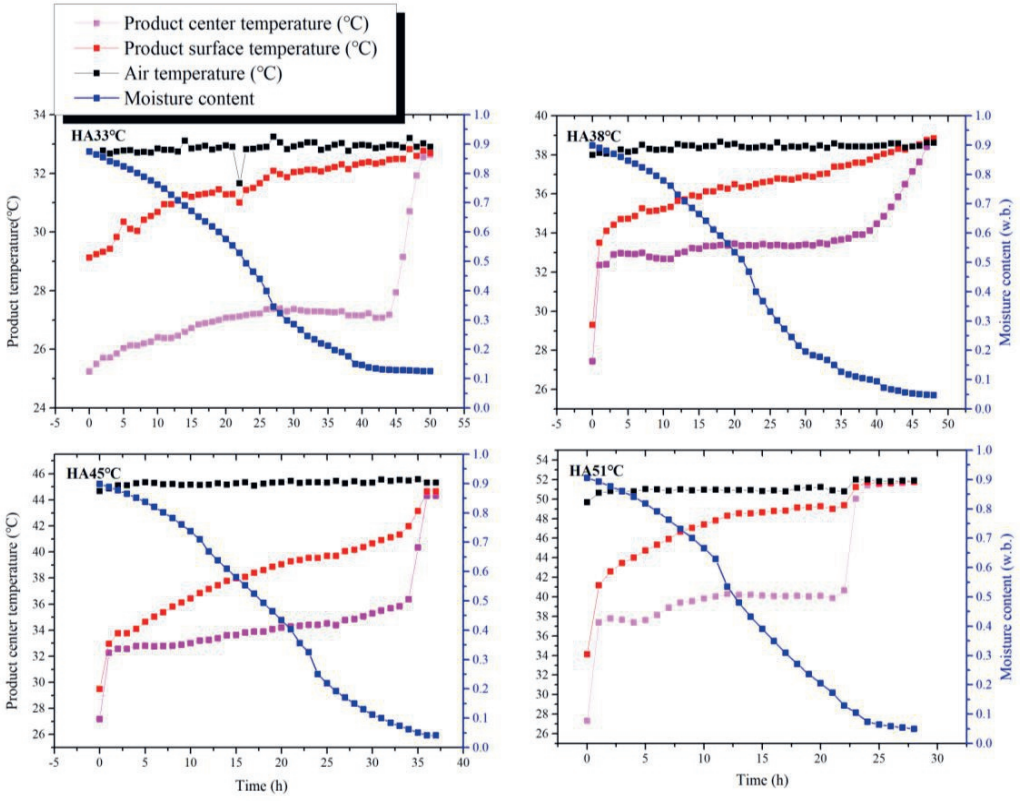
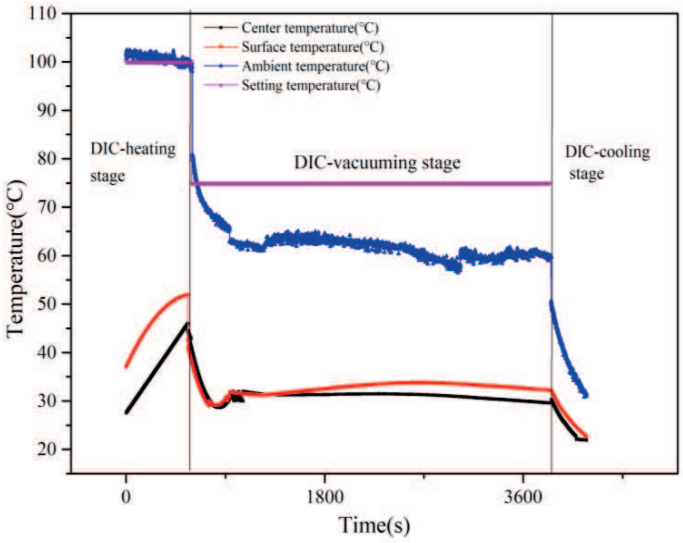
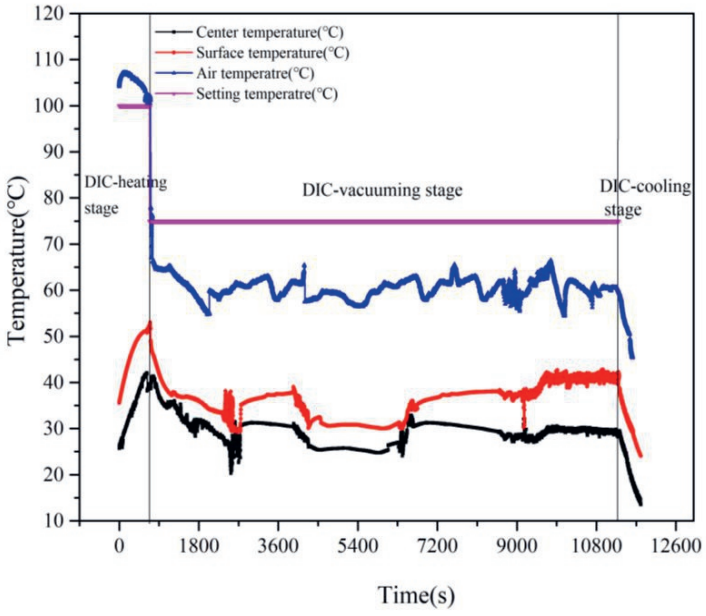


Fig. A3.1. *Product temperature and moisture content changes of mushrooms during hot air drying at 33, 38, 45, 51°C (air temperature in the dryer)*



(a) DIC-vacuuming at 75℃ for 1 h



(b) DIC-vacuuming at 75℃ for 3 h

Fig. A3.2. *Product temperature changes of mushrooms during DIC-vacuuming stages at 75℃ for 1h (a) and 3h (b)*

Chapter 4

Impact of physical changes in mushroom on variation in moisture sorption

This chapter has been published as Hu, L., Bi, J., Jin, X., & van der Sman, R. G. M. Impact of physical changes in mushroom on variation in moisture sorption. Journal of Food Engineering.2023, 351,111506. https://doi.org/10.1016/j.jfoodeng.2023.111506

Abstract

In this work, physical changes such as protein denaturation, cell membrane integrity, and the viscoelastic relaxation of mushrooms, as induced by drying treatments, were investigated as possible causes of the variation in moisture sorption isotherms (MSIs) and hysteresis. Our investigations involved both experimental and theoretical evaluation of MSIs. Via analysis with the Flory-Huggins (FH) theory, we concluded that 1) the protein denaturation does not significantly affect moisture sorption and hysteresis, and 2) cell membrane integrity only influences on the moisture sorption/water holding capacity at high relative humidity. Additional experiments show that mushrooms exhibit viscoelastic properties, which are temperature and moisture-dependent. As dynamic vapour sorption (DVS) experiments show signs of viscoelastic relaxation, we consider the latter to be the likely determining factor affecting the variations in MSI and hysteresis. The Flory-Rehner theory follows that one needs to include elastic stress into the driving force of drying. For viscoelastic media, a separate model, like the generalized Maxwell model, should describe the stress evolution linked to a drying model.

4.1 Introduction

Moisture sorption isotherms (MSIs) should ideally illustrate the equilibrium amount of water held by the food solids as a function of relative humidity at a constant temperature or equivalently as a function of water activity. Consequently, it can be used for the modelling and possible optimization of food drying procedures, as the water activity is related to the driving force for drying, i.e. the gradient in the chemical potential of water (Jin et al., 2014). However, many MSIs measurements conducted by food scientists via a single cycle of the sorption-desorption process do not exhibit equilibrium conditions, as evidenced by the existence of hysteresis (Burnett et al., 2006; Caurie, 2007). Hence, a good knowledge of the physical causes of the deviation of MSIs from equilibrium is essential (Dupas-Langlet et al., 2016).

Hysteresis has been given much attention in the field of wood drying. Several studies reported that during the multiple humid-dry cycles, the wood underwent a relaxation of internal mechanical stresses. The partial relaxation of stress results in wood samples, with different pre-treatments, to exhibit similar hysteresis when exposed to the second and third cycles. The different hysteresis values during the first sorption-desorption cycle is attributed to the different amounts of mechanical stress build up during the various drying pretreatments (Hill et al., 2012). Therefore, we assume that MSIs obtained after multiple sorption-desorption measurements would better reflect the equilibrium moisture sorption properties of samples, as a consequence of the relaxation of the internal stress.

When exploring the causes rendering the differences in moisture sorption isotherms of different samples, researchers tend to attribute these to the changes in 1) hygroscopic properties induced by protein denaturation (Paudel et al., 2015; van der Sman, 2012); 2) microstructure properties, such as loss of cell membrane integrity (Lee and Lee, 2008; Pedro et al., 2010), or 3) mechanical properties like viscoelasticity (Fredriksson and Thybring, 2018; Hill et al., 2012; Patera et al., 2016; Salmén and Larsson, 2018). However, a detailed mechanistic interpretation of these factors on moisture sorption behavior during multi-cycle dynamic vapour sorption (DVS) measurements, is still lacking.

In this work, we conducted dual cycle sorption-desorption DVS measurements on powdered dried *shiitake* mushroom samples obtained from different drying methods. Furthermore, we investigated the above mentioned factors affecting MSIs during the dual sorption-desorption cycle. The effect of protein denaturation on MSIs is illustrated via the comparison of experiments with theoretical predictions based on the Flory-Huggins theory (Jin et al., 2014;

Paudel et al., 2015; van der Sman, 2012).The cell membrane integrity of mushroom samples was identified by transmission electron microscopy (TEM). Subsequently, its effect on the MSIs of mushrooms is investigated by comparing the experimental data and the predicted MSIs calculated via the Flory-Huggins (FH) theory, while assuming cell wall and vacuole being a phase-separated system (Jin et al., 2014). We argue that overshoots observed in DVS experiments indicate the effect of stress relaxation and studied the viscoelastic properties of mushrooms via compression and stress relaxation tests on cylindrical mushroom samples with different moisture contents. Finally, we assume that the effect of stress relaxation can be explained by theory, where Flory-Rehner theory is coupled to a generalized Maxwell model, describing the viscoelastic property of the food material.

4.2 Material and Methods

4.2.1 Materials preparation

Fresh *shiitake* mushrooms were used in this study and were purchased from a mushroom farm in Beijing (China). After cutting off the stem and cleaning with tap water, mushrooms were divided into three batches on average. One batch of mushrooms was dried with a freeze dryer (abbreviated as FD) (Alpila-aplus 4Lplus, Christ Co. Ltd., Osterode am Harz, Germany) under the same conditions as described in our previous study (Hu et al., 2021); the other two batches underwent hot air drying at 35 °C, 80 °C (abbreviated as HA35, HA80) with a hot air drier (DHG-9123A, Shanghai Jinghong Experiment Facility Co., Ltd., Shanghai, China) with an air velocity of 1.2 m/s.

4.2.2 Measurement of moisture sorption isotherms on powdered dried mushrooms

Powdered dried mushroom samples (or dried mushroom powder) were obtained with a DFT-200 high-speed pulverizer (Linda, Wenling, China). The pulverization process lasted for 10 s, twice. The powder samples with relatively homogeneous particles were obtained after passing through 40 mesh sieves. Isotherms of powder samples weighing 22 mg ± 0.05 mg were determined at 25 °C with a dynamic vapor sorption analyzer (DVS) (Surface Measurement Systems Ltd., London, UK) equipped with a Cahn microbalance. Note that the powder samples were compacted on the specimen disc so that the structure of the pile of powder could be similar. Measurements were started by drying for 24 h at 0% RH, after which the RH was increased with 10% increments up to 90% RH, and then lowered again to

0% RH with 10% increments. This cycle of sorption/desorption was performed twice. A steady state was assumed when the weight change was less than 0.0005 min^{-1} over a window of 30 min. Isotherms were determined in duplicate.

4.2.3 Compression and stress relaxation test on cylindrical mushroom samples

Cylindrical mushroom samples were obtained from the cap of fresh mushrooms with a cylindrical steel tube cutter. The dimension of the fresh cylindrical samples was 10 mm ± 0.05 mm (diameter) × 10 mm ± 0.05 mm (height). These samples were dried to different moisture contents (Mc) at around 70%, 50%, 30%, and 10% (wet basis, w.b.) at 35 °C and 80 °C, respectively. Subsequently, compression stress relaxation tests were performed by TA.HD Plus Texture Analyzer (Stable Micro Systems, UK) with an AACC 36 mm cylinder probe with radius (P/36R) and Exponent 5.1.2.0 software, similar to (Myhan et al., 2015). The speed of the loading during compression was 1 mm/s. In the relaxation phase, the sample was held at constant strain (30% of the initial sample height) for 60 s. We performed ten test replications on mushrooms obtained from different drying treatments.

4.2.4 Transmission electron microscopy (TEM)

The cellular structure of fresh mushroom and powdered dried mushroom samples was observed with a Hitachi H-7500 TEM (Hitachi, Tokyo, Japan) according to the method of (Hayat, 2012). The samples were treated as described in our previous work (Qiu et al., 2021). Each piece was imaged at least six times. Here, the fresh mushroom is used as the reference showing the state of the intact cell membrane.

4.2.5 Statistical analysis

The values in tables were presented by the means ± standard deviation. Statistical analysis was performed with SPSS software (Version 18.0, SPSS, Inc., Chicago, IL, USA), using analysis of variance (ANOVA) and Tukey test. Significant differences (at the $p < 0.05$ level) were expressed with small letters a-f.

4.3. Model description

4.3.1 Moisture sorption model

In the moisture sorption model, we take into account the impact of the cell membrane

integrity of mushrooms on MSI. We view the mushroom powder with intact cell membranes as a phase-separated system, similar to our previous study (Jin et al., 2014). All solutes, such as sugars and ions, are located in the vacuole, which is considered a single-phase (Phase 1). On the other hand, all the biopolymers as proteins and fibers from the cytoplasm and cell wall, are assumed to be located in another phase (Phase 2). These phases are separated by the cell membrane (of the vacuole), whose permeability allows water to diffuse between the two phases. We assume local equilibrium between the two phases, leading to the partitioning of water over the two phases, such that the water activities of the two phases are equal. Therefore, the water activity of mushrooms with intact cell membranes follows:

$$a_{w,phase\ 1} = a_{w,phase\ 2} \tag{4.1}$$

But when the cell membrane is disrupted, the solutes from the vacuole can mix with the cell wall and cytoplasm, and hence we take the mushroom tissue as a single, homogeneous phase, with all compounds fully mixed.

The main compounds composing *shiitake* mushroom are listed in Table 4.1, with composition obtained from (Buwjoom et al., 2004; Carneiro et al., 2013; Julita Reguła, 2007; Reis et al., 2012). We display the averaged values from these data sources and list which phase they are located in (Phase 1: vacuole or Phase 2: cell wall/cytoplasm). We note that in all data sources, protein content is determined with a nitrogen-to-protein conversion factor of 4.38, which is required for the correction of nitrogen-containing chitin. The main ionic compound is potassium phosphate (KH_2PO_4) in mushrooms (Iiyama et al., 1996), which is considered that only 50% of the phosphate is soluble.

Table 4. 1 *Fraction of components in dry matter of shiitake mushrooms*

Component / Location / Content	Mannitol	Trehalose	Fiber	Protein	Ash (KH_2PO_4)
Phase1	√	√			√
Phase2			√	√	
	0.307±0.16	0.033±0.016	0.375±0.13	0.17±0.11	0.0335±0.007

Values are expressed as mean ± standard deviation

For a solution with both neutral and charged solutes, the chemical potential of water can be computed simply by adding the contributions of the involved solutes (van der Sman, 2012):

$$\Delta\mu_{tot} = \Delta\mu_{mix} + \Delta\mu_{ion} \tag{4.2}$$

$\Delta\mu_{mix}$ is the contribution of neutral solutes, and $\Delta\mu_{ionic}$ is the contribution of ions. In terms of water activity, the contributions to the water activity can be multiplied as:

$$a_{w,tot} = a_{w,mix} * a_{w,ion} \quad (4.3)$$

The contribution of neutral solutes, $a_{w,mix}$, follows the Flory-Huggins (FH) theory. The free volume contribution to moisture sorption is zero, as the glass transition temperature of fresh *shiitake* mushrooms is already lower than the room temperature (Zhao et al., 2016). The contribution of ions (ash) $a_{w,ion}$ is described by the Pitzer equation. In the cell wall/cytoplasm phase (Phase 2), ions are absent, and FH theory can be used to compute the water activity of the water/biopolymer mixture.

For the phase-separated system, the water activities are as follows:

$$a_{w,phase\,1} = a_{w,mix\_polymer} \quad (4.4)$$

$$a_{w,phase\,2} = a_{w,mix\_sugar} * a_{w,ion} \quad (4.5)$$

According to the local equilibrium between the two phases, the volume fraction of water $\phi_{w,phase\,1}, \phi_{w,phase\,2}$ are adjusted, such that equal water activities are achieved under the constraint of a constant total amount of water. For this partitioning of water, we have used the minimization procedure present in the Scipy toolbox of Python.

Flory Huggins theory for $a_{w,mix}$

Based on Flory Huggins theory (Jin et al., 2014; Paudel et al., 2015; van der Sman, 2012), the water activity $a_{w,mix}$ is:

$$ln a_{w,mix}\left(\phi_w, \chi_{eff}, N_{eff}\right) = ln\left(\phi_w\right) + \left(1 - \frac{1}{N_{eff}}\right)\left(1 - \phi_w\right) + \chi_{eff}(1 - \phi_w)^2 \quad (4.6)$$

in which ϕ_w is the volume fraction of water, which is the volume ratio of water and the sum of water and sugar, χ_{eff} is the effective interaction parameter, N_{eff} is the effective ratio of the molar volume of water versus solutes. The effective ratio of the molar volume of water versus that of the solutes (N_{eff}) is:

$$\frac{1}{N_{eff}} = \frac{\sum_i \frac{\phi_i}{N_i}}{\sum_i \phi_i} \quad (4.7)$$

ϕ_i is the volume fraction occupied by component i, N_i is the ratio of molar volumes of water and solute. For high molecular weight polymers like fiber and proteins, N_i could be 0.

χ_{eff} is the effective interaction parameter between components and water, which is given as:

$$\chi_{eff} = \frac{\sum_i \phi_i \chi_{iw}}{\sum_i \phi_i} \tag{4.8}$$

Here, χ_{iw} is the interaction parameter between component i and water, and ϕ_i is the volume fraction of component i. For trehalose and mannitol in mushrooms, the interaction parameters with water are constant with values of 0.5 and 0.37, respectively (van der Sman and Mauer, 2019). For polymers (fibers and protein), the interaction parameter is composition-dependent, which is as follows:

$$\chi_{iw} = \chi_{iw,0} + (\chi_{iw,1} - \chi_{iw,0}) * (1 - \tilde{\phi}_{w,eff})^2 \tag{4.9}$$

in which $\chi_{iw,0}$ equals 0.5, and holds universally for all bipolymers, and $\chi_{iw,1}$ is the interaction parameter with the dry polymers i, which is specific for each biopolymer. $\chi_{iw,1}$ is constant at 0.8 for fibers. For proteins $\chi_{iw,1}$ is temperature dependent due to its denaturation. Over a relatively large temperature range, it changes from 0.8 to 1.4, following a logistic (sigmoid) function (Paudel et al., 2015; van der Sman, 2012):

$$\chi_{pw,\ 1}(T) = \chi_{p1,0} + \frac{\chi_{p1,\infty} - \chi_{p1,0}}{1 + a * exp(b * (T - T_e))} \tag{4.10}$$

in which $\chi_{p1,0}$ = 0.8 and $\chi_{p1,\infty} = 1.4$ are the values attained by $\chi_{iw,1}$ when the proteins are in their native state and fully denatured states, respectively. T is the processing temperature. T_e, the mid-point of the sigmoid curve, equals 350K, which can be viewed as the protein denaturation temperature of *shiitake* mushrooms (Qiu et al., 2022). The values of a and b are 1.72 and -0.28, respectively, which is assumed similar to the values obtained for white button mushrooms (Paudel et al., 2015). Note that the irreversibility of denaturation implies that the interaction parameter retains the values according to the highest temperature experienced.

The effective water volume fraction $\tilde{\phi}_{w,eff}$ accounts for hydrogen bonding of all plasticizers present in the system, and it is defined as follows (van der Sman and Mauer, 2019):

$$\tilde{\phi}_{w,eff} = \phi_w + \sum_i \phi_{s,i} \left(\frac{N_{OH,s} v_w}{N_{OH,w} v_s}\right) \tag{4.11}$$

Here, ϕ_w and $\phi_{s,i}$ are the volume fraction of water and the solutes i, respectively. v_w and

v_s are the molar volume of water and solutes, respectively. The $\frac{N_{OH,S}}{v_s}$ represents the number of H-bonding sites effectively available within the molar volume of solutes for intermolecular interactions. The values of N_{OH} for water, mannitol, and trehalose are 2, 3.56, and 7.72, respectively (van der Sman, 2016; van der Sman and Mauer, 2019).

Pitzer theory for $a_{w,ion}$

Earlier for salted meat products, the Pitzer theory was combined with Flory Huggins Free Volume (FHFV) theory, based on the assumption of little interaction between salt and proteins (van der Sman, 2012). We take $a_{w,ionic}$ as the contribution from ash (phosphate, KH_2PO_4). In the Pitzer theory the state of electrolyte solutions is expressed in terms of the osmotic coefficient Φ:

$$(\Phi - 1) = -A_\Phi z_i^2 \frac{\sqrt{I}}{1+b\sqrt{I}} + (\beta_{ij}^{(0)} + \beta_{ij}^{(1)} exp^{-\alpha\sqrt{I}})m \tag{4.12}$$

with the relation between the osmotic coefficient and the water activity:

$$\ln(a_{w,ion}) = -\Phi * M_w \sum_i m \tag{4.13}$$

$A_\Phi = 0.391$ is the Debye factor, $Z_i = 1$ is the valency of the salt, $\alpha = 2$ and $b = 1.2$ are constants as determined by Pitzer, β_{ij}^n are parameters, which are specific for ion pairs ij. For KH_2PO_4, $\beta^0_{KH_2PO_4} = -0.0678$ and $\beta^1_{KH_2PO_4} = -0.1042$ (Pitzer and Mayorga, 1973). $I = \frac{1}{2}\sum z_i^2 m_i$ is the ionic strength on molality basis, m is the molality of the electrolyte, which is the number of mole of solute per kg of water. M_w is the molecular weight of water, 18 g/mol.

4.3.2 Viscoelastic relaxation model

A simple idealization of the viscoelastic characteristics of a material is the Maxwell model, which describes how mechanical stress changes with time:

$$\frac{d\sigma}{dt} = -\frac{\sigma}{\tau} + E_s \frac{d\epsilon}{dt} \tag{4.14}$$

τ is the viscoelastic relaxation time, ϵ is the total strain, and E_s is the elastic (shear) modulus. σ is the stress.

During the viscoelastic relaxation phase of a compression test, the total strain is constant, i.e. $\frac{d\epsilon}{dt} = 0$, and consequently, the stress relaxes via a single exponential function:

$$\sigma(t) = \sigma_0 \exp\left(-\frac{t}{\tau}\right) \tag{4.15}$$

$\sigma_0 = E_s \varepsilon_0$, ε_0 is the initial strain during the relaxation phase.

For complex materials like vegetables, a single relaxation time model is insufficient to describe their viscoelastic behavior (Ozturk, Oguz K. and Takhar, Pawan S., 2019). Hence, we have fitted the results of stress relaxation during the compression test with a stretched exponential model, also known as the Kohlraush–Slonimsky equation (Barua and Saha, 2016; Junisbekov et al., 2003).

$$\sigma(t) = (\sigma_0 - \sigma_\infty)\exp\left(-\frac{t}{\tau}\right)^{\beta} + \sigma_\infty \tag{4.16}$$

where σ_0 is the initial stress at the beginning of the stress relaxation phase; σ_∞ is the equilibrium modulus when $t \to \infty$; τ is the characteristic relaxation time. The stretched exponential model can be seen as the approximation of the fractional viscoelastic model (Simpson et al., 2013), which has been used for characterizing the viscoelastic properties of apples during drying (Mahiuddin et al., 2018). The applicability of fractional derivative models and stretched exponentials implies the existence of a broad distribution of relaxation times (Larson, 1985). Numerically, fractional derivative models are difficult to solve, therefore they are often approximated with a Prony series (Pettermann and Hüsing, 2012), which is similar to a generalized Maxwell model:

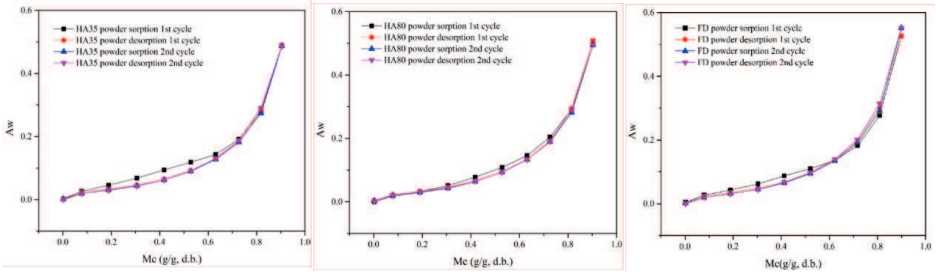
$$\sigma(t) = (\sigma_0 - \sigma_\infty)\exp\left(-\frac{t}{\tau}\right)^{\beta} + \sigma_\infty \approx \sum_1^k \sigma_i \exp\left(-\frac{t}{\tau_i}\right) + \sigma_\infty \tag{4.17}$$

4.4 Results and Discussion

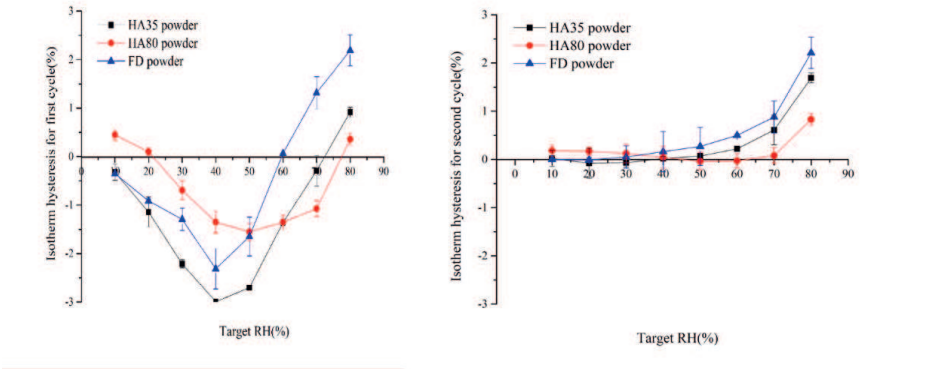
4.4.1 Sorption isotherms of powdered dried mushrooms

Fig.4.1a shows moisture sorption isotherms of powdered mushrooms with different drying treatments, obtained from dual sorption-desorption cycle measurements. One can observe the hysteresis between the sorption and desorption branches of the first cycle isotherms (with their difference shown in Fig.4.1b). The hysteresis phenomenon is also reported in previous studies for mushrooms (Argyropoulos et al., 2010; Pascual-Pineda et al., 2020). When mushroom samples were subjected to a second sorption-desorption cycle, we found that hysteresis was reduced for all drying treatments. Similarly, Keating et al. (2013) reported that hysteresis vanished in man-made hemicellulose (galactomannan) films above 75% RH at 25 °C and attributed it to the softening of the hemicelluloses at this humidity. Hill et al.(2012)

found a significant decrease in the sorption hysteresis for wood during the second and third cycles. The given explanation for this hysteresis reduction is the relaxation of internal stresses during the adsorption branch of the first cycle (Hill et al., 2012; Hill et al., 2009; Kohler et al., 2003). These studies induced our assumption that MSIs of dried mushroom samples obtained from multiple sorption-desorption measurements present the real moisture sorption equilibrium. Moreover, all second-cycle MSIs of the samples with different drying treatments largely overlap, as shown in Fig.A4.1b. This makes us confident that all samples have reached a similar equilibrium, irrespective of their drying pretreatments. We note in Fig.4.1b right, there are still differences in the high water activity range. We assume these differences are not attributed to the hysteresis but to the water holding capacity (WHC) differences.



(a)



(b)

Fig.4.1. *MSIs (a) and hysteresis (b) for HA35, HA80, and FD dried shiitake mushroom powders (b left: first sorption-desorption cycle; b right: second sorption-desorption cycle)*

4.4.2 Effect of protein denaturation on MSI interpreted with Flory-Huggins theory

In this section, we analyze the effect of protein denaturation on moisture sorption isotherms on 1) the hysteresis observed during the first sorption-desorption cycle and 2) the hysteresis variation in the "equilibrium" MSI between treatments as observed during the second cycle. One of the starting hypotheses was that hysteresis might be caused by protein denaturation. From the observation of MSIs for HA80 samples, we observe hysteresis during the first sorption-desorption cycle, which is almost reduced to zero during the second sorption-desorption cycle. We note that protein denaturation happened only in HA80 and FD treatments (due to cold denaturation). Given the mild product temperatures during HA35 treatment one can safely assume that the proteins remain in the native state. Protein denaturation happening at high temperatures, as during HA80, is commonly assumed to be irreversible, i.e. the protein will not fold back to the native state. Concerning the FD we note that in literature, there is no consensus on whether cold denaturation is (ir)reversible (Lau et al., 2013). Hence, we know for certain that the proteins have not changed their state during the DVS experiments of HA35 and HA80 samples. Consequently, we cannot attribute the hysteresis reduction to the protein denaturation, as the protein remained denatured throughout the DVS experiment.

Furthermore, we give an analysis based on the second-cycle MSIs of HA35 and HA80 dried samples. The protein denaturation degree can be quantified by the temperature-dependent interaction parameter between protein and water (van der Sman, 2012), based on FH theory. It is noted that after HA drying ($T > 35$ °C), the (partial) protein denaturation is irreversible (Baltacıoglu et al., 2015), implying that the interaction parameters between water and protein remain at the values of χ as imposed by the drying treatment. As depicted in Table 4.2, we calculated the interaction parameters ($\chi_{pro,w}$ and χ_{pro,w_1}) between protein and water according to Eq.4.10, assuming that product temperature has reached drying temperature at the end of drying. We found that the interaction parameters increased promptly when the drying temperature was over 80 °C. Coincidentally, the protein denaturation temperature of *shiitake* mushrooms was measured to be as high as 76 °C (Qiu et al., 2021), meaning the interaction parameter can quantitively describe the denaturation degree. Variation of the interaction parameters for samples obtained from different drying temperatures indicates the protein denaturation is supposed to affect the moisture sorption. Then we applied the FH theory model to predict the MSIs obtained at 35 °C and 80 °C. The predicted MSIs are comparable to the experimental curves measured during the second sorption-desorption cycle.

Thus, our calculations can accurately predict the equilibrium sorption isotherm (second cycle). However, a very limited difference is found between both predicted and measured MSIs of HA35 and HA80 dried samples, as shown in Fig.4.2. Consequently, we tend to conclude that protein denaturation should not be the cause for hysteresis reduction but present some influence on the equilibrium moisture sorption of mushrooms.

Table 4.2 Calculated interaction parameters of protein for shiitake mushroom

Temperature / Parameter	35℃	50℃	65℃	80℃
χ_{pro,w_1}	0.800	0.800	0.809	1.103
$\chi_{pro,w}$	0.734	0.734	0.741	0.970

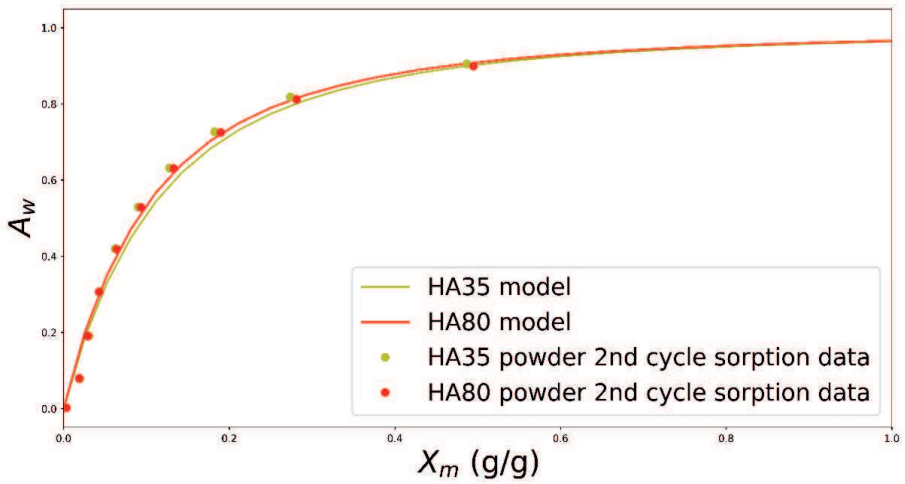


Fig.4.2. *Predictions and experimental data of sorption isotherms for HA35 and HA80 dried mushroom powders at 25 °C*

4.4.3 Effect of cell membrane integrity on MSI

4.4.3.1 Cell membrane integrity of mushrooms

The fate of cell membrane integrity due to the different drying methods of HA35, HA80, and FD was first investigated with transmission electron microscopy (TEM). Note, our dried samples were milled to powders to allow fast MSI measurements. As shown in Fig.4.3, when taking the TEM images of fresh mushrooms as the reference, we found that HA35 dried

powder samples retained intact cell membranes, while HA80 and FD dried ones present severe plasmolysis, cell membrane damage, and cell wall distortion. These results were consistent with our previous study (Qiu et al., 2021; Qiu et al., 2022). Cell membrane rupture might be due to the denaturation of membrane proteins, or the (liquid crystal/gel) phase transition of membrane lipids (Lewicki and Pawlak, 2003, 2005; Voda et al., 2012). Besides, there is an interesting finding from the intact cell membrane of HA35 dried samples; namely, no damage happens on the cell membrane during milling.

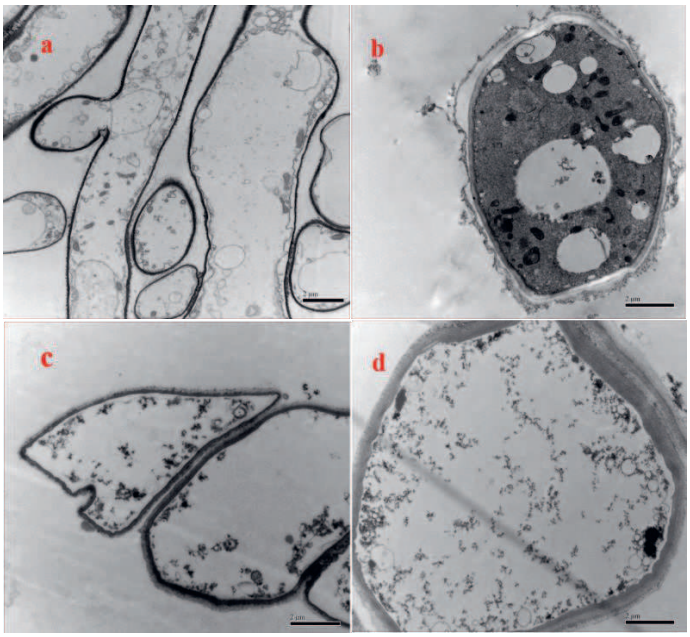


Fig.4.3. *TEM of mushroom samples(a: fresh mushroom; b: HA35 dried powder; c: HA80 dried powder; d: FD dried powder)*

4.4.3.2 Effect of cell membrane integrity on MSI interpreted with theory

As in the previous section, we first investigate the possible effect of cell membrane rupture on hysteresis. Likewise, cell membrane rupture is irreversible processes, happening at elevated temperatures (T>45 °C) (Hu et al., 2021), or during freezing (van der Sman, 2020). Hence, we can follow a similar line of reasoning concerning its effect on hysteresis. For there is no change in the state of the cell membrane during the DVS measurements, the hysteresis reduction during the second sorption-desorption cycle cannot be attributed to the loss of cell membrane integrity.

To evaluate the effect of cell membrane integrity on the “equilibrium” moisture sorption

isotherms, we compared theoretically calculated moisture sorption isotherms with experimental ones obtained from the second sorption-desorption cycle measurement. We assume all ingredients in the mushroom powder with ruptured membranes constitute a single, homogeneous mixed phase. While ingredients in the powder with intact membranes constitute a two-phase system, with solutes in the vacuole representing one phase, and the biopolymers existing in the cell wall and cytoplasm representing a second phase. The two-phase system is separated by the (vacuole) membrane, which allows the partitioning of water between phases until equilibrium is reached. Therefore, the HA35 dried sample having an intact cell membrane can be seen as a phase-separated system, while FD and HA80 dried samples presenting a ruptured cell membrane should be taken as a mixture system. Considering the more even distribution of ingredients in FD samples than that in HA80 ones (shown in Fig.4.3), we compared the measured second cycle MSIs of HA35 and FD samples with the predicted ones based on two-phase system and mixed system model, as shown in Fig.4.4. We observe little difference between the predictive MSIs of the two systems. Similarly, when the relative humidity is lower than 70% ($a_w < 0.7$), there is little difference in measured second-cycle MSIs between the HA35 and FD samples.

However, at high relative humidity ($a_w > 0.7$), the experimental data shows differences in water holding capacity (WHC) between HA35 and FD samples (shown in Fig.4.1b right). This difference could be due to the variation in cell membrane integrity, in which intact cell membranes can restore the water holding in the vacuole and thus the turgor pressure via the stretching of the cell walls. Furthermore, we assume this stretching, which indicates elastic properties of samples, after the cell membrane restoration varies with different drying treatments. For example, during freeze-drying, cell walls are compacted firmly, leading to an increase in crosslink density and elasticity (Voda et al., 2012). Therefore, from the theoretical and experimental evaluation, we conclude that the state of cell membrane integrity mainly affects the moisture sorption of mushroom samples due to its contribution to water holding capacity.

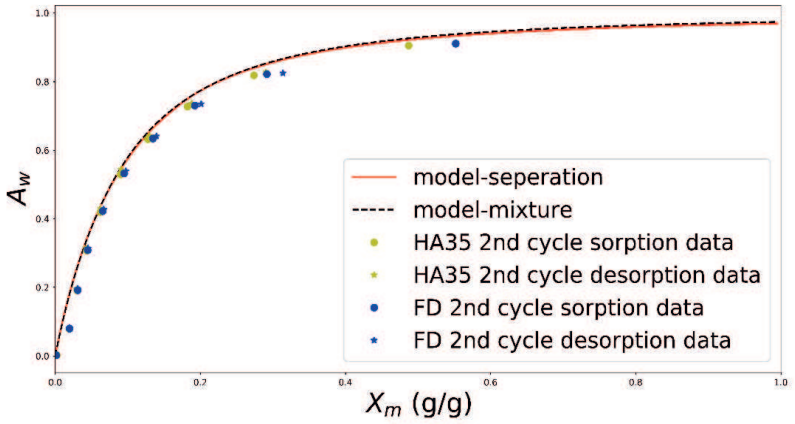


Fig.4.4 *Predictions and experimental data of sorption isotherms for HA35 and FD dried mushroom powders at 25 °C*

4.4.4 Effect of mechanical stress relaxation on MSI

Mechanical stress within the matrix has been reported in studies related to hydration (van der Sman et al., 2013b), and it is considered an important cause affecting the moisture sorption of samples at high water activities (Cornet et al., 2020; Hill et al., 2012; Paudel et al., 2015; Xie et al., 2011; Ying et al., 2013). (van der Sman et al., 2013b) presented the contributions from the elastic energy of the crosslinked network of cell wall materials to the hydration properties of carrots and mushrooms, which follows the Flory-Rehner theory. Other researchers pointed out that the viscoelastic properties could affect the moisture sorption via the stress relaxation (Champion et al., 2011; Hill and Xie, 2011; Oliver and Meinders, 2011; van der Sman and Meinders, 2011). Note that there can still be differences in moisture sorption if differences exist in pure elastic properties. Gels with different degrees of crosslinks will give a difference in moisture content at the same water activity, as described by Flory-Rehner theory. Therefore, the pure elastic properties should also be considered as equilibrium properties.

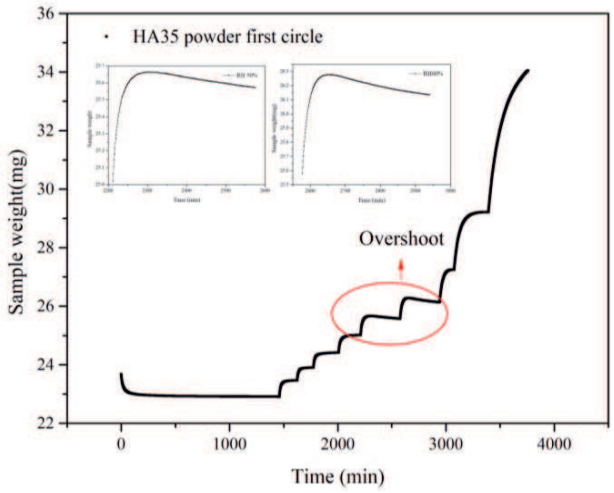
Many cellular food materials exhibit viscoelastic properties, such as strawberries, carrots, and apples, whose mechanical properties have been shown to be moisture and temperature-dependent (Mahiuddin et al., 2018; Ozturk, Oguz K. and Takhar, Pawan S., 2019; Ozturk, Oguz Kaan and Takhar, Pawan Singh, 2019). We note there is an interaction between water holding capacity, mechanical stress and cell membrane integrity. The cell wall can be considered a biopolymer network, and it provides structural rigidity under turgor conditions (Doulia et al., 2000; Veytsman and Cosgrove, 1998). At high a_w, solutes in the vacuole attract

water, and the volume expansion stretches the cell wall, rendering the turgor pressure (Veytsman and Cosgrove, 1998). The high turgor pressure makes the cell wall stretch, rendering high tensile stress due to cellulosic fibers. A requirement for maintaining the turgor pressure is the integrity of the cell membrane, which inhibits solutes from diffusing out from the vacuole. When the cell membrane of samples remains intact after drying, the vacuole will grow after absorbing water (rehydration or sorption) and the turgor recovers, and the cell wall will be stretched again, resulting in the rebuilt-up of stress and structural integrity. However, suppose the cell membrane integrity is lost during drying, the solute will diffuse out of the vacuole during rehydration (Gekas et al., 1993), and the cell wall will not be stretched, thus without stress build up.

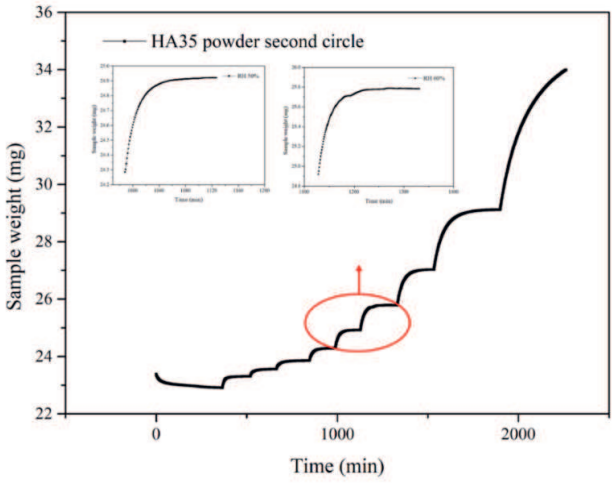
Hence, studying the viscoelastic properties of the cellular food matrix, which can also be caused by the cell membrane integrity change, provides valuable insights into its possible influence on MSI variations due to different processing histories.

4.4.4.1 Overshoot during dynamic vapor sorption

The occurrence of mechanical stress relaxation during moisture sorption of mushrooms is evident by the presence of overshoot in the dynamic responses, as measured by DVS (Oliver and Meinders, 2011). In Fig.4.5 we use HA35 dried mushrooms as an example and display typical dynamic moisture sorption curves obtained by DVS. The curve shows the sample weight varies with the environmental RH as a function of time. During the first cycle of moisture sorption measurement, several samples exhibit overshoots, i.e. the sample weight shows an initial increase while decreasing at a later stage, as depicted with the subgraphs in Fig.4.5a. Similarly, (Oliver and Meinders, 2011) also observed overshoots during the moisture sorption of gluten and starch films. They attributed it to the viscoelastic relaxation of the biopolymers. However, during the second cycle of sorption-desorption, the overshoots and the hysteresis disappear (as shown in the subgraphs of Fig.4.5b and in Fig.4.1b). Also, for the mushrooms, we assume the overshoot (and hysteresis reduction) is due to the stress relaxation during each RH step. At the end of the first sorption cycle, $T > T_g$, the sample eventually completes the relaxation of the stresses, leading to the absence of overshoots during the second cycle. Below, we will show experimentally that mushrooms indeed exhibit viscoelastic properties, enabling stress relaxation.



(a)



(b)

Fig.4.5. *The kinetic data obtained during the first (a) and second cycle (b) MSI measurements for HA35 dried mushroom powder*

4.4.4.2 Viscoelastic properties of mushrooms with different moisture contents

Since the viscoelastic property at the length scale of mushroom powder (micron scale) is hard to measure, we take a convenient way to measure the stress relaxation of mushroom powder via the compression and stress relaxation test on cylindrical mushroom samples. As shown in Fig.4.6, we examined the viscoelastic properties of cylindrical mushroom samples with different moisture contents obtained during hot air drying at 35 °C and 80 °C. It shows that

the stress-time curve mainly consists of two phases: compression and stress relaxation. During compression, all samples showed an increase in stress until the compression reached the expected strain. Subsequently, the stress gradually decreases over time in the relaxation phase, while holding the sample at the defined strain. This relaxation phase indicates the viscoelastic (stress relaxing) property of mushrooms.

In this study, we are mainly concerned about the initial and residual stress and the relaxation time (distribution) of cylindrical mushroom samples during the stress relaxation phase. It shows that all these parameters vary with moisture content. We observe decreasing initial stress in the range of moisture content (MC) larger than 0.91 g/g (d.b.) for HA35, and MC larger than 0.64 g/g (d.b.) for HA80. However, for smaller MC the initial stress increases again. A similar initial decrease of stress (relaxation modulus) was also found for apples, strawberries, and carrots using similar compression tests (Mahiuddin et al., 2018; Ozturk, Oguz K. and Takhar, Pawan S., 2019; Ozturk, Oguz Kaan and Takhar, Pawan Singh, 2019). Besides, it was also observed that the stress of carrots (relaxation modulus) increased again at low moisture contents. This range was not measured for strawberries or apples. The initial decrease of stress/relaxation modulus could be attributed to the turgor loss. The latter can be either due to the rupture of the cell membrane (as in the case of HA80), or the loss of stretching in the cell wall and possible plasmolysis (without rupture of the cell membrane, as in the case of HA35) (Prawiranto et al., 2018). This leads to the softening of the structure and the lowering of the stress levels (Ozturk, Oguz K. and Takhar, Pawan S., 2019). However, when the moisture contents of mushrooms drop below 0.91 g/g (d.b.), the stress increases, which can be attributed to the loss of the plasticization action of water of the cell wall material, similar to those studies given by (Ozturk, Oguz K. and Takhar, Pawan S., 2019).

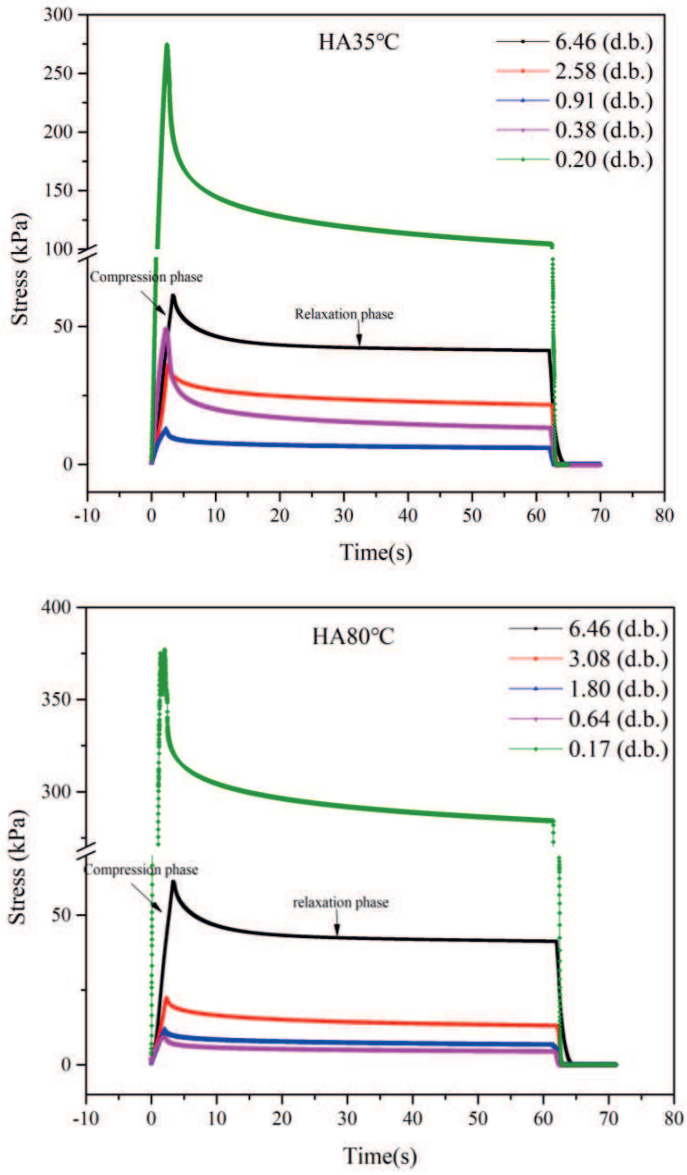


Fig.4.6. *Stress relaxation curves of cylindrical mushroom samples with different moisture contents during HA35 and HA80 drying*

4.4.4.3 Stress relaxation effect on MSI interpreted with viscoelasticity

The response of mushrooms in the stress relaxation phase cannot simply be described with a single relaxation-time Maxwell model, as evident by the long tailing of the stress relaxation.

As indicated by the use of the fractional derivative model by (Mahiuddin et al., 2018), there is a distribution of relaxation times. A fractional derivative model can be approximated by the stretched relaxation model Eq. (4.17). A detailed exposition of fractional viscoelastic models can be referred to (Katicha and Flintsch, 2012; Mainardi and Spada, 2011). The fitting plots of stress-time curves during the relaxation phase fitted with the stretched exponential model are shown in Figs.A4.2-A4.4. The values of $\boldsymbol{\sigma_0}$, τ, β, σ_∞ are given in Table 4.3, which were averaged from the fitting of stress-time curves with the stretched exponential model.

The initial stress (σ_0) and residual stress (σ_∞) during the compression phase of samples treated by HA35 and HA80 present the same trend as illustrated in 4.4.2. According to (Rathinaraj et al., 2022), the value of fractional order (similar to β) of about 0.3 indicates a broad distribution of relaxation times, meaning that some fraction of the stress takes a very long time to relax, as indicated by the long tailing in the stress relaxation. The power (β) of stretched exponential for most samples is quite similar, although these samples show different moisture content. This is consistent with similar exponents of the fractional model from the study conducted by (Mahiuddin et al., 2018). In theory, one can expect that both powers are similar for different moisture contents and temperatures. The residual stresses σ_∞, which will not relax, remain to give an elastic contribution to the chemical potential.

There are two kinds of elastic contributions in the moisture sorption of food. The first case is when the food material is in a glassy state, it has become elastic, with a prolonged structural relaxation time. Hence, it behaves as an elastic solid. Traditionally, this elastic contribution is described by the Free Volume extension of the FH theory, but it might also be replaced by a description similar to Flory-Rehner. The Leibler-Sekimoto model is an example of such a model that takes the elastic contribution of the glassy state into account (Leibler and Sekimotot, 1993). The second case is when the food material consists of a cross-linked biopolymer network in the rubbery state. Its moisture sorption/water holding behaviour is described by the Flory-Rehner theory, which is another extension of the FH theory (van der Sman et al., 2013a). Flory -Rehner theory learns that elastic stresses need to be accounted for in the chemical potential of water (Gosline, 1978; van der Sman, 2012):

$$\Delta\mu_{w\_poly} = \Delta\mu_{w,mix} + \Delta\mu_{w,elastic} = \nu_w(-\Pi_{mix} + \Pi_{elastic})$$

with ν_w the molar volume of water. The last term equals the elastic stress:

$\Pi_{elastic} = \sigma$

Initially, Flory-Rehner theory assumes a purely elastic material at large deformations. Mushrooms are viscoelastic materials as illustrated above, indicating the exist of elastic stress contribution to the moisture sorption. Hence, the above equation for the chemical potential of water still holds. However, based on the viscoelastic properties of mushrooms shown in study, we assume the stress relaxation effect on MSI should be coupled to the FH theory with a viscoelastic model, like the (generalized) Maxwell model that can describe the stress relaxation with time and has a distribution of relaxation times. The elastic modulus and relaxation time are, in general, temperature and moisture dependent as shown above. Furthermore, the generalized Maxwell model would need adaption to large deformations (van der Sman, 2015).

Table 4.3 *Elastic modules and parameters obtained from the fitting curves at different moisture contents (drying at 35,80 °C).*

Samples	Moisture content Mc (d.b.)	Initial stress σ_0 (kPa)	Relaxation time τ (s)	Power β	Residual stress σ_∞ (kPa)	Coefficient of determination R^2	Root Mean Square Error RMSE
Fresh	6.46 ±0.23	61.23 ±4.35^{d}	3.36 ±0.048^{cd}	0.56 ±0.032^{a}	41.31 ±15.89^{c}	0.9987	0.1141
HA 35	2.58 ±0.32	36.17 ±0.3^{d}	12.5 ±0.0089^{f}	0.31 ±0.056^{b}	17.06 ±2.15^{d}	0.9988	0.08623
	0.91 ±0.14	12.86 ±2.43^{d}	2.17 ±0.061^{c}	0.25 ±0.0029^{b}	4.83 ±0.81^{e}	0.9928	0.07985
	0.38 ±0.031	49.17 ±6.59^{c}	0.78 ±0.051^{a}	0.3 ±0.001^{b}	12.52 ±1.12^{de}	0.9840	0.5430
	0.2 ±0.032	274.62 ±19.83^{a}	1.45 ±0.029^{c}	0.26 ±0.0037^{b}	86.19 ±7.42^{b}	0.9912	2.0578
HA 80	3.08 ±0.081	22.32 ±4.95^{d}	15.8 ±0.079^{f}	0.36 ±0.28 ^{ab}	10.47 ±3.42^{de}	0.9998	0.02072
	1.8 ±0.1	11.86 ±2.37^{d}	9.09 ±0.023^{ef}	0.25 ±0.053^{b}	4.79 ±1.00^{e}	0.9976	0.039
	0.64 ±0.04	9.35^{d} ±2.92^{d}	5.00 ±0.047^{de}	0.25 ±0.0071^{b}	3.6 ±0.37^{e}	0.9977	0.0310
	0.17 ±0.03	377.09 ±0.72^{b}	1.35 ±0.086^{b}	0.21 ±0.022^{b}	267.37 ±18.77^{a}	0.9843	1.31

Values are mean ± standard deviation, values in the same column followed by different superscript letters are significantly ($p<0.05$) different.

4.5. Conclusion

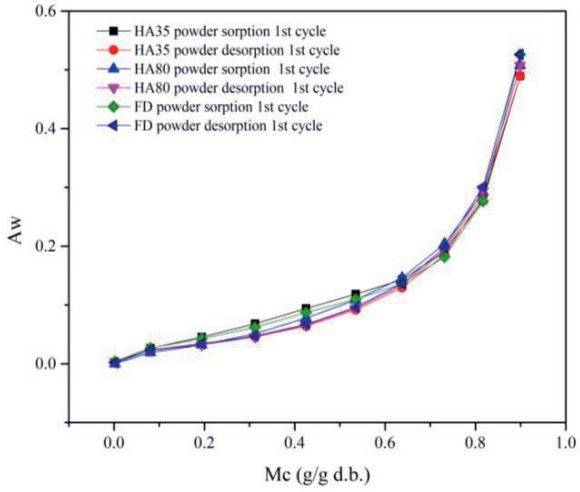
Different drying treatments (HA35, HA80, and FD) performed on mushrooms have led to different moisture sorption characteristics of dried mushroom powder, like the variation of hysteresis between the sorption and desorption branches of the isotherm. Hysteresis was reduced when the powdered dried mushroom samples were subjected to a second sorption-desorption cycle. Similar to (Oliver and Meinders, 2011), we pose that the hysteresis reduction is caused by the viscoelastic relaxation of the stress, that was built up during the drying treatments. We showed that neither protein denaturation nor cell membrane integrity significantly affect hysteresis. Retention of cell membrane integrity did influence the moisture sorption of dried mushroom samples in the high RH range, where it influences WHC. Furthermore, it helps restore turgor, and improved rehydration of mildly dried products, as shown in our previous study (Hu et al., 2021; Hu et al., 2022). Hence, retention of cell membrane integrity should be considered when designing drying systems for products aiming at high-volume recovery after rehydration. Severe drying conditions as HA80 lead to compacted cellular tissues, with high levels of stresses locked in after drying. The stress will relax away slowly, inhibiting restoration of initial microstructure during rehydration (Quang T. Ho et al. 2013; Voda,2012). For a quantitative description of drying processes, aimed at their design or optimization, one should incorporate the build-up of mechanical stresses due to the shrinkage of food materials during drying, their viscoelastic relaxation, and the inclusion of elastic stresses in driving forces of moisture sorption. This can be accomplished by modeling the stress via integration of the momentum balance, coupled to a viscoelastic constitutive model (generalized Maxwell) for the stress, and inclusion of this time-dependent stress in the Flory-Rehner theory, rendering the driving force for moisture transport (i.e. chemical potential of water).

Appendix 4

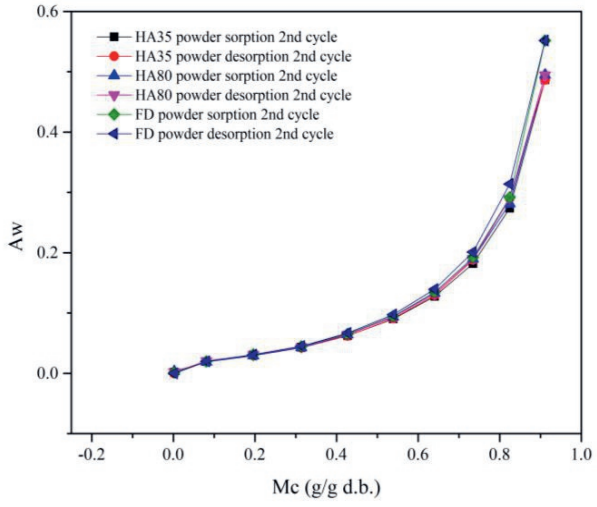
Supplementary data

Supplementary data to this article can be found online at:

https://doi.org/10.1016/j.jfoodeng.2023.111506



(a)



(b)

Fig. A4.1. *Comparison of MSIs measured from first (a) and second (b) cycles sorption-desorption for HA35, HA80, and FD dried mushroom powders at 25 °C*

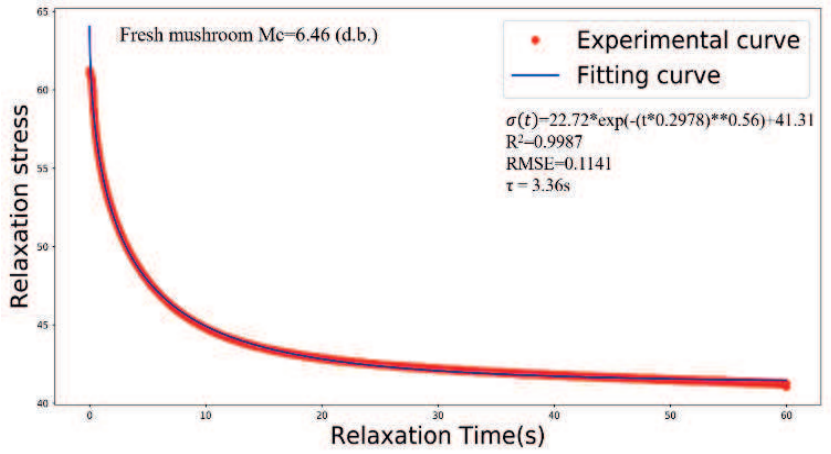


Fig. A4.2. *Experimental relaxation curve fitting with a fractional viscoelastic model for cylindrical fresh mushroom samples*

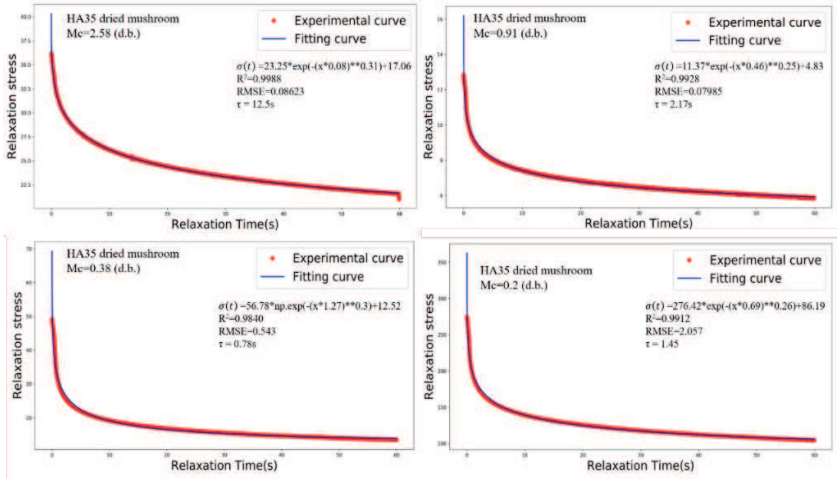


Fig. A4.3. *Experimental relaxation curve fitting with the fractional viscoelastic model for cylindrical mushroom samples with different moisture contents (MC) dried with hot air drying at 35 °C (HA35)*

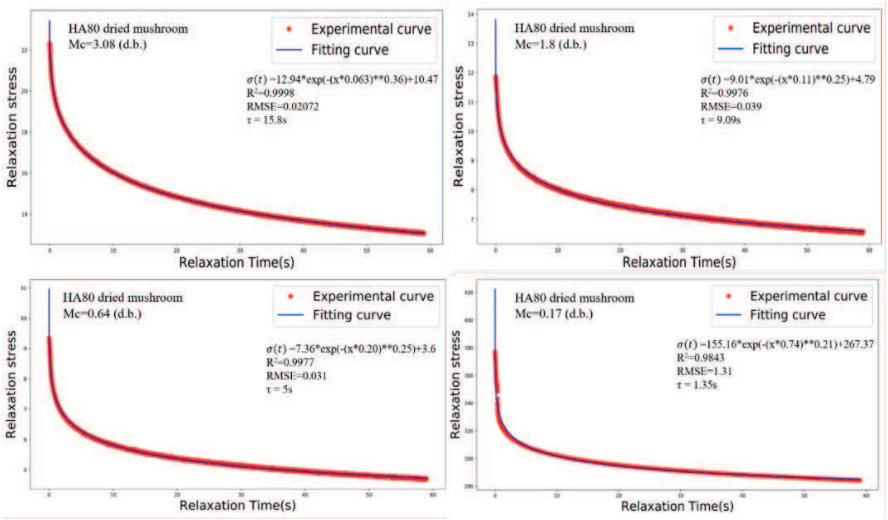


Fig. A4.4. *Experimental relaxation curve fitting with the fractional viscoelastic model for cylindrical mushroom samples with different moisture contents (MC) dried with hot air drying at 80 °C (HA80)*

Chapter 5

A multiphase and multiscale mechanistic model for hot air drying of *shiitake* mushroom

This chapter has been published as Hu, L., Jin, X., Xie Y., & Bi, J, van der Sman, R. G. M. (2026). A multiphase and multiscale mechanistic model for hot air drying of *shiitake* mushroom, Current Research in Food Science,12,101296 https://doi.org/10.1016/j.crfs.2025.101296

Abstract

A mechanistic multiphase, multiscale model is proposed to simulate mushroom drying, incorporating shrinkage, Flory-Huggins theory for water activity, viscoelasticity, alongside the heat and mass transfer. The model describes moisture and temperature evolution, capturing unique features of mushroom drying dynamics, such as sustained internal evaporative cooling, and a rapid increase in product temperature near the end of drying. This model enables the interpretation of T_2 NMR investigations of drying, thereby revealing the conditions for the loss of cell membrane integrity. By integrating conductivity and NMR data, critical thresholds for maintaining cell membrane integrity were identified. The findings support further optimization of serial drying processes, while preserving membrane integrity for optimal rehydration.

5.1. Introduction

Drying is a critical process for preserving the quality and extending the shelf life of *shiitake* mushrooms. However, it involves complex thermo-hydro-mechanical phenomena that affect final product properties, particularly the rehydration capacity. Currently, conventional optimization approaches of drying in the industry, particularly when adjusting factors such as air temperature, humidity, and velocity, are labor-intensive and energy-demanding. Mechanistic modeling offers an effective alternative, enabling detailed simulations of spatial temperature and moisture distributions. Such models provide insights that may be challenging to obtain directly from experiments (Castro et al., 2018). Compared with empirical methods, mechanistic modeling allows for the investigation of the individual roles of various transport mechanisms (Jiang et al., 2017). While numerous studies have focused on identifying empirical drying models that fit mushroom drying data (Dinani et al., 2014; Guo et al., 2014; Hou et al., 2024; Peter et al., 2021; Tran et al., 2020), few have systematically examined the underlying physical mechanisms. In contrast, mechanistic drying models have been well developed for other food materials, providing valuable insight into heat and mass transfer processes (Adduci et al., 2024; Castro et al., 2018; Datta et al., 2022; Datta, 2007a, b; Halder et al., 2011; Hou et al., 2020). Although a multiphase porous media model with coupled thermo-hydromechanical phenomena has been proposed for mushroom drying (Zhu et al., 2021), it has not yet incorporated physical aspects, such as changes in cell membrane integrity and viscoelastic properties during drying.

In previous studies (Hu et al., 2021; Hu et al., 2022, 2023), it was demonstrated that cell membrane integrity, which is closely linked to temperature and moisture content, critically governs the rehydration quality of dried *shiitake* mushrooms. In drying models, the relationship between water activity and moisture content, which is typically represented by moisture sorption isotherms (MSIs), is critical. For cellular food materials, both viscoelastic relaxation and cell membrane integrity have been reported to influence moisture sorption behavior (Fredriksson and Thybring, 2018; Hill and Beck, 2017; Hill et al., 2012; Lee and Lee, 2008; Patera et al., 2016; Pedro et al., 2010; Salmén and Larsson, 2018). For mushrooms, it has been found that viscoelastic relaxation contributes to sorption hysteresis, while the cell membrane integrity affects the water-holding capacity at high relative humidity (Hu et al., 2023). Therefore, incorporating viscoelastic relaxation into drying models can enhance the understanding of the heat and mass transfer phenomena during mushroom drying. To understand the changes in cell membrane integrity during drying, it necessitates an accurate knowledge of temperature and moisture evolution, which can be predicted with the drying

model and hence supports rational drying design and efficient optimization.

To predict moisture sorption isotherms, theoretical composition-based models, such as the Flory-Huggins Free Volume theory (FHFV), have been developed, which can then be integrated into drying models (Hu et al., 2023; Jin et al., 2014; Oliver and Meinders, 2011; van der Sman, 2013). In these models, the complex cellular structure of plant foods is approximated as two coexisting thermodynamic phases: one containing all biopolymers (cytoplasm and cell wall) and the other containing all solutes (vacuole), separated by a cell membrane. The membrane restricts solute transport but allows moisture exchange, with water partitioning determined by the local equilibrium (equal water activity in both phases) (Jin et al., 2014). Low-Field Nuclear Magnetic Resonance (LF-NMR) can identify distinct water populations within cells by measuring the transverse relaxation time (T_2), as water molecules in different chemical environments exhibit different T_2 values, with higher T_2 values corresponding to more mobile water, and lower T_2 values indicating less mobile water (Qiao et al., 2005 ; Xu et al., 2017; Zhang and McCarthy, 2012). The two thermodynamic phases in mushrooms may be identified by different peaks in the NMR relaxation time spectrum, potentially indicating the cell membrane integrity during drying.

The aim of this study is to develop a mechanistic model to examine mushroom drying processes, explicitly accounting for the complex heat and mass transfer phenomena within their porous structures. The model aims to be mechanistic, as much as possible, by incorporating: 1) a composition-based moisture sorption isotherm derived from the Flory-Huggins theory, considering cellular structure, stress effects, and viscoelastic relaxation; 2) a mechanistic description of moisture diffusion through bound water and the gas phase; and 3) thermal conductivity based on composition and porosity. Although ideally, deformation and stresses can be modelled by solving momentum balances, current theories for the large deformation of highly porous materials with high connectivity, such as mushrooms, are insufficiently developed (van der Sman et al., 2024). Therefore, an empirical approach was used with the assumption of ideal shrinkage of the solid (hyphae) phase and an empirical relationship between the porosity and moisture content (dry basis). The drying model was fitted to the experimental drying data at temperatures of 33°C, 38°C, and 51°C. The model was validated by experiments performed at 35°C. Furthermore, to validate the thermodynamic states of the two distinct water phases, which are critical for understanding cell membrane integrity, T_2-NMR measurements were performed on mildly dried mushroom samples. This experimental insight allowed the drying model to be applied to interpret earlier T_2 relaxation data for mushrooms dried at 30 °C, 40 °C, and 50 °C (Qiu et al., 2021). The T_2-

NMR data, which revealed the presence of one or two water populations, were integrated into an earlier state diagram based on conductivity measurements. This combined analysis helped identify the critical conditions associated with the loss of cell membrane integrity.

5.2. Theory model for aw prediction of viscoelastic mushroom

In this section, an improved theoretical model that accounts for viscoelastic properties was introduced to predict a_w. This model also describes the viscoelastic relaxation modes of mushrooms during drying.

5.2.1 The thermodynamic phase-separated system of mushroom

Mushrooms consist of hyphae, which resembles plant cells, containing cell walls and vacuoles. Water is partitioned among the cell wall, cytoplasm, and vacuole. As shown in Fig.5.1, the hypha of a mushroom is approximated as a thermodynamic phase-separated system, following (Jin et al., 2014). All solutes, including sugars (such as mannitol and trehalose) and ions, were localized in the vacuole and designated as **Phase1**. In contrast, all biopolymers, such as proteins in the cytoplasm and fibers in the cell wall, were assumed to reside in **Phase 2**. In principle, the cell wall and cytoplasm are separated by the cell membrane. However, as the cytoplasm and cell wall consist of biopolymer networks, they can be aggregated into a single phase with the same water activity (a_w). These two phases are separated by the cell membrane (of the vacuole), which allows water to diffuse between but prevents solute transport, provided that the membrane remains intact. Likewise, a local equilibrium can be achieved between the vacuole and biopolymer phases, with water partitioned over the two thermodynamic phases, such that their water activities are equal. Therefore, the water activity of mushrooms with intact cell membranes is as follows:

$$a_{w,1} = a_{w,2} \tag{5.1}$$

The water activity in each phase was calculated based on the composition of the respective phases. The main compounds in *shiitake* mushrooms have been reported in the previous work (Hu et al., 2023), and their details are given in the Table. A5.1 in the **Appendix 5 (Section A5.1.1)**. The fraction of water in each phase was determined via minimization procedures solved for the partitioning of a fixed amount of water, which adhered to the condition $a_{w,1}=a_{w,2}$.

The chemical potential of water in each phase, $\Delta\mu_{w,i}$, can be expressed as:

$$\Delta\mu_{w,i} = RTlna_{w,i} = \Delta\mu_{w,mix,i} + v_w p \tag{5.2}$$

where i indicates Phase1 (vacuole) or Phase 2 (cytoplasm and cell wall). The term $\Delta\mu_{w,mix,i}$ varies in each phase owing to differences in composition, following the Flory-Huggins theory. The constitutive relations and parameters for $\Delta\mu_{w,mix}$ have been provided in the previous publication (Hu et al., 2023). In contrast to existing moisture sorption models, an extra term, $v_w p$, is incorporated to account for the influence of osmotic pressure ($p, J/m^3$). This pressure arises from the attraction of water by the solutes present in the vacuole. v_w (m^3/mol) is the molar volume of water. The consequent cell volume expansion is hindered by the elastic cell wall, which encapsulates the cells, including the outer cell membrane. The cell wall is stretched, which renders mechanical stress and counter (turgor) pressure acting against cell expansion. At equilibrium, the turgor pressure is equale to the osmotic pressure inside the cell. Hence, in the case of phase2, $v_w p = -\Delta\mu_{elastic}$ is assumed owing to the elastic stress. Assuming isotropic deformation, the stress is represented by a scalar $\Pi_{elastic}$, yielding the stress tensor $\boldsymbol{\sigma} = -\Pi_{elastic}\boldsymbol{I}$ ($\boldsymbol{I}$ = identity tensor). The elastic chemical potential change is $\Delta\mu_{elastic} = v_w \Pi_{elastic}$ (v_w = molar volume of water). Based on the Flory-Rehner theory, $\Pi_{elastic}$ depends on the relative volume change $J = \frac{1}{\tilde{\varphi}} = \frac{\varphi_s}{\varphi_{ref}}$ (φ_s = polymer volume fraction, φ_{ref} = reference state) (van der Sman, 2023). For non-uniform large deformations, the displacement is characterized by the stretch parameter λ_i (total deformation in principal direction i). Simplifying with isotropic cell wall deformation and hydrogel incompressibility, $\frac{1}{\tilde{\varphi}} = \lambda^3$ ($= \lambda_i$). Note, at reference state ($\lambda = 1$, $\varphi_s = \varphi_{ref}$), the viscoelastic stress $\boldsymbol{\sigma}$ vanishes (van der Sman, 2023).

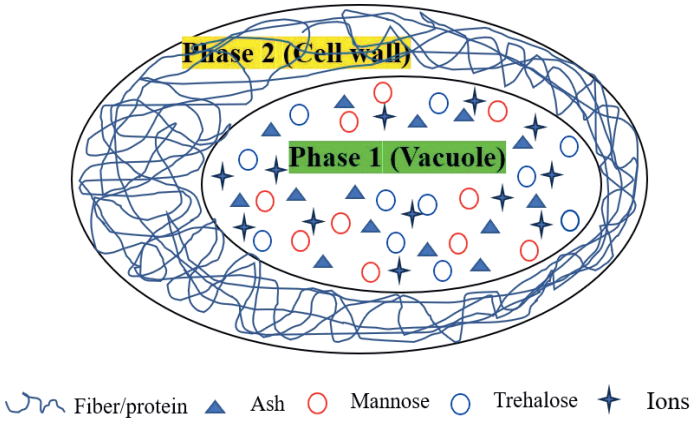


Fig.5.1. *The thermodynamic phase-separated system of hypha in mushroom*

5.2.2 Viscoelastic relaxation modes for mushrooms

The elastic modulus and viscoelastic behavior of mushrooms depend on both moisture content and temperature (Hu et al., 2022). Yet *shiitake* tissue at 15 % moisture (wet basis) shows a glass-transition temperature below −40 °C (Zhang et al., 2024; Zhao et al., 2016), which is far below the drying and sorption temperatures considered here. Therefore, temperature-induced changes in the modulus are neglected in this study. The elastic stress is assumed to relax over a spectrum of times. Although fractional-derivative and Marin–Graessley formulations can describe the stress (van der Sman, 2023; Xiao et al., 2016), a simplified dual-mode Maxwell model was adopted, supported by compression tests on mushroom tissue dried at 35 °C (Hu et al., 2023).

Because the experiments were constrained by moisture content, and there was insufficient data in the dry regime, the regression functions for the viscoelastic properties were extrapolated to a wider regime. Furthermore, viscoelastic properties are measured at the scale of the whole mushroom, but the viscoelastic properties relevant for sorption are those of the cell wall, which are probably higher due to the presence of fibers. Nevertheless, the dependencies on moisture and temperature are assumed to be comparable to those of the viscoelastic properties at the tissue scale. Two scaling factors, F_{Gi}, and $F_{\tau i}$, used for fitting to the dynamic vapor sorption measurements were introduced. Note, these fittings were performed independently of the fitting of the drying model to the drying experiments.

Following (van der Sman, 2023), the Maxwell model was extended to finite strains. The implementation details are given in the **Appendix 5 (Section 5.1.2).** The Maxwell model has two relaxation modes, slow and fast. The relaxation of each mode is governed by:

$$\frac{d\phi_{ref,i}}{dt} = \frac{\phi_s - \phi_{ref,i}}{\tau_{0,i}} \tag{5.3}$$

where $\phi_{ref,i}$ is the internal variable for each relaxation mode, and $\tau_{0,i}$ is the relaxation time, which is moisture content- and temperature- dependent.

The total stress σ is the sum of the contributions from both the relaxation modes:

$$\sigma = \sum_i G_i * \left(\widetilde{\varphi}_i^{\frac{1}{3}} - \widetilde{\varphi}_i\right) \tag{5.4}$$

where G_i is the elastic modulus for each mode, and $\widetilde{\varphi}_i = \frac{\phi_s}{\phi_{ref,i}}$ represents the relative volume change for each mode (i=1,2 for slow and fast modes, respectively).

5.3. Physical and mathematical model for drying process

5.3.1 Model assumptions

Based on the established framework of multiphase porous media transport phenomena, the drying model of *shiitake* mushroom (with a weight of 25×10^{-3} kg) was developed under the following assumptions:

1) Mushrooms are treated as porous media, consisting of hyphae (including liquid water and solid) and pores filled with air and vapor.

2) Both the hyphae and pore spaces are continuous phases.

3) Air and vapor are ideal gases.

4) The geometry of mushrooms is simplified as a hemisphere, and the consequent drying experiments are thus performed with mushrooms with stipe removed. As shown in Fig. 5.2, the mushroom is geometrically discretized into two distinct components: a hemispherical cap and a lamella layer. The cap is composed of a hyphal matrix interspersed with air-filled pores, and the lamella layer is modeled as a dual-porous structure characterized by air gaps between the porous lamellar tissues. The air gaps within the lamella account for 50% of the total volume of this dual-porous region (i.e., $\varphi_{hypha,lam} = \varphi_{air,lam} = 0.5$). The intrinsic material properties of the lamellar matrix are assumed to be consistent with those of the cap. These air gaps are excluded from the mass and energy balance calculations and are assumed to be explored under the same environmental conditions as the external drying atmosphere.

5) The heat and mass transfer during drying are primarily driven by convective airflow. Due to the mild drying temperature and long drying time, the mass transfer mechanism for water in mushrooms is assumed to include a) diffusion of liquid water within the matrix, following Fick's law, and b) the vapor transport by diffusion in the gas part (pores) of mushroom (Castro et al., 2018; Defraeye and Radu, 2018).

6) The moisture diffusion coefficient $\boldsymbol{D}_{w_{diff}}$ is based on the theory of (van der Sman and Meinders, 2013), as detailed in Supplementary Materials.

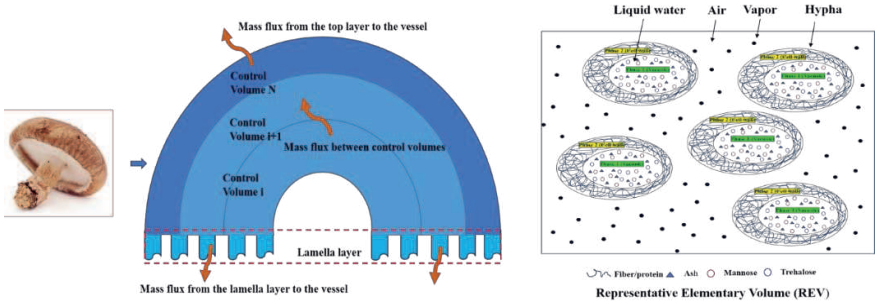


Fig.5.2. *Schematic of the division of the mushroom geometry in control volumes as used in the drying model and representation of multiple phases in the REV*

5.3.2 Governing equations

5.3.2.1 Mass equation

The total moisture concentration $c_{moisture}$ is defined as:

$$c_{moisture} = (1 - \varphi_{air})c_w + \varphi_{air}c_v \tag{5.5}$$

where φ_{air} is the porosity. c_w (kg/m^3) is the moisture concentration of the hyphae. c_v (kg/m^3) is the vapor concentration in the pores, which is assumed to reach the equilibrium state, and hence can be calculated with $c_v = a_w M_v \frac{p_{v,sat}(T_p)}{RT}$. The mass change of the total moisture is given by:

$$\frac{\partial c_{moisture}}{\partial t} = -\nabla \cdot \left(j_{w,diff} + j_{v,diff}\right) \tag{5.6}$$

where $j_{w,diff}$ and $j_{v,diff}$ (kg·s^{-1}·m^{-2}) are the liquid water and vapor mass flux density, respectively.

$$j_{w,diff} = -F_{w,diff}(1 - \varphi_{air})D_{w_{diff}}\nabla c_w \tag{5.7}$$

$$j_{v,diff} = -\varphi_{air}D_{gas_{vap}}\nabla c_v \tag{5.8}$$

$D_{w_{binary}}$ and $D_{gas_{vap}}$ are the diffusion coefficients of water and vapor, respectively.

$D_{w_{diff}}$ follows the theory of (van der Sman and Meinders, 2013), which has been shown to be valid for carbohydrate solutions. If this theory holds, cell wall material (CWM) and mannitol can be regarded as carbohydrates, as they are the main dry matter in mushroom. In the dry state, the predictions are largely independent of the molar weight of the carbohydrate, but in the wet regime, they depend on the molar weight. To account for the possible mismatch

between the theoretical and actual moisture diffusion in the wet regime, the theoretical diffusion coefficient is multiplied by a constant factor $F_{w,diff}$, to be estimated during model fitting. $F_{w,diff}$ is assumed to be of the order of 1, and hence $0.1<F_{w,diff}<10$. The detailed expression for $D_{w_{diff}}$ is given in the **Appendix 5 (Section A5.1.3)**.

5.3.2.2 Energy equation

The energy balance accounts for the heat convection due to water vapor and heat conduction through the mushroom.

$$\frac{\partial q}{\partial t} = -\nabla \cdot \left(j_w c_{\mathrm{p,w}}(T - T_0) + j_v c_{\mathrm{p,v}}(\mathrm{T} - T_0) + j_v h_{evap}\right) + \nabla \cdot \left(\lambda_{eff} \nabla \mathrm{T}\right) \tag{5.9}$$

$$q = \left(\varphi_s \rho_s c_{\mathrm{p,s}} + \varphi_w \rho_w c_{\mathrm{p,w}} + \varphi_{air} c_v c_{\mathrm{p,v}}\right) T + \varphi_{air} c_v h_{evap} \tag{5.10}$$

where q (J/ m^3) is the energy density, T (K) is the product temperature, and Zero Celsius T_0 (K) is taken as the reference temperature for the enthalpy; j_i (kg/(m^2·s)) indicates the mass flux for liquid water and vapor, and $c_{\mathrm{p,w}}$, $c_{\mathrm{p,v}}$ (J/kg/K) indicates the specific heat capacity of water and vapor, respectively. h_{evap} (J/kg) is the enthalpy of vaporization.

5.3.3 Boundary conditions

The boundary conditions for moisture and heat transport are as follows:

$$j_{w,diff} + j_{v,diff} = \mathrm{F}_{w,conv} h_{ext}\left(c_{v,surf} - c_{air}\right) \tag{5.11}$$

$$\lambda_{mushroom,eff} \nabla \mathrm{T} = h_{ext}(T_{air} - T) - \triangle H_{evap} \beta_{ext}\left(c_{v,surf} - c_{air}\right) \tag{5.12}$$

In Eq.5.11, $c_{v,surf} = a_w\, c_{sat}\left(T_{surf}\right)$ is the vapor concentration at the boundary layer, which is in equilibrium with the tissue at surface having a water activity of a_w. c_{sat} is the vapor concentration at saturated vapor pressure, T_{surf} indicates the surface temperature of mushroom. c_{air} is the vapor concentration in the air. In Eq.5.12, the term $h_{ext}(T_{air} - T)$ refers to the heat transfer from the air to mushroom on the boundary layer following Fourier's law. The term $\triangle H_{evap} \beta_{ext}\left(c_{v,surf} - c_{air}\right)$ accounts for the evaporative cooling, where $\triangle H_{evap}$ is the enthalpy of evaporation. The external heat transfer coefficient h_{ext} (W·m^{-2}·K^{-1}) is the sum of the coefficients of heat radiation (h_{rad}) and heat convection (h_{conv}). h_{rad} follows from the linearization of the Stefan's law, and h_{conv} is expressed with a convenient rule of thumb for heat transport in air at (nearly) flat surfaces (ASHRAE, 1997):

$$h_{rad} = e * 4 * \sigma * T_{wall}^3 \tag{5.13}$$

$$h_{conv} = 6 + 10 * u_{air} \quad (5.14)$$

The wall of the drying oven is assumed to have an emissivity of e which is unknown and needs to be estimated. For a perfect black body $e = 1$, the range of e is estimated to be between 0.1-0.9. σ is the Stefan constant with the value of 5.70×10^{-8} ($W\cdot m^{-2}\cdot K^{-4}$). T_{wall} is equal to T_{air}, as the absolute temperature in Kelvin of the walls in the drying oven. u_{air} (m/s) refers to the velocity at the surface of mushroom, which was estimated in this study. Normally, the external mass transfer coefficient β_{ext} is assumed to be largely related to the convective heat transfer coefficient h_{conv} via the Lewis relationship: $\beta_{ext} = F_{w,conv}\frac{h_{conv}}{\rho_{air}c_{p,air}}$. $F_{w,conv}$ accounts for possible deviations caused by: 1) temperature gradients across the boundary layer that can give rise to deviations in the Lewis relation. 2) due to the porosity, the effective surface area might also be slightly larger. 3) internal porosity can generate small convective/pressure driven flows (also enhancing the diffusion), and these convective flows leaving the mushroom surface can thin the boundary layer.

In the **Appendix 5 (Section A5.1.3-A5.1.4),** the material properties and model parameters are provided, as well as the details of the numerical implementation of the mathematical model.

5.4. Material and Methods

In this paper, material preparation, measurement of moisture content and product temperature of mushroom as well as the air temperature and relative humidity monitoring during drying, measurement of dynamic moisture sorption of mushroom are given in the **Appendix 5 (Section A5.2).**

5.4.1 NMR measurement and analysis

A mushroom cap was cut into four equal parts with a blade in a crisscross pattern, and used one of them to conduct the NMR measurement and analysis. A custom-built Niumag Pulsed NMR analyzer (Suzhou Niumag Analytical Instrument Corporation, Suzhou, China) was used, featuring a 0.5 T permanent magnet that corresponds to a proton resonance frequency of 23.2 MHz at 32.00 ± 0.02 °C, with 90° and 180° pulses set at 16 ms and 33 ms, respectively. A hot air drying device was positioned beneath the magnet, enabling upward air flow to facilitate the online NMR measurements during the drying process. The quartered sample was placed at the center of an NMR tube (outer diameter: 30 mm) and dried at a set temperature of 35°C for 10 h, during which the online NMR measurements were conducted.

The transverse relaxation times (T_2) were determined using Carr-Purcell-Meiboom-Gill (CPMG) pulse sequences. The main parameters for T_2 relaxation time measurements were TW (time waiting)= 2000 ms, TE (time echo)= 0.5 ms, NECH (number of echoes)= 12000, NS (number of scan) = 4. Logarithmic coordinates of raw data were used to construct the T_2 distribution curves with multi-exponential model under the program of the MultiExp Inv Analysis (Suzhou Niumag Analytical Instrument Corporation, Suzhou, China).

5.4.2 Relative humidity reconstruction for model parameters fitting

During drying modeling, parameters estimation was performed by fitting simulated moisture contents and center temperatures of HA33, HA38, and HA51 against experimental data obtained from the previous study (Hu et al., 2022). Due to the constraints of the experimental conditions at that time, it was impossible to simultaneously measure the variations in relative humidity during these drying processes. In this study, drying experiments at T=35°C (HA35) was performed, where the relative humidity was monitored simultaneously. This dataset was then used to validate the fitted model. The drying oven used for HA33, HA38, and HA51 is the same as for HA35 in this study. The absolute humidity in different drying experiments was assumed to be comparable and the relative humidity data can be reconstructed accordingly. This hypothesis was tested with supplementary experiments of HA33, HA38, and HA51, where relative humidity was monitored using the same method as for the HA35 experiments.

5.4.3 Parameter fitting and statistical analysis

For moisture sorption model, the unknown factors are F_{G0}, F_{G1}, $F\tau_{0_0}$, and $F\tau_{0_1}$, as described in viscoelastic property of mushroom in **Appendix 5 (SectionA5.1.3)**. This fitting was accomplished manually by comparing the experimental data (the desorption branch during the first sorption-desorption cycle and the adsorption branch measured during the second cycle) and the calculated results.

The drying model is based on existing predictive theories as much as possible. The remaining unknown factors are as follows: the emissivity e, $F_{w,diff}$ and $F_{w,conv}$, which are estimated by fitting simulated moisture contents and center temperatures to those of hot air drying experiments performed at T=33, 38, and 51°C (HA33, HA38, and HA51) obtained from our previous study (Hu et al., 2022).

Fitting was performed by minimizing the objective function with the squared difference

between the predicted and simulated temperatures and moisture content. The objective function is expressed as follows:

$$LSE\_sum = \sum_i \left(\left(\frac{\sum_j (\Theta_{p,exp} - \Theta_{p,pred})^2}{N_{T_{p,exp}}} \right) + 10 \left(\frac{\sum_j (y_{w,exp} - y_{w,pred})^2}{N_{y_{w,exp}}} \right) \right) \quad (5.15)$$

where i indicates the experiment (HA33, HA38, and HA51), and j indicates their datapoints. $T_{p,exp}$ and $T_{p,pred}$ represent the experimental and simulated temperatures respectively, while $y_{w,exp}$ and $y_{w,pred}$ denote the experimental and simulated moisture contents, respectively. As both the temperature and moisture content contribute to the sum of squares, the values must be properly rescaled to variances between 0 and 1. The mass fraction is already properly scaled, but the temperature is reduced using the air temperature and the initial product temperature: $\Theta = (T_p - T_{init})/(T_{air}-T_{init})$. As the number of data points for the temperature and moisture content recordings differed significantly, the sum of squares was rescaled by their respective numbers of data points: $N_{Tp,exp}$ and $N_{yw,exp}$. Because of the particular importance of moisture content on the prediction, a weight factor of 10 for the least squares error of moisture content was applied. In the initial stages of fitting, this weight factor was modified to make the objective function sensitive to its temperature and moisture variations similar. Because of the strong nonlinearity of the problem, the fitting process was performed manually.

To identify the optimal model parameters values that minimize the response variable (LSE_sum), a sequential single-factor optimization approach was employed. In each simulation series, one parameter (either e, $F_{w,conv}$, or $F_{w,diff}$) was varied while keeping the other parameters constant. The initial parameter ranges were chosen based on preliminary studies and relevant physical constraints. The corresponding LSE_sum values were recorded for each simulation. After each series, the parameter combination yielding the lowest LSE_sum was selected as the new working point for the next round of single-factor variations. This iterative refinement process was repeated until convergence was achieved—i.e., until further iterations did not yield a lower LSE_sum, indicating a local minimum of the objective function. A detailed description of the parameter refinement procedure is provided in the **Appendix 5 (Section A5.1.5)**.

The parameter fitting goodness and validation accuracy for the drying model was evaluated using statistical indicators, including the coefficient of determination (R^2), root mean square error (RMSE), and mean absolute error (MAE). The equations and meanings of the statistical indicators are provided in the **Appendix 5 (Section A5.1.6)**.

5.5. Results and Discussion

5.5.1 NMR results

The goal of the NMR measurement during drying at 35°C on fresh mushrooms is to examine the viability of the hypothesis- put up in a prior work by (Hu et al., 2023) - that the mushroom has two distinct thermodynamic phases. As demonstrated in Fig.5.3, two main peaks, denoted as T_{21} and T_{22}, are observed during the entire drying process. The T_{21} and T_{22} peaks have been used to identify water fractions in different cell compartments of cellular food materials such as broccoli and mushroom (Li et al., 2021; Qiu et al., 2021; Xu et al., 2017). The T_2 peaks are attributed to water populations with different molecular environments. The T_{21} peak, exhibiting T_2-relaxation times ranging from 10 to 100 ms, signifies water immobilized within the cell wall and cytoplasm. This immobilization is attributed to the bonding of water with biopolymers, such as proteins and polysaccharides, which restricts its mobility. The T_{22} peak, whose relaxation time spans from 100 to 1000 ms, signifies the presence of highly mobile water within the vacuole. This water is typically accompanied by small molecules such as sugars or minerals (Li et al., 2021; Qiu et al., 2021; Xu et al., 2017). Therefore, the NMR results presented in Fig.5.3 confirm the presence of two distinct thermodynamic phases in mushrooms throughout the drying process.

Furthermore, it was observed that the amplitudes of both T_2 peaks decreased during drying, and shifted to lower relaxation times. This indicates a reduction in the mobility of water within both phases towards the end of drying, which is a consequence of the decreasing moisture content relative to the fixed amount of solids, as well as the increase in concentrations of solutes in vacuoles. Toward the end of drying, there were no distinct populations, which could be due to the redistribution of water within the two main phases during hot air drying. When the cell membrane loses its integrity, free water in the vacuole is transformed into immobile water through bonding to carbohydrates (Li et al., 2021). It can be deduced that these two main water populations eventually mixed , and exhibited a single T_2 peak (Cheng et al., 2020).

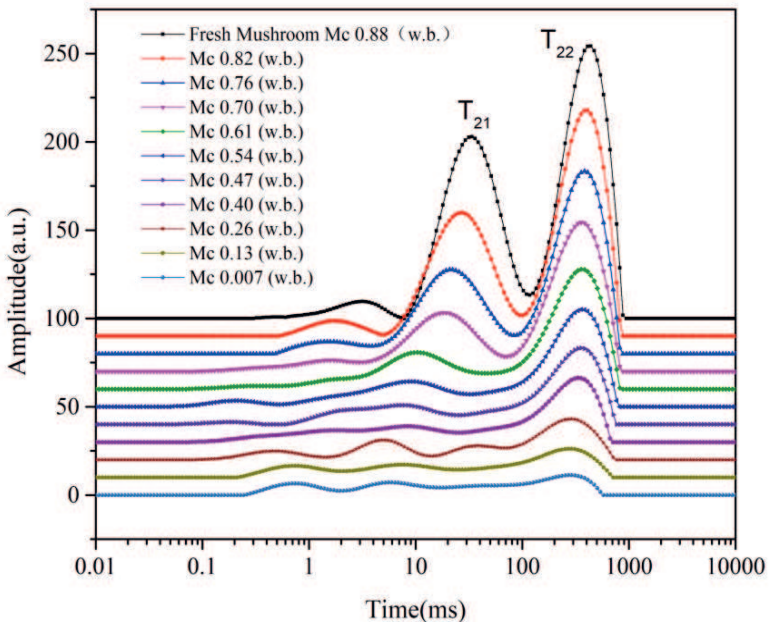


Fig.5.3. *The transverse relaxation curves (T2) of fresh shiitake mushrooms during the HA35 drying within 10 hours*

5.5.2 Moisture sorption prediction of mushroom with improved Flory Huggins theory model

Parameter fitting was performed for the dynamic vapor sorption response of a mushroom sample, and the results are presented in Fig.4. The parameter values that best fit the experimental data were: $F_{G0} = 0.1$; $F_{G1} = 3$; $F\tau_{0_0} = 10$; $F\tau_{0_1} = 100$.

Overall, the simulated moisture content values at the end of each relative humidity (RH) step are largely in agreement with the experimental data collected in the previous work (Hu et al., 2023), and the simulated curves present good fitting with the experimental ones, particularly in the range 0.2<RH<0.8. However, for the desorption branch of first cycle (left branch in Fig.5.4, data shown in previous paper), it is noted that the steady state experimental values are not attained at the end of the 'equilibration time', when the relative humidity (RH) is between 0.1- 0.2 or higher than 0.8. The experimental moisture content values were higher than those predicted by simulation. This difference can be attributed to the failure of dried samples to reach the true equilibration at RH=0.1-0.2, due to the stresses locked within the matrix after drying (van der Sman, 2023). The viscoelastic relaxation time of dry mushrooms is much longer than the practical time scales during DVS measurement, and the mechanical

stresses cannot be effectively relaxed, which impedes the attainment of a true equilibrium. Additionally, slow diffusion is another significant contributing factor. On the other hand, during moisture sorption at RH>0.8, the intact cell membranes of HA3 5 dried samples can restore the water holding capacity in the vacuole and thus increase the turgor pressure via stretching of the cell walls. Consequently, this physical process necessitates a longer period to achieve equilibration, as reported in the previous work (Hu et al., 2023).

When modeling the drying process, it is suspected that stress relaxation affects water sorption. In Fig.5.5, it shows the simulation results of the moisture sorption isotherms with the comparation with experimental data obtained in the previous study (Hu et al., 2023). The experimental moisture sorption isotherm (MSI) measured during the first cycle exhibits a distinct hysteresis phenomenon, which is barely noticeable from the second cycle onwards. This observed hysteresis can be attributed to the stress accumulated in the matrix during the rapid drying process of the samples. When the dried mushroom samples are exposed to a prolonged period of water absorption during the first cycle of MSI measurement, the internal stress within the samples gradually dissipates over this ample time span. As a result, the hysteresis disappears when the samples are subjected to the second cycle of MSI measurement. However, this hysteresis phenomenon is not addressed in this analysis, as the drying history of the freeze-dried sample is unknown. Its drying rate was definitely faster than during DVS experiments, leading to the locking-in of stresses. Furthermore, the information on the elastic modulus in the dry regime is lacking, which could not be obtained with the compression test (Hu et al., 2023).

Nevertheless, these results demonstrate that the satisfactory fitness allows us to utilize the updated moisture sorption theory model that accounts for viscoelastic relaxation to develop a drying model for mushrooms.

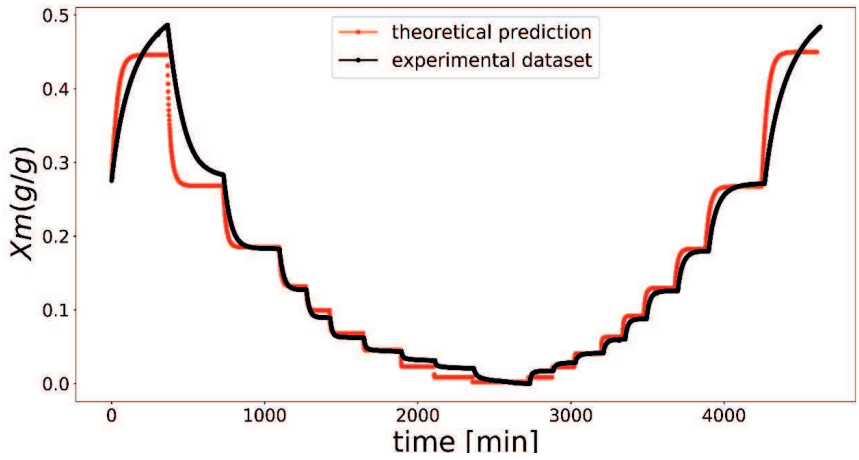


Fig.5.4. *Comparison between simulation and experiment of dynamic moisture sorption of HA35 dried mushroom powder (The left and right branches indicate desorption and absorption processes during the first and second sorption–desorption cycles, respectively).*

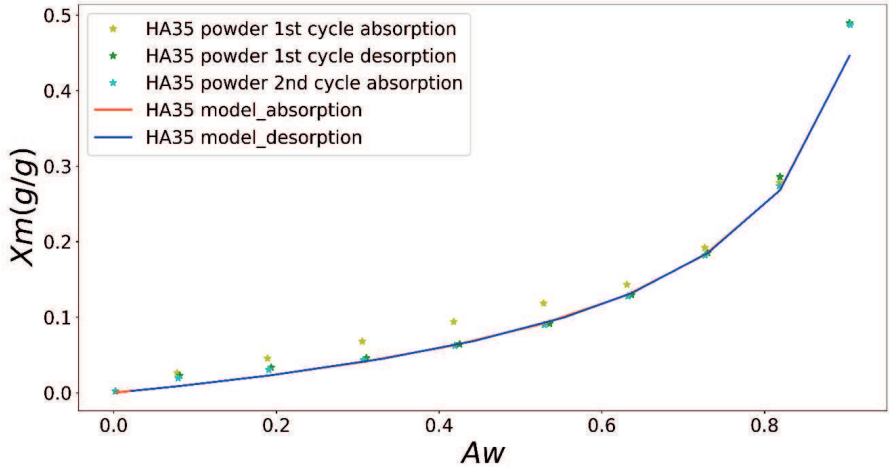


Fig.5.5. *Comparison between simulation and experimental MSI of HA33 dried mushroom*

5.5.3 The analysis of porosity evolution of mushrooms during drying

Moisture loss during the drying process leads to shrinkage of the mushroom, causing a change in its porosity. In principle, accurately determining these changes in porosity necessitates the resolution of the momentum balance. However, such computations are complex and demanding. Instead, a simulation of the porosity evolution of mushrooms was

presented by utilizing an empirical relation derived from the shrinkage ratio curves measured during the drying process. The detailed simulation process for predicting the porosity evolution based on the empirical relation is given below.

As depicted in Fig. 5.2, the mushroom exhibits a porous structure comprising hyphae (consisting of solid material and liquid water) and gas within the matrix (containing vapor and air). The solid, liquid water and gas fractions of the hyphae are distinguished. Due to the fact that the amount of solid material remains constant during drying and the amount of liquid water is governed by the mass balance, the gas fraction (porosity) is determined by the removal of water (in vapor form) and air from the matrix. Hence, the volume fractions undergo changes as water and air are lost. The variation in the gas phase (porosity) was represented as the change in the volume ratio between the air and solid material within the mushroom, and the derivation is given in the **Appendix 5 (Section A5.3.1)**:

$$\frac{\mathrm{V}_{mushroom}(\mathrm{t})}{\mathrm{V}_{solid}} = \frac{\mathrm{V}_{air}(t)}{\mathrm{V}_{solid}} + 1 + \mathrm{Xm}(t) * \frac{\rho_{solid}}{\rho_{water}} \tag{5.16}$$

The mushroom volume change $\mathrm{V}_{mushroom}(\mathrm{t})$, can be derived from an empirical relationship that describes the change in shrinkage ratio during hot air drying. Subsequently, the porosity evolution can be expressed by the relationship between the air volume fraction (relative to the constant solid volume) and moisture content (d.b.): $\frac{\mathrm{V}_{air}}{\mathrm{V}_{solid}} \sim \mathrm{Xm}$

To establish the relationship between $\frac{\mathrm{V}_{air}}{\mathrm{V}_{solid}}$ and X_m, exponential and linear fitting methods was applied to analyze the experimental data, as shown in Fig.5.6.

when $X_m < 0.95$,

$$\frac{dV_{gas}}{dV_{solid}} = 8.637e^{-4.034*\mathrm{Xm}} + 6.674 \tag{5.17}$$

when $X_m > 0.95$,

$$\frac{dV_{gas}}{dV_{solid}} = 2.467 * X_m + 4.33 \tag{5.18}$$

Subsequently, this empirical relation was incorporated into the modeling of hot air drying to account for the impact of mushroom shrinkage on heat and mass transfer.

From the porosity (air volume fraction) curve shown in Fig.5.6, it is observed that the porosity increases suddenly at the end of drying. This phenomenon is also observed by (Madiouli et al., 2007; Nguyen et al., 2018). According to (Gulati and Datta, 2015; Nguyen et al., 2018; van der Sman et al., 2024), it can be attributed to the formation of a tough skin, meanwhile the inside is soft, undergoing a mechanical (cavitation) instability due to the shrinkage of the

core. At the late stage of the drying process, as depicted in the mushroom image in Fig. 5.6, the surface layer stiffens upon drying. The wrinkled appearance on the surface serves as evidence of the mushrooms' case-hardening. Simultaneously, as drying progresses, the rubbery matrix in the core region shrink, leading to a sudden rise in porosity.

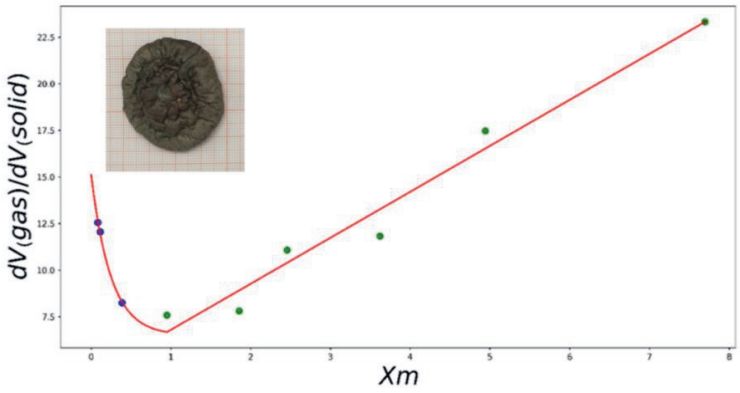


Fig.5.6. *Volume fraction ratio of gas and solid phases change of mushroom during HA35*

5.5.4 Model fitting and validation

Following the fitting of the moisture sorption model, the drying model was fitted to experiments via minimizing the objective function (Eq.5.15). The detailed fitting procedure and results of all parameter combinations are given in the Table S5.2 & Table S5.3 in the **Appendix 5 (Section A5.1.5),** showing that the best fit is obtained for e = 0.9, $F_{w,conv}$ = 5 and $F_{w,diff}$ = 8. All correction factors are in the expected range $0.1<F_i<10$.

Fig.5.7 presents the final fitting results for HA33, HA38, and HA51 with the optimal parameter combination. The moisture content curves fit well with the simulated ones. The coefficients of determination (R^2) for HA33, HA38, and HA51 are 0.9361, 0.9325, and 0.9849, respectively. The mean absolute errors (MAEs) are 0.068, 0.078, and 0.030, respectively. The root mean square errors (RMSEs) are 0.08205, 0.09371, and 0.04576, respectively. All experimental temperature curves ran below their simulated counterparts until the final drying stage. Yet, the moment of the rapid temperature rise is captured quite accurately for all experiments, which is probably driven more by the kinetics of moisture transport. This systematic deviation might arise from the fact that the relative humidity at these three temperatures were not directly measured, even though the environmental absolute humidity in the oven remained almost constant across different experimental periods, as

shown in Fig.A5.3 in the **Appendix 5 (Section A5.3.2)**. The actual relative humidity for HA33, HA38, and HA51 might have been lower than that of the auxiliary measurements taken later, which could be the main source of error. A consistent pattern is also observed in which all center temperatures stabilized near the wet-bulb temperature for a long time (approximately 25h for HA33,10h for HA38,12 h for HA51) and rapidly increase toward the air temperature at the late drying stage. This trend is primarily driven by internal evaporative cooling within the porous mushroom structure. If sufficient moisture is present, this cooling effect persists and maintains the central temperature near the wet-bulb level. However, when drying nears completion, with little moisture remaining in the core, the evaporation front shifts to the mushroom center, and the cooling effect diminishes, allowing the temperature to rise quickly toward the air temperature.

For model validation, a simulation of moisture content and surface and center temperatures of the mushroom during hot air drying at 35℃ (HA35) was conducted with the established model, and the results were compared with the experimental data in Fig. 5.8. As shown in Fig.5.8a, the simulated average moisture content across the entire sample layer exhibited strong agreement with the HA35 experiment, as validated by high coefficients of determination ($R^2 > 0.9875$), low mean absolute errors (MAEs = 0.02205), and low root mean square errors (RMSEs = 0.03656), confirming the reliability of the model for moisture content prediction.

As shown in Fig.5.8b, the model reasonably predicts the overall trends and final values of the surface and center temperatures; the simulated temperatures still consistently exhibit a lower bias than the experimental data, similar to Fig.5.7, although the air temperature and relative humidity were monitored synchronously with the product temperatures. Possible causes include the following:

a) Due to thermal contact limitations, thermocouple probes may not have perfect contact with the mushroom, failing to capture the exact local conditions, especially in the internal region. When measuring the surface temperature, the probes are additionally influenced by convective heat transfer from the surrounding hot air, which introduces measurement errors. Specifically, as shown in Fig.5.7&5.8b, the simulated temperatures are consistently lower than the experimental temperatures. This discrepancy might arise because the model outputs a simulated value at a single specific point, whereas the temperature sensor measures the temperatures across multiple points on the surface and outputs an average value. Mushroom shrinkage and case-hardening during drying result in geometric inconsistencies between the experimental sample and simulation model

(Zeineldin, 2008).

b) Simplified heat/mass transfer boundary conditions

The model assumes idealized surface conditions and overlooks the impact of non-uniform airflow on convective heat transfer coefficients. These airflow irregularities arise from the mesh structure supporting the mushrooms, which either conducts or blocks the airflow, thereby introducing variability in heat transfer that the model does not account for. Real-world air temperature/distribution variations around the mushroom create localized temperature differences that are unaccounted for in simulations, contributing to higher experimental readings.

Furthermore, it is observed that the surface and internal temperatures fluctuate upward as heat transfers inward in Fig.5.8. Surface temperature fluctuations mirrored thermodynamic equilibrium adjustments between aw and RH, while center temperature fluctuations arose from evaporative cooling in the porous structure, modulated by RH-dependent evaporation rates. RH fluctuations originate from dryer on/off control, consistent with observations in apple disks intermittent microwave drying by (Kumar et al., 2016). It is also observed that the surface and center temperatures stabilized at quasi-steady wet-bulb temperature for ~12 and 30 hours respectively, which might be directly correlated with its sustained high aw, as ongoing internal evaporation maintained the cooling effects. To determine the physical mechanism of mushroom drying, the moisture and temperature distributions was simulated and analyzed, as described in the next section.

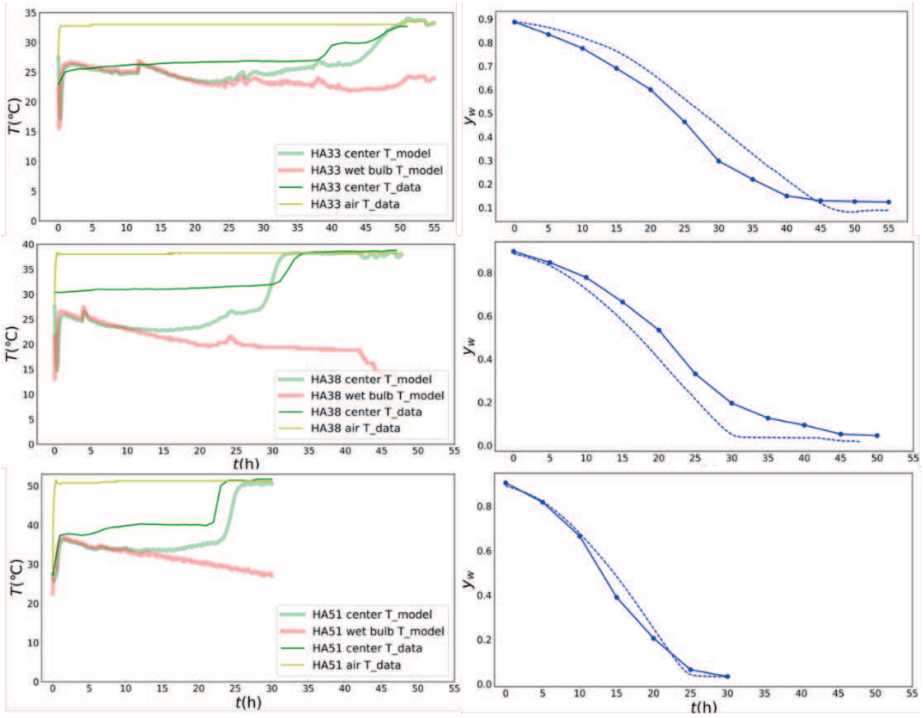


Fig. 5. 7. *Experimental and simulated temperatures and moisture contents of mushrooms dried by HA33, HA38, HA51 with the optimal parameter combination*

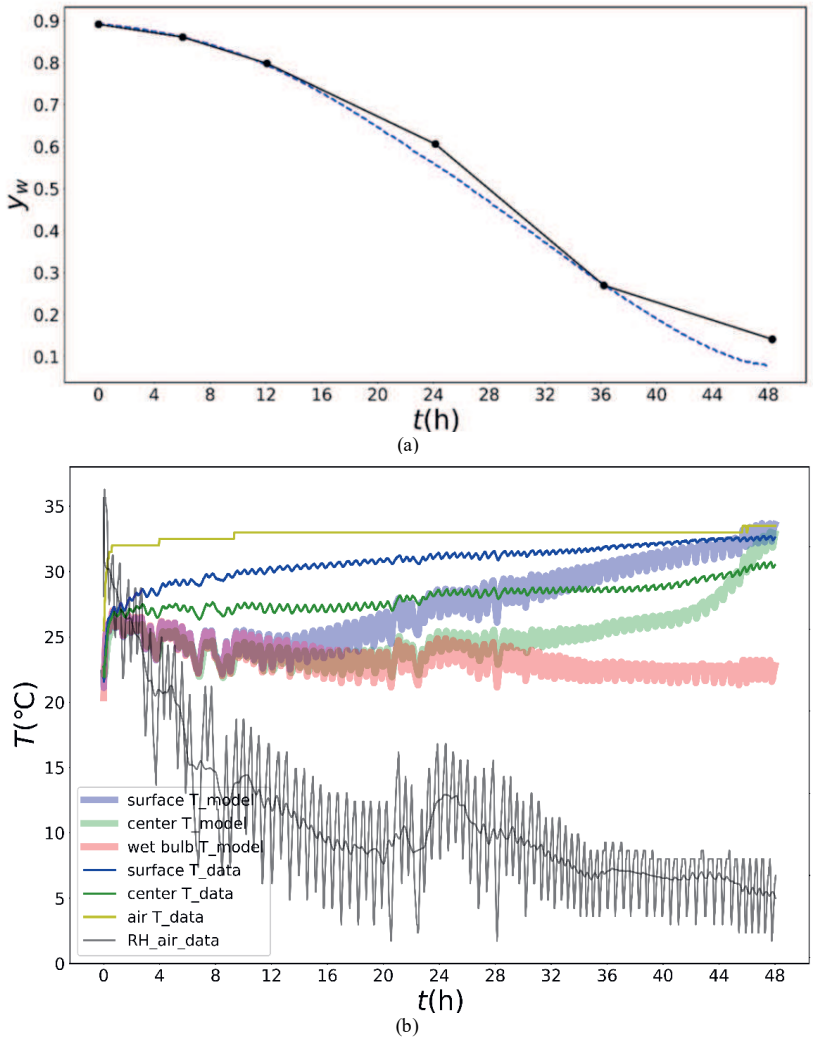


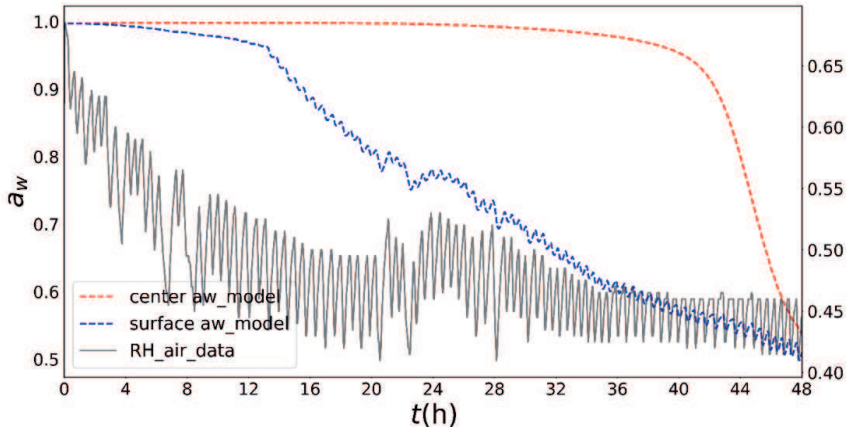
Fig.5.8. *Experimental and simulated moisture contents (a) and surface and center temperature evolution (b) of mushrooms dried by HA35 with the optimal parameter combination*

5.5.5 Drying Mechanism analysis

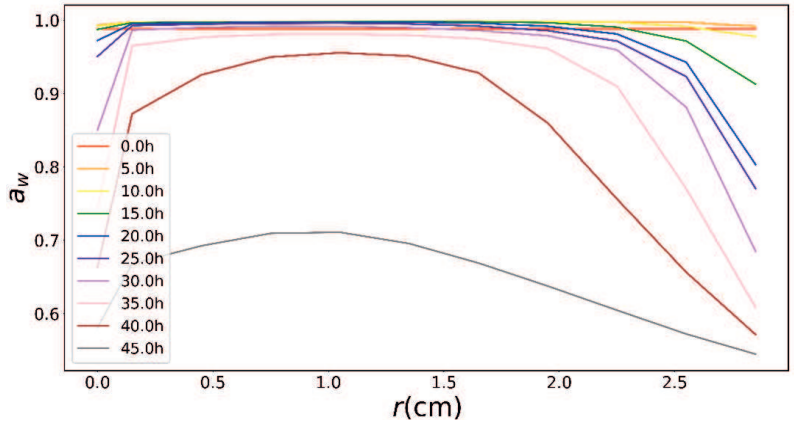
5.5.5.1 Water activity distribution

Water activity (aw) evolution provides insights into the evolution and distribution of moisture content and links the relationship between moisture and temperature dynamics. In Fig.5.9a, the surface aw decreases as drying progresses, in accordance with the reduction in the relative humidity (RH). In contrast, the central a_w remains approximately unity until the final drying

stage, a pattern directly tied to the prolonged maintenance of low central temperatures owing to internal evaporative cooling. Fig.5.9b presents the non-uniform spatial distribution of a_w at different time intervals during the drying process: layers near the cap surface (r = 3.0 cm) and lamella (r = 0.0 cm) dried faster than the internal layers. Approximately at t=15 h, the a_w of the outermost cap layer and the lamella decreased rapidly, while the center remains at initial aw until the drying front reaches the center after 40 hours, near the end of drying.



(a)



(b)

Fig.5.9. *Surface and center aw change during HA35 (a) and aw distribution evolution at different drying time intervals (b)*

5.5.5.2 Product temperature and distribution

Fig.5.10 depicts the model-derived temperature profiles showing changes in mushroom during drying. The initial drying stages exhibits flat and uniform profiles with minimal internal gradients. By 35 h, the surface and lamella temperatures exceeded those of the core, coinciding with their rapid aw reduction (Fig.5.10). Diminished evaporative cooling in these drier regions allowed heat accumulation, while the still-moist core retained its cooling capacity. In late drying, temperature gradients diminished as the outer layers approached ambient temperature, eventually equilibrating the entire product to ambient temperature, coinciding with the aw distribution.

Furthermore, it is observed that the simulated center temperature decreases during the intervals of 5 - 10 h, 10 - 15 h, 15 - 20 h, and 25- 30 h, as indicated by the red arrows in Fig.5.10, when the temperatures were expected to increase. The plots showing the changes in center temperature during these time periods were enlarged and presented in Fig. A5.4 of the **Appendix 5 (Section A5.3.3)**. These anomalous variations can be primarily attributed to fluctuations in relative humidity (RH), which intricately interact with the moisture dynamics within the mushroom.

Following the validation of the model's ability to predict the coupled evolution of moisture and temperature during drying and the clarification of its underlying mechanisms, the core innovations and advances of this model are summarized through a comparison with existing ones. Firstly, unlike previous studies (Tran et al., 2020; Zecchi et al., 2011; Zhu et al., 2021), which treat mushrooms as homogeneous porous media, this model explicitly divides mushrooms into two thermodynamic phases (cell wall/cytoplasm and vacuoles) separated by intact cell membranes validated via NMR measurements, and distinguished the mushroom into cap and lamellar parts. This distinction captures water partitioning between phases and local distribution in mushroom, which is critical for understanding the real moisture sorption and transport mechanism (Jin et al., 2014). Secondly, this model integrates cellular-level thermodynamics (via the Flory-Huggins theory based on composition), the effect of viscoelastic relaxation on moisture sorption/diffusion (via Maxwell Model and Flory-Rehner theory), and multiphase heat/mass transfer. It bridges microstructural features (cell membrane integrity, rheological property) with macroscopic drying behavior, addressing gaps in existing multiphase models that ignore biological complexity of cellular food materials (Onwude et al., 2021; Purlis, 2019; Zhu et al., 2021). Additionally, this model employs predictive properties, such as the mutual moisture diffusion coefficient and composition-weighted thermal conductivity, which adapt to temperature and moisture

changes. This captures the evolving physical nature of mushroom tissue during drying, which is missing in simplified models (Tran et al., 2020; Zecchi et al., 2011). However, it must be noted the current model is missing a mechanistic model, describing the large deformation and wrinkling of the mushroom during drying.

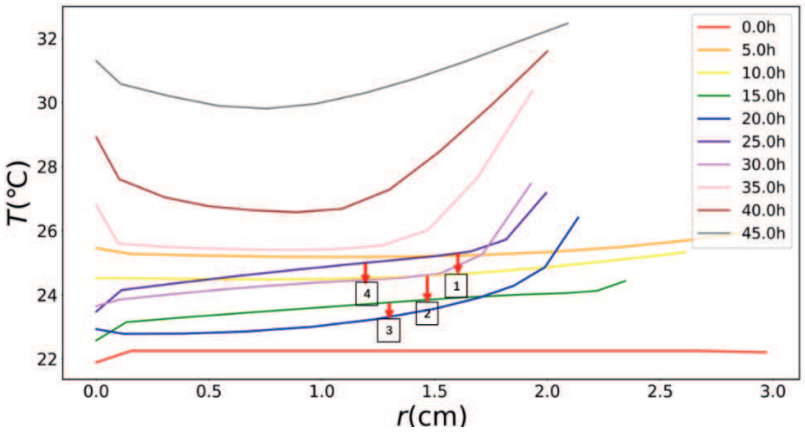


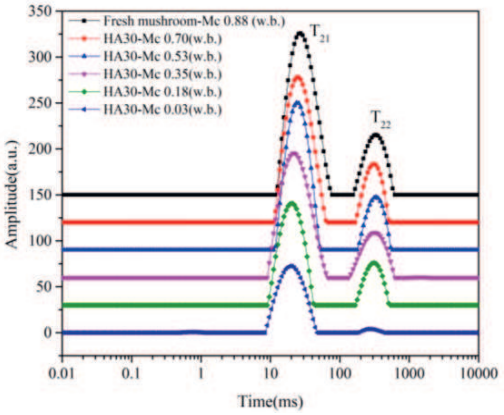
Fig.5.10. *Product temperature distribution evolution at different time intervals during the drying (red arrows 1-4 indicate the change during the intervals of 5 - 10 h, 10 - 15 h, 15 - 20 h, and 25 - 30 h)*

5.5.6 Identification of cell membrane integrity change with NMR measurement

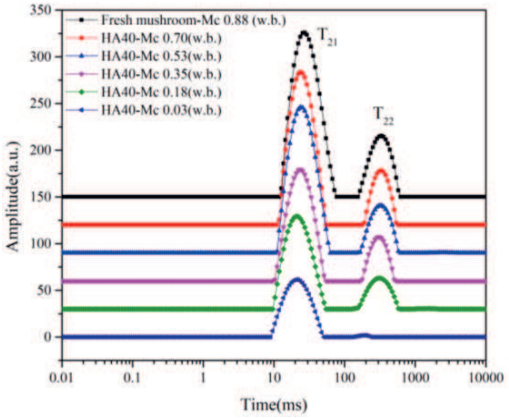
With NMR, two distinct thermodynamic phases in hyphae were identified, separated by the cell membrane and distinguishable by their respective T_2 peaks (as detailed in Section 5.1). In an earlier study using the conductivity method, it showed that the loss of cell membrane integrity occurred in a critical temperature regime ($T \approx 40$℃) (Hu et al., 2022). While the conductivity method is straightforward, it is an indirect measurement, and via T_2-NMR, one obtains a direct, non-destructive indication of the cell membrane integrity via the number of water populations. Upon loss of cell membrane integrity, it is expected the T_{21} and T_{22} populations to merge into one. Here, the NMR results of mushroom during in-situ hot air drying at 30,40,50 °C in another study was reproduced (Qiu et al., 2021), as shown in Fig.5.11. These results were compared with the data based on conductivity. However, during NMR measurement the product temperature was not recorded, whereas the moisture content was recorded. The validated drying model can be used for the prediction of product temperature. Based on the predicted product temperature and measured moisture content, the product state is known, and the NMR-results can be plotted (i.e. the presence of one or two water

populations) in the previous contour plot based on conductivity(Hu et al., 2022). To objectively infer the presence of one or two peaks, a threshold of 5% (relative to the peak of the fresh mushroom) was used, and the presence of peaks above this threshold was counted.

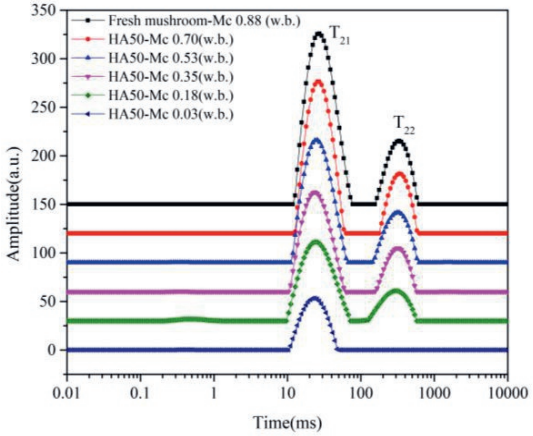
The evolution of the product state (T_p and y_w), as predicted by the validated drying model, is plotted in the conductivity contour plot, together with symbols indicating the presence of one or two peaks, as shown in Fig.5.12 The color bar indicates the values of conductivity. Lower conductivity indicates less cell membrane damage (Hu et al., 2022). From the contour plot, it is observed that two critical conditions for the loss of cell membrane integrity: T_p>40℃ or y_w<3%. The first threshold is imposed by a (fluid-to-gel) phase transition of the lipid bilayer (Gonzalez et al., 2010; Singhal et al., 2020). This second condition is probably caused by osmotic stress. However, it is expected that under these conditions, the loss of cell membrane integrity is reversible, as shown in the previous study that mushrooms after HA35 drying treatment can restore turgor after rehydration.



(a)



(b)



(c)

Fig.5.11. *The reproduced T2 inversion spectra curves of fresh and dried mushrooms from (Qiu et al., 2021)*

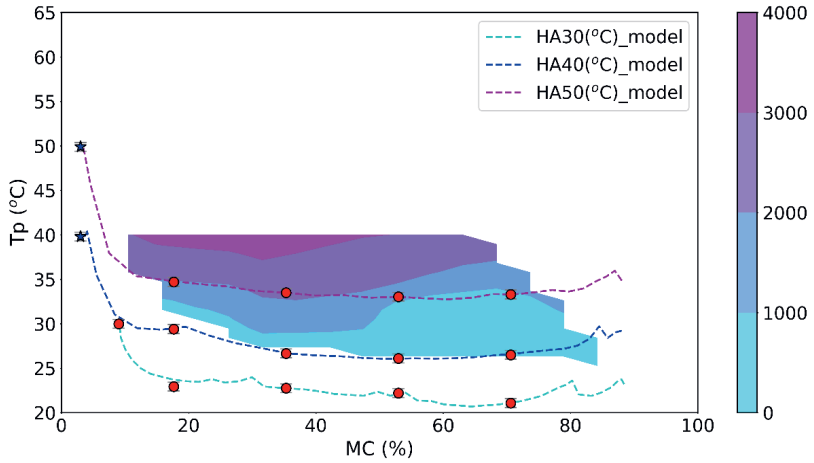


Fig.5.12. *Model-simulated moisture–temperature state diagram of hot air-dried mushrooms with contour lines for the electrical conductivity (μS/cm) of rehydration liquid (The red circles denote samples with two T2 peaks, and blue stars represent those with one T2 peak.)*

5.6. Conclusion

This study presents a mechanistic multiphase and multiscale model for mushroom drying. This model reasonably captures the moisture content evolution and gradients variation, accounting for the thermal equilibrium between the two thermodynamic phases within the hypha via the Flory-Huggins theory, viscoelastic relaxation of the cell wall by Maxwell relaxation modes, and the heat and mass transfer mechanism accounting for the unique porous structure of mushroom filled with vapor and air. The analysis of experiments with the model shows the particular drying behavior of mushrooms: the inclusion of these factors enables the reasonable prediction of moisture and temperature evolution, such as the prolonged high central aw due to internal evaporation cooling. Furthermore, the model was used to predict the product temperature profile during hot air drying at 30°C, 40°C, 50°C. Integration of these predictions with conductivity and NMR data allowed us to determine that preserving membrane integrity requires maintaining temperatures below 40°C and moisture content above a threshold of 3% (w.b.). As the study showed preservation of the cell membrane integrity is required for optimal rehydration of *shiitake* mushrooms, the moisture-temperature-conductivity contour plot integrated with T_2 relaxation results indicating the cell membrane status provides a convenient tool for the optimization for critical drying conditions of serial combined drying processes of cellular food materials.

Appendix 5

A5.1. Supplementary for modeling description

A5.1.1 The main compounds composing shiitake mushroom

The main compounds present in *shiitake* mushroom are listed in Table A5.1.

Table. A5.1 *Mass fraction of components in dry matter of shiitake mushrooms*

Component / Location / Content	Mannitol	Trehalose	Fiber	Protein	Ash (KH_2PO_4)
Phase1	√	√			√
Phase2			√	√	
	0.307	0.033	0.375	0.17	0.0335

A5.1.2 The large deformation version of the Maxwell mode

The classical Maxwell model is applicable to small deformations of viscoelastic media. For our discussion later, it is convenient to rewrite the Maxwell model in terms of the elastic strain ϵ_{el} and inelastic strain $\epsilon_{in} = \epsilon - \epsilon_{el}$. The inelastic strain can relax as:

$$\frac{d\epsilon_{in}}{dt} = \frac{\epsilon - \epsilon_{in}}{\tau_0} \tag{A5.1}$$

τ_0 is the viscoelastic relaxation time.

The stress is only due to the elastic part, which means

$$\boldsymbol{\sigma} = G\epsilon_{el} \tag{A5.2}$$

G is the elastic (shear) modulus.

In our case we have to deal with the large deformation of the cell wall, then we need to convert the Maxwell model. For large deformations one use stretch parameter $\lambda = 1 + \epsilon$ to express the strain. To describe the viscoelasticity of large deformation, we apply multiplicative decomposition to λ :

$$\lambda = \lambda_{el}\lambda_{in} = (1 + \epsilon_{el})(1 + \epsilon_{in}) \tag{A5.3}$$

with the elastic part λ_{el} and the inelastic part λ_{in}, respectively. We can find this definition is consistent with the small deformation when expanding this equation, due to the $\epsilon_{el}\epsilon_{in}$ is very small and can be neglected.

We assume isotropic deformation of mushroom, then we can use the volume fraction to indicate the deformation as done in the Flory-Rehner theory. Hence, we can apply multiplicative decomposition to $\frac{\phi_s}{\phi_{dry}}$, as for plastic deformations.

$$\frac{\phi_s}{\phi_{dry}} = \frac{\phi_s}{\phi_{ref}}\frac{\phi_{ref}}{\phi_{dry}} = \frac{1}{\lambda_{el}^3 \lambda_{in}^3} \tag{A5.4}$$

φ_s is the polymer volume fraction, and φ_{ref} is a reference value. $\phi_{dry} = 1$.

The stress is the function of elastic deformation (Sman, 2023).

$$\boldsymbol{\sigma} = G * \left(\tilde{\varphi}^{\frac{1}{3}} - \tilde{\varphi}\right) \tag{A5.5}$$

We reinterpret φ_{ref} as the internal variable describing the viscoelastic state, as in case of transient networks models (Curatolo et al., 2018; Reese, 2003). Based on the transient network hypothesis, the distance between physical crosslinks along the polymer backbone changes due to the mechanical deformations, presenting the viscoelastic relaxation of polymers, which is represented by φ_{ref}, as follows from the c*-theorem from deGennes (van der Sman, 2015).

A single relaxation time viscoelastic process at large deformations can be captured via the following relaxation of φ_{ref}(Sman, 2023):

$$\frac{d\phi_{ref}}{dt} = \frac{\phi_s - \phi_{ref}}{\tau_0} \tag{A5.6}$$

whose physical meaning is that the intermediate (stress free) reference state of polymer networks tends to relax towards the current state, as represented by ϕ_s. The process is schematically shown in Fig.A5.2.

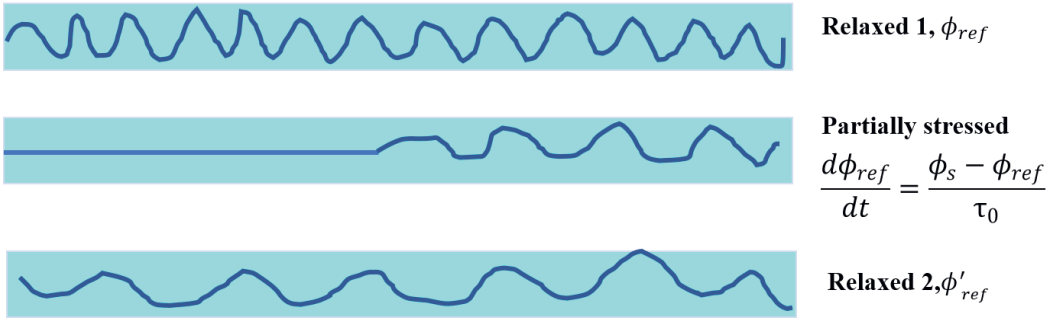


Fig. A5.1. *Volume fraction of viscoelastic polymer changes with time*

A5.1.3 Material properties

The constant parameters used to solve the mathematical model in Table A5.2.

Table A5.2 Values of parameters present in the model

	Parameter	Value	Unit	Reference
ρ_{water}	Density of water	998	kg/m ^{3}	(Çengel and Boles, 2006)
ρ_{solid}	Density of solid matrix	1591	kg/m	(Oikonomopoulou and Krokida, 2012)
ρ_{carb}	Density of carbohydrate	1550	kg/m ^{3}	(van der Sman, 2008)
ρ_{pro}	Density of protein	1330	kg/m ^{3}	(van der Sman, 2008)
ρ_{ash}	Density of ash	2440	kg/m ^{3}	(van der Sman, 2008)
ρ_{fat}	Density of fat	930	kg/m ^{3}	(van der Sman, 2008)
η_f	Effective viscosity of mannitol	1.00× 10 $^{-3}$		(van der Sman and Meinders, 2013)
K_{ss}	Free volume parameter	69.21	K	(van der Sman and Meinders, 2013)
K_{ws}	Free volume parameter	3.36× 10 $^{-4}$	K	
K_{sw}	Free volume parameter	-19.73	K	(van der Sman and Meinders, 2013)
K_{ww}	Free volume parameter for water	1.95× 10 $^{-3}$	K	(van der Sman and Meinders, 2013)
K_{ss}	Free volume parameter	69.21	K	(van der Sman and Meinders, 2013)
T_{gs}	Glass translation temperature of solid	347.15	K	(Zhu et al., 2021)
T_{gw}	Glass temperature of water	136	K	(van der Sman and Meinders, 2013)
r_H	Hydrodynamic radius of mannitol molecule	0.448× 10 $^{-9}$		(van der Sman and Meinders, 2013)
h_{evap}	Latent heat of evaporation	2.26 × 10 ^{6}	KJ/kg	(Zhu et al., 2021)
δ	Shape factor	0.79		
V_{cs}	Specific free volume fraction for solute	0.91		(van der Sman and Meinders, 2013)
V_{cw}	Specific free volume fraction for water	0.59		(van der Sman and Meinders, 2013)
$c_{p,solid}$	Specific heat capacity of solid matrix	1500	J/kg/K	(Tansakul and Lumyong, 2008)
$c_{p,w}$	Specific heat capacity of water	4182	J/kg/K	(Rakesh et al., 2012)
$c_{p,v}$	Specific heat capacity of vapor	2062	J/kg/K	(Rakesh et al., 2012)
$c_{p,air}$	Specific heat capacity of air	1006	J/kg/K	(Rakesh et al., 2012)
λ_{air}	Thermal conductivity of air	0.026	W/m/K	(Rakesh et al., 2012)
λ_{carb}	Thermal conductivity of carbohydrate	0.2	W/m/K	(van der Sman, 2008)
λ_{pro}	Thermal conductivity of protein	0.18	W/m/K	(van der Sman, 2008)
λ_{ash}	Thermal conductivity of ash	0.33	W/m/K	(van der Sman, 2008)
λ_{fat}	Thermal conductivity of fat	0.18	W/m/K	(van der Sman, 2008)
λ_{water}	Thermal conductivity of water	0.599	W/m/K	(Rakesh et al., 2012)

Moisture diffusion coefficient $\boldsymbol{D_{w_{diff}}}$

To make the model as mechanistical as possible, we assume the moisture diffusion coefficient $\boldsymbol{D_{w_{diff}}}$ as a mutual diffusion coefficient, which is based on three theories: the free volume theory for the water self diffusivity; the generalized Stokes–Einstein relation for the solute self diffusivity and the Darken relation linking the mutual diffusivity to the self diffusivities of water and solutes (van der Sman and Meinders, 2013).

$$D_{w_{diff}} = \phi_w * D_{s,s} + (1 - \phi_w) * D_{s,w} \tag{A5.7}$$

$D_{s,s}$ and $D_{s,w}$ are the self diffusivities of the solute and water respectively. During drying, the moisture within the mushroom is unevenly distributed. In the low moisture regime, diffusion is dominated by the water self diffusivity $D_{s,w}$, while in the high moisture regime, it is governed by the solute self diffusivity $D_{s,s}$ However, a major part of the dry matter of mushrooms consists of biopolymers located in cell wall and cell cytoplasm which do not include the generalized Stokes–Einstein as solutes. Hence, to account for these deviations from theory, we multiply the diffusivity with a pre-factor $F_{w,diff}$ as shown in Eq.A5.7.

We approximate the solute self diffusivity with a variable simplification by taking the molecule of mannitol, which is the main component in mushroom dry matter, to describe the hydrodynamic radius r_H.

$$D_{self diffusion\ solute} = \frac{k_B T}{6\pi\eta_f r_H} \tag{A5.8}$$

With k_B the Boltzmann constant (1.380649×10^{-23} J/K), T the product temperature, r_H the hydrodynamic radius of the mannitol molecule, and η_f the effective viscosity of the mannitol.

$$D_{self diffusion\ water} = D_0 * e^{\frac{-\Delta E}{RT}} * e^{\frac{-y_w * V_{cw} + \delta * y_s * V_{cs}}{y_w * K_{ww} * (K_{sw} - T_{gw} + T_p) + y_s * K_{ws} * (K_{ss} - T_{gs} + T_p)}} \tag{A5.9}$$

With ΔE the activation energy, R universal gas constant (8.314 J/mol/K) K_{ij} free volume parameters, δ is a shape factor. y_w and y_s are the mass fraction of water and solutes, respectively, and V_{cw} and V_{cs} are related to the specific free volume fraction for water and solute respectively. These parameter values are obtained from (van der Sman and Meinders, 2013), which are listed in Table A5.2.

Air/vapor diffusion coefficient

The air/vapor diffusion coefficient in gas within the control volumes, $D_{gas_{air}}$ and $D_{gas_{vap}}$, are multicomponent Fick diffusivities (Bird et al., 2002), and can be written as:

$$D_{gas_{vap}} = 0.129e^{-4} + 0.18e^{-6}(T - T_0) \quad \text{(A5.10)}$$

Thermal parameters

The physical thermal parameters of mushroom are based on composition and effective medium theory. In porous materials, such as mushroom containing air (gas phase) dispersed in the hypha matrix (composed of water and solids), the thermal conductivity λ is determined by the complex interplay of hypha and gas phases. According to the Maxwell-Eucken model, the dispersed phase (air in the mushroom) is modeled as spherical particles uniformly distributed in the continuous phase (hypha matrix of the mushroom).

The thermal conductivity $\lambda_{mushroom,eff}$ and specific heat capacity $c_{p,mushroom}$ (J/kg/K) are calculated as follows:

$$\lambda_{mushroom,eff} = \lambda_{hypha}\frac{1+(\varphi_{air}+\varphi_{hypha}*\mathrm{Q})*\zeta}{(1+\varphi_{hypha}*\mathrm{Q}*\delta)} \quad \text{(A5.11)}$$

$$\lambda_{mushroom,lam,eff} = \varphi_{lamella}\lambda_{mushroom,eff} + (1-\varphi_{lamella})\lambda_{air} \quad \text{(A5.12)}$$

$\mathrm{Q} = \frac{1}{3}$ (isotropic), $\zeta = (\lambda_{\mathrm{air}} - \lambda_{\mathrm{hypha}})/\lambda_{\mathrm{hypha}}$,

$$\lambda_{\mathrm{hypha}} = (\varphi_s\lambda_{\mathrm{solid}} + \varphi_w\lambda_{water})/(1-\varphi_{air}) \quad \text{(A5.13)}$$

$$\lambda_{\mathrm{solid}} = \varphi_{carb}\lambda_{carb} + \varphi_{pro}\lambda_{pro} + \varphi_{ash}\lambda_{ash} + \varphi_{fat}\lambda_{fat}$$

$$c_{p,mushroom} = \frac{\varphi_w c_{p,water}\rho_{water} + \varphi_s c_{p,solid}\rho_{solid}}{\rho_{mushroom}} \quad \text{(A5.14)}$$

Here,

$$\rho_{mushroom} = \rho_{water}\varphi_w + \rho_{solid}\varphi_s + \rho_{air}\varphi_{air} \quad \text{(A5.15)}$$

With $\rho_{solid} = \frac{\sum X_i}{\sum\frac{X_i}{\rho_i}}$; $c_{p,solid} = \sum \rho_i \Phi_i$; $\Phi_i = \frac{X_i}{\rho_i \sum\frac{X_i}{\rho_i}}$

X_i is the mass fraction based on the total dry matter, as listed in Table1, and Φ_i represents the volume fraction. i indicates carbohydrate, protein, ash, and fat, respectively. Note, we assume that the contribution of vapor (gas) to the specific heat capacity of mushroom is negligible because of its low density.

Viscoelastic property of mushroom

From the compression measurement on mushrooms with the moisture contents ranging from 0.20-6.46 g/g dry basis (d.b.). dried at 35 ℃ at the tissue scale (Hu et al., 2023), we established the moisture-dependency functions for the elastic modules G_0 and relaxation time τ_0. Note, the values of G_0 for the cell wall of mushroom are assumed to be higher than those at the tissue scale. This is because of the existence of stiff chitin fibers in the cell wall, and at the tissue scale, easy sliding of hyphae leads to a moderately effective G (Ene et al., 2015). Therefore, in this study these functions are applied to mushroom samples, and multiplied with unknown pre-factors F_{G_i} and $F_{\tau 0_i}$ which need to be fitted. Here, i indicates the slow and fast viscoelastic relaxation modes as mentioned above. Therefore, the generalized functions between the modules/relaxation time and moisture content (y_w d.b.) of on the powder scale can be expressed as follows:

when $y_w > 0.91$,

$$G_0 = F_{G_i} * (42.85 + 161.26 * \left(\frac{y_w - 0.91}{5.54}\right)) \quad \text{(A5.16)}$$

$$\tau_0 = F_{\tau 0_i} * \left(2.17 + 1.19 * \left(\frac{y_w - 0.91}{5.54}\right)\right) \quad \text{(A5.17)}$$

when $y_w < 0.91$,

$$G_0 = F_{G_i} * (42.85 + 872.55 * \left(\frac{y_w - 0.91}{-0.7}\right)) \quad \text{(A5.18)}$$

$$\tau_0 = F_{\tau 0_i} * \ (2.17 - 0.72 * \left(\frac{y_w - 0.91}{5.54}\right)) \quad \text{(A5.19)}$$

A5.1.4 Numerical implementation

Finite Volume Mass equations for liquid water, gas and water vapor (Eqs. A5--A14) were solved by finite volume analysis, central differencing and Euler forward. The total simulation time is set to be consistent with the end time of drying experiments, and the time step is set based on the heat transfer penetration on the surface and lamellar layer of the mushroom. The Fourier number Fo^* is defined as the ratio of the rate of heat conduction to the rate of heat storage. For an explicit scheme to be stable in a one-dimensional heat conduction problem, the Grid Fourier number must satisfy the condition $Fo^* \leq 0.2$. We take the minimum value of the multiplication of the Grid Fourier number ($Fo^* = 0.2$) and thermal capacity and resistance as the time step. The mesh is applied to discretize computational domain. As shown in Fig.2, the cap mushroom is divided into hemispherical shells as the control volumes with

the equal thickness $\triangle r = \frac{Radius}{10}$ .The lamella part is a single control volume, which connects all hemispherical shells at its top, and the environment at its bottom surface. Python was used to solve the discretized governing equations. The shrinkage of *shiitake* mushroom results in changes in diameter of the mushroom and the $\triangle r$ of control volumes, which are recalculated and updated at every time step according to the changes in the volume of water and gas during drying.

A5.1.5 Parameter fitting results for hot air drying model

Single factor tests were conducted on parameters e, $F_{w,conv}$ and $F_{w,diff}$, respectively. The parameter range and values of the objective function are listed in Table A5.2. The initial guess of these parameters are as follows: e ranges from 0.1 to 0.9, $F_{w,conv}$ ranges from 1 to 20, $F_{w,diff}$ ranges from 1 to 20. From the single-factor tests, we obtained the optimal parameter set, as shown in test 10.

Table A5.2. *Single-factor tests*

Test code	e	$F_{w,conv}$	$F_{w,diff}$	LSE_sum
1	0.1	5	5	1.181
2	0.5	5	5	0.996
3	0.9	5	5	0.832
4	0.9	1	5	1.088
5	0.9	5	5	0.832
6	0.9	10	5	0.814
7	0.9	20	5	1.544
8	0.9	10	1	2.196
9	0.9	10	5	0.814
10	0.9	10	10	0.765
11	0.9	10	20	0.949

Subsequently, multiple rounds of parameter refinement were performed to further optimize the identified optimal parameter set. As shown in Table A3, to explore the local parameter space around the initial optimal values, the first round (tests 12-16) refined values were selected for each parameter: for e, values of 0.5 and 0.7 were added to verify if 0.9 was indeed the optimal maximum; for $F_{w,conv}$, values of 5 and 15 were tested, bracketing the initially optimal value of 10; for $F_{w,diff}$, 5 and 15 were examined. The results of this round revealed a new optimal combination (test 14): e = 0.9, $F_{w,conv}$ = 5, and $F_{w,diff}$ = 10, which improved the response variable compared with the previous optimal.

Consequently, in test 17-20, we continued the parameter refinement for the second round to further explored the local parameter space, and revealed a new optimal combination (test 19): e = 0.9, $F_{w,conv}$ = 5, and $F_{w,diff}$ = 8, with a response value of 0.7418249 (representing a 2.3% improvement over the previous optimal value of 0.759156). In test 21-24, a third round of refinement was designed to further explore potential improvements. A focused set of experiments was conducted to investigate the effects of adjusting the parameters within narrower intervals around the newly identified optimal values. To determine whether values of $F_{w,diff}$ smaller than 8 could yield further improvements, two additional levels 6,7 were tested. Given that $F_{w,conv}$ = 5 was optimal in the first-round tests (among 4, 5, and 6), smaller values of 3 was explored to check for potential hidden minima. The combination of $F_{w,conv}$ = 3 and $F_{w,diff}$ =7 was selected to evaluate the interaction between the smaller $F_{w,conv}$ and adjusted $F_{w,diff}$ values.

The results showed that despite testing multiple combinations, the new optimal response value of 0.745802 (corresponding to e = 0.9, $F_{w,conv}$ = 5, $F_{w,diff}$= 7) was higher than the previous optimum. This indicates that reducing $F_{w,conv}$or $F_{w,diff}$ within the current parameter refinement did not improve the outcome; instead, it led to a worse response. Therefore, after multiple rounds of parameter refinement, the combination of e = 0.9, $F_{w,conv}$ = 5 and $F_{w,diff}$= 8 remains the optimal solution.

Table A5.3. *Parameter Refinement tests*

Test code	e	$F_{w,conv}$	$F_{w,diff}$	LSE_sum
12	0.5	10	10	0.799
13	0.7	10	10	0.773
14	0.9	5	10	0.759
15	0.9	15	10	0.906
16	0.9	10	15	0.857
17	0.9	4	10	0.756
18	0.9	6	10	0.761
19	0.9	5	8	0.742
20	0.9	5	12	0.790
21	0.9	5	7	0.746
22	0.9	5	6	0.771
23	0.9	3	8	0.750
24	0.9	3	7	0.762

A5.1.6 The calculation and meanings of the statistical parameters

Coefficient of Determination (R^2), assesses the goodness-of-fit. It is given by:

$$R^2 = 1 - \frac{\Sigma(y_{exp} - y_{pred})^2}{\Sigma(y_{exp} - \bar{y}_{pred})^2} \quad \text{(A5.20)}$$

where y_{exp} represents the experimental values, y_{pred} are the predicted values, and $\bar{y}_{pred}$ is the mean of the experimental values.

Root Mean Square Error (RMSE), which measures the differences between the predicted and observed values:

$$RMSE = \sqrt{\frac{\Sigma(y_{exp} - \bar{y}_{pred})^2}{N}} \quad \text{(A5.21)}$$

where n is the number of observations.

Mean Absolute Error (MAE), which provides the average of absolute errors between the predicted and experimental values:

$$\text{MAE} = \frac{\Sigma|y_{exp} - y_{pred}|}{N} \quad \text{(A5.22)}$$

A5.2. Material and methods

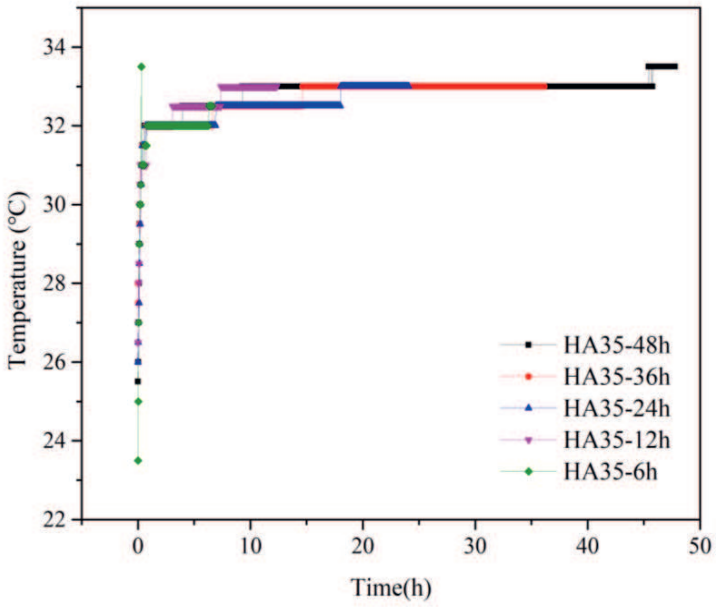
A5.2.1 Material preparation

Fresh *shiitake* mushrooms were purchased from a mushroom farm in Beijing (China) and stored in plastic bags at 4 ℃ until further use. The mushroom stems were cut, leaving mushroom caps with a diameter of 60 ×10⁻³ m for experiments. The thickness of lamella layer of mushroom cap is about 2×10⁻³ m. The average moisture content of mushrooms was 89.14 ± 2.0% (wet basis: w.b.), which was measured in a drying oven (DHG-9123A, Shanghai Jinghong Experiment Facility Co., Ltd., Shanghai, China) at 105 ◦C for 24 h (AOAC, 1990).

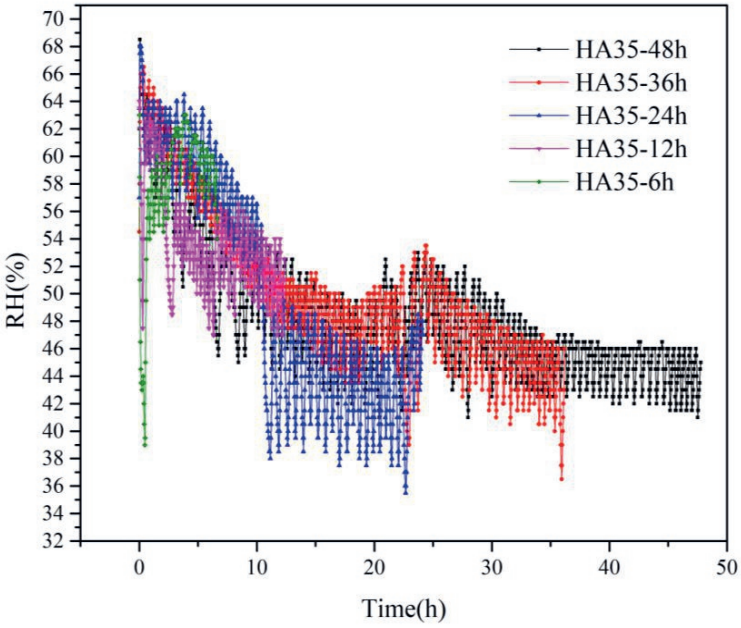
A5.2.2 Moisture content and temperature monitoring during drying

The moisture content and temperature of the mushroom were measured during hot air drying at 35 ◦C (HA35), with an air velocity maintained at 2 m/s. A precisely measured quantity of fresh *shiitake* mushrooms (200.0 ± 1.0 g) was placed and evenly spread on a wire mesh tray. The moisture contents of mushrooms were measured after various drying durations: 6h, 12h, 24h, 36h, 48h. The surface (measured at a depth of 0.2 mm depth below the skin of the

mushroom cap) and center (measured at a depth of 10 mm) temperatures of mushrooms were recorded using a K-type thermocouple probe (Omega Engineering Inc., Stamford, Connecticut, USA) connected to a data recorder (PicoLogTC-08, Pico Technology, England) (Hu et al., 2022).The air temperature and relative humidity within the drying oven were monitored synchronously using a humidity and temperature data logger (EL-USB-2-LCD+, Lascar Electronics, Hong Kong, China) during each experiment. These measurements were taken performed consecutively for each drying duration. The monitored air temperature and relative humidity results are given below, which provide the real information about the drying environment.



(a)



(b)

Fig. A5.2. *The air temperature (a) and relative humidity (b) in the drying oven*

A5.2.3 Measurement of dynamic moisture sorption of mushroom

The dynamic moisture sorption (DVS) measurements were conducted on HA35 dried mushroom samples. The sample preparation and DVS measurement procedure are the same as those used in our previous study (Hu et al., 2023).

A5.3 Supplementary for results

A5.3.1 The derivation procedure for the porosity evolution of mushrooms during drying

$$\mathrm{V}_{mushroom}(\mathrm{t}) = \mathrm{V}_{air}(t) + \mathrm{V}_{solid} + \mathrm{V}_{water}$$

$$\frac{\mathrm{V}_{mushroom}(\mathrm{t})}{\mathrm{V}_{solid}} = \frac{\mathrm{V}_{air}(t)}{\mathrm{V}_{solid}} + 1 + \frac{\mathrm{V}_{water}(t)}{\mathrm{V}_{solid}}$$

$$\frac{\mathrm{V}_{mushroom}(\mathrm{t})}{\mathrm{V}_{solid}} = \frac{\mathrm{V}_{air}(t)}{\mathrm{V}_{solid}} + 1 + \frac{\frac{m_{water}(t)}{\rho_{water}}}{\frac{m_{solid}}{\rho_{solid}}}$$

$$\frac{\mathrm{V}_{mushroom}(\mathrm{t})}{\mathrm{V}_{solid}} = \frac{\mathrm{V}_{air}(t)}{\mathrm{V}_{solid}} + 1 + \mathrm{Xm}(t) * \frac{\rho_{solid}}{\rho_{water}}$$

$$\frac{\mathrm{V}_{mushroom}(\mathrm{t})}{\mathrm{V}_{solid}} = \frac{\mathrm{V}_{air}(t)}{\mathrm{V}_{solid}} + 1 + \mathrm{Xm}(t) * \frac{\rho_{solid}}{\rho_{water}}$$

A5.3.2 Absolute humidity changes in the drying oven

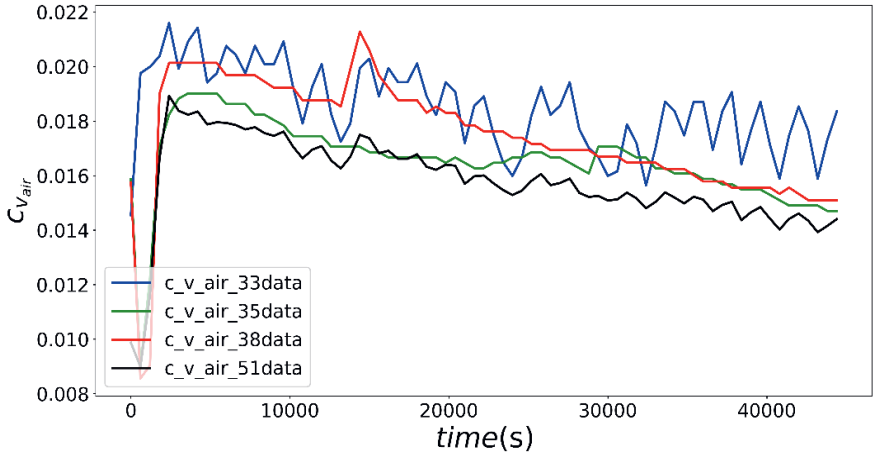
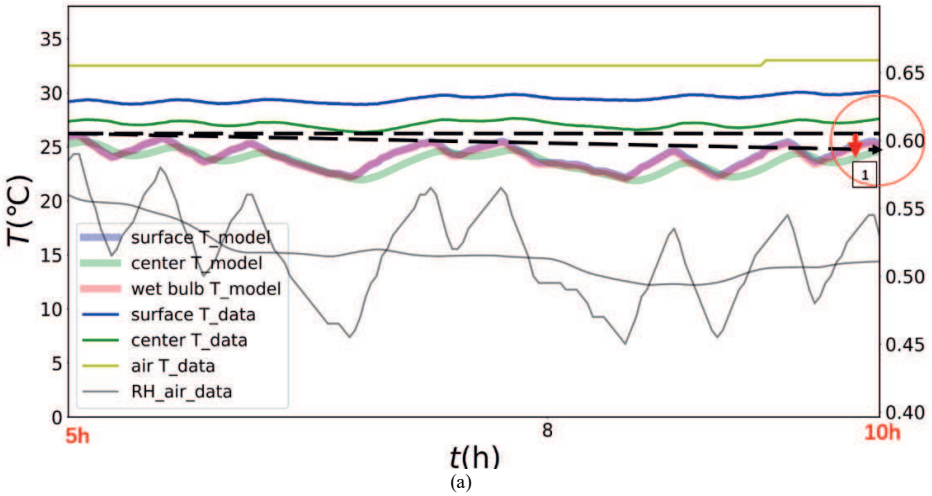
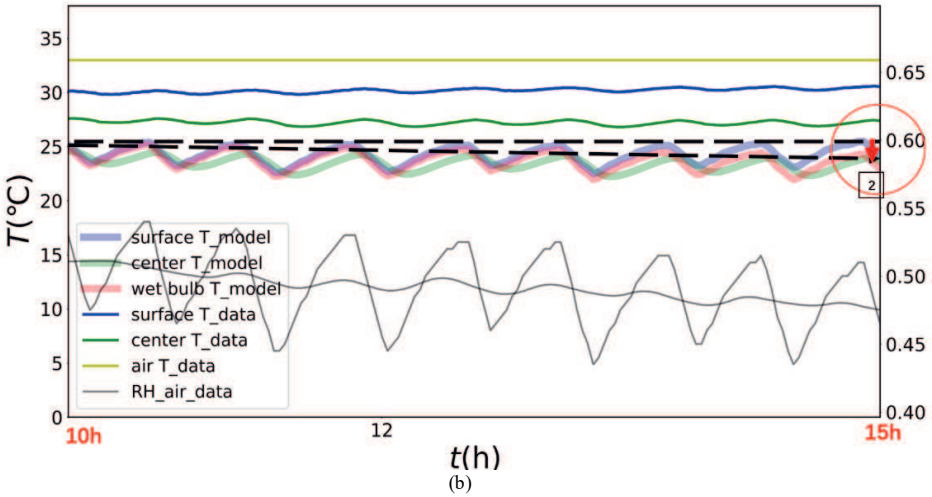


Fig.A5.3. *Absolute humidity change in the drying oven during HA33, HA35, HA38, HA51*

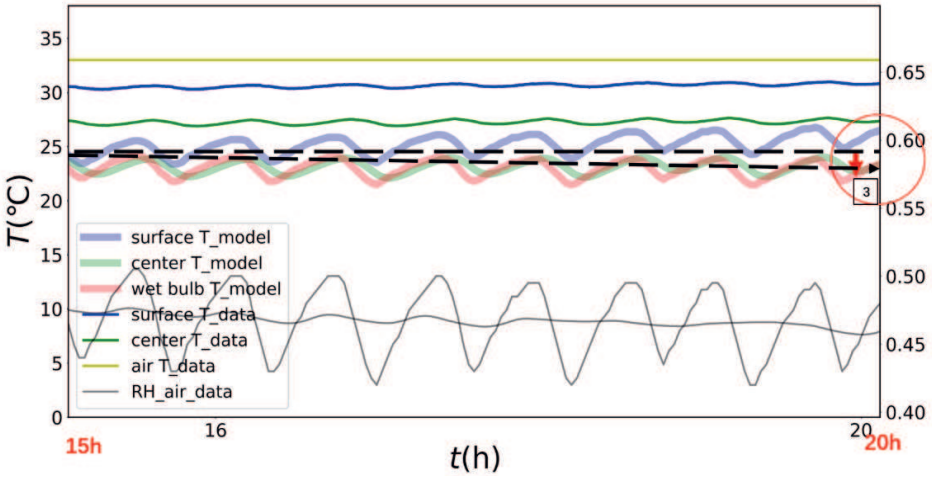
A5.3.3 Product temperature fluctuations during drying



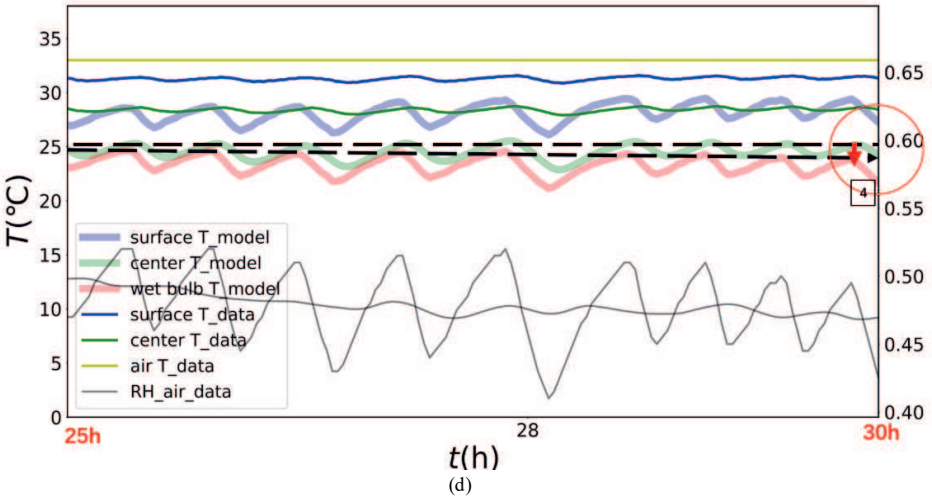
(a)



(b)



(c)



(d)

Fig. A5.4. *Product temperature fluctuations align with relative humidity at different time intervals during the drying (red arrows 1-4 indicate the decrease during the intervals of 5 - 10 h(a), 10 - 15 h(b), 15 - 20 h(c), and 25 - 30 h(d))*

Chapter 6

General discussion

6.1. Introduction

This thesis investigated serial combined drying technology to achieve both good rehydration and texture retention in *shiitake* mushrooms. After the initial experimental evaluation of various serial combined drying techniques, we found the instant controlled pressure drop (DIC) combined with hot air (HA) drying at 35°C as the promising drying technology for good rehydration performance (Chapter 2). We formulated the hypothesis that good rehydration after the DIC/HA treatment was due to the slight porosity enhancement during the DIC stage, and preservation of the cell membrane integrity throughout the drying process. Subsequently, we investigated the microstructural evolution of mushrooms throughout the DIC treatments. We found that DIC increases sub-surface layer porosity, without disrupting the cell membrane, if the product temperature remains below the critical threshold of 40°C during drying (Chapter 3). Then, we aimed to develop a mechanistic drying model to optimize the serial combined drying process. Before modeling the whole drying process, we examined how the cell membrane and viscoelasticity in mushrooms impacted their moisture sorption behavior, resulting in a theoretical model predicting moisture sorption isotherms (MSIs) (chapter 4 and 5). We improved the Flory-Huggins model for water activity prediction via 1) incorporating elastic stress in the driving force for moisture transport; and 2) the modelling of two water-holding compartments, namely, cell wall/cytoplasm and vacuole-separated by the tonoplast membrane, but in thermodynamic equilibrium. Thereafter, we developed an overall drying model describing heat and mass transfer during hot air (HA) mushroom drying (Chapter 5), supplemented by the extended Flory-Huggins MSI model, and an empirical relation for shrinkage. The mathematical complexity of describing the shrinkage of open pore systems precluded the development of a fully mechanistic model. After validating the full drying model against hot air drying experiments, we interpreted NMR experiments conducted on *shiitake* mushrooms during drying at different temperatures and established reliable conditions for the loss of cell membrane integrity.

In this chapter, we reflect on our main findings, and compare them with contemporary research, and conclude with recommendations for future investigations.

6.2 Reflections on serial combined drying method

6.2.1 Porosity enhancement

Initially, DIC treatment was selected because our initial expectation was that the structure of

mushroom can be expanded significantly. However, the experiments did not yield the expected expansion and only a slight porosity enhancement was observed. This was attributed to the fact that the mushroom is too wet to achieve this expansion, because pore formation requires a hard skin (also known as case hardening) (van der Sman et al., 2024). Based on the glass transition and state diagram for mushrooms (Zhao et al., 2016), the absence of case hardening in mushrooms after DIC treatment can be explained by the too low glass transition temperature (Tg) properties of the *shiitake* mushroom via the presence of a large portion of mannitol in its vacuole. Although the rapid decompression during DIC-puffing causes instantaneous surface dehydration, the mushroom retains most of its internal moisture. Although, the wrinkling observed on the surface of the mushroom during drying (as shown in Fig.6 in Chapter 4), shows the skin has sufficient strength for deformation, it might be due to the elastic properties of the compact skin via its crosslinked/entangled hyphae network structure. Another possible explanation is that when the cell membrane remains intact and the mannitol remains in the vacuole, the cell wall will present a (separate) high Tg due to its high polysaccharide composition (Rathore et al., 2017), and develops elasticity when it enters the glassy state. The stiff skin allows for the observed slight increase in porosity within the sub-surface layer of the mushroom after DIC treatment. The different Tg of vacuole and cell wall is not accounted yet for in our model, but it is recommended to be included in future drying models. Such differences in Tg between the cell wall and vacuole also exist in fruits and vegetables, as they have small sugars like glucose, fructose, and saccharose in their vacuoles, which also have a low Tg (Goula et al., 2008; Li et al., 2019; Xu, C. et al., 2017).Drying models of fruits and vegetables may also benefit from a two-compartment model for moisture sorption and drying. However, the initial porosity of most fruits and vegetables (except for eggplant, okra, etc.) is significantly lower than that of mushrooms, with tiny pores in between cells in extracellular junctions. Therefore, we question that whether there is potential for the application of DIC to other "wet" fruits and vegetables. An alternative pretreatment before DIC to create initial porosity is partial-freeze-drying (Peng et al., 2018; Siebert et al., 2018), which may cause, however, cell damage if the ice crystals puncture the cell membranes.

6.2.2 Other combined drying technologies to enhance rehydration

In recent years, there has been an abundance of literatures on combined drying methods reporting improved rehydration, including serial and parallel combined drying, such as hot air combined with radio frequency vacuum drying(Chen et al., 2024), pulse-spouted

microwave vacuum drying (PSMVD) (Hao Zhang a, 2025), ultrasonic-assisted infiltration vacuum freeze-drying combined with hot air drying (Sun et al., 2022), microwave vacuum drying (MVD) combined with hot air drying (HAD) (Xu et al., 2020), freeze vacuum drying (FVD) combined with hot air drying (HAD) (Zhang et al., 2019), microwave-assisted hot air drying (MAHD) (Zhao et al., 2023), vacuum drying (VD) combined with heat pump drying (HPD) (Han and Jin 2024), etc. However, these methods (except for VD+HPD) involve intense thermal effects such as microwave heating, or ice crystal formation during freeze drying, which can lead to irreversible damage to the cell membranes. This contradicts the primary objective conclusion of our study that membrane maintenance is beneficial for good rehydration performance. In principle, vacuum drying can minimize thermal damage by lowering the boiling point of water below a critical temperature, and thus further improve rehydration. However, none of these studies give a mechanistic/microstructural explanation for rehydration improvement.

Meanwhile the research of this thesis, other researchers further investigated serial or parallel combined drying to shorten drying time and improve final quality of dried products (Guo et al., 2024; Zhang et al., 2017). In literature we found that parallel combined drying received more attention than serial combined drying (Maftoonazad et al., 2022, Kumar et al., 2024; Ozbek et al., 2022), as well as rehydration ratio and rate (Hao Zhang a, 2025; Jeon et al., 2024). From an academic perspective, parallel combined drying methods have a more innovative character than serial-combined drying (which simply means application of existing techniques in sequence). Hence, this research direction would attract more attention and funding. However, this does not mean that serial combined drying is less performing with regard to product quality, and from industrial perspective they remain of interest because of their higher Technology-Readiness-Level (TRL).

6.2.3 Critical conditions for cell membrane integrity

The preservation of cell membrane integrity was attributed to the long maintenance of the product temperature at the wet bulb temperature (Chapter 3&5). This effect ceases in the falling rate period, where moisture loss causes the temperature to rise beyond critical thresholds (e.g., M_c>3% w.b. and T_p<40°C for mushrooms). During pre-treatments, such as blanching, this critical temperature is often exceeded (Wang et al., 2024), leading to the loss of cell membrane integrity and reduced rehydration performance.

Given that similar conditions have been observed in yeast and seeds (Fine and Gervais, 2005; Veser et al., 2025), the underlying mechanism, where low temperature and sufficient moisture

jointly mitigate membrane damage during drying, may apply broadly across biological materials, including fruits and vegetables. This can be attributed to the similar sensitivity of cell membranes to thermal and dehydration stress. Nevertheless, variations in cell wall structure and solute composition across species could influence the precise critical values of these parameters. Therefore, experimental validation across different produce types is required to confirm the generalizability of these thresholds and clarify any species-specific adaptations, thereby strengthening their practical applicability in food preservation and processing.

6.3 Mechanistic modeling of mushroom drying

Our initial research objective was to develop a fully mechanistic model of mushroom drying. In principle, a complete mechanistic model incorporating all key processes is possible. However, this is constrained by its requirement for extensive and precise physical parameters, as well as the inherent mathematical complexity of the large deformation mechanics of soft matter, which has a steep learning curve. The latter limited us to develop a fully mechanistic model, and we used an empirical relation for the volume shrinkage as a function of moisture content.

We note, that our two-compartment model is a first step towards a multiscale model of drying for fruits and vegetables, and the lack of properties at the cellular level limits its applicability. As the drying model conceptualized moisture sorption at the cell-scale, it necessitates the requirement of material properties at the cellular scale, as the cell wall contains (chitin) fibers restraining large deformations in their transversal direction. Accounting for rheology at the cellular scale would improve accuracy. However, this cannot be obtained via Texture Profile Analysis (TPA) compression tests. A more accurate viscoelastic properties might be obtained with the Dynamic Mechanical Analysis (DMA) (Kovalenko et al., 2016; Rzigue et al., 2016), which applies an oscillating mechanical force to a sample, allowing researchers to observe how the material deforms and recovers over time, providing information about the material's stiffness, energy dissipation, and transition behaviors. The nano indentation could be an alternative method to measure the mechanical properties at the cellular scale. In nanoindentation, a tip applies a milli-Newton-force to penetrate a sample nanometer deep. The resulting force-displacement curve is used to calculate mechanical properties like elastic modulus, and to identify phenomena such as creep, strain hardening, and fracture toughness (Mahmoud et al., 2024).

During drying, moisture transport is intrinsically coupled with stress development and

microstructural evolution. Its principle driving force (the chemical potential) has two contributions: the osmotic pressure and stress, which enforces the coupling between moisture transport, shrinkage and stress (Gulati and Datta, 2016; Hong et al., 2008b; van der Sman, 2023). This coupling is missing in the current drying model, as we did not solve the momentum balance, which delivers the stress field. Ultimately, this coupling of shrinkage and stress can initiate pore formation, altering the microstructure. Therefore, we propose future models to solve the momentum balance equation.

For modeling the large deformation during drying, there are two mechanistic approaches: 1) the poro-mechanics framework followed by Datta (Rakesh and Datta, 2011), and 2) the monophasic approach developed by (Hong et al., 2008a) – which extends Flory-Rehner – as we used in our MSI model. Datta's group has developed a wide variety of multiphysics models for porosity development and deformation during intensive heating processes (Datta et al., 2012; Gulati and Datta, 2015, 2016; Gulati et al., 2016; Rakesh and Datta, 2011), where deformation is primarily driven by internal pressure generated from the rapid evaporation of liquid water, and mass transport is governed by pressure-driven Darcy flow. The solid mechanics are described using a hyperplastic Neo-Hookean model to account for large deformations, and coupled with Darcy's law for fluid transport, while also tracking porosity evolution with the assumption of incompressibility of the solid phase. Following the theory of poromechanics, this approach does not explicitly account for bound water or couple the stress with the moisture transport. In contrast, Hong et al. (2008a) presented a theory that coupled mass transport and large deformation in polymeric gels. Water and polymers constitute a single thermodynamic phase, following the Flory- Rehner theory. The theory's foundation of this theory is a free-energy function comprising two parts: the strain energy of the polymer network, described by Flory Rehner theory, and the mixing energy of polymers and solvent molecules, based on the Flory-Huggins theory. However, they did not consider the capillary water,. Abedi et al. (2023) developed a hybrid mixture theory (HMT)-based model, which distinguishes between bound water and capillary water. However, the HMT-based model does not account for large deformations.

Materials like mushrooms in this study present an initial open pore structure. However, a comprehensive mechanical model for such structures has not yet been fully developed (van der Sman et al., 2024). Within the theoretical framework proposed by Suo (Zhao et al., 2008), it remains an open question on how to effectively couple the gas pressure and stress in the gel phase for an open pore system. Although Datta's model addresses open-pore systems (Gulati and Datta, 2016), it does not adopt the Flory-Huggins/Flory-Rehner perspective. Thus,

the key challenge is to bridge the gap between the two approaches. By integrating pressure-driven flow and large deformation with the thermodynamically consistent diffusion-deformation theory, the hybrid model can better capture the multi-physics of moisture transport—from initial internal vapor flow to late-stage molecular diffusion—enabling optimized control over shrinkage and final product quality.

6.4 The potential of NMR to be used for drying research

As demonstrated in previous studies (Gonzalez et al., 2010; Qiao et al., 2005 ; Xu, F. et al., 2017; Zhang and McCarthy, 2012), the transverse relaxation time (T_2) serves as an effective non-destructive indicator for tracking water populations in cellular food materials, and for cell membrane integrity during drying, which has been validated in the studies of (Jiang et al., 2019; Qiu et al., 2021). The multi-exponential relaxation behavior reflects the distinct physical states of water in different cellular compartments (e.g., vacuoles, cytoplasm, cell walls) (As and Duynhoven, 2013). As illustrated by (As and Duynhoven, 2013; Hills and Reson., 1999), the confinement of water within the microstructures of biological tissues directly influences its dynamics, causing reduced T_2 relaxation times in NMR. In dried foods, the spectrum of T_2 relaxation time, as revealed by a multi-exponential model, informs cellular integrity (Musse et al., 2025). Upon membrane rupture during severe drying, the water populations mix, causing the merging of the T_2 peaks to a single-exponential.

T_2-NMR/MRI holds significant potential for advancing drying research, particularly in validating multiphysics/multiscale simulation models by providing rich, spatially-resolved datasets for direct comparison. For instance, MRI can directly and non-invasively observe full-field sample shrinkage during drying, quantifying spatial displacement (Jiang et al., 2019), while techniques like Magnetic Resonance Elastography (MRE) can map material properties such as shear modulus by measuring wave-induced displacements of the body using an external actuation system like ultrasound (Carvalho et al., 2025; Manduca et al., 2001). This enables multimodal validation that moves beyond conventional temperature and moisture content measurements. Furthermore, NMR presents a promising pathway for at-line, non-destructive quality monitoring, such as the assessment of cell membrane integrity. Future efforts should focus on developing integrated NMR systems for industrial dryers, equipped with controlled environmental supply and synchronized sensors for air/product temperature and humidity. Such systems would allow for the real-time adjustment of drying parameters to preserve quality attributes and optimize the process directly in a factory setting.

6.5 Future work directions

Our original objective of this thesis was to develop a model for whole drying process of mushroom, including the DIC step, and the optimization of the drying process for rehydration improvement. From the conclusions and reflections drawn from this thesis, we know that a physics-based computational model will offer researchers a powerful tool to interpret experimental processes, including moisture sorption isotherms and drying, and to test different scenarios during the design and optimization of the processing of different food materials.

Note, a key requirement for applying the moisture sorption model to other fruits and vegetables is the precise definition of the sample's initial state for the DVS experiment — specifically, whether residual stress is locked within the matrix prior to the DVS measurement. The initial state of a wet product is well defined, as it is stress free. The initial drying step must be performed under well controlled and measured conditions, but it can even be performed within the DVS equipment.

The established hot air drying model for *shiitake* mushroom in this work is the first step for further modeling of the complete DIC treatment, which consists of a sequence of different processing units. For instance, the DIC- heating stage can be described with the hot air model with the assumption that the air velocity in the DIC chamber equals zero. However, the modeling of heat and mass transfer at the moment of DIC- puffing and the continued evaporative cooling under the DIC-vacuuming still needs to be investigated, which requires solving momentum balance and convective gas transport within the mushroom tissue. Particularly, the sudden pressure drop, causes expansion of the gas inside the mushroom, combined with pressure-gradient driven flows - which occur at a fast timescale, and thus constitutes a challenge for the model. Inertial effects may need to be considered in the momentum balance, which is still poorly investigated in the field of soft matter mechanics.

We assume that a validated DIC model would serve as the core of a simulation-driven optimization framework. However, the state diagram, as shown in Fig.5.12 in Chapter 5, might already be insightful for designing an optimization strategy, such as a multi-stage drying stages for DIC treatment or vacuum drying. Namely, at the beginning of HA drying or DIC heating stage, the wet materials remain at or below the wet bulb temperature when air temperature is above the wet bulb temperature but still have a low relative humidity. The DIC heating stage can be enhanced by incorporating microwave/RF or infrared radiation as the heat source, provided that the wet bulb temperature remains below the critical condition.

The DIC vacuum stage can be improved via cyclic evacuation, as proposed by pulsed-vacuum drying (Wang et al., 2018; Yi et al., 2016).

In conclusion, this thesis not only provides a potential combined drying strategy, but also an important step forward in the modeling framework for cellular food materials. By addressing these future directions, the development of next-generation, quality-sensitive drying processes for a wider range of vegetables and fruits can be accelerated.

References

Abdollah Hajalilou, L.S.G. (2019). Evaluation Technologies for Food Quality. https://doi.org/10.1016/B978-0-12-814217-2.00030-5.

Abedi, F., Kumar, S., Kumar, N., Kumar, D., & Takhar, P.S. (2023). Moisture transport and stress development in rice during drying, a Hybrid Mixture Theory-based model. *Drying Technology*,41(13), 2119-2142. https://doi.org/10.1080/07373937.2023.2220019.

Adduci, G., Petrosino, F., Manoli, E., Cardaropoli, E., Coppola, G., & Curcio, S. (2024). Transport phenomena in pasta drying a dough-air double domain advanced modelling. *Journal of Food Engineering*,376, 112052. https://doi.org/ 10.1016/j.jfoodeng.2024.112052.

Aguilera, J.M. (2006). Seligman lecture 2005 food product engineering: building the right structures. *Journal of the Science of Food and Agriculture*, 86(8), 1147-1155. https://doi.org/ 10.1002/jsfa.2468.

Ajani, C.K., Zhu, Z., & Sun, D.-W. (2023). Shrinkage during vacuum cooling of porous foods: Conjugate mechanistic modelling and experimental validation. *Journal of Food Engineering*, 337, 111220. https://doi.org/ 10.1016/j.jfoodeng.2022.111220.

Allaf, T., & Allaf, K. (2014). Instant Controlled Pressure Drop (D.I.C.) in Food Processing. New York: Springer-Verlag.

Angersbach, A., Heinz, V., & Knorr, D. (1999). Electrophysiological model of intact and processed plant tissues: Cell disintegration criteria. *Biotechnology Progress*, 15, 753-762. https://doi.org/10.1021/bp990079f

Antal, T.; Sikolya, L.;Kerekes, B.(2014). Quality evaluation of different pre-treatments and combined convective-freeze drying of sour cherry (*Prunus Cerasus L.*). *Progress in Agricultural Engineering Sciences*, 10, 17-33. https://doi.org/10.1556/progress.10.2014.2

Aregawi, W.A., Abera, M.K., Fanta, S.W., Verboven, P., & Nicolai, B. (2014). Prediction of water loss and viscoelastic deformation of apple tissue using a multiscale model. *Journal of physics: condensed matter*,26(46), 464111. https://doi.org/10.1088/0953-8984/26/46/464111

Arganda-Carreras, I., Kaynig, V., Rueden, C., Eliceiri, K. W., Schindelin, J., Cardona, A., & Seung, H. S. (2017). Trainable weka segmentation: A machine learning tool for microscopy pixel classification. *Bioinformatics*, 33 (15), 2424--2426.

https://doi.org/10.1093/bioinformatics/btx180

Argyropoulos, D., Alex, R., & Mueller, J., (2010). Establishing moisture sorption isotherms of wild mushroom varieties using a dynamic vapor sorption method, XVIIth World Congress of the International Commission of Agricultural Engineering (CIGR) - Section VI: Postharvest Technology and Process Engineering, Quebec City, Canada. pp. 13 -17.

Argyropoulos, D., Heindl, A., & Müller, J. (2011). Assessment of convection, hot-air combined with microwave-vacuum and freeze-drying methods for mushrooms with regard to product quality. *International Journal of Food Science & Technology*,46(2), 333-342. https://doi.org/ 10.1111/j.1365-2621.2010.02500.x.

Artnaseaw, A.; Theerakulpisut, S.;Benjapiyaporn, C.(2010). Drying characteristics of *shiitake* mushroom and Jinda chili during vacuum heat pump drying. *Food and Bioproducts Processing*, 88, 105-114. https://doi.org/ 10.1016/j.fbp.2009.09.006

As, H.V., & Duynhoven, J.v. (2013). MRI of plants and foods. *Journal of Magnetic Resonance*,229 25--34. https://doi.org/ 10.1016/j.jmr.2012.12.019.

ASHRAE (1997).1997 ASHRAE Handbook---Fundamentals. (SI Edition) . American Society of Heating, Refrigerating and Air-Conditioning Engineers, Inc. Atlanta, GA.

Baltacıoglu, H., Bayındırlı, A., Severcan, M., & Severcan, F. (2015). Effect of thermal treatment on secondary structure and conformational change of mushroom polyphenol oxidase (PPO) as food quality related enzyme: A FTIR study. *Food Chemistry*, 187, 263--269. https://doi.org/ 10.1016/j.foodchem.2015.04.097.

Banaszak, J., & Kowalski, S.J. (2002). Drying induced stresses estimated on the base of elastic and viscoelastic models. *Chemical Engineering Journal*,86, 139--143.

Barua, B., & Saha, M.C. (2016). Incorporating density and temperature in the stretched exponential model for predicting stress relaxation behavior of polymer foams. *Journal of Engineering Materials and Technology*, 138, 1. https://doi.org/ 10.1115/1.4031426.

Beney, L., de Maranon, I. M., Marechal, P. A., & Gervais, P. (2000). Influence of thermal and osmotic stresses on the viability of the yeast Saccharomyces cerevisiae. *International Journal of Food Microbiology*, 55, 275--279. https://doi.org/10.1016/S0168-1605(00)00203-8

Benseddik, A., Azzi, A., Zidoune, M.N., Khanniche, R., & Besombes, C. (2019). Empirical and diffusion models of rehydration process of differently dried pumpkin slices.

Journal of the Saudi Society of Agricultural Sciences,18, 401--410. https://doi.org/10.1016/j.jssas.2018.01.003.

Bird, R.B., Stewart, W.E., & Lightfoot, E.N. (2002). *Transport Phenomena* (2nd Ed)_ (2nd Ed ed. John Wiley & Sons, Inc., New York / Chichester / Weinheim / Brisbane / Singapore / Toronto.

Borompichaichartkul, C., Moran, G., Srzednicki, G., & Price, W.S. (2005). Nuclear magnetic resonance (NMR) and magnetic resonance imaging (MRI) studies of corn at subzero temperatures. *Journal of Food Engineering*,69(2), 199-205. https://doi.org/10.1016/j.jfoodeng.2004.07.018.

Burnett, D.J., Garcia, A.R., & Thielmann, F. (2006). Measuring moisture sorption and diffusion kinetics on proton exchange membranes using a gravimetric vapor sorption apparatus. *Journal of Power Sources*, 160, 426--430. https://doi.org/10.1016/j.jpowsour.2005.12.096.

Buwjoom, T., Suchon Tangtaweewipat, Thongwittaya, N., & Yamauchi, K.-e. (2004). Chemical composition, nutritent digestibility and metabolizable energy of *shiitake* mushroom stalk meal. *Journal of Poultry Science*, 41, 322-328. https://doi.org/10.2141/jpsa.41.322.

Cantre, D., Herremans, E., Verboven, P., Ampofo-Asiama, J., & Nicolaï, B. (2014). Characterization of the 3-D microstructure of mango (Mangifera indica L. cv. Carabao) during ripening using X-ray computed microtomography. *Innovative Food Science & Emerging Technologies*, 24, 28-39. http://dx.doi.org/10.1016/j.ifset.2013.12.008

Carneiro, A.A., Ferreira, I.C., Duenas, M., Barros, L., Da Silva, R., Gomes, E., & Santos-Buelga, C. (2013). Chemical composition and antioxidant activity of dried powder formulations of Agaricus blazei and Lentinus edodes. *Food and Chemical Toxicology*,138, 2168-2173. https://doi.org/ 10.1016/j.foodchem.2012.12.036.

Carvalho, L., Pereira, I.D.O., Andreani, L., Cunha, F.R., Luz, S.M., Dias, R.M., Silva, A.M.A., Valadares, L.F., & Monteiro, S. (2025). Production of oleogels from cellulose and starch cryogels: Morphological, thermal, mechanical, and viscoelastic properties. *LWT - Food Science and Technology*, 217, 117406. https://doi.org/10.1016/j.lwt.2025.117406.

Castro, A.M., Mayorg, E.Y., & Moreno, F.L. (2018). Mathematical modelling of convective drying of fruits: A review. *Journal of Food Engineering*, 223,152-167. https://doi.org/

10.1016/j.jfoodeng.2017.12.012.

Caurie, M. (2007). Hysteresis phenomenon in foods. *International Journal of Food Science and Technology*,42, 45-49. https://doi.org/ 10.1111/j.1365-2621.2006.01203.x.

Çengel, Y., & Boles, M. (2006).Thermodynamics: An Engineering Approach. McGraw Hill Higher Education.

Champion, D., Loupiac, C., Simatos, D., Lillford, P., & Cayot, P. (2011). Structural relaxation during drying and rehydration of food materials---the water effect and the origin of hysteresis. *Food Biophysics*, 6, 160--169. https://doi.org/ 10.1007/s11483-011-9204-5.

Chanvrier, H., Jakubczyk, E., Gondek, E., & Gumy, J.-C. (2014). Insights into the texture of extruded cereals: Structure and acoustic properties. *Innovative Food Science & Emerging Technologies*,24, 61-68. https://doi.org/ 10.1016/j.ifset.2013.11.013.

Chen, A., EL, G., Achkar, Liu, B., & Bennacer, R. (2021). Experimental study on moisture kinetics and microstructure evolution in apples during high power microwave drying process. *Journal of Food Engineering*. https://doi.org/ 10.1016/j.jfoodeng.2020.110362.

Chen, A., Wan, F., Ma, G., Ma, J., Xu, Y., Zang, Z., Ying, X., Jia, H., & Huang, X. (2024). Radio frequency vacuum drying study on the drying characteristics and quality of cistanche slices and analysis of heating uniformity. Foods 13, 2672. https://doi.org/ 10.3390/foods13172672.

Chen, Z.;Lamb, F.M. (2001). Vacuum drying of small wood components at room temperature. *Forest Products Journal*, 51,55-57.

Cheng, S., Li, R., Yang, H., Wang, S., & Tan, M. (2020). Water status and distribution in *shiitake* mushroom and the effects of drying on water dynamics assessed by LF NMR and MRI. *Drying Technology*,38(8), 1001-1010. https://doi.org/10.1080/07373937.2019.1625364.

Contreras, C.; MartÍn-Esparza, M.E.;MartÍnez-Navarrete, N.(2012). Influence of drying method on the rehydration properties of apricot and apple. *Journal of Food Process Engineering*, 35, 178-190. https://doi.org/ 10.1111/j.1745-4530.2010.00579.x

Cornet, S.H.V., van der Goot, A.J., & van der Sman, R.G.M. (2020). Effect of mechanical interaction on the hydration of mixed soy protein and gluten gels. *Current Research in*

Food Science, 3, 134-145. https://doi.org/ 10.1016/j.crfs.2020.03.007.

Curatolo, M., Nardinocchi, P., & Teresi, L. (2018). Driving water cavitation in a hydrogel cavity. *Soft Matter*.14, 2310. https://doi.org/ 10.1039/C8SM00100F.

Dadmohammadi, Y., & Datta, A.K. (2020). Food as porous media: a review of the dynamics of porous properties during processing. *Food Reviews International*, 38(5), 953–985. https://doi.org/ 10.1080/87559129.2020.1761376.

Datta, A., Erdogdu, F., Nicolaï, B., Marra, F., Vitrac, O., Verboven, P., Sarghini, F., & Koh, C. (2022). Computer-aided food engineering. *Nature Food*,3, 894--904. https://doi.org/ 10.1038/s43016-022-00617-5.

Datta, A.K. (2007a). Porous media approaches to studying simultaneous heat and mass transfer in food processes. I: Problem formulations. *Journal of Food Engineering*,80 80--95. https://doi.org/ 10.1016/j.jfoodeng.2006.05.013.

Datta, A.K. (2007b). Porous media approaches to studying simultaneous heat and mass transfer in food processes. II: Property data and representative results. *Journal of Food Engineering*,80, 96--110. https://doi.org/ 10.1016/j.jfoodeng.2006.05.012.

Datta, A.K., van der Sman, R., Gulati, T., & Warning, A. (2012). Soft matter approaches as enablers for food macrosccale simulation. *Faraday Discuss,*158, 435-459; discussion 493-522. https://doi.org/ 10.1039/c2fd20042b.

Defraeye, T. (2014). Advanced computational modelling for drying processes -- A review. *Applied Energy*,131, 323--344. https://doi.org/ 10.1016/j.apenergy.2014.06.027.

Defraeye, T., & Radu, A. (2018). Insights in convective drying of fruit by coupled modeling of fruit drying, deformation, quality evolution and convective exchange with the airflow. *Applied Thermal Engineering*,129, 1026-1038. https://doi.org/ 10.1016/j.applthermaleng.2017.10.082.

Demir, H., Cihan, E., & Demir, H. (2020). 3D simulation of transport phenomena of onion drying with moving boundary in a vacuum oven. *Journal of Food Process Engineering*,43(4). https://doi.org/ 10.1111/jfpe.13361.

Demirkesen, I., Kelkar, S., Campanella, O.H., Sumnu, G., Sahin, S., & Okos, M. (2014). Characterization of structure of gluten-free breads by using X-ray microtomography. *Food Hydrocolloids*,36, 37-44. https://doi.org/ 10.1016/j.foodhyd.2013.09.002.

Deng, Y., Luo, Y., Wang, Y., Yue, J., Liu, Z., Zhong, Y., Zhao, Y., & Yang, H. (2014).

Drying-induced protein and microstructure damages of squid fillets affected moisture distribution and rehydration ability during rehydration. *Journal of Food Engineering*,123,23-31. https://doi.org/ 10.1016/j.jfoodeng.2013.09.006.

Dinani, S.T., Hamdami, N., Shahedi, M., & Havet, M. (2014). Mathematical modeling of hot air/electrohydrodynamic (EHD) drying kinetics of mushroom slices. *Energy Conversion and Management*,86, 70--80. https://doi.org/ 10.1016/j.enconman.2014.05.010.

Doulia, D., Tzia, K., & Gekas, V. (2000). A knowledge base for the apparent mass diffusion coefficient (DEFF) of foods. *International Journal of Food Properties*, 3(1), 1-14. https://doi.org/ 10.1080/10942910009524613.

Doymaz, I. (2012). Infrared drying of sweet potato (*Ipomoea batatas L.*) slices. *Journal of Food Science & Engineering*, 49, 760-766. https://doi.org/ 10.1007/s13197-010-0217-8

Duangkhamchan, W.; Wiset, L.; Poomsa-ad N. (2013). Evaluation of drying and moisture sorption characteristics models for *shiitake* mushroom (*Lentinussquarrosulus* Mont.) and grey oyster mushroom.Suranaree. *Journal of Science and Technology*, 20 (2):151-166.

Dupas-Langlet, M., Dupas, J., Samain, S., Giardiello, M.-I., Meunier, V., & Forny, L. (2016). A new method to determine "equilibrated" water activity and establish sorption isotherm by erasing surface history of the samples. *Journal of Food Engineering*, 184, 53-62. https://doi.org/ 10.1016/j.jfoodeng.2016.03.023.

Ene, I.V., Walker, L.A., Schiavone, M., Lee, K.K., Martin-Yken, H., Dague, E., Gow, N.A.R., Munro, C.A., & Brown, A.J.P. (2015). Cell Wall Remodeling Enzymes Modulate Fungal Cell Wall Elasticity and Osmotic Stress Resistance. *mBio*.6(4), e00986-00915. https://doi.org/ 10.1128/mBio.00986-15.

Erriguible, A., Bernada, P., Couture, F., & Roques, M.-A. (2007). Simulation of vacuum drying by coupling models. *Chemical Engineering and Processing*: *Process Intensification*,46(12), 1274-1285. https://doi.org/10.1016/j.cep.2006.10.011.

Fan, X. P., Wang, Y. J., Zou, Z. J., Wu, F. Y., & Ying, D. Y. (2018). A review on explosion puffing technology for fruits and vegetables. *International Journal of Food Engineering*, 332-336. http://dx.doi.org/10.18178/ijfe.4.4.332-336

Fine, F., & Gervais, P. (2005). Thermal destruction of dried vegetative yeast cells and dried

bacterial spores. *Environmental Microbiology*,7(1),40--46. https://doi.org/ 10.1111/j.1462-2920.2004.00689.x.

Foley, D.A., Dunn, A.L., & Zell, M.T. (2016). Reaction monitoring using online vs tube NMR spectroscopy: seriously different results. *Magnetic resonance in chemistry*: MRC54(6), 451--456. https://doi.org/10.1002/mrc.4259.

Fredriksson, M., & Thybring, E.E. (2018). Scanning or desorption isotherms? Characterising sorption hysteresis of wood. *Cellulose*,25, 4477--4485. https://doi.org/ 10.1007/s10570-018-1898-9.

Gao, K.; Chen, Q.; Bi, J.; Liu, X.; Wu, X.;Wang, X. (2016). Changes in browning-related components of apple slices during different stages of instant controlled pressure drop-assisted hot air drying (AD-DIC). *International Journal of Food Science & Technology*, 51, 2242-2250. https://doi.org/ 10.1111/ijfs.13195

Gekas, V., Öste, R., & Lamberg, I. (1993). Diffusion in heated potato tissues. *Journal of food science*, 58, 827-831. https://doi.org/ 10.1111/j.1365-2621.1993.tb09368.x.

Gonzalez, M.E., Barrett, D.M., Michael J. McCarthy, Frank J. Vergeldt, Edo Gerkema, Matser, A.M., & As, H.V. (2010). H-NMR Study of the Impact of High Pressure and Thermal Processing on Cell Membrane Integrity of Onions. *Journal of Food Science*,75(7), 417-425. https://doi.org/ 10.1111/j.1750-3841.2010.01766.x.

Gosline, J.M. (1978). The temperature-dependent swelling of elastin. *Biopolymers*, 17, 697-707 https://doi.org/ 10.1002/bip.1978.360170312.

Goula, A.M., Karapantsios, T.D., Achilias, D.S., & Adamopoulos, K.G. (2008). Water sorption isotherms and glass transition temperature of spray dried tomato pulp. *Journal of Food Engineering*, 85 73--83. https://doi.org/ 10.1016/j.jfoodeng.2007.07.015.

Gruber, S., Vorhauer-Huget, N., & Foerst, P. (2021). In situ micro-computed tomography to study microstructure and sublimation front during freeze-drying. *Food Structure*,29, 100213. https://doi.org/10.1016/j.foostr.2021.100213.

Gulati, T., & Datta, A.K. (2015). Mechanistic understanding of case-hardening and texture development during drying of food materials. *Journal of Food Engineering*,166, 119-138. https://doi.org/ 10.1016/j.jfoodeng.2015.05.031.

Gulati, T., & Datta, A.K. (2016). Coupled multiphase transport, large deformation and phase transition during rice puffing. *Chemical Engineering Science*,139,75-98.

https://doi.org/ 10.1016/j.ces.2015.08.057.

Gulati, T., Zhu, H., & Datta, A.K. (2016). Coupled electromagnetics, multiphase transport and large deformation model for microwave drying. *Chemical Engineering Science*,156 206--228. https://doi.org/ 10.1016/j.ces.2016.09.004.

Gundersen, H. J. G., Boyce, R. W., Nyengaard, J. R., & Odgaard, A. (1993). The conneulor: Unbiased estimation of connectivity using physical disectors under projection. *Bone*, 14, 217-222. https://doi.org/10.1016/8756-3282(93)90144-Y

Guo, Q., Zhang, M., Mujumdar, A.S., & Yu, D. (2024). Drying technologies of novel food resources for future foods: Progress, challenges and application prospects. Food Bioscience 60, 104490. https://doi.org/ 10.1016/j.fbio.2024.104490.

Guo, X.-h., Xia, C.-y., HongsingTan, Chen, A., & Ming, J. (2014). Mathematical Modeling and Effect of Various Hot-Air Drying on Mushroom (*Lentinus edodes*). J*ournal of Integrative Agriculture*,13(1), 207-216. https://doi.org/ 10.1016/S2095-3119(13)60265-8.

Halder, A., Dhall, A., & Datta, A.K. (2011). Modeling Transport in Porous Media with Phase Change: Applications to Food Processing. *Journal of Heat Transfer*,133. https://doi.org/ 10.1115/1.4002463 10.1115/1.4002463.

Han, L.-c., & Jin, T.-x. (2024). Effects of combined vacuum and heat pump drying on drying characteristics and physicochemical properties of pineapple. *LWT - Food Science and Technology*,192 115727. https://doi.org/ 10.1016/j.lwt.2024.115727.

Hancock, B.C., & Zografi, G. (1993). The Use of Solution Theories for Predicting Water Vapor Absorption by Amorphous Pharmaceutical Solids: A Test of the Flory--Huggins and Vrentas Models. *Pharmaceutical Research*,10, 1262--1267. https://doi.org/10.1023/A:1018901325842.

Harnkarnsujarit, N., Kawai, K., Watanabe, M., & Suzuki, T. (2016). Effects of freezing on microstructure and rehydration properties of freeze-dried soybean curd. *Journal of Food Engineering*, https://doi.org/ 10.1016/j.jfoodeng.2016.03.014.

Hayat, M. A. (2012). Basic techniques for transmission electron microscopy. Netherlands: Academic Press, Elsevier.

Heila, M., Hazela, A.L., & Smith, J.A. (2008). The mechanics of airway closure. *Respiratory Physiology & Neurobiology*,163, 214--221. https://doi.org/

10.1016/j.resp.2008.05.013.

Herremans, E., Melado-Herreros, A., Defraeye, T., Verlinden, B., Hertog, M., Verboven, P., Val, J., Fernández-Valle, M.E., Bongaers, E., Estrade, P., Wevers, M., Barreiro, P., & Nicolaï, B.M. (2014). Comparison of X-ray CT and MRI of watercore disorder of different apple cultivars. *Postharvest Biology and Technology*,87, 42-50. https://doi.org/ 10.1016/j.postharvbio.2013.08.008.

Hertig, D., Maddah, S., Memedovski, R., Kurth, S., Moreno, A., Pennestri, M., Felser, A., Nuoffer, J.M., & Vermathen, P. (2021). Live monitoring of cellular metabolism and mitochondrial respiration in 3D cell culture system using NMR spectroscopy. *The Analyst*,146(13), 4326--4339. https://doi.org/10.1039/d1an00041a.

Hill, C., & Beck, G. (2017). On the applicability of the Flory--Huggins and Vrentas models for describing the sorption isotherms of wood. *International Wood Products Journal*,8(1), 50-55. https://doi.org/ 10.1080/20426445.2016.1275094.

Hill, C.A.S., & Xie, Y. (2011). The dynamic water vapour sorption properties of natural fibres and viscoelastic behaviour of the cell wall: is there a link between sorption kinetics and hysteresis? *Journal of Materials Science*, 46, 3738--3748. https://doi.org/ 10.1007/s10853-011-5286-1.

Hill, C.A.S., Keating, B., Rautkari, L., Ramsay, J., Laine, K., Hughes, M., & Constant, B. (2012). The water vapour sorption properties of thermally modified and densified wood. *Journal of Materials Science*,47, 3191--3197. https://doi.org/ 10.1007/s10853-011-6154-8.

Hill, C.A.S., Norton, A., & Newman, G. (2009). The water vapor sorption behavior of natural fibers. *Journal of Applied Polymer Science*, 112, 1524--1537. https://doi.org/ 10.1002/app.29725.

Hills, B.P., Nott, K.P. , & Reson., A.M. (1999). NMR studies of water compartmentation in carrot parenchyma tissue during drying and freezing. *Applied Magnetic Resonance*,17, 521--535. https://doi.org/10.1007/BF03162084.

Hiraide, M., Miyazaki, Y., & Shibata, Y. (2004). The smell and odorous components of dried *shiitake* mushroom, Lentinula edodes I: relationship between sensory evaluations and amounts of odorous components. *Journal of Wood Science*, 50(4), 358-364. https://doi.org/ 10.1007/s10086-004-0689-0.

Hong, W., Liu, Z., & Suo, Z. (2009a). Inhomogeneous swelling of a gel in equilibrium with

a solvent and mechanical load. *International Journal of Solids and Structures*,46(17), 3282-3289. https://doi.org/ 10.1016/j.ijsolstr.2009.04.022.

Hong, W., Liu, Z., & Suo, Z. (2009b). Inhomogeneous swelling of a gel in equilibrium with a solvent and mechanical load. *International Journal of Solids and Structures*,46, 3282--3289. https://doi.org/ 10.1016/j.ijsolstr.2009.04.022.

Hong, W., Zhao, X., Zhou, J., & Suo, Z. (2008a). A theory of coupled diffusion and large deformation in polymeric gels. *Journal of the Mechanics and Physics of Solids,*56 1779--1793. https://doi.org/ 10.1016/j.jmps.2007.11.010.

Hong, W., Zhao, X., Zhou, J., & Suo, Z. (2008b). A theory of coupled diffusion and large deformation in polymeric gels. *Journal of the Mechanics and Physics of Solids*, 56(5), 1779-1793. https://doi.org/10.1016/j.jmps.2007.11.010.

Hou, L., Zhou, X., & Wang, S. (2020). Numerical analysis of heat and mass transfer in kiwifruit slices during combined radio frequency and vacuum drying. *International Journal of Heat and Mass Transfer*,154. https://doi.org/ 10.1016/j.ijheatmasstransfer.2020.119704.

Hou, Y., Wua, W., Wang, J., Yang, Y., & Zhang, H. (2024). Heat pump drying kinetics modeling and prediction for Lentinus edodes based on orthogonal experimental. *Case Studies in Thermal Engineering*,63, 105305. https://doi.org/ 10.1016/j.csite.2024.105305.

Hu, L., Bi, J., Jin, X., Qiu, Y., & van der Sman, R.G.M. (2021). Study on the rehydration quality improvement of *shiitake* mushroom by combined drying methods. *Foods*,10, 769. https://doi.org/ 10.3390/foods10040769.

Hu, L., Bi, J., Jin, X., & Sman, R.v.d. (2022). Microstructure evolution affecting the rehydration of dried mushrooms during instant controlled pressure drop combined hot air drying (DIC-HA). *Innovative Food Science and Emerging Technologies*,79 103056. https://doi.org/ 10.1016/j.ifset.2022.103056.

Hu, L., Bi, J., Jin, X., & Sman, R.v.d. (2023). Impact of physical changes in mushroom on variation in moisture sorption. *Journal of Food Engineering*, 351, 111506. https://doi.org/ 10.1016/j.jfoodeng.2023.111506.

Huang, L., Zhang, M., Wang, L., Mujumdar, A.S., & Sun, D. (2012). Influence of combination drying methods on composition, texture, aroma and microstructure of apple slices. *LWT - Food Science and Technology,*47(1), 183-188. https://doi.org/

10.1016/j.lwt.2011.12.009.

Iiyama, K., Stone, B.A., & Macauley, B.J. (1996). Changes in the concentration of soluble anions in compost during composting and mushroom (Agaricus bisporus) growth. *Journal of the Science of Food and Agriculture*, 72, 243-249. https://doi.org/10.1002/(SICI)1097-0010(199610)72:2243::AID-JSFA6483.0.CO;2-U.

Inkson, B.J. (2016). Scanning electron microscopy (SEM) and transmission electron microscopy (TEM) for materials characterization. https://doi.org/ 10.1016/B978-0-08-100040-3.00002-X.

Jayan, H., Yin, L., Zhou, R., Zou, X., & Guo, Z. (2025). Future horizons of Raman spectroscopy in food science: Emerging techniques and innovations for enhanced analysis. *Food chemistry*,493, 145777. https://doi.org/10.1016/j.foodchem.2025.145777.

Jeon, S., Choi, M.-J., Lee, J., Lee, M., & Lee, M.-Y. (2024). Comparative study on the characteristics of low-mineral paprika powder using combined drying and soaking methods. LWT - Food Science and Technology 214, 117141. https://doi.org/ 10.1016/j.lwt.2024.117141.

Jiang, H., Zhang, M., & Mujumdar, A.S. (2010). Microwave Freeze-Drying Characteristics of Banana Crisps. *Drying Technology*,28(12), 1377--1384. https://doi.org/10.1080/07373937.2010.482702.

Jiang, J., Dang, L., Yuensin, C., Tan, H., Pan, B., & Wei, H. (2017). Simulation of microwave thin layer drying process by a new theoretical model. *Chemical Engineering Science*,162, 69--76. https://doi.org/ 10.1016/j.ces.2016.12.040.

Jiang, Y., Jin, X., Xu, F., & Chen, X.D. (2019). Quantifying food drying rates from NMR/MRI experiments: Development of an online calibration system. *Drying Technology*,37(16), 2047-2058. https://doi.org/ 10.1080/07373937.2018.1552291.

Jin, X., & van der Sman, R.G.M. (2022). Interaction between large deformation and moisture transport during dehydration of vegetables. *Food Structure*,32,100269. https://doi.org/ 10.1016/j.foostr.2022.100269.

Jin, X., van der Sman, R.G.M., van Maanen, J.F.C., van Deventer, H.C., van Straten, G., Boom, R.M., & van Boxtel, A.J.B. (2014). Moisture sorption isotherms of broccoli interpreted with the Flory-Huggins Free Volume theory. *Food Biophysics*,9(1), 1-9. https://doi.org/ 10.1007/s11483-013-9311-6.

Joardder, M.U.H.; Kumar, C.;Karim, M.A.(2018). Prediction of porosity of food materials during drying: Current challenges and directions. *Critical Reviews in Food Science and Nutrition*, 58, 2896-2907. https://doi.org/ 10.1080/10408398.2017.1345852

Joardder, M.U.H.;Karim, M.A. Development of a porosity prediction model based on shrinkage velocity and glass transition temperature (2019). *Drying Technology*, 37, 1988-2004. https://doi.org/ 10.1080/07373937.2018.1555540

Julita Reguła, M.S. (2007). Dried *shiitake* (*lentinulla edodes*) and oyster (*pleurotus ostreatus*) mushrooms as a good source of nutrient. *Acta Scientiarum Polonorum, Technologia Alimentaria* 6(4), 135-142.

Junisbekov, T.M., Kestelman, V.N., & Malinin, N.I. (2003). Stress relaxation in viscoelastic materials. Science Publishers, Enfield, NH.

Katicha, S.W., & Flintsch, G.W. (2012). Fractional viscoelastic models: master curve construction, interconversion, and numerical approximation. *Rheologica Acta*, 51, 675--689 https://doi.org/ 10.1007/s00397-012-0625-y.

Keating, B.A., Hill, C.A.S., Sun, D., English, R., Davies, P., & McCue, C. (2013). The water vapor sorption behavior of a galactomannan cellulose nanocomposite film analyzed using parallel exponential kinetics and the Kelvin--Voigt viscoelastic model. *Journal of Applied Polymer Science,* 129(4), 2352-2359. https://doi.org/ 10.1002/app.39132.

Kohler, R., Dück, R., Ausperger, B., & Alex, R. (2003). A numeric model for the kinetics of water vapor sorption on cellulosic reinforcement fibers. *Composite Interfaces*, 10, 2-3, 255-276. https://doi.org/ 10.1163/156855403765826900.

Kovalenko, A., Zimny, K., Mascaro, B., Brunet, T., & Mondain-Monval, O. (2016). Tailoring of the porous structure of soft emulsion-templated polymer materials. *Soft Matter*,12(23), 5154-5163. https://doi.org/ 10.1039/c6sm00461j.

Krokida, M.K., & Philippopoulos, C. (2005). Rehydration of Dehydrated Foods. *Drying Technology*,23(4), 799-830. https://doi.org/ 10.1081/drt-200054201.

Kumar, C., Joardder, M.U.H., Farrell, T.W., & Karim, M.A. (2016). Multiphase porous media model for intermittent microwave convective drying (IMCD) of food. *International Journal of Thermal Sciences*, 104104, 304-314. https://doi.org/ 10.1016/j.ijthermalsci.2016.01.018.

Kumar, M., Madhumita, M., Prabhakar, P.K., & Basu, S. (2024). Refractance window drying

of food and biological materials: Status on mechanisms, diffusion modelling and hybrid drying approach. Critical Reviews in Food Science and Nutrition 64(11), 3458-3481. https://doi.org/ 10.1080/10408398.2022.2132210.

Larson, R.G. (1985). Constitutive relationships for polymeric materials with power-law distributions of relaxation times. *Rheologica Acta*, 24, 327-334 https://doi.org/ 10.1007/BF01333961.

Lau, C.-C., Abdullah, N., Aminudin, N., & Shuib, A.S. (2013). Effect of freeze-drying process on the property of angiotensin I-converting enzyme inhibitory peptides in grey oyster mushrooms. *Drying Technology*, 31, 13-14, 1693-1700. https://doi.org/ 10.1080/07373937.2013.779584.

Lawless, H.T.;Heymann, H. Sensory Evaluation of Food: Principles and Practices. 2 ed; Springer Science+Business Media: LLC, 233 Spring Street, New York, NY 10013, USA, 2010; pp. 149-174.

Lee, J.H., & Lee, M.J. (2008). Effect of drying method on the moisture sorption isotherms for Inonotus obliquus mushroom. *LWT - Food Science and Technology*,41(8), 1478-1484. https://doi.org/ 10.1016/j.lwt.2007.08.016.

Leibler, L., & Sekimoto, K. (1993). On the sorption of gases and liquids in glassy polymers. *Macromolecules*,26, 6937--6939. https://pubs.acs.org/sharingguidelines.

Lewicki, P.P. (1998). Effect of pre-drying treatment, drying and rehydration on plant tissue properties: A review. *International Journal of Food Properties*, 1, 1-22. https://doi.org/ 10.1080/10942919809524561

Lewicki, P.P. (2006). Design of hot air drying for better foods. *Trends in Food Science & Technology*,17(4), 153-163. https://doi.org/ 10.1016/j.tifs.2005.10.012.

Lewicki, P.P., & Pawlak, G. (2003). Effect of drying on microstructure of plant tissue. *Drying Technology*,21(4), 657-683. https://doi.org/ 10.1081/drt-120019057.

Lewicki, P.P., & Pawlak, G. (2005). Effect of mode of drying on microstructure of potato. *Drying Technology*, 23(4), 847-869. 10.1081/DRT-200054233

Li, K., Zhao, L., Ren, J., & He, B. (2025). Lignin's effect on cellulose fiber bonding and inter-fiber interface design for enhancing densified wood. *Carbohydrate Polymers*, 359, 123573. https://doi.org/10.1016/j.carbpol.2025.123573.

Li, X., Bi, J., Chen, Q., Jin, X., Wu, X., & Zhou, M. (2019). Texture improvement and

deformation inhibition of hot air-dried apple cubes via osmotic pretreatment coupled with instant control pressure drop (DIC). *International Journal of Food Science & Technology*, 101, 351-359. https://doi.org/ 10.1016/j.lwt.2018.11.035

Li, X., Bi, J., Chen, Q., Jin, X., Wu, X., & Zhou, M. (2019). Texture improvement and deformation inhibition of hot air-dried apple cubes via osmotic pretreatment coupled with instant control pressure drop (DIC). *LWT - Food Science and Technology*, 101, 351-359. https://doi.org/10.1016/j.lwt.2018.11.035

Li, X., Bi, J., Jin, X., Li, X., Wu, X., & Lyu, J. (2019). Characterization of Water Binding Properties of Apple Pectin Modified by Instant Controlled Pressure Drop Drying (DIC) by LF-NMR and DSC Methods. *Food and Bioprocess Technology*,13(2), 265-274. https://doi.org/ 10.1007/s11947-019-02387-8.

Li, X., Bi, J., Jin, X., Lyu, J., Wu, X., Li, B., & Li, X. (2021). Study on the mechanism of volume expansion and texture formation of apple cube dried by instant controlled pressure drop drying (DIC). *Journal of Food Engineering*,293, 110379. https://doi.org/ 10.1016/j.jfoodeng.2020.110379.

Li, X., Bi, J., Jin, X., Wu, X., Lyu, J., Li, X., & Hu, L. (2020). Effect of the moisture equilibrium process on the expansion behavior of instant controlled pressure drop (DIC) drying of dried apple cubes. *Journal of the Science of Food Agriculture*, 100 (4), 1635-1642. https://doi.org/10.1002/jsfa.10175

Lomolino, G., Morari, F., Dal Ferro, N., Vincenzi, S., & Pasini, G. (2017). Investigating the einkorn (Triticum monococcum) and common wheat (Triticum aestivum) bread crumb structure with X-ray microtomography: Effects on rheological and sensory properties. *International Journal of Food Science and Technology*, 52 (6), 1498-1507. https://doi.org/10.1111/ijfs.13425

Lopez-Quiroga, E., Prosapio, V., Fryer, P.J., Norton, I.T., & Bakalis, S. (2019). Model discrimination for drying and rehydration kinetics of freeze-dried tomatoes. *Journal of Food Process Engineering*,43(5). https://doi.org/ 10.1111/jfpe.13192.

Lormand, C., Zellmer, G. F., Németh, K., Kilgour, G., Mead, S., Palmer, A. S., Sakamoto, N., Yurimoto, H., & Moebis, A. (2018). Weka trainable segmentation plugin in ImageJ: A semi-automatic tool applied to crystal size distributions of microlites in volcanic rocks. *Microscopy and Microanalysis*, 24, 667--675. https://doi.org/10.1017/S1431927618015428

Louka, N., & Allaf, K. (2004). Expansion ratio and color improvement of dried vegetables texturized by a new process "controlled sudden decompression to the vacuum" application to potatoes, carrots and onions. *Journal of Food Engineering*, 65 (2), 233-243. https://doi.org/10.1016/j.jfoodeng.2004.01.020

Lyu, J., Zhou, L.-y., Bi, J.-f., Liu, X., & Wu, X.-y. (2015). Quality evaluation of yellow peach chips prepared by explosion puffing drying. *Journal of Food Science and Technology*,52, 8204--8211 https://doi.org/10.1007/s13197-015-1906-0.

Madiouli, J., Lecomte, D., Nganya, T., Chavez, S., Sghaier, J., & Sammouda, H. (2007). A Method for Determination of Porosity Change from Shrinkage Curves of Deformable Materials. *Drying Technology*,25(4), 621-628. https://doi.org/ 10.1080/07373930701227185.

Maftoonazad, N., Dehghani, M.R., & Ramaswamy, H.S. (2022). Hybrid microwave-hot air tunnel drying of onion slices: Drying kinetics, energy efficiency, product rehydration, color, and flavor characteristics. Drying Technology 40(5), 966-986. https://doi.org/ 10.1080/07373937.2020.1841790.

Mahiuddin, M., Khan, M.I.H., Duc Pham, N., & Karim, M.A. (2018). Development of fractional viscoelastic model for characterizing viscoelastic properties of food material during drying. *Food Bioscience*, 23, 45-53. https://doi.org/ 10.1016/j.fbio.2018.03.002.

Mahmoud, Z.H., AL-Salman, H.N.K., & Kianfar, E. (2024). Nanoindentation: Introduction and applications of a non-destructive analysis. *Nano TransMed*,3 100057. https://doi.org/ 10.1016/j.ntm.2024.100057.

Mainardi, F., & Spada, G. (2011). Creep, relaxation and viscosity properties for basic fractional models in rheology. *The European Physical Journal Special Topics*, 193, 133--160 https://doi.org/ 10.1140/epjst/e2011-01387-1.

Malik, N., Gouseti, O.,Bakalis, S.(2018). Effect of freezing on microstructure and reconstitution of freeze-dried high solid hydrocolloid-based systems. *Food Hydrocolloids*, 83, 473-484. https://doi.org/ 10.1016/j.foodhyd.2018.05.008

Manduca, A., Oliphant, T.E., Dresner, M.A., Mahowald, J.L., Kruse, S.A., Amromin, E., Felmlee, J.P., Greenleaf, J.F., & Ehman, R.L. (2001). Magnetic resonance elastography: Non-invasive mapping of tissue elasticity. *Medical Image Analysis*,5(4), 237-254. https://doi.org/10.1016/S1361-8415(00)00039-6.

Marabi, A., Dilak, C., Shah, J., & Saguy, I. S. (2004). Kinetics of solids leaching during

rehydration of particulate dry vegetables. *Food Engineering and Physical Properties*, 69 (3), 91-96. https://doi.org/10.1111/j.1365-2621.2004.tb13369.x

Marabi, A., & Saguy, I.S. (2004). Effect of porosity on rehydration of dry food particulates. *Journal of Food and Agriculture*.84(10), 1105-1110. https://doi.org/ 10.1002/jsfa.1793.

Marabi, A., Thieme, U., Jacobson, M., & Saguy, I.S. (2006). Influence of drying method and rehydration time on sensory evaluation of rehydrated carrot particulates. *Journal of Food Engineering*,72(3), 211-217. https://doi.org/10.1016/j.jfoodeng.2004.11.011.

Mari, A., Parisouli, D.N., & Krokida, M. (2024). Exploring Osmotic Dehydration for Food Preservation: Methods, Modelling, and Modern Applications. *Foods*,13,2783. https://doi.org/ 10.3390/foods13172783.

Marques, L.G., Prado, M.M., & Freire, J.T. (2009). Rehydration characteristics of freeze-dried tropical fruits. *LWT - Food Science and Technology*,42, 1232--1237. https://doi.org/ 10.1016/j.lwt.2009.02.012.

Mattila, P., Lampi, A.-M., Ronkainen, R., Toivo, J., & Piironenb, V. (2002). Sterol and vitamin D2 contents in some wild and cultivated mushrooms. *Food Chemistry*,76, 293--298. https://doi.org/10.1016/S0308-8146(01)00275-8

Metilli, L., Francis, M., Povey, M., Lazidis, A., Marty-Terrade, S., Ray, J., & Simone, E. (2020). Latest advances in imaging techniques for characterizing soft, multiphasic food materials. *Advances in Colloid and Interface Science*,279, 102154. https://doi.org/10.1016/j.cis.2020.102154

Mounir, S., Allaf, T., Berka, B., Hassani, A.,Allaf, K.(2014). Instant controlled pressure drop technology: From a new fundamental approach of instantaneous transitory thermodynamics to large industrial applications on high performance-high controlled quality unit operations. *Comptes Rendus Chimie*, 17, 261-267. https://doi.org/10.1016/j.crci.2013.10.019

Mounir, S., Allaf, T., Mujumdar, A.S., & Allaf, K. (2012). Swell Drying: coupling instant controlled pressure drop DIC to standard convection drying processes to intensify transfer phenomena and improve quality---an overview. *Drying Technology*,30(14), 1508-1531. https://doi.org/10.1080/07373937.2012.693145.

Mounir, S., Allaf, T., Mujumdar, A. S., & Allaf, K. (2012). Swell Drying: coupling instant controlled pressure drop DIC to standard convection drying processes to intensify transfer phenomena and improve quality---an overview. *Drying Technology*, 30 (14),

1508-1531. https://doi.org/10.1080/07373937.2012.693145

Mounir, S., Amami, E., Allaf, T., Mujumdar, A. S., & Allaf, K. (2020). Instant controlled pressure drop (DIC) coupled to intermittent microwave/airflow drying to produce shrimp snacks: Process performance and quality attributes. *Drying Technology*, 38 (5-6), 695-711. https://doi.org/10.1080/07373937.2019.1694537

Mounir, S., Besombes, C., Al-Bitar, N., & Allaf, K. (2011). Study of instant controlled pressure drop DIC treatment in manufacturing snack and expanded granule powder of apple and onion. *Drying Technology*, 29 (3), 331-341. https://doi.org/10.1080/07373937.2010.491585

Mounir, S., Téllez-Pérez, C., Alonzo-Macías, M.,Allaf, K. (2014). Swell-Drying, in instant controlled pressure drop (D.I.C.) in food processing, T.A.a.K. Allaf, Editor. Springer Science+Business Media New York p. 3-43. https://doi.org/10.1007/978-1-4614-8669-5

Mujumdar, A.S. (2007). An overview of innovation in industrial drying: current status and R&D needs. *Transport in Porous Media*,66, 3-18. https://doi.org/ https://doi.org/10.1007/s11242-006-9018-y.

Musse, M., Traore, A., Leca, A., Lahaye, M., Lorho, C.e., Pierre, G., Traubenberg, N.R.d., Garcia, C., Diascorn, Y., Quellec, S.e., Bourvellec, C.L., Clerjon, S., Challois, S., Collewet, G., & Bertin, N. (2025). Insights into the mechanisms involved in the evolution of the structural and physicochemical properties of tomato during air drying -- A study combining MRI, unilateral NMR and conventional techniques. *Food Research International*,212, 116385. https://doi.org/ 10.1016/j.foodres.2025.116385.

Muziri, T., Theron, K. I., Cantre, D., Wang, Z., Verboven, P., Nicolai, B. M., & Crouch, E. M. (2016). Microstructure analysis and detection of mealiness in 'Forelle' pear (Pyrus communis L.) by means of X-ray computed tomography. *Postharvest Biology and Technology*, 120, 145-156. http://dx.doi.org/10.1016/j.postharvbio.2016.06.006

Myhan, R., Markowski, M., Daszkiewicz, T., Zapotoczny, P., & Sadowski, P. (2015). Non-linear stress relaxation model as a tool for evaluating the viscoelastic properties of meat products. *Journal of Food Engineering*, 146, 107-115. https://doi.org/ 10.1016/j.jfoodeng.2014.09.006.

Nadi, F., & Tzempelikos, D. (2018). Vacuum drying of apples (cv. Golden Delicious): drying characteristics, thermodynamic properties, and mass transfer parameters. *Heat and*

Mass Transfer,54, 1853--1866. https://doi.org/ 10.1007/s00231-018-2279-5.

Naji-Tabasi, S., & Mohebbi, M. (2015). Evaluation of cress seed gum and xanthan gum effect on macrostructure properties of gluten-free bread by image processing. *Food Measure*,9, 10--119. https://doi.org/ 10.1007/s11694-014-9216-1.

Nguyen, T.K., Khalloufi, S., Mondor, M., & Ratti, C. (2018). Shrinkage and porosity evolution during air-drying of non-cellular food systems: Experimental data versus mathematical modelling. *Food Research International*,103, 215--225. https://doi.org/ 10.1016/j.foodres.2017.10.013.

Ogawa, K., Tachibana, K., Tai, T.U.T., Yamashita, N., & Miyauchi, N.T.R. (2001). High-resolution scanning electron microscopic evaluation of cell-membrane porosity by ultrasound. *Medical Electron Microscopy*,34, 249--253. https://doi.org/10.1007/s007950100022

Oikonomopoulou, V.P., & Krokida, M.K. (2012). Structural Properties of Dried Potatoes, Mushrooms, and Strawberries as a Function of Freeze-Drying Pressure. *Drying Technology*.30(4), 351--361. https://doi.org/10.1080/07373937.2011.639475

Oliver, L., & Meinders, M.B.J. (2011). Dynamic water vapour sorption in gluten and starch films. *Journal of Cereal Science*,54, 409-416. https://doi.org/ 10.1016/j.jcs.2011.08.005

Onipe, O.O., Beswa, D., & Jideani, A.I.O. (2020). Confocal Laser Scanning Microscopy and Image Analysis for Elucidating Crumb and Crust Microstructure of Bran-Enriched South African Fried Dough and Batter.*Foods*,9, 605. https://doi.org/ 10.3390/foods9050605

Onwude, D.I., Hashim, N., Chen, G., Putranto, A., & Udoenoh, N.R. (2021). A fully coupled multiphase model for infrared-convective drying of sweet potato. *Journal of the Science of Food and Agriculture*,101(2), 398--413. https://doi.org/ 10.1002/jsfa.10649.

Özbek, H. N., Elik, A., Koçak Yanık, D., Işınay, B., Sever, M., Bulut, E., Topçam, H., Dalgıç, A. C., Erdoğdu, F., & Göğüş, F. (2022). Effect of sequential-combined solar energy assisted hot air and hot air assisted radio frequency drying on the physical and chemical properties of dried apricots. Journal of food science and technology, 59(7), 2894–2904. https://doi.org/10.1007/s13197-021-05314-y

Ozturk, O.K., & Takhar, P.S. (2019). Physical and viscoelastic properties of carrots during

drying. *Journal of Texture Studies*, 51, 532--541. https://doi.org/ 10.1111/jtxs.12496.

Ozturk, O.K., & Takhar, P.S. (2019). Selected physical and viscoelastic properties of strawberries as a function of heated-air drying conditions. *Drying Technology*, 37(14), 1833-1843. https://doi.org/ 10.1080/07373937.2018.1543701.

Pang, S., & Xu, C.S. (2023). Methods of enhanced FIB-SEM sample preparation and image acquisition. Methods in cell biology, 177, 269–300. https://doi.org/10.1016/bs.mcb.2023.01.019

Pasquale M. Falcone, Baiano, A., Conte, A., Mancini, L., Tromba, G., Zanini, F., & Nobile, M. A. D. (2006). Imaging Techniques for the Study of Food Microstructure: A Review. *Advances in Food and Nutrition Research*,51, 205-263. https://doi.org/10.1016/S1043-4526(06)51004-6.

Pascual-Pineda, L.A., Hernández-Marañon, A., Castillo-Morales, M., Uzárraga-Salazar, R., Rascón-Díaz, M.P., & Flores-Andrade, E. (2020). Effect of water activity on the stability of freeze-dried oyster mushroom (Pleurotus ostreatus) powder. *Drying Technology*, 1-14. https://doi.org/ 10.1080/07373937.2020.1739064.

Patera, A., Derluyn, H., Derome, D., & Carmeliet, J. (2016). Influence of sorption hysteresis on moisture transport in wood. *Wood Science and Technology*,50, 259--283. https://doi.org/ 10.1007/s00226-015-0786-9.

Paudel, E., Boom, R.M., & Van der Sman, R.G.M. (2016). Effects of Porosity and Thermal Treatment on Hydration of Mushrooms. *Food and Bioprocess Technology*,9(3), 511-519. https://doi.org/ 10.1007/s11947-015-1641-6.

Paudel, E., Boom, R.M., & van der Sman, R.G.M. (2015). Change in water-holding capacity in mushroom with temperature analyzed by Flory-Rehner theory. *Food and Bioprocess Technology*, 8(5), 960-970. https://doi.org/ 10.1007/s11947-014-1459-7.

Pedro, M.A.M., Telis-Romero, J., & Telis, V.R.N. (2010). Effect of drying method on the adsorption isotherms and isosteric heat of passion fruit pulp powder. *Food Science and Technology*,30(4), 993-1000. https://doi:10.1590/S0101-20612010000400024

Pedro, M.A.M., Telis-Romero, J., &Telis, V.R.N. (2010). Effect of drying method on the adsorption isotherms and isosteric heat of passion fruit pulp powder. Pedro, M.A., Telis-Romero, J., & Telis, V.R. (2010). Effect of drying method on the adsorption isotherms and isosteric heat of passion fruit pulp powder. Food Science and Technology International, 30, 993-1000. https://doi:10.1590/S0101-

20612010000400024

Pei, F., Shi, Y., Mariga, A.M., Yang, W.J., Tang, X.Z., Zhao, L.Y., An, X.X.,Hu, Q.H.(2014). Comparison of freeze-drying and freeze-drying combined with microwave vacuum drying methods on drying kinetics and rehydration characteristics of button mushroom (*Agaricus bisporus*) slices. *Food and Bioprocess Technology*, 7, 1629-1639. https://doi.org/ 10.1007/s11947-013-1199-0

Peng, J., Bi, J., Yi, J., Chen, Q., Wu, X., Zhou, M., & Liu, J.n. (2018). Freezing as pretreatment in instant controlled pressure drop (DIC) texturing of dried carrot chips: Impact of freezing temperature. *LWT-Food Science and Technology*,89, 365-373. https://doi.org/10.1016/j.lwt.2017.11.009.

Peng, J., Bi, J., Yi, J., Chen, Q., Wu, X., Zhou, M., & Liu, J. n. (2018). Freezing as pretreatment in instant controlled pressure drop (DIC) texturing of dried carrot chips: Impact of freezing temperature. *LWT-Food Science and Technology*, 89, 365-373. https://doi.org/10.1016/j.lwt.2017.11.009

Peng, J., Bi, J., Yi, J., Wu, X., Zhou, M., Lyu, J.,Liu, J.n.(2018). Engineering texture properties of instant controlled pressure drop (DIC) dried carrot chips via modulating osmotic conditions. *Food and Bioproducts Processing*, 11, 1674-1685. https://doi.org/10.1007/s11947-018-2133-2

Peter, M., Liu, Z., Fang, Y., Dou, X., Awuah, E., Soomro, S.A., & Chen, K. (2021). Computational intelligence and mathematical modelling in chanterelle mushrooms' drying process under heat pump dryer. *Biosystems Engineering*,212, 143e159. https://doi.org/ 10.1016/j.biosystemseng.2021.10.002.

Pettermann, H.E., & Hüsing, J. (2012). Modeling and simulation of relaxation in viscoelastic open cell materials and structures. *International Journal of Solids and Structures*, 49(19-20), 2848-2853. https://doi.org/ 10.1016/j.ijsolstr.2012.04.027.

Pitzer, K.S., & Mayorga, G. (1973). Thermodynamics of electrolytes. II. Activity and osmotic coefficients for strong electrolytes with one or both Ions univalent. *The Journal of Physical Chemistry*, 77(19), 2300-2308. https://doi.org/ 10.1021/j100638a009.

Prawiranto, K., Defraeye, T., Derome, D., Verboven, P., Nicolai, B., & Carmeliet, J. (2018). New insights into the apple fruit dehydration process at the cellular scale by 3D continuum modeling. *Journal of Food Engineering*, 239, 52--63. https://doi.org/

10.1016/j.jfoodeng.2018.06.023.

Prothon, F., Ahrne, L., & Sjoholm, I. (2003). Mechanisms and prevention of plant tissue collapse during dehydration: a critical review. *Critical reviews in food science and nutrition*, 43(4), 447-479. https://doi.org/ 10.1080/10408690390826581.

Pu, Y.-Y., & Sun, D.-W. (2017). Combined hot-air and microwave-vacuum drying for improving drying uniformity of mango slices based on hyperspectral imaging visualisation of moisture content distribution. *Biosystems Engineering,*156, 108-119. https://doi.org/ 10.1016/j.biosystemseng.2017.01.006.

Purlis, E. (2019). Modelling convective drying of foods: A multiphase porous media model considering heat of sorption. *Journal of Food Engineering*, 263, 132--146. https://doi.org/ 10.1016/j.jfoodeng.2019.05.028.

Qi, L.-L., Zhang, M., Mujumdar, A.S., Meng, X.-Y., Chen, H.-Z. (2014). Comparison of drying characteristics and quality of *shiitake* mushrooms (*lentinus edodes*) using different drying methods. *Drying Technology*. 32, 1751-1761. https://doi.org/ 10.1080/07373937.2014.929588

Qiao, Y., Galvosas, P., & Callaghan, P.T. (2005). Diffusion Correlation NMR Spectroscopic Study of Anisotropic Diffusion of Water in Plant Tissues. *Biophysical Journal Volume*,89, 2899--2905. https://doi.org/ 10.1529/biophysj.105.064709.

Qiu, Y., Bi, J., Jin, X., Hu, L., Lyu, J., & Wu, X. (2021). An understanding of the changes in water holding capacity of rehydrated *shiitake* mushroom (Lentinula edodes) from cell wall, cell membrane and protein. *Food chemistry*,351, 129230. https://doi.org/ 10.1016/j.foodchem.2021.129230.

Qiu, Y., Bi, J., Jin, X., Wu, X., Hu, L., & Chen, L. (2022). Investigation on the rehydration mechanism of freeze-dried and hot-air dried *shiitake* mushrooms from pores and cell wall fibrous material. *Food chemistry*,383 132360. https://doi.org/ 10.2141/jpsa.41.322.

Quintero Ruiz, N.A., Demarchi, S.M.,Giner, S.A. (2014).Effect of hot air, vacuum and infrared drying methods on quality of rose hip (*Rosa rubiginosa*) leathers. *International Journal of Food Science & Technology*, 49, 1799-1804. https://doi.org/10.1111/ijfs.12486

Rahman, M.M., Joardder, M.U.H., Khan, M.I.H., Pham, N.D., & Karim, M.A. (2018). Multi-scale model of food drying: Current status and challenges. *Critical reviews in food science and nutrition*, 58(5), 858-876. https://doi.org/

10.1080/10408398.2016.1227299.

Rahyan, A. R., Henning, W. L., & Westcott, D. E. (1971). Histological and physical changes in carrots as affected by blanching, cooking, freeze drying and compression. *Journal of Food Science*, 36, 500-502. https://doi.org/10.1111/j.1365-2621.1971.tb06399.x

Rakesh, V., & Datta, A.K. (2011). Microwave puffing: Determination of optimal conditions using a coupled multiphase porous media -- Large deformation model. *Journal of Food Engineering*,107, 152--163. https://doi.org/ 10.1016/j.jfoodeng.2011.06.031.

Rakesh, V., Datta, A.K., Walton, J.H., McCarthy, K.L., & McCarthy, M.J. (2012). Microwave combination heating: Coupled electromagnetics- multiphase porous media modeling and MRI experimentation..*AIChE Journal*.58(4), 1262--1278. https://doi.org/10.1002/aic.12659

Ranjbaran, M., & Datta, A.K. (2019). Pressure-driven infiltration of water and bacteria into plant leaves during vacuum cooling: A mechanistic model. *Journal of Food Engineering*,246, 209-223. https://doi.org/10.1016/j.jfoodeng.2018.10.032.

Rathinaraj, J.D.J., Keshavarz, B., & FRS, G.H.M. (2022). Why the Cox-Merz rule and Gleissle mirror relation work: A quantitative analysis using the fractional K-BKZ model. https://doi.org/ 10.13140/RG.2.2.36735.33448.

Rathore, H., Prasad, S., & Sharma, S. (2017). Mushroom nutraceuticals for improved nutrition and better human health: A review. *Pharma Nutrition*,5(2), 35-46. https://doi.org/ 10.1016/j.phanu.2017.02.001.

Ratti, C. (2001). Hot air and freeze-drying of high-value foods: a review. *Journal of Food Engineering*, 49, 311-319. https://doi.org/10.1016/S0260-8774(00)00228-4

Reese, S. (2003). A micromechanically motivated material model for the thermo-viscoelastic material behaviour of rubber-like polymers. *International Journal of Plasticity*.19(7), 909--940. https://doi.org/10.1016/S0749-6419(02)00086-4

Reis, F.S., Barros, L., Martins, A., & Ferreira, I.C. (2012). Chemical composition and nutritional value of the most widely appreciated cultivated mushrooms: An inter-species comparative study. *Food and Chemical Toxicology*, 50(2), 191-197. https://doi.org/ 10.1016/j.fct.2011.10.056.

Reyes, A., Vega, R., Bustos, R., &Araneda, C. (2008). Effect of processing conditions on drying kinetics and particle microstructure of carrot. *Drying Technology*, 26, 1272-

1285. https://doi.org/10.1080/07373930802307282

Rojas, M.L., & Augusto, P.E.D. (2018). Microstructure elements affect the mass transfer in foods: The case of convective drying and rehydration of pumpkin. *LWT- Food Science and Technology*,93, 102-108. https://doi.org/ 10.1016/j.lwt.2018.03.031.

Rzigue, A., Monteau, J.-Y., Marmi, K., Le Bail, A., Chevallier, S., Réguerre, A.-L., & Jury, V. (2016). Bread collapse. Causes of the technological defect and impact of depanning time on bread quality. *Journal of Food Engineering*,182, 72-80. https://dx.doi.org/10.1016/j.jfoodeng.2016.03.007.

Sam Saguy, I., Marabi, A., & Wallach, R. (2005). New approach to model rehydration of dry food particulates utilizing principles of liquid transport in porous media. *Trends in food science & technology*,16(11), 495-506. https://doi.org/ 10.1016/j.tifs.2005.07.006.

Salmén, L., & Larsson, P.A. (2018). On the origin of sorption hysteresis in cellulosic materials. *Carbohydrate Polymers*,182 15--20. https://doi.org/ 10.1016/j.carbpol.2017.11.005.

Schoeman, L., Williams, P., du Plessis, A., & Manley, M. (2016). X-ray micro-computed tomography (μCT) for non-destructive characterisation of food microstructure. *Trends in food science & technology*,47, 10-24. https://doi.org/ 10.1016/j.tifs.2015.10.016.

Seremet Ceclu, L., Botez, E., Nistor, O.V., Andronoiu, D.G., &Mocanu, G.D. (2016). Effect of different drying methods on moisture ratio and rehydration of pumpkin slices. *Food Chemistry*, 195, 104-109. https://doi.org/ 10.1016/j.foodchem.2015.03.125

Si, X., Chen, Q., Bi, J., Wu, X., Yi, J., Zhou, L.,Li, Z.(2016). Comparison of different drying methods on the physical properties, bioactive compounds and antioxidant activity of raspberry powders. *Journal of the Science of Food and Agriculture*, 96, 2055-62. https://doi.org/ 10.1002/jsfa.7317

Siebert, T., Becker, A., Bunzel, M., Zuber, M., Hamann, E., Baumbach, T., Karbstein , H.P., & Gaukel, V. (2019). Evaluation of the usefulness of serial combination processes for drying of apples. *Drying Technology*, 38, 1274-1290. https://doi.org/ 10.1080/07373937.2019.1637888

Siebert, T., Becker, A., Bunzel, M., Zuber, M., Hamann, E., Baumbach, T., Karbstein, H. P., & Gaukel, V. (2020). Evaluation of the usefulness of serial combination processes for drying of apples. *Drying Technology*, 38 (10), 1274-1290. https://doi.org/10.1080/07373937.2019.1637888

Siebert, T., Gall, V., Karbstein, H.P., & Gaukel, V. (2018). Serial combination drying processes: A measure to improve quality of dried carrot disks and to reduce drying time. *Drying Technolog*.36(13), 1578-1591. https://doi.org/10.1080/07373937.2017.1418374.

Siebert, T., Gall, V., Karbstein, H.P., & Gaukel, V. (2018). Serial combination drying processes: A measure to improve quality of dried carrot disks and to reduce drying time. *Drying Technology*, 36 (13), 1578-1591. https://doi.org/10.1080/07373937.2017.1418374

Siebert, T., Zuber, M., Hamann, E., Baumbach, T., Karbstein, H.P., & Gaukel, V. (2019). Micro-CT visualization of structure development during freeze-drying processes. *Drying Technology*, 38, 376-384. https://doi.org/ 10.1080/07373937.2019.1572619

Siebert, T., Zuber, M., Hamann, E., Baumbach, T., Karbstein, H. P., & Gaukel, V. (2020). Micro-CT visualization of structure development during freeze-drying processes. *Drying Technology*, 38 (3), 376-384. https://doi.org/10.1080/07373937.2019.1572619

Simonin, H., Beney, L., &Gervais, P. (2007). Sequence of occurring damages in yeast plasma membrane during dehydration and rehydration: mechanisms of cell death. *Biochimica et Biophysica Acta* , 1768, 1600-10. https://doi.org/ 10.1016/j.bbamem.2007.03.017

Simpson, R., Ramirez, C., Jaques, A., Nun˜ez, H., & Almonacid, A. (2013). Fractional calculus as a mathematical tool to improve the modeling of mass transfer phenomena in food processing. *Food Engineering Reviews*, 5, 45--55 https://doi.org/ 10.1007/s12393-012-9059-7

Singh, F., Katiyar, V.K., & Singh, B.P. (2014). Analytical study of turgor pressure in apple and potato tissues. *Postharvest Biology and Technology*,89, 44-48. https://doi.org/ 10.1016/j.postharvbio.2013.11.007.

Singhal, S., Rasane, P., Kaur, S., Singh, J., & Gupta, N. (2020). Thermal degradation kinetics of bioactive compounds in button mushroom (Agaricus bisporus) during tray drying process. *Journal of Food Process Engineering*,43, e13555. https://doi.org/ 10.1111/jfpe.13555.

Sman, R.G.M.v.d. (2020). Impact of processing factors on quality of frozen vegetables and fruits. *Food Engineering Reviews*, 12, 399--420. https://doi.org/ 10.1007/s12393-020-09216-1.

Sman, R.G.M.v.d. (2023). Effects of viscoelasticity on moisture sorption of maltodextrins.

Food Hydrocolloids,139, 108481. https://doi.org/ 10.1016/j.foodhyd.2023.108481.

Stadtländer, C.T.K.-H. (2007). Scanning Electron Microscopy and Transmission Electron Microscopy of Mollicutes: Challenges and Opportunities.

Stokes, D.J. (2013). Environmental scanning electron microscopy (ESEM): principles and applications to food microstructures. In V.J. Morris, K. Groves (Eds.), Food Microstructures (pp. 3-26). Woodhead Publishing, Cambridge, England. https://doi.org/10.1533/9780857098894.1.3.

Sun, Q., Yu, X., Zhang, L., Abu ElGasim A. Yagoub, Tang, Y., Wahia, H., & Zhou, C. (2022). Effects of vacuum ultrasonic infiltration and combined drying on rehydration quality of ginger (Zingiber officinale Roscoe). Industrial Crops and Products 187, 115381. https://doi.org/10.1016/j.indcrop.2022.115381.

Tansakul, A., & Lumyong, R. (2008). Thermal properties of straw mushroom. *Journal of Food Engineering*,87(1), 91-98. https://doi.org/10.1016/j.jfoodeng.2007.11.016.

Taylor, N.W., Cluskey, J.E., & Senti, F.R. (1961). Water sorption by dextrans and wheat starch at high humidities. *The Journal of Physical Chemistry*,65(10), 1810-1816.

Tian, Y., Zhao, Y., Huang, J., Zeng, H., &Zheng, B. (2016). Effects of different drying methods on the product quality and volatile compounds of whole *shiitake* mushrooms. *Food Chemistry*, 197, 714-722. https://doi.org/10.1016/j.foodchem.2015.11.029

Tran, T.N.T., Khoo, K.S., Chew, K.W., Phan, T.Q., Nguyen, H.S., Nguyen-Sy, T., Nguyen, T.D.P., Chen, W.-H., & Show, P.L. (2020). Modelling drying kinetic of oyster mushroom dehydration -- The optimization of drying conditions for dehydratation of Pleurotus species. *Materials Science for Energy Technologies*,3, 840--845. https://doi.org/ 10.1016/j.mset.2020.10.005.

van der Sman, R.G. (2015). Hyperelastic models for hydration of cellular tissue. *Soft Matter*, 11(38), 7579-7591. https://doi.org/ 10.1039/c5sm01032b.

van der Sman, R.G., & Meinders, M.B. (2013). Moisture diffusivity in food materials. *Food Chemistray*,138(2-3), 1265-1274. https://doi.org/ 10.1016/j.foodchem.2012.10.062.

van der Sman, R.G., & Meinders, M.B. (2013). Moisture diffusivity in food materials. *Food Chemistray,* 138(2-3), 1265-1274. https://doi.org/ 10.1016/j.foodchem.2012.10.062.

van der Sman, R.G.M. (2008). Prediction of enthalpy and thermal conductivity of frozen meat and fish products from composition data. *Journal of Food Engineering*,84(3),

400-412. https://doi.org/ 10.1016/j.jfoodeng.2007.05.034.

van der Sman, R.G.M. (2012). Thermodynamics of meat proteins. *Food Hydrocolloids*,27(2), 529-535. https://doi.org/ 10.1016/j.foodhyd.2011.08.016.

van der Sman, R.G.M. (2013). Moisture sorption in mixtures of biopolymer, disaccharides and water. *Food Hydrocolloids*,32(1), 186-194. https://doi.org/ 10.1016/j.foodhyd.2012.12.029.

van der Sman, R.G.M. (2015). Biopolymer gel swelling analysed with scaling laws and Flory--Rehner theory. *Food Hydrocolloids*,48, 94-101. https://doi.org/ 10.1016/j.foodhyd.2015.01.025.

van der Sman, R.G.M. (2016). Sugar and polyol solutions as effective solvent for biopolymers. *Food Hydrocolloids*, 56, 144-149. https://doi.org/ 10.1016/j.foodhyd.2015.12.001.

van der Sman, R.G.M. (2020). Impact of processing factors on quality of frozen vegetables and fruits. *Food Engineering Reviews*,12, 399--420. https://doi.org/ 10.1007/s12393-020-09216-1.

van der Sman, R.G.M. (2023). Effects of viscoelasticity on moisture sorption of maltodextrins. *Food Hydrocolloids*,139 108481. https://doi.org/ 10.1016/j.foodhyd.2023.108481.

van der Sman, R.G.M., & Mauer, L.J. (2019). Starch gelatinization temperature in sugar and polyol solutions explained by hydrogen bond density. *Food Hydrocolloids*, 94, 371-380. https://doi.org/ 10.1016/j.foodhyd.2019.03.034.

van der Sman, R.G.M., & Meinders, M.B.J. (2011). Prediction of the state diagram of starchwater mixtures using the Flory--Huggins free volume theory. *Soft Matter*,7(2), 429-442. https://doi.org/ 10.1039/c0sm00280a.

van der Sman, R.G.M., Curatolo, M., & Teresi, L. (2024). Pore development in viscoelastic foods during drying. *Soft Matte*r,20, 5183. https://doi.org/ 10.1039/D4SM00201F.

van der Sman, R.G.M., Jin, X., & Meinders, M.B.J. (2013). A paradigm shift in drying of food materials via Free-Volume concepts. *Drying Technology*,31(15), 1817-1825. https://doi.org/ 10.1080/07373937.2013.829089.

van der Sman, R.G.M., Jin, X., & Meinders, M.B.J. (2013a). A paradigm shift in drying of food materials via Free-Volume concepts. *Drying Technology*, 31(15), 1817-1825.

https://doi.org/ 10.1080/07373937.2013.829089.

van der Sman, R.G.M., Paudel, E., Voda, A., & Khalloufi, S. (2013b). Hydration properties of vegetable foods explained by Flory--Rehner theory. *Food Research International*, 54(1), 804-811. https://doi.org/ 10.1016/j.foodres.2013.08.032.

Van der Sman, R.G.M. (2008). Prediction of enthalpy and thermal conductivity of frozen meat and fish products from composition data. *Journal of Food Engineering*, 84, 400-412. https://doi.org/ 10.1016/j.jfoodeng.2007.05.034

Vergeldt, F.J., van Dalen, G., Duijster, A.J., Voda, A., Khalloufi, S., van Vliet, L.J., Van As, H., van Duynhoven, J.P.M., & van der Sman, R.G.M. (2014). Rehydration kinetics of freeze-dried carrots. *Innovative Food Science and Emerging Technologies,*24, 40-47. https://doi.org/ http://dx.doi.org/10.1016/j.ifset.2013.12.002.

Veser, J., Hartman, W., Guidry, S., Schutyser, M.A.I., & Sman, van der Sman, R.G.M. (2025). Optimisation of primed cabbage seed drying via quality models, state diagrams and two-stage drying. *Future Foods*,12, 100803. https://doi.org/ 10.1016/j.fufo.2025.100803.

Veser, J., Peeters, W., Schutyser, M.A.I., & Sman, van der Sman, R.G.M. (2025). Prediction of cabbage seed drying at lab and industrial scale using a 'non-equilibrium' sorption isotherm model. *Current Research in Food Science*,11, 101239. https://doi.org/ 10.1016/j.crfs.2025.101239.

Veytsman, B.A., & Cosgrove, D.J. (1998). A model of cell wall expansion based on thermodynamics of polymer networks. *Biophysical Journal*, 75, 2240--2250. https://doi.org/ 10.1016/S0006-3495(98)77668-4.

Voda, A., Homan, N., Witek, M., Duijster, A., van Dalen, G., van der Sman, R., Nijsse, J., van Vliet, L., Van As, H., & van Duynhoven, J. (2012). The impact of freeze-drying on microstructure and rehydration properties of carrot. *Food Research International,*49(2), 687-693. https://doi.org/ 10.1016/j.foodres.2012.08.019.

Vrentas, J.S., & Vrentas, C.M. (1991). Sorption in glassy polymers. *Macromolecules*,24(9). https://doi.org/10.1021/ma00009a043.

Wang, B., Jia, Y., Li, Y., Wang, Z., Wen, L., He, Y., & Xu, X. (2023). Dehydration--rehydration vegetables: Evaluation and future challenges. *Food Chemistry: X*,20(100935). https://doi.org/ 10.1016/j.fochx.2023.100935.

Wang, B., Li, Y., Lv, Y., Jiao, X., Wang, Z., He, Y., & Wen, L. (2024). Dehydration--rehydration mechanism of vegetables at the cell-wall and cell-membrane levels and future research challenges. *Critical Reviews in Food Science and Nutrition*,64(30), 11179-11195. https://doi.org/ 10.1080/10408398.2023.2233620.

Wang, H., Zhang, M., &Adhikari, B. (2015). Drying of *shiitake* mushroom by combining freeze-drying and mid-infrared radiation. *Food and Bioproducts Processing*, 94, 507-517. https://doi.org/ 10.1016/j.fbp.2014.07.008

Wang, J., Law, C.-L., Nema, P.K., Zhao, J.-H., Liu, Z.-L., Deng, L.-Z., Gao, Z.-J., & Xiao, H.-W. (2018). Pulsed vacuum drying enhances drying kinetics and quality of lemon slices. *Journal of Food Engineering*,224, 129-138. https://doi.org/10.1016/j.jfoodeng.2018.01.002.

Welsh, Z.G., Thathsaranee, V., Thuppahige, W., & Karim, M.A. (2026). Multiscale modeling for food drying: A downscaling approach. *Journal of Food Engineering*,402 112695. https://doi.org/ 10.1016/j.jfoodeng.2025.112695.

Winiczenko R.; Górnicki K.; Kaleta A.; Mańkowska M.J.; Choińska A.; Trajer J. (2018b). Apple cubes drying and rehydration. *Multi-objective Optimization of the Processes Sustainability*, 10, 4126. https://doi.org/ 10.3390/su10114126

Winiczenko R.; Górnicki K.; Kaleta A.; Mańkowska M.J.; Trajer J.(2018a). Multi-objective optimization of the apple drying and rehydration processes parameters. *Emirates Journal of Food and Agriculture,* 30, 1--9. https://doi.org/ 10.9755/ejfa.2018.v30.i1.1595

Witrowa-Rajchert, D., & Lewicki, P.P. (2006). Rehydration properties of dried plant tissues. *International Journal of Food Science and Technology*,41, 1040--1046. https://doi.org/ 10.1111/j.1365-2621.2006.01164.x.

Wolf, W., Spiess, W.E.L., & Jung, G. (1985). Standardization of Isotherm Measurements (Cost-Project 90 and 90 BIS). In D. Simatos, J.L. Multon (Eds.),Properties of Water in Foods: in Relation to Quality and Stability(pp. 661-679). Springer Netherlands, Dordrecht. https://doi.org/ 10.1007/978-94-009-5103-7_40.

Xiao, R., Sun, H., & Chen, W. (2016). An equivalence between generalized Maxwell model and fractional Zener model. *Mechanics of Materials*,100, 148--153. https://doi.org/ 10.1016/j.mechmat.2016.06.016.

Xie, Y., Hill, C.A.S., Jalaludin, Z., & Sun, D. (2011). The dynamic water vapour sorption

behaviour of natural fibres and kinetic analysis using the parallel exponential kinetics model. *Cellulose*, 18, 517-530. https://doi.org/ 10.1007/s10570-011-9512-4.

Xin, Y., Zhang, M., Xu, B., Adhikari, B., & Sun, J. (2015). Research trends in selected blanching pretreatments and quick freezing technologies as applied in fruits and vegetables: A review. *International Journal of Refrigeration*, 2015, 11-25. https://doi.org/10.1016/j.ijrefrig.2015.04.015.

Xu, C., Liu, D., Li, Y., Li, G., Zhang, J., & Gao, R. (2017). Implication of water state on glass transition temperature in hot air-dried carrot slices. *LWT - Food Science and Technology*,84, 780-787. https://doi.org/ 10.1016/j.lwt.2017.06.052.

Xu, F., Jin, X., Zhang, L., & Chen, X.D. (2017). Investigation on water status and distribution in broccoli and the effects of drying on water status using NMR and MRI methods. *Food Research International*,96, 191-197. https://doi.org/ 10.1016/j.foodres.2017.03.041.

Xu, Y., Xiao, Y., Lagnika, C., Li, D., Liu, C., Jiang, N., Song, J., & Zhang, M. (2020). A comparative evaluation of nutritional properties, antioxidant capacity and physical characteristics of cabbage (Brassica oleracea var. Capitate var L.) subjected to different drying methods. Food chemistry 309, 124935. https://doi.org/ 10.1016/j.foodchem.2019.06.002.

Xu, Y., Zhang, M., Mujumdar, A.S., Duan, X., & Jin-cai, S. (2006). A two-stage vacuum freeze and convective air drying method for strawberries. *Drying Technology*, 24(8), 1019-1023. https://doi.org/ 10.1080/07373930600776209.

Xu, Y., Zhang, M., Mujumdar, A.S., Duan, X.,Jin-Cai, S. (2006). A Two-Stage vacuum freeze and convective air drying method for strawberries. *Drying Technology*, 24, 1019-1023. https://doi.org/10.1080/07373930600776209

Xu, Y., Zhang, M., Tu, D., Sun, J., Zhou, L., & Mujumdar, A.S. (2005). A two-stage convective air and vacuum freeze-drying technique for bamboo shoots. *International Journal of Food Science and Technology*,40(6), 589-595. https://doi.org/ 10.1111/j.1365-2621.2005.00956.x.

Yang, Z., Fan, H., Li, R., Li, B., Fan, J., Ge, J., Xu, X., Pan, S., & Liu, F. (2023). Potential role of cell wall pectin polysaccharides, water state, and cellular structure on twice "increase--decrease" texture changes during kohlrabi pickling process. *Food Research International*,173, 113308. https://doi.org/10.1016/j.foodres.2023.113308

Yi, J.-Y., Lyu, J., Bi, J.-F., Zhou, L.-Y., &Zhou, M.(2017). Hot air drying and freeze drying pre-treatments coupled to explosion puffing drying in terms of quality attributes of mango, pitaya, and papaya fruit chips. *Journal of Food Processing and Preservation*, 41. https://doi.org/10.1111/jfpp.13300

Yi, J.-Y., Zhou, L.-Y., Bi, J.-F., Wang, P., Liu, X., & Wu, X.-Y. (2016). Influence of number of puffing times on physicochemical, color, texture, and microstructure of explosion puffing dried apple chips. *Drying Technology*,34(7), 773-782. https://dx.doi.org/10.1080/07373937.2015.1076838.

Yi, J., Wang, P., Bi, J., Liu, X., Wu, X., &Zhong, Y. (2015). Developing novel combination drying method for jackfruit bulb chips: instant controlled pressure drop (DIC)-assisted freeze drying. *Food and Bioproducts Processing*, 9, 452-462. https://doi.org/ 10.1007/s11947-015-1643-4

Yi, J., Zhou, L., Bi, J., Liu, X., Qinqin, C., &Wu, X. (2016). Influences of microwave pre-drying and explosion puffing drying induced cell wall polysaccharide modification on physicochemical properties, texture, microstructure and rehydration of pitaya fruit chips. *LWT - Food Science and Technology,* 70, 271-279. https://doi.org/ 10.1016/j.lwt.2016.03.001

Ying, R., Rondeau-Mouro, C., Barron, C., Mabille, F., Perronnet, A., & Saulnier, L. (2013). Hydration and mechanical properties of arabinoxylans and β-D-glucans films. *Carbohydrate Polymers*, 96 31-- 38. https://doi.org/ 10.1016/j.carbpol.2013.03.090.

Zecchi, B., Clavijo, L., Martínez Garreiro, J., & Gerla, P. (2011). Modeling and minimizing process time of combined convective and vacuum drying of mushrooms and parsley. *Journal of Food Engineering*,104(1), 49-55. https://doi.org/ 10.1016/j.jfoodeng.2010.11.026.

Zeineldin, T. (2008). Modeling the process of drying stationary objects inside a tumble dryer Using COMSOL Multiphysics. InCOMSOL Conference 2008 .

Zhang, H., Wang, B., Lv, W., & Xiao, H. (2025). Optimizing crispness and nutrient retention in carrot snacks: Multi-stage drying via microwave-infrared and negative pressure puffing with moisture-dependent transition. Innovative Food Science and Emerging Technologies 105, 104171. https://doi.org/ 10.1016/j.ifset.2025.104171.

Zhang, L., Jiang, L., Adnouni, M., Li, S., & Zhang, X. (2024). Numerical Study on the Variable-Temperature Drying and Rehydration of *Shiitake*. *Foods*,13, 3356.

https://doi.org/ 10.3390/foods13213356.

Zhang, L., & McCarthy, M.J. (2012). Black heart characterization and detection in pomegranate using NMR relaxometry and MR imaging. *Postharvest Biology and Technology*,67, 96--101. https://doi.org/ 10.1016/j.postharvbio.2011.12.018.

Zhang, L., Qiao, Y., Wang, C., Liao, L., Liu, L., Shi, D., An, K., Hu, J., &Xu, Q.(2019). Effects of freeze vacuum drying combined with hot air drying on the sensory quality, active components, moisture mobility, odors, and microstructure of kiwifruits. *Journal of Food Quality*, 1-11. https://doi.org/ 10.1155/2019/8709343

Zhang, M., Chen, H., Mujumdar, A.S., Tang, J., Miao, S., & Wang, Y. (2017). Recent developments in high-quality drying of vegetables, fruits, and aquatic products. *Critical reviews in food science and nutrition*, 57(6), 1239-1255. https://doi.org/ 10.1080/10408398.2014.979280.

Zhang, M., Jiang, H., & Lim, R.-X. (2010). Recent Developments in Microwave-Assisted Drying of Vegetables, Fruits, and Aquatic Products---Drying Kinetics and Quality Considerations. *Drying Technology*,28(11), 1307-1316. https://doi.org/ 10.1080/07373937.2010.524591.

Zhang, M., Tang, J., Mujumdar, A.S., & Wang, S. (2006). Trends in microwave-related drying of fruits and vegetables. *Trends in food science & technology*,17(10), 524-534. https://doi.org/10.1016/j.tifs.2006.04.011.

Zhang, Z., Wei, Q., Nie, M., Jiang, N., Liu, C., Liu, C., Li, D., & Xu, L. (2018). Microstructure and bioaccessibility of different carotenoid species as affected by hot air drying: Study on carrot, sweet potato, yellow bell pepper and broccoli. *LWT - Food Science and Technology*,96, 357-363. https://doi.org/ 10.1016/j.lwt.2018.05.061.

Zhao, J.-H., Ding, Y., Nie, Y., Xiao, H.-W., Zhang, Y., Zhu, Z., & Tang, X.-M. (2016). Glass transition and state diagram for freeze-dried Lentinus edodes mushroom. *Thermochimica Acta*,637, 82-89. https://doi.org/ 10.1016/j.tca.2016.06.001.

Zhao, S.-y., An, N.-n., Zhang, K.-y., Li, D., Wang, L.-j., & Wang, Y. (2023). Evaluation of drying kinetics, physical properties, bioactive compounds, antioxidant activity and microstructure of Acanthopanax sessiliflorus fruits dried by microwave-assisted hot air drying method. Journal of Food Engineering 357, 111642. https://doi.org/10.1016/j.jfoodeng.2023.111642

Zhao, X., Hong, W., & Suo, Z. (2008). Inhomogeneous and anisotropic equilibrium state of

a swollen hydrogel containing a hard core. *Applied Physics Letters*,92, 051904. https://doi.org/ 10.1063/1.2840158.

Zhao, Y., Bi, J., Yi, J., Njoroge, D.M., Peng, J., & Hou, C. (2019). Comparison of dynamic water distribution and microstructure formation of *shiitake* mushrooms during hot air and far infrared radiation drying by low-field nuclear magnetic resonance and scanning electron microscopy. *Journal of the Science of Food and Agriculture*, 99(6), 2826–2834. https://doi.org/10.1002/jsfa.9494

Zhao, Y., Bi, J., Yi, J., Jin, X., Wu, X., &Zhou, M. (2019). Evaluation of sensory, textural, and nutritional attributes of *shiitake* mushrooms (*Lentinula edodes*) as prepared by five types of drying methods. *Journal of Food Process Engineering*, 42. https://doi.org/ 10.1111/jfpe.13029

Zhou, L., Wang, X., Bi, J., Liu, X., Yi, J., & Wu, X. (2018). Effect of different moisture equilibration process on the quality of apple chips dried by instant controlled pressure drop (dic)-assisted hot air drying. *Journal of Food Processing and Preservation*, 42(4), e13316. https://dx.doi.org/10.1080/07373937.2015.1076838

Zhu, Y., Wang, P., Sun, D., Qu, Z., & Yu, B. (2021). Multiphase porous media model with thermo-hydro and mechanical bidirectional coupling for food convective drying. *International Journal of Heat and Mass Transfer,*175, 121356. https://doi.org/ 10.1016/j.ijheatmasstransfer.2021.121356.

Zielinska, M., Ropelewska, E., & Markowski, M. (2017). Thermophysical properties of raw, hot-air and microwave-vacuum dried cranberry fruits (*Vaccinium macrocarpon*). *LWT - Food Science and Technology*,85, 204-211. https://doi.org/ 10.1016/j.lwt.2017.07.016.

Zou, K., Teng, J., Huang, L., Dai, X., &Wei, B. (2013). Effect of osmotic pretreatment on quality of mango chips by explosion puffing drying. *LWT - Food Science and Technology*, 51, 253-259. https://doi.org/ 10.1016/j.lwt.2012.11.005

Summary

Dried fruits, vegetables, and mushrooms can be stored and transported without refrigeration, significantly extending their shelf life. However, improper drying methods can adversely affect the texture, color, sensory qualities, and nutritional value. Air-dried products often become tough and rehydrate poorly, while freeze-dried products generally rehydrate well but tend to have an excessively soft texture. With existing drying technologies, maintaining the original quality of food remains a significant challenge, making it difficult for dried products to match the quality of fresh ones **(Chapter 1)**.

In this thesis, we explore whether serially combining different drying techniques can improve the quality retention of rehydrated mushrooms. We also seek to identify the critical factors influencing rehydration performance by studying microstructural evolution during the drying. Additionally, we have developed a mechanistic model of mushroom drying to better understand the heat and mass transfer processes that shape microstructure formation.

In Chapter 2 we took *shiitake* mushroom as the case study, and studied various combinations of drying techniques such as instant controlled pressure drop drying (DIC) and freeze drying (FD) for porosity enhancement that improves the rehydration performance. These treatments were applied either before or after an additional drying step at low (35 °C) or high (65 °C) temperatures. Based on the principal component analysis (PCA) on quality indicators including relative volume, rehydration rate, dry matter loss and sensory scores, the DIC treatment before hot air drying at 35 °C was shown to be the most promising combination for improving the rehydration quality.

To validate the hypothesis from Chapter 2, we conducted a follow-up study **in Chapter 3**. Focusing on the microstructural development induced by DIC, we compared overall porosity and connectivity among three groups: hot air dried samples at 35°C (HA35), DIC treated samples, and samples subjected to DIC combined with HA35. Our findings confirmed that the critical temperature range for cell membrane damage lies between 30°C and 40°C. Importantly, DIC pretreatment creates a porous microstructure with increased porosity, provided the product temperature remains below the critical threshold of 40°C during the subsequent drying.

To develop a theoretical model that accurately represents the physical process of mushroom drying, we investigated the moisture sorption isotherms (MSIs) of mushrooms **in Chapter 4**, through both experimental measurement and theoretical modeling. Our analysis revealed variations in MSIs and hysteresis among mushrooms dried using different methods. We explored potential causes of these variations.

Based on the Flory-Huggins (FH) theory, our findings suggest that protein denaturation does not significantly influence moisture sorption or hysteresis. Cell membrane integrity primarily affects the moisture sorption and water-holding capacity at high relative humidity. Instead, we attribute the observed differences in MSI and hysteresis to viscoelastic relaxation. This conclusion is supported by dynamic vapor sorption (DVS) experiments, which revealed temperature- and moisture-dependent viscoelastic behavior in mushrooms.

In light of these findings, we propose incorporating elastic stress into the driving force of drying, consistent with the Flory-Rehner theory. To accurately describe the stress evolution in viscoelastic media during drying, we suggest adopting a separate model, such as the generalized Maxwell model.

In Chapter 5 we introduce a mechanistic and multiphase model for simulating the hot air drying of *shiitake* mushrooms. The model integrates several key physical phenomena, including shrinkage, water activity prediction based on Flory-Huggins theory, viscoelastic relaxation described by an extended Maxwell model, and coupled heat and mass transfer in a porous medium. It captures the distinctive drying behavior of mushrooms, such as prolonged internal evaporative cooling and a sharp temperature rise toward the end of drying process. The model was validated against experimental data across multiple drying temperatures, and it was then applied to interpret low-field NMR results, which verified the presence of two thermodynamic phases with the two distinct water populations corresponding to different cellular compartments. By integrating model predictions with electrical conductivity and NMR data, critical thresholds for the cell membrane integrity were identified—specifically, when the product temperature exceeds 40°C or moisture content falls below 3% (w.b.). These findings provide a valuable tool for further optimization of the drying processes to maintain membrane integrity, thereby improving the rehydration quality.

In Chapter 6 we reflect on our findings in a broader context. We discuss DIC treatments in the context of current literature of serial and parallel combined drying. Furthermore, state the found conditions for the preservation of cell membrane integrity for *shiitake* mushrooms are likely applicable to other biological materials. The state diagram of mushrooms can guide the design of optimized drying protocols. We also acknowledge the developed model's current limitation in mechanistically describing large deformations and shrinkage, which is due to the complexity of soft materials and the lack of cellular-level material properties. Future models should incorporate momentum balance to couple moisture transport, stress, and shrinkage, potentially integrating poromechanics and diffusion-deformation theories. Besides, the potential of T_2-NMR as a non-destructive tool for monitoring water dynamics

and microstructure during drying is discussed. The NMR/MRI methods can validate multiphysics models, quantify spatial changes, and enable real-time quality monitoring in industrial drying processes. Finally, future work is recommended to focus on the complete DIC/HA process, generalizing the findings to other fruits and vegetables with the considerations of the instinct material properties like Tg and initial porosity, and developing simulation-driven optimization frameworks for multi-stage drying.

In conclusion, this thesis advances the understanding of serial combined drying for *shiitake* mushrooms and provides a foundational modeling framework for cellular food materials. By addressing the identified research gaps, future work can accelerate the development of quality-sensitive drying technologies for a wider range of fruits and vegetables.

Appendices

Acknowledgments

About the author

Publications

Overview of completed training activities

Acknowledgements

The thesis book summarizes my PhD work over the past few years. I would like to express my sincere gratitude to the Food Process and Engineering Group (FPE) at Wageningen University (WUR) and the Institute of Food Science and Technology (IFST), Chinese Academy of Agricultural Sciences (CAAS) for funding this work. I also would like to acknowledge all those who involved in this research.

First and foremost, I wish to express my heartfelt thanks to my promotors and supervisors: Prof. Ruud van der Sman, Prof. Remko Boom, Prof. Jinfeng Bi and Dr. Xin Jin. Your combined knowledge, creativity and great passion were invaluable to the completion of this work, and I am truly grateful for the opportunity to have worked with you.

My distinguished promoter and supervisor, Ruud van der Sman, words cannot fully express my gratitude. Over the past years, you have devoted tremendous patience and time to guiding my PhD research. As a beginner in modelling, I deeply appreciated your supervision, which was extremely important to me. Especially during the COVID-19 pandemic, I am grateful to you and your wife for inviting me to meet virtually at your home, which ensured effective communication and allowed my modeling work to continue smoothly despite quarantine. I also admirable for your meticulous scientific spirit. Through your high standards in my proposal, experimental design, data analysis, and scientific writing—always grounded in consistent logical and critical thinking—I have received rigorous training and now feel confident to become a qualified scientific researcher. Thank you for your efforts in the past years. Thank you.

Prof. Remko Boom, I was deeply impressed by your sharp intellect and extensive experience across a wide range of scientific and technological challenges. You have inspired me and offered excellent suggestions after every discussion we have had. When I worked in the office (X1120) next to yours and observed PhD students coming to you one after another, I felt that you were a remarkable doctor—always able to provide an accurate diagnosis and prescribe the right solution for each student working in different fields. Of course, I am one of the beneficiaries of your excellent “art of healing”. I truly appreciate it.

My gratitude also extends to my Chinese promoter, Professor Dr. Jinfeng Bi, for the opportunity you provided me to participate in the WUR-CAAS collaboration program. Thank you for your time and effort in supporting my PhD work. Furthermore, thanks to your many years of experience and achievements in the field of fruit and vegetable processing, I had valuable opportunities to meet many outstanding entrepreneurs and learn from them, which

is very important for my future career. I also admire your passionate enthusiasm and perseverance in your work. Your success in both academia and industry, along with your excellent ability to lead a large group, sets an inspiring example for everyone in the team.

Dr. Xin Jin, my daily supervisor in China, thank you very much for your help and support. Thanks to your help, I was eventually accepted as Ruud's PhD after a long period of trying and waiting. Your support and trust greatly encouraged me at that time. In the years that followed, no matter what difficulties I encountered, you were always patient, supportive, and willing to help. I am deeply grateful for that. I also appreciate the opportunities you provide for me to participate in project work like managing project progress, reporting, communicating with the cooperating teams, which helped train me to become an independent researcher. I really appreciate it.

I would also like to thank the technicians at Axis, who have been essential to my work. Dear Jos, Maurice, Martin, Wouter, Jarno—thank you for all your support for our entire FPE team and labs, for your help with my project, and for all the wonderful lunch breaks we shared. Martin, I am especially grateful for your help with important financial and organizational matters throughout my PhD project. Jos, Maurice, Wouter and Jarno, thank you for always being ready to help with all kinds of questions during my time at Axis. It was a true pleasure working with all of you. Your expertise and teamwork made everything possible. My thanks also go to Evelyn and Ilona for their kind help and support from the secretaries' office. I am equally grateful to Yvonne and the other VLAG colleagues for their assistance with my PhD project.

Being part of both FPE, WUR and IFST, CAAS allowed me to meet many excellent colleagues across the university in the Netherlands and the institute in China. First, I would like to thank my office mates at IFST, CAAS, where I began my sandwich PhD work. Many thanks to the staff at the Institute of Food Science and Technology, CAAS. Qinqin Chen, Xuan Liu, Jianyong Yi, Xinye Wu, Jian Lyu, Xuan Li and Mo Zhou. Thank you all for your help with my experimental work at CAAS.

A big thank you to Yitong Xie, Meilin Xian, Wanjia Yu, Yue Song, Yang Qiu, Jian Peng, Jianxin Song, Xiao Li, Noor, Chongting Guo, Dazhi Liu, Jianing Liu, Ying Lv, Yening Qiao, YuanyuanZhao, Jiaxin Chen, Min Gou, Xiyu Jiang, Shuhan Feng, Jin Xie, Meng Liu, Wenyue, Wang , Fengzhao Wang, Youchuan Ma for the selfless assistance with my work, for the enriching time spend together in various scientific activities, and for the chats and the shared food that makes the office and labs such a pleasant places to be. I also cherish the countless meals and working hours we have spent together. Congting Guo, Xiao Li, Jin Xie, thank you

for the accompany on those nights walking back to the dormitory from the lab.

I also would like to thank my FPE office mates and colleagues. Andrea, Nynke, Anouk, Luc, Sirinan, Joanna, Koen, Jiarui and Somayeh—thank you for your kindness and for welcoming me as a new member of the office when I conducted my PhD work at Wageningen in 2020 and 2022. Thank you again for your warm farewell gift and dinner before I left for China. I really enjoyed the time I spent with you all. Qinhui, thank you for introducing me to new people in FPE group and for showing me interesting places when I first arrived in Wageningen. Julia, Nynke E., thank you both for sharing your modeling skills with me. Yu and Wanqing, thank you for your encouragement and suggestions regarding my future career. Boxin, Sicong, Yifeng, Ruihao, Chenqiang, Yizhou, Lingfeng, Ruoxuan, Mingzhao, Steven, Isabel, Eric, Anna, Pina, Konstantina, thanks for the enjoyable conversations we had in the office. A special thanks to Julia Veser and Jingwei Liu. Thank you for being my paranymphs! Thank you for all your help with my defense issue.

I also want to express my gratitude to my friends in the WUR-CAAS program. Many thanks for Panpan Fan, Jingjing Mao, Yusi Liu, Ran Wang, Yingxia Liu, Qingbo Qu, Dengke Hua, Qian Li, Xiaoxiao Xie, Jingyan Zhang, Yan Wang, Hongwei Yu, Zhuo Xu, Xiaojie Qin, Feilong Yang, Yaowu Wang, Jiaqi Zhang, Qitong Huang. Because of you all, I have "comrade-in-arms" to persevere together through this PhD journey. Thank you to Lei Deng, Keli Li, Zhenxiang Zhou, Taojun Wang, Shuangwei Li, Mingming Zhong, Yufan Sun, Honglei Wang for inviting me to join your parties. Shanshan, Panpan, Yusi, Xiaojie thank you for your feeding when I was in quarantine due to the corona. Jianing, Yening, Xiyu, Dazhi, I really enjoyed our happy travels together in Belgium and the Netherlands. Thanks to all of you. The parties, dinners, and sports activities we shared will remain among my most precious and unforgettable memories of Wageningen.

最后我要特别感谢我的爸爸妈妈，谢谢你们这么多年来对我的理解和支持，没有你们的托举和兜底，不会有我今天的收获与成绩。谢谢爸爸妈妈，谢谢你们给予我最坚实的铠甲和直面人生的勇气。还要感谢舅舅舅妈、姨妈姨父，叔叔婶婶、姑姑以及我的兄弟姐妹们，谢谢你们在我最困难的时候对我的鼓励和照顾。你们的关心和帮助让我感受到了亲人间的支持、温暖与爱，谢谢你们！

About the author



Lina Hu was born on December 20, 1989, in Luohe, Henan Province, China. She obtained her bachelor's degree in Food Nutrition and Inspection Education from Henan Agricultural University in 2012. In 2013, she pursued her master's studies at the Zhengzhou Fruit Research Institute, Chinese Academy of Agricultural Sciences (CAAS). For her master's thesis, she investigated the post-harvest enrichment of bioactive compounds in fruits. She received her master's degree in Food Science in 2016. Subsequently, she worked as a research assistant at the institute for one year. In May 2018, she began her joint PhD research at Wageningen University and Research (WUR) and CAAS, under the supervision of Prof. Dr. Ruud van der Sman from WUR and Prof. Dr. Jinfeng Bi and Dr. Xin Jin from CAAS. Her research focused on the mechanism of mushroom drying, aiming to improve the quality of the dried product after rehydration. The results of her PhD project are described in this thesis.

Contact: hulina2008@163.com

Publications

This thesis

Hu, L., Bi, J., Jin, X., Qiu, Y., & van der Sman, R. G. M. (2021). Study on the rehydration quality improvement of *shiitake* mushroom by combined drying methods. Foods, 10 (4), 769. https://doi.org/10.3390/foods10040769

Hu, L., Bi, J., Jin, X., & van der Sman, R. G. M. (2022). Microstructure evolution affecting the rehydration of dried mushrooms during instant controlled pressure drop combined hot air drying (DIC-HA). Innovative Food Science and Emerging Technologies, 79, 103056. https://doi.org/10.1016/j.ifset.2022.103056

Hu, L., Bi, J., Jin, X., & van der Sman, R. G. M. (2023). Impact of physical changes in mushroom on variation in moisture sorption. Journal of Food Engineering, 351, 111506. https://doi.org/10.1016/j.jfoodeng.2023.111506

Hu, L., Xie, Y., Jin, X., Bi, J., & van der Sman, R. G. M. (2026). A multiphase and multiscale mechanistic model for hot air drying of *shiitake* mushroom, Current Research in Food Science,101296. https://doi.org/10.1016/j.crfs.2025.101296.

Hu, L., Bi, J., Jin, X., & van der Sman, R. G. M. Rehydration capacity improvement of mushrooms dried by combined methods. IDS'2020 – 22nd International Drying Symposium.

Other publications:

Xian, M., Bi, J., **Hu, L.**, Xie Y, Zhao Y, Jin, X. (2024). Synergistic mechanism of steam blanching and freezing conditions on the texture of frozen yellow peaches based on macroscopic and microscopic properties. Journal of Texture Studies,55(2): e12830 https://doi.org/10.1111/jtxs.12830

Qiu, Y., Bi, J., Jin, X., Wu, X., **Hu, L.**, & Chen, L. (2022). Investigation on the rehydration mechanism of freeze-dried and hot-air dried *shiitake* mushrooms from pores and cell wall fibrous material. Food Chemistry, 383, 132360.

https://doi.org/10.1016/j.foodchem.2022.132360

Qiu, Y., Bi, J., Jin, X., **Hu, L.**, Lyu, J., & Wu, X. (2021). An understanding of the changes in water holding capacity (WHC) of rehydrated *shiitake* mushroom (Lentinula edodes) from cell wall, cell membrane and protein. Food Chemistry, 351, 129230.

https://doi.org/10.1016/j.foodchem.2021.129230

Li, X., Bi, J., Jin, X., Wu, X., Lyu, J., Li, X., and Hu, L. (2020). Effect of the moisture equilibrium process on the expansion behavior of instant controlled pressure drop (DIC) drying of dried apple cubes. Journal of the Science of Food and Agriculture, 100(4), 1635–1642. https://doi.org/10.1002/jsfa.10175

Overview of completed training activities

Discipline specific activities

	Organiser	*Year*
Courses		
Progress in Agricultural Science	CAAS	2017
COMSOL Multiphysics® Intensive Training (online)	COMSOL	2019
Rheology: the do`s and don`ts"	VLAG	2020
VLAG Online lecture series	VLAG	2020-2022
Advanced Organic Chemistry	VLAG	2021-2022
VLAG Course Advanced Food Analysis	VLAG	2022
Conferences		
5th Food Drying Workshop& 10th LF-NMR National Conference	Jiangnan University, Wuxi, China	2018
NWGD symposium	Wageningen, The Netherlands	2019
6th Food Drying International conference&7th Symposium for Space Nutrition and Food Engineering[o]	Jiangnan University, Wuxi, China	2020
Wageningen Food Science symposium	Wageningen, The Netherlands	2020
International Drying Symposium (on line)[o]	Worcester Polytechnic Institute (WPI),Worchester, United States	2022
NWGD symposium	Wageningen, The Netherlands	2022
2nd Edible Soft Matter Workshop & Conference[p]	Wageningen, The Netherlands	2022

General courses

Searching and Organising Literature	WGS	2020
Scientific Writing	WGS	2020
The Essentials of Scientific Writing & Presenting Wageningen,	WGS	2020 2020
Introduction to R	VLAG	2020
Scientific Publishing	WGS	2022
Career Perspectives	WGS	2022

Other activities

Preparation of research proposal	CAAS, FPE	2018
FPE group meetings[o]	CAAS, FPE	2018-2022
Physical Transport Phenomena	BET	2020
FPE group days[p]	FPE	2022

[p] *Poster presentation,* [o] *Oral presentation*

List of abbreviations

CAAS: Chinese Academy of Agricultural Sciences
VLAG: The Graduate School VLAG (Advanced Studies in Food Technology, Agrobiotechnology, Nutrition and Health Sciences)
WGS: Wageningen Graduate Schools
FPE: Food Process and Engineering group
BET: Biobased Chemistry and Technology group

The research described in this thesis was financially supported by the Joint PhD Program between Wageningen University & Research and Chinese Academy of Agricultural Sciences (MOE11NL1A20151701N), National Key R&D Program of China (2018YFD0700203), National Natural Science Foundation of China (32001719), Ningxia Key R&D Program (No.2024BBF02026) and Agricultural Science and Technology Innovation Program of Food Science and Technology, Chinese Academy of Agricultural Sciences (CAAS-ASTIP-G2025-IFST-02). and China Scholarship Council (CSC).

Financial support from Wageningen University for printing this thesis is gratefully acknowledged.

Cover design by Lina Hu
Printed by ProefschriftMaken ‖ www.proefschriftmaken.nl